

# **Programming supramolecular peptide materials for immunological applications**

Chun Yin Jerry Lau

2021

**Programming supramolecular peptide materials for immunological applications**

Chun Yin Jerry Lau

Department of Pharmaceutics, Utrecht Institute for Pharmaceutical Sciences (UIPS), Faculty of Science, Utrecht University, Utrecht, the Netherlands

**Author:** Chun Yin Jerry Lau

**Cover design:**

**Printed by:** Gilderprint

**ISBN:** 978-94-6419-359-6

The research described in this thesis has been done within the NANOMED network. The funding was provided from the European Union's Horizon 2020 research and innovation programme Marie Skłodowska-Curie Innovative Training Networks (ITN) under grant No. 676137.

Printing of this thesis was partially supported by Utrecht Institute for Pharmaceutical Sciences (UIPS), Faculty of Science, Utrecht University, Utrecht, the Netherlands.

© Chun Yin Jerry Lau, 2021

All rights reserved. No parts of this thesis may be reproduced, stored in a retrieval system or transmitted in any form or by any means without permission of the author

# **Programming supramolecular peptide materials for immunological applications**

**Programmering van supramoleculaire peptidematerialen voor immunologische toepassingen**  
(met een samenvatting in het Nederlands)

## **Proefschrift**

ter verkrijging van de graad van doctor aan de  
Universiteit Utrecht  
op gezag van de  
rector magnificus, prof.dr. H.R.B.M. Kummeling,  
ingevolge het besluit van het college voor promoties  
in het openbaar te verdedigen op

maandag 6 december 2021 des middags om 12.15 uur

door

**Chun Yin Lau**

geboren op 3 juli 1991  
te Hong Kong, Hongkong

## **Promotoren:**

Prof. dr. E. Mastrobattista

Prof. dr. W.E. Hennink

To my family

‘What I really need is to get clear about *what I must do*, not what I must know ... the crucial thing is to find a truth which is truth *for me*, to find *the idea for which I am willing to live and die.*’

Søren Kierkegaard (1813-55)



# Table of Content

<b>Chapter 1:</b> Introduction .....	9
<b>Chapter 2:</b> Programming supramolecular peptide materials by modulating the intermediate steps in the complex assembly pathway: implications for biomedical applications .....	23
<b>Chapter 3:</b> Control over the fibrillization yield by varying the oligomeric nucleation propensities of self-assembling peptides .....	45
<b>Chapter 4:</b> The hierarchical structure of peptide nanofibers formed by self-assembly .....	85
<b>Chapter 5:</b> Tuning surface charges of supramolecular nanofibers for induction of antigen-specific immune tolerance: an introductory study .....	103
<b>Chapter 6:</b> Complementary hydrophobic-electrostatic interactions enhance albumin association with dexamethasone-antigen conjugates leading to a more robust tolerogenic response .....	125
<b>Chapter 7:</b> Summary and Perspective .....	149
<b>Appendices:</b> Nederlandse Samenvatting, Curriculum Vitae, List of Publications, Acknowledgement .....	159





# **Chapter 1**

## **Introduction**

### 1. General introduction

Self-assembly of molecules can bring about disorder-to-order transition to give discrete structures at different length scales. Supramolecular chemistry, the chemistry of noncovalent interactions between molecules and/or ions, is key to advancing the field of self-assembly for molecular systems<sup>1,2</sup>. Through manipulating the intermolecular non-covalent interactions between the molecular building blocks (e.g., van der Waals forces, hydrogen bonding, electrostatic interactions), supramolecular materials can be programmed with novel properties such as multicomponent modularity<sup>3-5</sup>, semiconductivity<sup>6,7</sup> and evolution-like adaptivity<sup>8</sup>. These novel properties impart new possibilities to biomedical applications such as cardiac tissue engineering<sup>9</sup> and self-boosting antitumor nanoreactors<sup>10</sup>. Peptides are frequently used to construct supramolecular materials in which the non-covalent interactions are moderated through the backbone and side-chain interactions of the self-assembling peptides. Specific strategies to design and fabricate supramolecular peptide materials at different length scales have been reported, such as zero-dimensional spherical assemblies<sup>11</sup>, one-dimensional peptide nanofibers<sup>12</sup>, two-dimensional peptide nanosheets<sup>13</sup>, and three-dimensional matrices<sup>14</sup>. However, many of these reported approaches are system-specific. Therefore, further understanding of the mechanisms underlying self-assembly is needed to devise more general engineering methodologies.

### 2. Programmable supramolecular peptide materials: from self-assembly to non-covalent synthesis

Accumulating evidence shows that supramolecular structures are formed via a multistep mechanism rather than a single spontaneous event, which leads to a paradigm shift of our engineering approach to devising supramolecular materials with higher molecular complexity<sup>15-17</sup> (Figure 1). Following the trajectory of multistep covalent synthesis, there is an increasing focus on the importance of the intermediate states towards the properties of the fabricated materials<sup>16</sup>. In particular, as the magnitude of non-covalent interactions is smaller than their covalent counterparts, there is a larger share of entropy to the construction of supramolecular materials<sup>15</sup>. With this delicate structure-energy balance in each intermediate state, many supramolecular material properties are under kinetic rather than thermodynamic control<sup>17</sup>. For example, the polymorphic structures of supramolecular peptide fibrils are controlled by their kinetic intermediates<sup>18</sup>. However, parallel/competing non-covalent synthetic pathways are often present in one supramolecular system<sup>19</sup>. To navigate this pathway complexity, there are continuous efforts to decipher the precise pathways in each non-covalent synthetic process<sup>19-21</sup>. Therefore, to fully unleash the potential of supramolecular peptide materials, increasing efforts are spent on characterizing and optimizing the intermediate states.

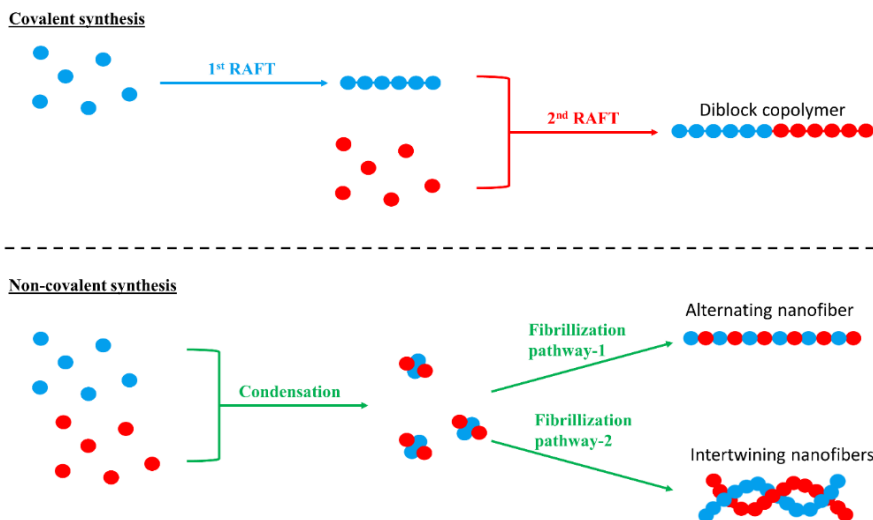


**Figure 1** demonstrates the versatility of noncovalent synthesis to construct structures with higher molecular complexity. For example, we can employ reversible addition–fragmentation chain-transfer (RAFT) polymerization with two stages trigger to synthesize a diblock copolymer via covalent synthesis. With noncovalent synthesis, we can obtain complex polymeric structures (e.g., alternating nanofiber) through modulating the intermediate states.

### 3. The non-covalent synthetic strategy of supramolecular peptide materials

The multistep non-covalent synthetic pathway of supramolecular peptide materials is amongst the most studied supramolecular systems<sup>22-24</sup>. To successfully overcome the desolvation barrier, peptides undergo liquid-liquid-phase separation as the common first step to form dynamic oligomeric particles<sup>22, 25, 26</sup>. Next, through secondary structure induction (e.g.,  $\alpha$ -helix,  $\beta$ -sheet), higher-order nucleates (e.g., cross- $\beta$  protofilaments) are formed within the oligomeric particles, which can trigger the formation of supramolecular materials with increasing structural complexity<sup>27</sup>. Several researchers explored molecular<sup>28, 29</sup>, physical<sup>24</sup>, or chemical<sup>30</sup> strategies to modulate the intermediate states of peptide assembly, thereby influencing the resultant properties of the supramolecular peptide materials. For example, Cui et al. studied how the helicity of the peptide nanofibers can be modulated through surface electrostatic interactions<sup>29</sup>. However, the generality of all these intermediate engineering approaches lies heavily on understanding the link between the modified parameters and the molecular arrangement of the resultant supramolecular products. Hence, robust characterization of the supramolecular materials is essential for further optimization of the non-covalent synthetic strategy.

### 4. Characterization of the supramolecular peptide materials

Given that most supramolecular peptide materials exist in a kinetically trapped rather than the thermodynamic state<sup>16</sup>, an in-depth understanding of the physicochemical properties of the supramolecular structures not only can aid our understanding of the structural

organization but also of the energy constraints these structures are encountering. With the advancement in biophysical characterization techniques, we can now resolve the molecular organization of structures in dynamic<sup>31, 32</sup> and static<sup>31, 32</sup> states. For example, using cryo-EM tomography analysis, Meijer et al. resolved the double helix nanofiber structures formed by supramolecular polymers in water<sup>33</sup>; while using high-speed atomic force microscopy, Sugiyasu et al. captured and manipulated the event of dynamic assembly of supramolecular polymers<sup>34</sup>. Since the functionality of supramolecular materials is closely correlated to the systemic energy landscape<sup>20</sup>, our increased understanding of the structural properties paves the way to better manipulate the material properties for functional applications<sup>32</sup>.

### **5. From programming material properties to functional system integration**

Successful application of designer supramolecular peptide materials requires not only tailored properties but also good compatibility with the application sites. For supramolecular peptide materials targeting biological applications, effective integration into the biological system is an essential prerequisite to delivering the overarching functionality. Currently, two major system integration approaches are being pursued ---1) reconciling the fabricated supramolecular materials with the biological systems<sup>35, 36</sup>; or 2) incorporating the supramolecular materials as modalities in the biological systems<sup>37-39</sup>. As an example of the first approach, Meijer et al. investigate the use of dynamic covalent chemistry to anchor supramolecular nanofibers to human erythrocytes<sup>35</sup>, which can serve as a potential means for targeted tumor delivery<sup>40</sup>. Regarding the second approach, Kataoka et al. explore the use of electrostatic association of supramolecular peptide materials to transiently modify the liver sinusoidal wall, which enhances the longevity of gene delivery vectors<sup>39</sup>. These system integration strategies unleash a new facet of the application potential of the supramolecular peptide materials.

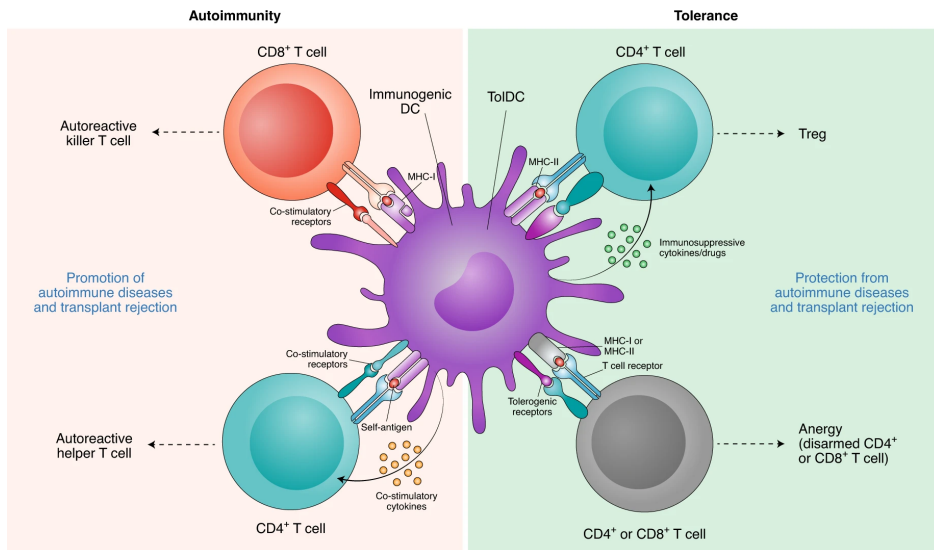


**Figure 2** Diagram shows the critical parameters governing the induction of autoimmune or tolerance response. Adapted from Voelcker et al<sup>45</sup>.

## 6. Immunological applications of the supramolecular peptide materials

Being proteinaceous material, supramolecular peptide materials offer an inherent advantage towards immunological application. By incorporating functional vaccine epitopes into the peptide sequences, upon uptake by antigen-presenting cells (APCs, e.g., dendritic cells and macrophages), the supramolecular peptide materials can activate APCs and promote the presentation of vaccine epitopes in the major histocompatibility complex (MHC)<sup>41-44</sup>. Presentation of vaccine epitopes bound to MHC class I generally propagate CD8+ T cell response, while MHC class II epitope presentation propagates CD4+ T cell response. Furthermore, the type of co-receptors and cytokines released from the APCs play a significant role in determining the state of the immune response (tolerance versus autoimmunity, Figure 2)---expression of co-stimulatory receptors and production of pro-inflammatory cytokines will lead to an autoimmune response. In contrast, the absence of co-stimulatory receptors and the production of immunosuppressive cytokines will lead to tolerogenic response<sup>45</sup>. Accordingly, the two major approaches of functional system integration have been explored for the immunological application of supramolecular peptide materials. Below are two exemplary strategies.

**Use of supramolecular peptide nanofibers for immunomodulation.** Thanks to their excellent biocompatibility<sup>46, 47</sup>, high thermostability<sup>48</sup>, and multicomponent modularity<sup>49</sup>, supramolecular peptide nanofibers are extensively studied for engineering immunomodulation<sup>50-52</sup>. The structural dimension of nanofibers (high aspect ratio) governs higher uptake by phagocytic cells (e.g., APCs) than non-phagocytic cells<sup>53</sup>, which serve as a means to augment vaccine epitope delivery to the target immune cells. To elicit a desirable immune response upon *in vivo* application, it is paramount for the peptide

nanofibers to reach the secondary lymphoid organs, such as draining lymph nodes and spleen. In this regard, Collier et al. showed that peptide nanofibers can successfully reach the draining lymph nodes and elicit systemic immune response upon parenteral administration<sup>54</sup>. Moreover, the magnitude of the immune response can be modulated by its physicochemical properties (such as charge<sup>54</sup>) and/or composition (such as the ratio of different vaccine epitopes presenting in the same nanofiber<sup>3, 49, 55</sup>).

**Use of peptide-drug/albumin supramolecular complexes for lymphatic delivery.** Being the most abundant plasma protein in the body, albumin plays a crucial role in regulating the oncotic pressure in the body through its movement between blood circulation and lymphatic system---albumin leaves the blood through capillaries to reach the interstitial fluid, from which it can rejoin the blood circulation via the lymphatic system<sup>56</sup>. Besides, albumin is also a major transporter of endogenous and exogenous molecules<sup>57, 58</sup>. To exploit the biological functionality of albumin, several peptide vaccines have been developed to implement the modular integration with albumin<sup>59, 60</sup>. For example, Chen et al. utilized hydrophobic interactions to guide albumin complexation with a peptide-based molecular vaccine, which can deliver potent antitumor immune response<sup>59</sup>. Since the modular integration of the molecular peptide vaccine with albumin is a supramolecular complexation process (e.g., guided by hydrophobic interaction<sup>61</sup>), supramolecular chemistry can be deployed for encoding this assembly process.

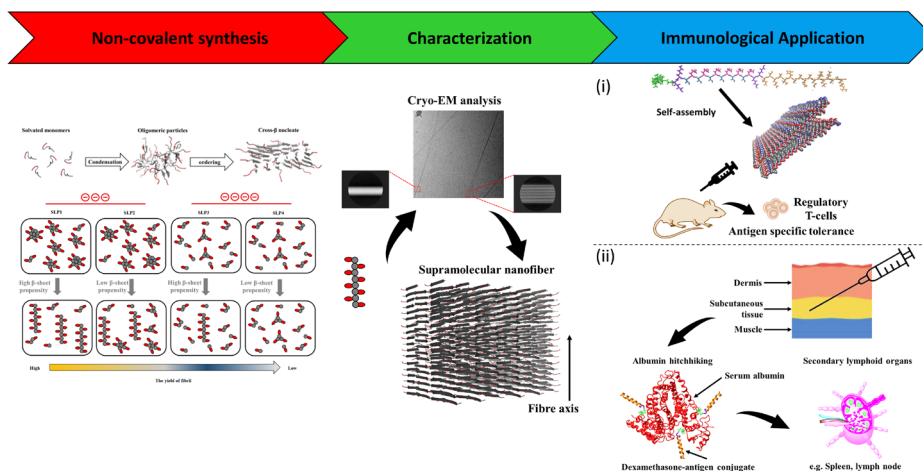


**Figure 3** Summary of the work in this doctoral thesis

### 7. Aim of this thesis

The overarching aims of this doctoral thesis are 1) to gain a better understanding of the mechanisms underlying peptide self-assembly to form hierarchical supramolecular structures and 2) to apply this knowledge to fabricate and characterize supramolecular peptide materials as vaccines to modulate the immune response in inflammatory or autoimmune diseases. Two approaches will be followed for this, which include the use of (i) supramolecular nanofibers and (ii) molecular peptide vaccine/albumin supramolecular complexes (Figure 3). The research reported in this thesis contributed as part of the NANOMED network, a consortium aiming to train a new generation of multi-disciplinary nanotechnology experts capable of supporting and managing the effective translation of molecular innovations into clinically applicable therapeutic solutions. Financial support was provided by European Union's Horizon 2020 research and innovation program Marie Skłodowska-Curie Innovative Training Networks (ITN) under grant No. 676137.

### 8. Outline

#### Chapter 2: Programming supramolecular peptide materials by modulating the intermediate steps in the complex assembly pathway: implications for biomedical applications

This chapter provides a general overview of the strategies to better control the supramolecular material properties by modulating the intermediate steps in the self-assembly pathway. This engineering approach is exemplified in the fabrication of the  $\beta$ -sheet based zero-/one-dimensional nanostructures. In addition, examples of biomedical applications using these steered peptide assemblies in drug delivery and tissue engineering are provided.

#### Chapter 3: Control over the fibrillization yield by varying the oligomeric nucleation propensities of self-assembling peptides

An extensive study of the multistep process of peptide self-assembly was presented, which offers fundamental insights into the design of supramolecular biomaterials in this study. This is done by integrating an array of experimental techniques (cryo-MAS solid-state NMR, TEM, AFM, FCS) with computational approaches. Findings in this chapter guide the molecular design of peptides in Chapter 5 to guide higher yield of the supramolecular nanofiber.

#### Chapter 4: The hierarchical structure of peptide nanofibers formed by self-assembly of a surfactant-like peptide under physiological conditions

In this chapter, the supramolecular organization of the nanofibers forms by self-assembly of a designer surfactant-like peptide (SLP 1) studied in chapter 3 was characterized using cryo-EM analysis.

#### Chapter 5: Tuning surface charges on supramolecular nanofibers for induction of antigen-specific immunotolerance

## Chapter 1

---

This study investigates supramolecular peptide nanofibers as scaffolds for the co-delivery of immunosuppressive drugs and peptide epitopes. Besides peptide and drug concentration, the overall charge of the peptide assemblies is the subject of investigation in this chapter.

### Chapter 6: Attenuating albumin-hitchhiking by linker charges of dexamethasone-antigen conjugate for tolerogenic immunotherapy

Here we optimize the exploration of dexamethasone-antigen conjugates for tolerogenic immunotherapy by attenuating the supramolecular complexation propensities with albumin. We explore the use of complementary electrostatic and hydrophobic interactions to enhance the dexamethasone-antigen conjugate/albumin complexation.



### References

1. Palmer, L. C.; Velichko, Y. S.; Olvera de la Cruz, M.; Stupp, S. I., Supramolecular self-assembly codes for functional structures. *Philosophical Transactions of the Royal Society A: Mathematical, Physical and Engineering Sciences* **2007**, *365* (1855), 1417.
2. Hashim, P. K.; Bergueiro, J.; Meijer, E. W.; Aida, T., Supramolecular Polymerization: A Conceptual Expansion for Innovative Materials. *Progress in Polymer Science* **2020**, *105*, 101250.
3. Hudalla, G. A.; Sun, T.; Gasiorowski, J. Z.; Han, H.; Tian, Y. F.; Chong, A. S.; Collier, J. H., Graded assembly of multiple proteins into supramolecular nanomaterials. *Nature Materials* **2014**, *13*, 829.
4. Bakker, M. H.; Lee, C. C.; Meijer, E. W.; Dankers, P. Y. W.; Albertazzi, L., Multicomponent Supramolecular Polymers as a Modular Platform for Intracellular Delivery. *ACS Nano* **2016**, *10* (2), 1845-1852.
5. Shah, R. N.; Shah, N. A.; Del Rosario Lim, M. M.; Hsieh, C.; Nuber, G.; Stupp, S. I., Supramolecular design of self-assembling nanofibers for cartilage regeneration. *Proceedings of the National Academy of Sciences* **2010**, *107* (8), 3293.
6. Tao, K.; Makam, P.; Aizen, R.; Gazit, E., Self-assembling peptide semiconductors. *Science* **2017**, *358* (6365).
7. Kumar, M.; Ing, N. L.; Narang, V.; Wijerathne, N. K.; Hochbaum, A. I.; Ulijn, R. V., Amino-acid-encoded biocatalytic self-assembly enables the formation of transient conducting nanostructures. *Nature Chemistry* **2018**, *10* (7), 696-703.
8. Sadownik, J. W.; Mattia, E.; Nowak, P.; Otto, S., Diversification of self-replicating molecules. *Nature Chemistry* **2016**, *8* (3), 264-269.
9. Chakraborty, P.; Oved, H.; Bychenko, D.; Yao, Y.; Tang, Y.; Zilberzwige-Tal, S.; Wei, G.; Dvir, T.; Gazit, E., Nanoengineered Peptide-Based Antimicrobial Conductive Supramolecular Biomaterial for Cardiac Tissue Engineering. *Advanced Materials* **2021**, *n/a* (n/a), 2008715.
10. Li, J.; Anraku, Y.; Kataoka, K., Self-Boosting Catalytic Nanoreactors Integrated with Triggerable Crosslinking Membrane Networks for Initiation of Immunogenic Cell Death by Pyroptosis. *Angewandte Chemie International Edition* **2020**, *59* (32), 13526-13530.
11. Fatouros, D. G.; Lamprou, D. A.; Urquhart, A. J.; Yannopoulos, S. N.; Vizirianakis, I. S.; Zhang, S.; Koutsopoulos, S., Lipid-like Self-Assembling Peptide Nanovesicles for Drug Delivery. *ACS Applied Materials & Interfaces* **2014**, *6* (11), 8184-8189.
12. Cormier, A. R.; Pang, X.; Zimmerman, M. I.; Zhou, H.-X.; Paravastu, A. K., Molecular Structure of RADA16-I Designer Self-Assembling Peptide Nanofibers. *ACS Nano* **2013**, *7* (9), 7562-7572.
13. Dai, B.; Li, D.; Xi, W.; Luo, F.; Zhang, X.; Zou, M.; Cao, M.; Hu, J.; Wang, W.; Wei, G.; Zhang, Y.; Liu, C., Tunable assembly of amyloid-forming peptides into nanosheets as a retrovirus carrier. *Proceedings of the National Academy of Sciences* **2015**, *112* (10), 2996.
14. Chau, Y.; Luo, Y.; Cheung, A. C. Y.; Nagai, Y.; Zhang, S.; Kobler, J. B.; Zeitels, S. M.; Langer, R., Incorporation of a matrix metalloproteinase-sensitive substrate into self-assembling peptides – A model for biofunctional scaffolds. *Biomaterials* **2008**, *29* (11), 1713-1719.

15. Vantomme, G.; Meijer, E. W., The construction of supramolecular systems. *Science* **2019**, *363* (6434), 1396.
16. Mattia, E.; Otto, S., Supramolecular systems chemistry. *Nature Nanotechnology* **2015**, *10* (2), 111-119.
17. Matern, J.; Dorca, Y.; Sánchez, L.; Fernández, G., Revising Complex Supramolecular Polymerization under Kinetic and Thermodynamic Control. *Angewandte Chemie International Edition* **2019**, *58* (47), 16730-16740.
18. Pellarin, R.; Schuetz, P.; Guarnera, E.; Caflisch, A., Amyloid Fibril Polymorphism Is under Kinetic Control. *Journal of the American Chemical Society* **2010**, *132* (42), 14960-14970.
19. Korevaar, P. A.; George, S. J.; Markvoort, A. J.; Smulders, M. M. J.; Hilbers, P. A. J.; Schenning, A. P. H. J.; De Greef, T. F. A.; Meijer, E. W., Pathway complexity in supramolecular polymerization. *Nature* **2012**, *481* (7382), 492-496.
20. Tantakitti, F.; Boekhoven, J.; Wang, X.; Kazantsev, R. V.; Yu, T.; Li, J.; Zhuang, E.; Zandi, R.; Ortony, J. H.; Newcomb, C. J.; Palmer, L. C.; Shekhawat, G. S.; de la Cruz, M. O.; Schatz, G. C.; Stupp, S. I., Energy landscapes and functions of supramolecular systems. *Nature Materials* **2016**, *15* (4), 469-476.
21. Fukui, T.; Kawai, S.; Fujinuma, S.; Matsushita, Y.; Yasuda, T.; Sakurai, T.; Seki, S.; Takeuchi, M.; Sugiyasu, K., Control over differentiation of a metastable supramolecular assembly in one and two dimensions. *Nature Chemistry* **2017**, *9* (5), 493-499.
22. Michaels, T. C. T.; Šarić, A.; Curk, S.; Bernfur, K.; Arosio, P.; Meisl, G.; Dear, A. J.; Cohen, S. I. A.; Dobson, C. M.; Vendruscolo, M.; Linse, S.; Knowles, T. P. J., Dynamics of oligomer populations formed during the aggregation of Alzheimer's A $\beta$ 42 peptide. *Nature Chemistry* **2020**, *12* (5), 445-451.
23. Dear, A. J.; Michaels, T. C. T.; Meisl, G.; Klenerman, D.; Wu, S.; Perrett, S.; Linse, S.; Dobson, C. M.; Knowles, T. P. J., Kinetic diversity of amyloid oligomers. *Proceedings of the National Academy of Sciences* **2020**, 201922267.
24. Auer, S.; Dobson, C. M.; Vendruscolo, M.; Maritan, A., Self-Templated Nucleation in Peptide and Protein Aggregation. *Physical Review Letters* **2008**, *101* (25), 258101.
25. Yuan, C.; Levin, A.; Chen, W.; Xing, R.; Zou, Q.; Herling, T. W.; Challa, P. K.; Knowles, T. P. J.; Yan, X., Nucleation and Growth of Amino Acid and Peptide Supramolecular Polymers through Liquid-Liquid Phase Separation. *Angewandte Chemie International Edition* **2019**, *58* (50), 18116-18123.
26. Hsieh, M.-C.; Lynn, D. G.; Grover, M. A., Kinetic Model for Two-Step Nucleation of Peptide Assembly. *The Journal of Physical Chemistry B* **2017**, *121* (31), 7401-7411.
27. Aggeli, A.; Nyrkova, I. A.; Bell, M.; Harding, R.; Carrick, L.; McLeish, T. C. B.; Semenov, A. N.; Boden, N., Hierarchical self-assembly of chiral rod-like molecules as a model for peptide  $\beta$ -sheet tapes, ribbons, fibrils, and fibers. *Proceedings of the National Academy of Sciences* **2001**, *98* (21), 11857.
28. Clover, T. M.; O'Neill, C. L.; Appavu, R.; Lokhande, G.; Gaharwar, A. K.; Posey, A. E.; White, M. A.; Rudra, J. S., Self-Assembly of Block Heterochiral Peptides into Helical Tapes. *Journal of the American Chemical Society* **2020**, *142* (47), 19809-19813.

29. Hu, Y.; Lin, R.; Zhang, P.; Fern, J.; Cheetham, A. G.; Patel, K.; Schulman, R.; Kan, C.; Cui, H., Electrostatic-Driven Lamination and Untwisting of  $\beta$ -Sheet Assemblies. *ACS Nano* **2016**, *10* (1), 880-888.
30. Tan, J.; Zhang, L.; Hsieh, M.-C.; Goodwin, J. T.; Grover, M. A.; Lynn, D. G., Chemical control of peptide material phase transitions. *Chemical Science* **2021**, *12* (8), 3025-3031.
31. Boicchio, D.; Salvalaglio, M.; Pavan, G. M., Into the Dynamics of a Supramolecular Polymer at Submolecular Resolution. *Nature Communications* **2017**, *8* (1), 147.
32. Torchi, A.; Boicchio, D.; Pavan, G. M., How the Dynamics of a Supramolecular Polymer Determines Its Dynamic Adaptivity and Stimuli-Responsiveness: Structure–Dynamics–Property Relationships From Coarse-Grained Simulations. *The Journal of Physical Chemistry B* **2018**, *122* (14), 4169-4178.
33. Lafleur, R. P. M.; Herziger, S.; Schoenmakers, S. M. C.; Keizer, A. D. A.; Jahzolah, J.; Thota, B. N. S.; Su, L.; Bomans, P. H. H.; Sommerdijk, N. A. J. M.; Palmans, A. R. A.; Haag, R.; Friedrich, H.; Böttcher, C.; Meijer, E. W., Supramolecular Double Helices from Small C<sub>3</sub>-Symmetrical Molecules Aggregated in Water. *Journal of the American Chemical Society* **2020**, *142* (41), 17644-17652.
34. Fukui, T.; Uchihashi, T.; Sasaki, N.; Watanabe, H.; Takeuchi, M.; Sugiyasu, K., Direct Observation and Manipulation of Supramolecular Polymerization by High-Speed Atomic Force Microscopy. *Angewandte Chemie International Edition* **2018**, *57* (47), 15465-15470.
35. Morgese, G.; de Waal, B. F. M.; Varela-Aramburu, S.; Palmans, A. R. A.; Albertazzi, L.; Meijer, E. W., Anchoring Supramolecular Polymers to Human Red Blood Cells by Combining Dynamic Covalent and Non-Covalent Chemistries. *Angewandte Chemie International Edition* **2020**, *59* (39), 17229-17233.
36. Newcomb, C. J.; Sur, S.; Lee, S. S.; Yu, J. M.; Zhou, Y.; Snead, M. L.; Stupp, S. I., Supramolecular Nanofibers Enhance Growth Factor Signaling by Increasing Lipid Raft Mobility. *Nano Letters* **2016**, *16* (5), 3042-3050.
37. Zhan, J.; Cai, Y.; He, S.; Wang, L.; Yang, Z., Tandem Molecular Self-Assembly in Liver Cancer Cells. *Angewandte Chemie International Edition* **2018**, *57* (7), 1813-1816.
38. Li, J.; Kuang, Y.; Shi, J.; Zhou, J.; Medina, J. E.; Zhou, R.; Yuan, D.; Yang, C.; Wang, H.; Yang, Z.; Liu, J.; Dinulescu, D. M.; Xu, B., Enzyme-Instructed Intracellular Molecular Self-Assembly to Boost Activity of Cisplatin against Drug-Resistant Ovarian Cancer Cells. *Angewandte Chemie International Edition* **2015**, *54* (45), 13307-13311.
39. Dirisala, A.; Uchida, S.; Toh, K.; Li, J.; Osawa, S.; Tockary, T. A.; Liu, X.; Abbasi, S.; Hayashi, K.; Mochida, Y.; Fukushima, S.; Kinoh, H.; Osada, K.; Kataoka, K., Transient stealth coating of liver sinusoidal wall by anchoring two-armed PEG for retargeting nanomedicines. *Science Advances* **2020**, *6* (26), eabb8133.
40. Zhao, Z.; Ukidve, A.; Krishnan, V.; Fehnel, A.; Pan, D. C.; Gao, Y.; Kim, J.; Evans, M. A.; Mandal, A.; Guo, J.; Muzykantov, V. R.; Mitragotri, S., Systemic tumour suppression via the preferential accumulation of erythrocyte-anchored chemokine-encapsulating nanoparticles in lung metastases. *Nature Biomedical Engineering* **2021**, *5* (5), 441-454.
41. Rad-Malekshahi, M.; Lempsink, L.; Amidi, M.; Hennink, W. E.; Mastrobattista, E., Biomedical Applications of Self-Assembling Peptides. *Bioconjugate Chemistry* **2016**, *27* (1), 3-18.

42. Mansukhani, N. A.; Peters, E. B.; So, M. M.; Albaghdadi, M. S.; Wang, Z.; Karver, M. R.; Clemons, T. D.; Laux, J. P.; Tsihlis, N. D.; Stupp, S. I.; Kibbe, M. R., Peptide Amphiphile Supramolecular Nanostructures as a Targeted Therapy for Atherosclerosis. *Macromolecular Bioscience* **2019**, *19* (6), 1900066.
43. So, M. M.; Mansukhani, N. A.; Peters, E. B.; Albaghdadi, M. S.; Wang, Z.; Rubert Pérez, C. M.; Kibbe, M. R.; Stupp, S. I., Peptide Amphiphile Nanostructures for Targeting of Atherosclerotic Plaque and Drug Delivery. *Advanced Biosystems* **2018**, *2* (3), 1700123.
44. Kassam, H. A.; Bahnson, E. M.; Cartaya, A.; Jiang, W.; Avram, M. J.; Tsihlis, N. D.; Stupp, S. I.; Kibbe, M. R., Pharmacokinetics and biodistribution of a collagen-targeted peptide amphiphile for cardiovascular applications. *Pharmacology Research & Perspectives* **2020**, *8* (6), e00672.
45. Cifuentes-Rius, A.; Desai, A.; Yuen, D.; Johnston, A. P. R.; Voelcker, N. H., Inducing immune tolerance with dendritic cell-targeting nanomedicines. *Nature Nanotechnology* **2021**, *16* (1), 37-46.
46. Newcomb, C. J.; Sur, S.; Ortony, J. H.; Lee, O.-S.; Matson, J. B.; Boekhoven, J.; Yu, J. M.; Schatz, G. C.; Stupp, S. I., Cell death versus cell survival instructed by supramolecular cohesion of nanostructures. *Nature Communications* **2014**, *5* (1), 3321.
47. Chen, J.; Pompano, R. R.; Santiago, F. W.; Maillat, L.; Sciammas, R.; Sun, T.; Han, H.; Topham, D. J.; Chong, A. S.; Collier, J. H., The use of self-adjuvanting nanofiber vaccines to elicit high-affinity B cell responses to peptide antigens without inflammation. *Biomaterials* **2013**, *34* (34), 8776-8785.
48. Sun, T.; Han, H.; Hudalla, G. A.; Wen, Y.; Pompano, R. R.; Collier, J. H., Thermal stability of self-assembled peptide vaccine materials. *Acta Biomaterialia* **2016**, *30*, 62-71.
49. Shores, L. S.; Kelly, S. H.; Hainline, K. M.; Suwanpradid, J.; MacLeod, A. S.; Collier, J. H., Multifactorial Design of a Supramolecular Peptide Anti-IL-17 Vaccine Toward the Treatment of Psoriasis. *Frontiers in Immunology* **2020**, *11*, 1855.
50. Rudra, J. S.; Tian, Y. F.; Jung, J. P.; Collier, J. H., A self-assembling peptide acting as an immune adjuvant. *Proceedings of the National Academy of Sciences of the United States of America* **2010**, *107* (2), 622-627.
51. Al-Halifa, S.; Babych, M.; Zottig, X.; Archambault, D.; Bourgault, S., Amyloid self-assembling peptides: Potential applications in nanovaccine engineering and biosensing. *Peptide Science* **2019**, *111* (1), e24095.
52. Rad-Malekshahi, M.; Fransen, M. F.; Krawczyk, M.; Mansourian, M.; Bourajjaj, M.; Chen, J.; Ossendorp, F.; Hennink, W. E.; Mastrobattista, E.; Amidi, M., Self-Assembling Peptide Epitopes as Novel Platform for Anticancer Vaccination. *Molecular pharmaceutics* **2017**, *14* (5), 1482-1493.
53. Mougou, J.; Bourgaux, C.; Couvreur, P., Elongated self-assembled nanocarriers: From molecular organization to therapeutic applications. *Advanced Drug Delivery Reviews* **2021**, *172*, 127-147.
54. Wen, Y.; Waltman, A.; Han, H.; Collier, J. H., Switching the Immunogenicity of Peptide Assemblies Using Surface Properties. *ACS Nano* **2016**, *10* (10), 9274-9286.
55. Pompano, R. R.; Chen, J.; Verbus, E. A.; Han, H.; Fridman, A.; McNeely, T.; Collier, J. H.; Chong, A. S., Titration of T-Cell Epitopes within Self-Assembled Vaccines Optimizes CD4+ Helper T Cell and Antibody Outputs. *Advanced Healthcare Materials* **2014**, *3* (11), 1898-1908.

56. Ellmerer, M.; Schaupp, L.; Brunner, G. A.; Sendlhofer, G.; Wutte, A.; Wach, P.; Pieber, T. R., Measurement of interstitial albumin in human skeletal muscle and adipose tissue by open-flow microperfusion. *American Journal of Physiology-Endocrinology and Metabolism* **2000**, *278* (2), E352-E356.
57. Fanali, G.; di Masi, A.; Trezza, V.; Marino, M.; Fasano, M.; Ascenzi, P., Human serum albumin: From bench to bedside. *Molecular Aspects of Medicine* **2012**, *33* (3), 209-290.
58. Czub, M. P.; Venkataramany, B. S.; Majorek, K. A.; Handing, K. B.; Porebski, P. J.; Beeram, S. R.; Suh, K.; Woolfork, A. G.; Hage, D. S.; Shabalina, I. G.; Minor, W., Testosterone meets albumin – the molecular mechanism of sex hormone transport by serum albumins. *Chemical Science* **2019**, *10* (6), 1607-1618.
59. Zhu, G.; Lynn, G. M.; Jacobson, O.; Chen, K.; Liu, Y.; Zhang, H.; Ma, Y.; Zhang, F.; Tian, R.; Ni, Q.; Cheng, S.; Wang, Z.; Lu, N.; Yung, B. C.; Wang, Z.; Lang, L.; Fu, X.; Jin, A.; Weiss, I. D.; Vishwasrao, H.; Niu, G.; Shroff, H.; Klinman, D. M.; Seder, R. A.; Chen, X., Albumin/vaccine nanocomplexes that assemble in vivo for combination cancer immunotherapy. *Nature Communications* **2017**, *8* (1), 1954.
60. Wang, P.; Zhao, P.; Dong, S.; Xu, T.; He, X.; Chen, M., An Albumin-binding Polypeptide Both Targets Cytotoxic T Lymphocyte Vaccines to Lymph Nodes and Boosts Vaccine Presentation by Dendritic Cells. *Theranostics* **2018**, *8* (1), 223-236.
61. Tian, R.; Zeng, Q.; Zhu, S.; Lau, J.; Chandra, S.; Ertsey, R.; Hettie, K. S.; Teraphongphom, T.; Hu, Z.; Niu, G.; Kiesewetter, D. O.; Sun, H.; Zhang, X.; Antaris, A. L.; Brooks, B. R.; Chen, X., Albumin-chaperoned cyanine dye yields superbright NIR-II fluorophore with enhanced pharmacokinetics. *Science Advances* **2019**, *5* (9), eaaw0672.



# **Chapter 2**

## **Programming supramolecular peptide materials by modulating the intermediate steps in the complex assembly pathway: implications for biomedical applications**

Chun Yin Jerry Lau, Enrico Mastrobattista

*Utrecht Institute for Pharmaceutical Sciences, Department of Pharmaceutics, Faculty of Science, Utrecht University Universiteitsweg 99, 3584 CG Utrecht (The Netherlands)*

### Abstract

Self-assembling peptides form a prominent class of supramolecular materials with, in general, good biocompatibility. To afford better control over the material properties, tremendous progress has been made in studying the supramolecular organization of the peptide assemblies. This knowledge has helped us understand the correlation between the molecular structure of the peptide building blocks and the properties of the supramolecular products. However, peptide self-assembly consists of a complex pathway rather than a spontaneous thermodynamic process. This implies that the assembly pathway critically governs the outcome of the self-assembly. Here, we are going to discuss how peptide self-assembly can be modulated at the intermediate steps in the self-assembly pathway. The focus will be to demonstrate this engineering approach on the example of 0D/1D nanostructure selectivity over the  $\beta$ -sheet assembly pathway. In addition, we provide examples of biomedical applications of such steered peptide assemblies in the field of drug delivery and tissue engineering



# Programming supramolecular peptide materials by modulating the intermediate steps in the complex assembly pathway: implications for biomedical applications

---

## 1. Introduction

Supramolecular materials with biomimetic properties are fabricated by manipulating non-covalent interactions such as hydrogen-bonding, van der Waal's forces, and electrostatic interactions. Self-assembling peptides form a prominent class of supramolecular materials that have, in general good biological compatibility. Self-assembling peptides can form supramolecular structures at different length scales, such as zero-dimensional (0D) micelles or vesicles and one-dimensional (1D) nanofibers or nanotubes, through a combination of side-chain and backbone interactions. The formation of secondary structure in peptides ( $\alpha$ -helix or  $\beta$ -sheet) is a common molecular transition that drives controlled peptide supramolecular assembly, with cross- $\beta$ <sup>1</sup> and coiled-coil structures<sup>2</sup> as two notable examples of the resulting molecular arrangement. These supramolecular assemblies have been explored for different biomedical applications, including the formation of discrete nanoparticles for drug delivery<sup>3-9</sup> and scaffolds for regenerative medicine and tissue engineering<sup>10-13</sup>.

There is currently a good number of experimental accounts investigating the supramolecular organization of the final structure of peptide assemblies, which has offered us atomic insights into the peptide interaction within these supramolecular structures<sup>1, 11, 14, 15</sup>. However, for supramolecular peptide structure, rather than a spontaneous thermodynamic process, their assembly pathway is signified by its high complexity, along which metastable intermediates are formed before eventual conversion to the more thermodynamically stable end products<sup>16, 17</sup>. This implies that the outcome of the peptide assembly process is critically governed by the self-assembly pathway that is being followed and thus can be influenced by directly modulating these intermediate steps<sup>18-20</sup>. Indeed, this explains why, though cross- $\beta$  fibers are generally the most thermodynamically stable structural organization in physiological condition<sup>21</sup>, we can still access a variety of peptide assemblies with alternative structural ordering, such as coiled-coil nanofibers<sup>14</sup>.

Currently, several excellent reviews have discussed the biomedical applications of self-assembling peptide nanomaterials<sup>22-24</sup>. However, comparatively few have discussed the biomedical implications in light of the complex assembly pathway. Here, on the example of  $\beta$ -sheet peptide assemblies, we will demonstrate how manipulating the complex peptide self-assembly pathway can afford better control over the structures and properties of the resulting materials. Since the kinetic pathway of  $\beta$ -sheet assembly is highly complexed<sup>25</sup>, to stay focused on the objective of this review, we have chosen to exemplify this engineering approach with the 0D/1D nanostructure selectivity over the  $\beta$ -sheet assembly pathway (Figure 1), as nanostructures at these length scales are widely used in biomedical application<sup>26</sup>. Subsequently, we will discuss the common approaches used to modulate the self-assembly pathway. Finally, we will highlight the possibilities and considerations for the biomedical application of peptide nanostructures in light of the pathway complexity.

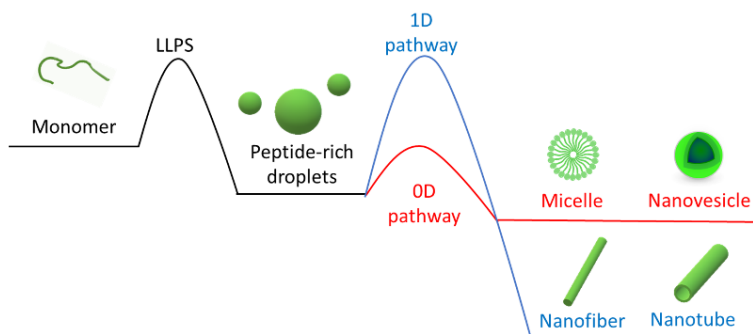


**Figure 1** Schematic representation of the complex pathway of  $\beta$ -sheet peptide self-assembly that direct formation of 0D nanostructures (e.g., micelle, nanovesicle) and 1D nanostructures (nanofiber, nanotube). LLPS: Liquid-liquid phase separation; 0D: zero-dimensional; 1D: one dimensional

## 2. Parallel and competing kinetic pathways of 0D and 1D nanostructures formation Liquid-liquid phase separation as the common first step before pathway divergence.

Unlike supramolecular structures composed of low molecular weight polymers, peptides possess a relatively significant desolvation barrier in water, making it energetically improbable to assemble into ordered structures spontaneously. To overcome the desolvation barrier, liquid-liquid phase separation (LLPS) is a common first step in peptide self-assembly<sup>17, 27, 28</sup> (Figure 2a, b). The LLPS process is entropically driven, in which the entropic gain is rooted in the increase in peptide conformational freedom and the gain of water entropy through peptide desolvation<sup>27</sup>. The LLPS process will lead to the formation of peptide-rich droplets, or oligomeric particles, which create an alternative environment for peptide arrangement into more ordered assemblies<sup>28-30</sup>. Recent work by Michaels et al. has outlined the probabilistic nature for the assemblies to progress through different stages of the assembly pathway<sup>29</sup>. Section 3 will describe the common strategies to direct the assembly process towards a particular kinetic pathway.

## Programming supramolecular peptide materials by modulating the intermediate steps in the complex assembly pathway: implications for biomedical applications

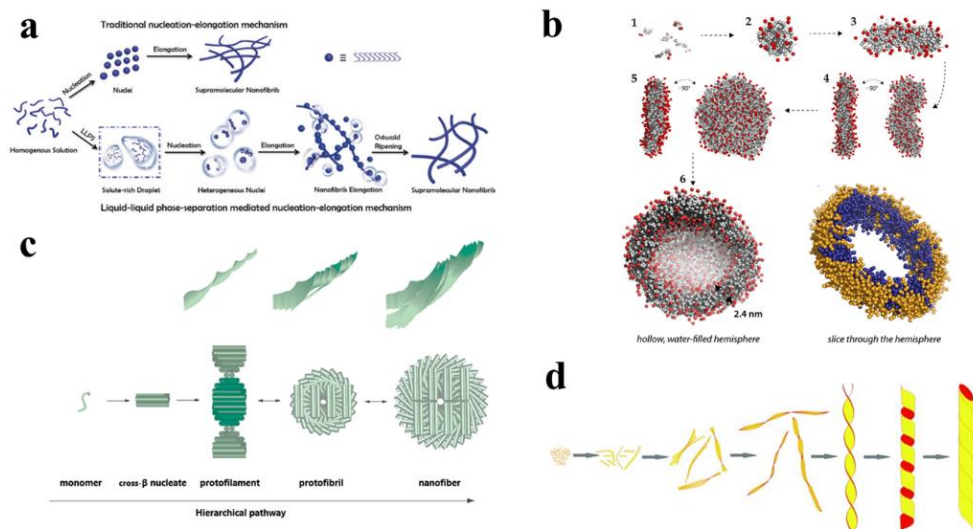


**Figure 2** The self-assembly mechanisms of peptide structures **a**) Difference in supramolecular fibrillization between small-molecule supramolecular polymers (traditional nucleation-elongation) and self-assembling peptides (LLPS mediated nucleation-elongation). Adapted by permission from Wiley Publishers Ltd: *Angewandte Chemie* ref. <sup>27</sup> copyright (2019); **b**) The bottom-up self-assembly mechanism of peptide nanovesicles. It shows that both nanovesicle and nanofiber pathways undergo LLPS as the first step before diverting to their respective pathway. Adapted by permission from American Chemical Society: *JACS.*, ref. <sup>31</sup> copyright (2015); **c**) Hierarchical self-assembly of peptide nanofibers. Supramolecular structures with ascending structural sophistication are shown from left to right. Adapted by permission from future medicine Ltd: *Nanomedicine*, ref. <sup>22</sup> copyright (2013); **d**) Hierarchical self-assembly of peptide nanotubes. The self-assembly mechanisms deviate from that of nanofibers at the protofibril stage to form helical ribbon intermediates. Permission from Wiley Publishers Ltd: *Angewandte Chemie* ref <sup>32</sup> copyright (2011)

**0D nanostructure pathway selection if no cross- $\beta$  nucleates are formed.** Cross- $\beta$  nucleation is the critical event that decides the bifurcation between the 0D and 1D nanostructure assembly pathways. If no cross- $\beta$  nucleate is formed, the oligomeric particles will transform into 0D nanostructures (e.g., micelles <sup>6, 33, 34</sup> and nanovesicles <sup>31, 35</sup>). Our group has previously integrated state-of-the-art experimental techniques with large- and multi-scale molecular dynamic (MD) simulation to elucidate the self-assembly pathway of an amphiphilic peptide (SA2: Ac-AAVVLLLWEE-COOH) that will form nanovesicles when dispersed in aqueous media<sup>31</sup>. In good agreement with recent in-situ studies on amphiphilic self-assembly<sup>36</sup>, we have detected that the oligomeric particles condensed via LLPS adopt a micellar arrangement. The micellar oligomers will then grow by monomer addition and evolve into elongated micelles, followed by the formation of interdigitated bilayers and disks, and eventually into water-filled hemispheres<sup>31</sup> (Figure 2b). Interestingly, structural analysis of these 0D nanostructures revealed that, although they are not following templated elongation with cross- $\beta$  nucleates, the orthogonal  $\beta$ -sheet pattern (inter-strand distance at  $\sim 4.7\text{\AA}$ , inter-sheet distance at  $\sim 10\text{\AA}$ ) could still be observed <sup>6, 31</sup>. This implies

that cross- $\beta$  interactions also contributed to the structural organization in these assemblies but with lower periodicity than the 1D nanostructures.

### **Hierarchical pathway for 1D nanostructure formation**

**1D nanostructure pathway selection through the formation of cross- $\beta$  nucleates.** The formation of cross- $\beta$  nucleates in the oligomeric particles can trigger the hierarchical assembly of cross- $\beta$  fibers (Figure 2a). As described earlier, the cross- $\beta$  structures are signified by orthogonal  $\beta$ -sheet interactions, characterized by a distinctive X-ray diffraction pattern with reflection at  $\sim 4.7\text{\AA}$  that represent the inter- $\beta$ -strand repeats and a perpendicular reflection at  $\sim 10\text{\AA}$  that represent the inter- $\beta$ -sheet repeats<sup>1</sup>. Formation of cross- $\beta$  nucleates within the oligomeric particles is an enthalpy-driven process---the entropic penalty (increased molecular order) is compensated by the enthalpic gain of the cooperative non-covalent interactions (hydrogen-bonding, van der Waal's forces, electrostatic interactions)<sup>27</sup>. The nucleates are formed when a critical number of cross- $\beta$  arranged peptides are reached<sup>28</sup>. After reaching that threshold, replication of the cross- $\beta$  molecular ordering thereafter will become energetically favorable<sup>37</sup>. The propensity of cross- $\beta$  nucleation is influenced by the sequence length,  $\beta$ -sheet propensities, side-chain molecular compatibility of the peptide, and the size of the oligomeric particles formed<sup>28, 38, 39</sup>.

**Protofilaments formation via a nucleation-elongation mechanism.** Through a nucleation-elongation mechanism, the replication of cross- $\beta$  molecular order will yield protofilaments, or  $\beta$ -sheet ribbon, as the primary units leading to the build-up of the hierarchical 1D nanostructures<sup>40</sup>. As the lowest level structure in the assembly hierarchy, the protofilaments adopt an elementary supramolecular organization with a single cross- $\beta$  interface<sup>1</sup>. Previous studies reveal that the prime hindrance in the elongation process is desolvating the peptide monomers<sup>41</sup>. Therefore, the sequence length and residual hydrophobicity of the peptides are significant factors influencing the propensity of the elongation mechanism<sup>41</sup>.

**1D nanofiber pathway selection via protofilament association.** After protofilaments have been formed, the next step in the hierarchical pathway is the association of protofilaments into protofibrils<sup>40</sup>. In the hierarchical 1D nanostructures, the assembly of protofilaments is driven by a side-chain interface with higher association force; a side-chain interface drives the assembly of secondary units (protofibril) with weaker association force, which drives the lateral association of protofilaments. The final structure (nanofiber) is formed via the edge-to-edge  $\beta$ -strand interaction, which drives the longitudinal association of protofibrils<sup>40</sup> (Figure 2c). Notably, due to the chemical anisotropy between side-chain (mostly van der Waal's forces) and backbone interactions (hydrogen bonding), all these filament structures are twisted<sup>42, 43</sup>. The structural twisting can halt the unlimited growth of the fibrous structures in lateral and longitudinal directions<sup>40, 43</sup>. Previous studies have revealed that the assembled nanofibers are mainly kinetically trapped species, which shows the fiber morphology is under kinetic control, *i.e.*, the energy barrier for each step

## **Programming supramolecular peptide materials by modulating the intermediate steps in the complex assembly pathway: implications for biomedical applications**

---

determines the resultant fibre morphology<sup>44</sup>. This explains why the chirality of natural L-amino acids should give left-handed twisted nanofiber; the hierarchical process can counteract the twist-handedness to generate right-handed twisted fibers<sup>45</sup>.

**1D nanotube pathway selection via formation helical ribbon intermediate.** The 1D nanotube pathway deviates from the protofibril step in the 1D nanofiber pathway. Rather than undergoing longitudinal association, the protofibrils are transformed to helical ribbon intermediates; the closure of these helical ribbons will give 1D nanotubes<sup>32, 46-48</sup> (Figure 2d). The closure mechanism of the helical ribbon is a relatively slow process, which generally takes weeks to conclude<sup>32, 46-48</sup>. Furthermore, the nanotube's diameter is determined by the magnitude of the lateral interactions in the helical ribbon, which is influenced by the side-chain interface association forces<sup>46</sup>. Besides, 1D nanofibers are often detected alongside the nanotube structures within one supramolecular system<sup>32, 46</sup>.

### **3. Common strategies to modulate peptide assembly pathways**

#### **Internal factors**

**Hydrophobic-hydrophilic residue arrangement.** A common approach to modulate the self-assembly pathway is to program the arrangement of hydrophobic/hydrophilic amino acids in the peptide sequence<sup>35, 46, 49</sup>. Previous studies reveal that an increase in the hydrophobic to hydrophilic ratio (*i.e.*, increase in hydrophobicity) favors the kinetic selection of 1D nanostructures over 0D nanostructures<sup>35</sup>. This can be partly explained by the fact that more hydrophobic peptides generally form larger-sized oligomeric particles, which in turn increases the chance of cross- $\beta$  nucleation<sup>28</sup>. Furthermore, the nanotube pathway is favored by increasing the repulsive forces between the protofibrils in the longitudinal direction. This can be achieved by placing mutually repulsive residues at both ends of the  $\beta$ -strand<sup>46</sup> or by end-capping the peptide to prevent electrostatic attraction between the amino- and carboxy-terminal<sup>32</sup>. Besides, most of the reported 0D nanovesicle forming peptides adopt a surfactant-like sequence arrangement, in which the hydrophobic and hydrophilic amino acids are arranged in two modular compartments<sup>31, 49</sup>. The modular hydrophobic-hydrophilic pattern can likely facilitate the micelle to nanovesicle transition<sup>36</sup>.

**Molecular geometry and  $\beta$ -sheet propensities.** Altering the molecular geometry of peptides is another approach to moderate the assembly pathway. For example, the molecular geometry can be adjusted by engineering the conformational ( $\beta$ -sheet) propensities of the peptide sequence<sup>50</sup> and the molecular volume of the side-chain groups<sup>51, 52</sup>. Increasing the  $\beta$ -sheet propensities of peptides can increase the probability of cross- $\beta$  nucleation, thereby favoring kinetic selection of the 1D pathway<sup>38</sup>. The  $\beta$ -sheet propensities can be increased by instigating molecular frustration in peptide sequences (*i.e.*, patterning peptide sequences with alternating hydrophobic and hydrophilic residues)<sup>50, 53, 54</sup> or incorporation of  $\beta$ -branched amino acids<sup>55, 56</sup> and lowering the content of  $\beta$ -sheet disrupting residues, *e.g.*, proline<sup>57</sup>. Besides, the steric compatibility between the side chain interface in the  $\beta$ -strand can also influence the propensity of cross- $\beta$  nucleation<sup>39, 51, 52</sup>.

**Complimentary directional non-covalent interactions.** The backbone-backbone hydrogen bonding interactions confer the directionality of cross- $\beta$  structures. The directionality can complement other directional non-covalent interactions such as  $\pi$ - $\pi$ -stacking<sup>54, 58</sup> and electrostatic attraction in the side-chain interfaces<sup>54, 59-62</sup>. For example, Shao et al. has demonstrated how the side chain charge complementary interaction can direct precise ABAB molecular pattern in the resultant cross- $\beta$  nanofibers<sup>62</sup>. Implementing these complementary interactions can therefore favor the formation of 1D nanostructures.

### External factors

**Solvent composition.** The assembly pathway can also be extrinsically modulated through varying the solvent composition, such as the solvent polarity and pH. For zwitterionic peptides, adjusting the pH from 7.4 can increase the mutual electrostatic repulsive force between oligomeric particles. Increasing the mutual repulsive forces can stabilize oligomeric particles at a smaller size range, which lowers the probability of cross- $\beta$  nucleation<sup>28</sup>. However, if cross- $\beta$  nucleates are formed, changing the pH value can potentially alter the sequence alignment in the cross- $\beta$  structures. For example, for the peptide containing charged residues, changes in pH can potentially alter the electrostatic interactions between the side chains, thereby moderating the sequence alignment<sup>59</sup>. Such changes in sequence alignment can potentially facilitate nanotube formation by inducing repulsive longitudinal forces between protofibrils<sup>59, 63</sup>. Concerning organic solvents, the addition of dimethyl sulfoxide (DMSO)<sup>64</sup>, hexafluoro-2-propanol (HFIP)<sup>6</sup>, and acetonitrile (MeCN)<sup>65</sup> can favor the formation of 0D nanostructures through disrupting interpeptide hydrogen bonding networks, thereby lowering the chance of cross- $\beta$  nucleation. Besides, since the gain of water entropy through peptide desolvation is a significant driver of LLPS<sup>27</sup>, the rate of initial peptide solvation (e.g., rate of water addition) can serve as a potential moderator of the LLPS process.

**Concentration.** Regarding the LLPS of peptides, the condensation process is concentration-dependent<sup>38, 66</sup>. Furthermore, like other supramolecular systems, concentration-dependent phase transition behavior is observed in self-assembling peptides<sup>40, 48</sup>. Higher concentrations generally favor the formation of higher-order supramolecular structures. For example, Aggeli et al. have demonstrated that by increasing the concentration of the P-11 peptide, 1D nanostructures with the increasing sophistication of structural ordering are detected (from protofilament, through protofibril to fiber)<sup>40</sup>; Prassl et al. have also demonstrated that a superstructure of nanofibers can be induced by increasing the peptide concentration<sup>48</sup>.

**Temperature & external fields.** The effect of temperature is more complex. On one end, LLPS can only take place when the solution temperature drops below a certain threshold<sup>66</sup>. However, further reduction in temperature can freeze the molecular conformation in the oligomeric phase<sup>38</sup>. On the other hand, high temperatures in general disfavor the condensation process<sup>38</sup>, but if cross- $\beta$  nucleates are formed, the increase in molecular motion can, in return, speed up the supramolecular polymerization process. Besides, by

## Programming supramolecular peptide materials by modulating the intermediate steps in the complex assembly pathway: implications for biomedical applications

varying the temperature (4–37°C), the kinetic pathways of nanofiber formation can be varied, leading to the formation of nanofibers with different morphology using the same peptide as building block<sup>67,68</sup>. Regarding external fields, such as electromagnetic fields or ultrasound, the influence of thermal effects can be referred to in the above discussion on temperature. Regarding the nonthermal effects of the external fields, previous studies showed that the application of electromagnetic fields can alter the  $\beta$ -sheet propensities<sup>69,70</sup>, the aggregation propensities<sup>71</sup> of the peptide. In addition, the application of external fields can also promote directionality in a molecular arrangement through peptide dipole alignment<sup>72</sup>. These changes can influence the likelihood of 1D nanofiber formation.

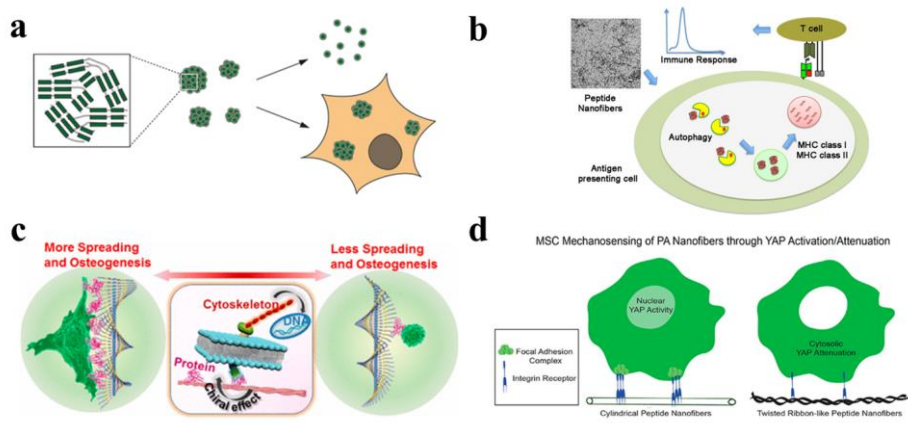


**Figure 3 Biomedical application of kinetic control over self-assembling peptides** a) Selective uptake of 0D peptide nanostructures to professional antigen-presenting cells (e.g., macrophage and dendritic cells). Adapted by permission from American Chemical Society: ACS Nano, ref. <sup>6</sup> copyright (2014); b) Engagement of autophagy mechanism of 1D peptide nanofiber upon uptake by professional antigen-presenting cells. Adapted by permission from American Chemical Society: ACS Omega, ref. <sup>83</sup> copyright (2017); c) Effect of nanofiber chirality on stem cell spreading and differentiation. Left-handed twisted nanofiber has a better ability to induce osteogenesis than right-handed twisted nanofiber. Adapted by permission from American Chemical Society: ACS Applied Materials & Interfaces, ref. <sup>87</sup> copyright (2019); d) Effect of nanofiber helicity on mechanotransduction of stem cell. The untwisted/cylindrical peptide nanofiber incurs higher stem cell osteogenic potential through the activation of nuclear YAP, while the twisted nanofiber caused YAP confinement in the cytosol. Adapted by permission from American Chemical Society: Biomacromolecules, ref. <sup>10</sup> copyright (2017)

### 4. Implications for biomedical applications

**Engineer nanostructures for therapeutic delivery.** Both 0D and 1D  $\beta$ -sheet assemblies have been extensively explored for drug delivery applications thanks to their good biocompatibility and comparatively stable structural order (cross- $\beta$ ). Strategies to incorporate therapeutics into the peptide nanostructures using physical encapsulation<sup>6, 52, 73, 74</sup> or chemical ligation approaches<sup>4, 7, 75, 76</sup> have been extensively explored. Seminal work in drug targeting has revealed that 0D and 1D therapeutic carriers have distinctive biodistribution profiles<sup>26, 77</sup>. Concerning peptide assemblies, Yang et al. has reported that 1D peptide nanofibers exhibit short circulating time upon intravenous injection<sup>78</sup>, while Tanisaka et al. has reported a 0D peptide nanovesicle that displays a comparatively long circulation profile<sup>79</sup>. Hence, the peptide-based therapeutic carriers' biodistribution profile can potentially be adjusted by altering the morphology of peptide assemblies. Regarding targeting at the cell level, both 0D<sup>4, 6</sup>, and 1D<sup>80</sup> peptide nanostructures are preferentially taken up by antigen presentation cells (macrophages, dendritic cells, Figure 3a-b). Taking advantage of the immune cell targetability, these peptide nanostructures have been extensively explored as a delivery carrier for vaccine epitopes<sup>4, 76, 80</sup> or immunomodulators<sup>7, 74</sup>. Furthermore, the capability to trigger membrane translocation or endosome disruption is instrumental for transporting the therapeutic cargo into the cytosol for further processing and loading of the peptide epitopes into the MHC molecules. In this regard,  $\beta$ -sheet peptide assemblies have demonstrated good cell-membrane permeability, which can trigger endosomal escape, but the underlying mechanisms of endosomal escape remain unresolved<sup>49, 81</sup>. Once the peptide assemblies reach the cytosol, their cellular fate is highly dependent on their supramolecular organization---the less ordered structure (e.g., dynamic oligomers) will be directed to the ubiquitin-proteasome pathway. In contrast, the more ordered cross- $\beta$  structures (e.g., 0D nanovesicle, 1D nanofiber) will be directed to the autophagy degradation pathway<sup>82-84</sup> (Figure 3b). In particular, since autophagy is an important cellular regulator of immune responsiveness<sup>85</sup>, the autophagy-engagement capability of these cross- $\beta$  structures can be utilized in the development of onco-<sup>86</sup> or immuno-therapies<sup>76, 83, 84</sup>.

**Altering cell behavior by changing the morphology of 1D nanofibers.** The self-assembly pathway control approach can also be employed to optimize nanofiber applications in tissue engineering. Peptide nanofibers are an established building block of natural extracellular matrix (ECM)-mimicking matrix scaffolds that support three-dimensional tissue cultures of primary or stem cells<sup>22</sup>. These artificial viscoelastic fibrous mesh networks can be composed through non-specific inter-nanofiber interactions<sup>24</sup> or specific nanofiber crosslinking<sup>13</sup>. Like fibrillar proteins present in the natural ECM, chirality<sup>87-89</sup> (Figure 3c) and helicity<sup>10</sup> (Figure 3d) of the peptide nanofibers are critical modulators of cell behavior, such as adhesion, spreading, and proliferation. The chirality (right or left-handed twist) of the nanofiber is generally altered by switching the chirality of the amino acids (D-vs L-amino acid) in the peptide<sup>88, 90</sup>, while the helicity (pitch and twist) are commonly altered by switching to different sequence<sup>10</sup>. However, altering the molecular chirality of amino acids can also change the cellular behavior<sup>88</sup>. The pathway control approach can be a more subtle alternative to adjust the chirality and helicity of the



## **Programming supramolecular peptide materials by modulating the intermediate steps in the complex assembly pathway: implications for biomedical applications**

---

nanofibers. Besides, natural ECM transmits biological signals through cell-binding sites or functional motifs to trigger cell growth and differentiation. Taking advantage of the modularity of peptide nanofibers<sup>62</sup>, multiple functional motifs can be co-incorporated into such nanofibers<sup>91</sup>. The fiber morphology can alter the spatial arrangement of the functional motifs, directly affecting their avidity and exposure to the targeted cell receptors<sup>92</sup>. By optimizing the nanofiber morphology via pathway control, we can directly modulate the interaction of functional motifs with target cells<sup>93</sup>.

**Co-existence of supramolecular products.** One complication caused by self-assembling pathway complexity is the co-existence of assembled products within one supramolecular system<sup>94</sup>. For example, Liberta et al. demonstrated the prevalent co-existence of polymorphic peptide nanofibers and oligomers within one supramolecular system<sup>45</sup>. This system heterogeneity can alter the functional profiles of the peptide assemblies, e.g., the drug-release profile will change if different 0D and 1D nanostructures co-exist. Alternatively, mixtures of polymorphic peptide nanofibers for 3D scaffolds for tissue engineering may cause differences in cell behavior. The composition of the supramolecular products must therefore be carefully characterized to give more predictable and repeatable results.

### **5. Conclusion and Outlook**

Self-assembling peptides form a prominent class of biomaterial for biomedical applications such as drug delivery and tissue engineering. Several studies have explored the molecular organization of the final supramolecular peptide assemblies to fully unleash the biomedical application potential of self-assembling peptides. This understanding of the molecular interaction at the atomic level within the assemblies has tremendously facilitated the search for a correlation between the primary peptide sequence and the supramolecular nanostructures. As a result, a few programmable peptide supramolecular systems have been developed and applied biomedically. Successful as it is, though, most of these engineering approaches require significant molecular changes.

Increasing evidence suggests that peptide nanostructures are constructed through a multistep mechanism. This means that their assembly pathway critically influences the outcome of the self-assembly process. Without significant changes in the peptide sequence, nanostructures of distinctive properties can be fabricated by influencing the assembly pathway. In this review, on the example of  $\beta$ -sheet assemblies, we have highlighted the strategies to derive 0D and 1D nanostructures through pathway selection. We have also discussed how this subtle engineering approach can benefit applications of self-assembling peptides for drug delivery and tissue engineering.

To further the applicability of the pathway control approach, there are a few challenges present ahead. First, the self-assembly process, in general, does not achieve full completion due to the activation energy barrier, which can lead to the co-existence of side-products alongside the main products. To avoid that such side-products complicating the functionality of the peptide nanostructures, robust purification methods should be explored to select the desired products. Alternatively, the intrinsic system heterogeneity can also be explored as extra functionality. By deciphering the supramolecular products' ratio, we can

collectively employ the assemblies to devise synergistic applications. For instance, in tissue engineering applications, the formation of 1D nanostructures can serve as infrastructural scaffolds, while the co-existence of 0D nanostructures can serve as delivery systems for growth factors.

At last, recent studies have explored the possibility of bridging dynamic covalent interactions to the non-covalent interactions in the build-up of 1D peptide nanostructures<sup>95</sup>.<sup>96</sup> For example, the reversible disulfide exchange reaction has been explored as a complementary driver for the self-assembly of 1D peptide nanostructures<sup>95</sup>. These complementary covalent and non-covalent interactions can be explored as a stabilization strategy to generate biomaterials with enhanced longevity in the often complex biological environment.

### **6. Acknowledgment**

The authors would like to acknowledge the support from the European Union Horizon 2020 NANOMED Grant 676137

## Programming supramolecular peptide materials by modulating the intermediate steps in the complex assembly pathway: implications for biomedical applications

---

### References

1. Fitzpatrick, A. W. P.; Debelouchina, G. T.; Bayro, M. J.; Clare, D. K.; Caporini, M. A.; Bajaj, V. S.; Jaroniec, C. P.; Wang, L.; Ladizhansky, V.; Müller, S. A.; MacPhee, C. E.; Waudby, C. A.; Mott, H. R.; De Simone, A.; Knowles, T. P. J.; Saibil, H. R.; Vendruscolo, M.; Orlova, E. V.; Griffin, R. G.; Dobson, C. M., Atomic structure and hierarchical assembly of a cross- $\beta$  amyloid fibril. *Proceedings of the National Academy of Sciences* **2013**, *110* (14), 5468.
2. Beesley, J. L.; Woolfson, D. N., The de novo design of  $\alpha$ -helical peptides for supramolecular self-assembly. *Current Opinion in Biotechnology* **2019**, *58*, 175-182.
3. Ueda, M.; Seo, S.; Nair, B. G.; Müller, S.; Takahashi, E.; Arai, T.; Iyoda, T.; Fujii, S.-i.; Tsuneda, S.; Ito, Y., End-Sealed High Aspect Ratio Hollow Nanotubes Encapsulating an Anticancer Drug: Torpedo-Shaped Peptidic Nanocapsules. *ACS Nano* **2019**, *13* (1), 305-312.
4. Rad-Malekshahi, M.; Fransen, M. F.; Krawczyk, M.; Mansourian, M.; Bourajjaj, M.; Chen, J.; Ossendorp, F.; Hennink, W. E.; Mastrobattista, E.; Amidi, M., Self-Assembling Peptide Epitopes as Novel Platform for Anticancer Vaccination. *Molecular pharmaceutics* **2017**, *14* (5), 1482-1493.
5. Rahman, M. M.; Ueda, M.; Hirose, T.; Ito, Y., Spontaneous Formation of Gating Lipid Domain in Uniform-Size Peptide Vesicles for Controlled Release. *Journal of the American Chemical Society* **2018**, *140* (51), 17956-17961.
6. Kumar, S. T.; Meinhardt, J.; Fuchs, A.-K.; Aumüller, T.; Leppert, J.; Büchele, B.; Knüpfer, U.; Ramachandran, R.; Yadav, J. K.; Prell, E.; Morgado, I.; Ohlenschläger, O.; Horn, U.; Simmet, T.; Görlach, M.; Fändrich, M., Structure and Biomedical Applications of Amyloid Oligomer Nanoparticles. *ACS Nano* **2014**, *8* (11), 11042-11052.
7. Tang, W.; Zhao, Z.; Chong, Y.; Wu, C.; Liu, Q.; Yang, J.; Zhou, R.; Lian, Z.-X.; Liang, G., Tandem Enzymatic Self-Assembly and Slow Release of Dexamethasone Enhances Its Antihepatic Fibrosis Effect. *ACS Nano* **2018**, *12* (10), 9966-9973.
8. Li, S.; Zou, Q.; Li, Y.; Yuan, C.; Xing, R.; Yan, X., Smart Peptide-Based Supramolecular Photodynamic Metallo-Nanodrugs Designed by Multicomponent Coordination Self-Assembly. *Journal of the American Chemical Society* **2018**, *140* (34), 10794-10802.
9. Li, Y.; Zou, Q.; Yuan, C.; Li, S.; Xing, R.; Yan, X., Amino Acid Coordination Driven Self-Assembly for Enhancing both the Biological Stability and Tumor Accumulation of Curcumin. *Angewandte Chemie International Edition* **2018**, *57* (52), 17084-17088.
10. Arslan, E.; Hatip Koc, M.; Uysal, O.; Dikecoglu, B.; Topal, A. E.; Garifullin, R.; Ozkan, A. D.; Dana, A.; Hermida-Merino, D.; Castelletto, V.; Edwards-Gayle, C.; Baday, S.; Hamley, I.; Tekinay, A. B.; Guler, M. O., Supramolecular Peptide Nanofiber Morphology Affects Mechanotransduction of Stem Cells. *Biomacromolecules* **2017**, *18* (10), 3114-3130.
11. Jekhmane, S.; Prachar, M.; Pugliese, R.; Fontana, F.; Medeiros-Silva, J.; Gelain, F.; Weingarth, M., Design Parameters of Tissue-Engineering Scaffolds at the Atomic Scale. *Angewandte Chemie International Edition* **2019**, *58* (47), 16943-16951.
12. Roberts, S.; Harmon, T. S.; Schaal, J. L.; Miao, V.; Li, K.; Hunt, A.; Wen, Y.; Oas, T. G.; Collier, J. H.; Pappu, R. V.; Chilkoti, A., Injectable tissue integrating networks from recombinant polypeptides with tunable order. *Nature Materials* **2018**, *17* (12), 1154-1163.

13. Pugliese, R.; Marchini, A.; Saracino, G. A. A.; Zuckermann, R. N.; Gelain, F., Cross-linked self-assembling peptide scaffolds. *Nano Research* **2018**, *11* (1), 586-602.
14. Christofferson, A. J.; Al-Garawi, Z. S.; Todorova, N.; Turner, J.; Del Borgo, M. P.; Serpell, L. C.; Aguilar, M.-I.; Yarovsky, I., Identifying the Coiled-Coil Triple Helix Structure of  $\beta$ -Peptide Nanofibers at Atomic Resolution. *ACS Nano* **2018**, *12* (9), 9101-9109.
15. Gremer, L.; Schölzel, D.; Schenk, C.; Reinartz, E.; Labahn, J.; Ravelli, R. B. G.; Tusche, M.; Lopez-Iglesias, C.; Hoyer, W.; Heise, H.; Willbold, D.; Schröder, G. F., Fibril structure of amyloid- $\beta$ (1-42) by cryo-electron microscopy. *Science* **2017**, *358* (6359), 116.
16. Nambiar, M.; Wang, L.-S.; Rotello, V.; Chmielewski, J., Reversible Hierarchical Assembly of Trimeric Coiled-Coil Peptides into Banded Nano- and Microstructures. *Journal of the American Chemical Society* **2018**, *140* (40), 13028-13033.
17. Hsieh, M.-C.; Lynn, D. G.; Grover, M. A., Kinetic Model for Two-Step Nucleation of Peptide Assembly. *The Journal of Physical Chemistry B* **2017**, *121* (31), 7401-7411.
18. Mattia, E.; Otto, S., Supramolecular systems chemistry. *Nature Nanotechnology* **2015**, *10* (2), 111-119.
19. Raeburn, J.; Zamith Cardoso, A.; Adams, D. J., The importance of the self-assembly process to control mechanical properties of low molecular weight hydrogels. *Chemical Society Reviews* **2013**, *42* (12), 5143-5156.
20. Tantakitti, F.; Boekhoven, J.; Wang, X.; Kazantsev, R. V.; Yu, T.; Li, J.; Zhuang, E.; Zandi, R.; Ortony, J. H.; Newcomb, C. J.; Palmer, L. C.; Shekhawat, G. S.; de la Cruz, M. O.; Schatz, G. C.; Stupp, S. I., Energy landscapes and functions of supramolecular systems. *Nature Materials* **2016**, *15* (4), 469-476.
21. Baldwin, A. J.; Knowles, T. P. J.; Tartaglia, G. G.; Fitzpatrick, A. W.; Devlin, G. L.; Shammas, S. L.; Waudby, C. A.; Mossuto, M. F.; Meehan, S.; Gras, S. L.; Christodoulou, J.; Anthony-Cahill, S. J.; Barker, P. D.; Vendruscolo, M.; Dobson, C. M., Metastability of Native Proteins and the Phenomenon of Amyloid Formation. *Journal of the American Chemical Society* **2011**, *133* (36), 14160-14163.
22. Maude, S.; Ingham, E.; Aggeli, A., Biomimetic self-assembling peptides as scaffolds for soft tissue engineering. *Nanomedicine* **2013**, *8* (5), 823-847.
23. Hainline, K. M.; Fries, C. N.; Collier, J. H., Progress Toward the Clinical Translation of Bioinspired Peptide and Protein Assemblies. *Advanced Healthcare Materials* **2018**, *7* (5), 1700930.
24. Sarkar, B.; Nguyen, P. K.; Gao, W.; Dondapati, A.; Siddiqui, Z.; Kumar, V. A., Angiogenic Self-Assembling Peptide Scaffolds for Functional Tissue Regeneration. *Biomacromolecules* **2018**, *19* (9), 3597-3611.
25. Yuan, C.; Ji, W.; Xing, R.; Li, J.; Gazit, E.; Yan, X., Hierarchically oriented organization in supramolecular peptide crystals. *Nature Reviews Chemistry* **2019**, *3* (10), 567-588.
26. Geng, Y.; Dalhaimer, P.; Cai, S.; Tsai, R.; Tewari, M.; Minko, T.; Discher, D. E., Shape effects of filaments versus spherical particles in flow and drug delivery. *Nature Nanotechnology* **2007**, *2* (4), 249-255.
27. Yuan, C.; Levin, A.; Chen, W.; Xing, R.; Zou, Q.; Herling, T. W.; Challa, P. K.; Knowles, T. P. J.; Yan, X., Nucleation and Growth of Amino Acid and Peptide Supramolecular Polymers through Liquid-Liquid Phase Separation. *Angewandte Chemie International Edition* **2019**, *58* (50), 18116-18123.

## Programming supramolecular peptide materials by modulating the intermediate steps in the complex assembly pathway: implications for biomedical applications

---

28. Sementilli, A.; Rengifo, R.; Kim, Y.; Liang, C.; Li, N.; Mehta, A.; Lynn, D., Liquid-like phases pre-order peptides for supramolecular assembly. *ChemSystemsChem* **2020**, *n/a* (n/a).
29. Michaels, T. C. T.; Šarić, A.; Curk, S.; Bernfur, K.; Arosio, P.; Meisl, G.; Dear, A. J.; Cohen, S. I. A.; Dobson, C. M.; Vendruscolo, M.; Linse, S.; Knowles, T. P. J., Dynamics of oligomer populations formed during the aggregation of Alzheimer's A $\beta$ 42 peptide. *Nature Chemistry* **2020**, *12* (5), 445-451.
30. Dear, A. J.; Michaels, T. C. T.; Meisl, G.; Klenerman, D.; Wu, S.; Perrett, S.; Linse, S.; Dobson, C. M.; Knowles, T. P. J., Kinetic diversity of amyloid oligomers. *Proceedings of the National Academy of Sciences* **2020**, 201922267.
31. Rad-Malekshahi, M.; Visscher, K. M.; Rodrigues, J. P.; de Vries, R.; Hennink, W. E.; Baldus, M.; Bonvin, A. M.; Mastrobattista, E.; Weingarth, M., The Supramolecular Organization of a Peptide-Based Nanocarrier at High Molecular Detail. *Journal of the American Chemical Society* **2015**, *137* (24), 7775-7784.
32. Adamcik, J.; Castelletto, V.; Bolisetty, S.; Hamley, I. W.; Mezzenga, R., Direct Observation of Time-Resolved Polymorphic States in the Self-Assembly of End-Capped Heptapeptides. *Angewandte Chemie International Edition* **2011**, *50* (24), 5495-5498.
33. Yu, X.; Wang, Q.; Zheng, J., Structural determination of Abeta25-35 micelles by molecular dynamics simulations. *Biophysical journal* **2010**, *99* (2), 666-674.
34. Morel, B.; Carrasco, M. P.; Jurado, S.; Marco, C.; Conejero-Lara, F., Dynamic micellar oligomers of amyloid beta peptides play a crucial role in their aggregation mechanisms. *Physical Chemistry Chemical Physics* **2018**, *20* (31), 20597-20614.
35. Meng, Q.; Kou, Y.; Ma, X.; Liang, Y.; Guo, L.; Ni, C.; Liu, K., Tunable Self-Assembled Peptide Amphiphile Nanostructures. *Langmuir* **2012**, *28* (11), 5017-5022.
36. Ianiro, A.; Wu, H.; van Rijt, M. M. J.; Vena, M. P.; Keizer, A. D. A.; Esteves, A. C. C.; Tuinier, R.; Friedrich, H.; Sommerdijk, N. A. J. M.; Patterson, J. P., Liquid-liquid phase separation during amphiphilic self-assembly. *Nature Chemistry* **2019**, *11* (4), 320-328.
37. Tsemekhman, K.; Goldschmidt, L.; Eisenberg, D.; Baker, D., Cooperative hydrogen bonding in amyloid formation. *Protein Science* **2009**, *16* (4), 761-764.
38. Auer, S.; Dobson, C. M.; Vendruscolo, M.; Maritan, A., Self-Templated Nucleation in Peptide and Protein Aggregation. *Physical Review Letters* **2008**, *101* (25), 258101.
39. Louros, N.; Konstantoulea, K.; De Vleeschouwer, M.; Ramakers, M.; Schymkowitz, J.; Rousseau, F., WALTZ-DB 2.0: an updated database containing structural information of experimentally determined amyloid-forming peptides. *Nucleic Acids Research* **2019**, *48* (D1), D389-D393.
40. Aggeli, A.; Nyrkova, I. A.; Bell, M.; Harding, R.; Carrick, L.; McLeish, T. C. B.; Semenov, A. N.; Boden, N., Hierarchical self-assembly of chiral rod-like molecules as a model for peptide  $\beta$ -sheet tapes, ribbons, fibrils, and fibers. *Proceedings of the National Academy of Sciences* **2001**, *98* (21), 11857.
41. Buell, A. K.; Dhulesia, A.; White, D. A.; Knowles, T. P. J.; Dobson, C. M.; Welland, M. E., Detailed Analysis of the Energy Barriers for Amyloid Fibril Growth. *Angewandte Chemie International Edition* **2012**, *51* (21), 5247-5251.
42. Forman, C. J.; Fejer, S. N.; Chakrabarti, D.; Barker, P. D.; Wales, D. J., Local Frustration Determines Molecular and Macroscopic Helix Structures. *The Journal of Physical Chemistry B* **2013**, *117* (26), 7918-7928.

43. Hall, D. M.; Bruss, I. R.; Barone, J. R.; Grason, G. M., Morphology selection via geometric frustration in chiral filament bundles. *Nature Materials* **2016**, *15* (7), 727-732.
44. Pellarin, R.; Schuetz, P.; Guarnera, E.; Cafilisch, A., Amyloid Fibril Polymorphism Is under Kinetic Control. *Journal of the American Chemical Society* **2010**, *132* (42), 14960-14970.
45. Liberta, F.; Loerch, S.; Rennegarbe, M.; Schierhorn, A.; Westermark, P.; Westermark, G. T.; Hazenberg, B. P. C.; Grigorieff, N.; Fändrich, M.; Schmidt, M., Cryo-EM fibril structures from systemic AA amyloidosis reveal the species complementarity of pathological amyloids. *Nature Communications* **2019**, *10* (1), 1104.
46. Zhao, Y.; Yang, W.; Wang, D.; Wang, J.; Li, Z.; Hu, X.; King, S.; Rogers, S.; Lu, J. R.; Xu, H., Controlling the Diameters of Nanotubes Self-Assembled from Designed Peptide Bolophiles. *Small* **2018**, *14* (12), 1703216.
47. Middleton, D. A.; Madine, J.; Castelletto, V.; Hamley, I. W., Insights into the Molecular Architecture of a Peptide Nanotube Using FTIR and Solid-State NMR Spectroscopic Measurements on an Aligned Sample. *Angewandte Chemie International Edition* **2013**, *52* (40), 10537-10540.
48. Kornmueller, K.; Letofsky-Papst, I.; Gradauer, K.; Mikl, C.; Cacho-Nerin, F.; Leybold, M.; Keller, W.; Leitinger, G.; Amenitsch, H.; Prassl, R., Tracking morphologies at the nanoscale: Self-assembly of an amphiphilic designer peptide into a double helix superstructure. *Nano Research* **2015**, *8* (6), 1822-1833.
49. Mello, L. R.; Aguiar, R. B.; Yamada, R. Y.; Moraes, J. Z.; Hamley, I. W.; Alves, W. A.; Reza, M.; Ruokolainen, J.; Silva, E. R., Amphipathic design dictates self-assembly, cytotoxicity and cell uptake of arginine-rich surfactant-like peptides. *Journal of Materials Chemistry B* **2020**, *8* (12), 2495-2507.
50. Lopez-Silva, T. L.; Leach, D. G.; Li, I. C.; Wang, X.; Hartgerink, J. D., Self-Assembling Multidomain Peptides: Design and Characterization of Neutral Peptide-Based Materials with pH and Ionic Strength Independent Self-Assembly. *ACS Biomaterials Science & Engineering* **2019**, *5* (2), 977-985.
51. Bera, S.; Arad, E.; Schnaider, L.; Shaham-Niv, S.; Castelletto, V.; Peretz, Y.; Zaguri, D.; Jelinek, R.; Gazit, E.; Hamley, I. W., Unravelling the role of amino acid sequence order in the assembly and function of the amyloid- $\beta$  core. *Chemical Communications* **2019**, *55* (59), 8595-8598.
52. Cao, M.; Lu, S.; Zhao, W.; Deng, L.; Wang, M.; Wang, J.; Zhou, P.; Wang, D.; Xu, H.; Lu, J. R., Peptide Self-Assembled Nanostructures with Distinct Morphologies and Properties Fabricated by Molecular Design. *ACS Applied Materials & Interfaces* **2017**, *9* (45), 39174-39184.
53. Brack, A.; Orgel, L. E.,  $\beta$  structures of alternating polypeptides and their possible prebiotic significance. *Nature* **1975**, *256* (5516), 383-387.
54. Wychowanec, J. K.; Patel, R.; Leach, J.; Mathomes, R.; Chhabria, V.; Patil-Sen, Y.; Hidalgo-Bastida, A.; Forbes, R. T.; Hayes, J. M.; Elsayy, M. A., Aromatic Stacking Facilitated Self-Assembly of Ultrashort Ionic Complementary Peptide Sequence:  $\beta$ -Sheet Nanofibers with Remarkable Gelation and Interfacial Properties. *Biomacromolecules* **2020**.
55. Zhou, P.; Deng, L.; Wang, Y.; Lu, J. R.; Xu, H., Interplay between Intrinsic Conformational Propensities and Intermolecular Interactions in the Self-Assembly of Short Surfactant-like Peptides Composed of Leucine/Isoleucine. *Langmuir* **2016**, *32* (18), 4662-4672.

## Programming supramolecular peptide materials by modulating the intermediate steps in the complex assembly pathway: implications for biomedical applications

---

56. Street, A. G.; Mayo, S. L., Intrinsic  $\beta$ -sheet propensities result from van der Waals interactions between side chains and the local backbone. *Proceedings of the National Academy of Sciences* **1999**, *96* (16), 9074.
57. Hamley, I. W.; Castelletto, V.; Dehsorkhi, A.; Torras, J.; Aleman, C.; Portnaya, I.; Danino, D., The Conformation and Aggregation of Proline-Rich Surfactant-Like Peptides. *The Journal of Physical Chemistry B* **2018**, *122* (6), 1826-1835.
58. Baram, M.; Gilead, S.; Gazit, E.; Miller, Y., Mechanistic perspective and functional activity of insulin in amylin aggregation. *Chemical Science* **2018**, *9* (18), 4244-4252.
59. Hsieh, M.-C.; Liang, C.; Mehta, A. K.; Lynn, D. G.; Grover, M. A., Multistep Conformation Selection in Amyloid Assembly. *Journal of the American Chemical Society* **2017**, *139* (47), 17007-17010.
60. Sahoo, J. K.; VandenBerg, M. A.; Ruiz Bello, E. E.; Nazareth, C. D.; Webber, M. J., Electrostatic-driven self-sorting and nanostructure speciation in self-assembling tetrapeptides. *Nanoscale* **2019**, *11* (35), 16534-16543.
61. Wong, K. M.; Wang, Y.; Seroski, D. T.; Larkin, G. E.; Mehta, A. K.; Hudalla, G. A.; Hall, C. K.; Paravastu, A. K., Molecular complementarity and structural heterogeneity within co-assembled peptide  $\beta$ -sheet nanofibers. *Nanoscale* **2020**, *12* (7), 4506-4518.
62. Shao, Q.; Wong, K. M.; Seroski, D. T.; Wang, Y.; Liu, R.; Paravastu, A. K.; Hudalla, G. A.; Hall, C. K., Anatomy of a selectively coassembled  $\beta$ -sheet peptide nanofiber. *Proceedings of the National Academy of Sciences* **2020**, *117* (9), 4710.
63. Lu, K.; Jacob, J.; Thiyagarajan, P.; Conticello, V. P.; Lynn, D. G., Exploiting Amyloid Fibril Lamination for Nanotube Self-Assembly. *Journal of the American Chemical Society* **2003**, *125* (21), 6391-6393.
64. Dahlgren, K. N.; Manelli, A. M.; Stine, W. B.; Baker, L. K.; Krafft, G. A.; LaDu, M. J., Oligomeric and Fibrillar Species of Amyloid- $\beta$  Peptides Differentially Affect Neuronal Viability. *Journal of Biological Chemistry* **2002**, *277* (35), 32046-32053.
65. Jones, O. G.; Mezzenga, R., Inhibiting, promoting, and preserving stability of functional protein fibrils. *Soft Matter* **2012**, *8* (4), 876-895.
66. Wang, Y.; Lomakin, A.; Kanai, S.; Alex, R.; Benedek, G. B., Liquid-Liquid Phase Separation in Oligomeric Peptide Solutions. *Langmuir* **2017**, *33* (31), 7715-7721.
67. Tanaka, M.; Chien, P.; Naber, N.; Cooke, R.; Weissman, J. S., Conformational variations in an infectious protein determine prion strain differences. *Nature* **2004**, *428* (6980), 323-328.
68. Ohhashi, Y.; Ito, K.; Toyama, B. H.; Weissman, J. S.; Tanaka, M., Differences in prion strain conformations result from non-native interactions in a nucleus. *Nature Chemical Biology* **2010**, *6* (3), 225-230.
69. Muscat, S.; Stojceski, F.; Danani, A., Elucidating the Effect of Static Electric Field on Amyloid Beta 1-42 Supramolecular Assembly. *Journal of Molecular Graphics and Modelling* **2020**, *96*, 107535.
70. Budi, A.; Legge, F. S.; Treutlein, H.; Yarovsky, I., Electric Field Effects on Insulin Chain-B Conformation. *The Journal of Physical Chemistry B* **2005**, *109* (47), 22641-22648.
71. Todorova, N.; Bentvelzen, A.; Yarovsky, I., Electromagnetic field modulates aggregation propensity of amyloid peptides. *The Journal of Chemical Physics* **2020**, *152* (3), 035104.

72. Calabrò, E.; Magazù, S., Parallel  $\beta$ -sheet vibration band increases with proteins dipole moment under exposure to 1765 MHz microwaves. *Bioelectromagnetics* **2016**, *37* (2), 99-107.
73. Karavasili, C.; Andreadis, D. A.; Katsamenis, O. L.; Panteris, E.; Anastasiadou, P.; Kakazanis, Z.; Zoumpourlis, V.; Markopoulou, C. K.; Koutsopoulos, S.; Vizirianakis, I. S.; Fatouros, D. G., Synergistic Antitumor Potency of a Self-Assembling Peptide Hydrogel for the Local Co-delivery of Doxorubicin and Curcumin in the Treatment of Head and Neck Cancer. *Molecular Pharmaceutics* **2019**, *16* (6), 2326-2341.
74. Leach, D. G.; Dharmaraj, N.; Piotrowski, S. L.; Lopez-Silva, T. L.; Lei, Y. L.; Sikora, A. G.; Young, S.; Hartgerink, J. D., STINGel: Controlled release of a cyclic dinucleotide for enhanced cancer immunotherapy. *Biomaterials* **2018**, *163*, 67-75.
75. Leach, D. G.; Newton, J. M.; Florez, M. A.; Lopez-Silva, T. L.; Jones, A. A.; Young, S.; Sikora, A. G.; Hartgerink, J. D., Drug-Mimicking Nanofibrous Peptide Hydrogel for Inhibition of Inducible Nitric Oxide Synthase. *ACS Biomaterials Science & Engineering* **2019**, *5* (12), 6755-6765.
76. Chesson, C. B.; Huante, M.; Nusbaum, R. J.; Walker, A. G.; Clover, T. M.; Chinnaswamy, J.; Endsley, J. J.; Rudra, J. S., Nanoscale Peptide Self-assemblies Boost BCG-primed Cellular Immunity Against Mycobacterium tuberculosis. *Scientific Reports* **2018**, *8* (1), 12519.
77. Ma, H.; Bolster, C.; Johnson, W. P.; Li, K.; Pazmino, E.; Camacho, K. M.; Anselmo, A. C.; Mitragotri, S., Coupled Influences of Particle Shape, Surface Property and Flow Hydrodynamics on Rod-Shaped Colloid Transport in Porous Media. *Journal of Colloid and Interface Science* **2020**.
78. Yang, C.; Chu, L.; Zhang, Y.; Shi, Y.; Liu, J.; Liu, Q.; Fan, S.; Yang, Z.; Ding, D.; Kong, D.; Liu, J., Dynamic Biostability, Biodistribution, and Toxicity of l/d-Peptide-Based Supramolecular Nanofibers. *ACS Applied Materials & Interfaces* **2015**, *7* (4), 2735-2744.
79. Tanisaka, H.; Kizaka-Kondoh, S.; Makino, A.; Tanaka, S.; Hiraoka, M.; Kimura, S., Near-Infrared Fluorescent Labeled Peptosome for Application to Cancer Imaging. *Bioconjugate Chemistry* **2008**, *19* (1), 109-117.
80. Si, Y.; Wen, Y.; Kelly, S. H.; Chong, A. S.; Collier, J. H., Intranasal delivery of adjuvant-free peptide nanofibers elicits resident CD8<sup>+</sup> T cell responses. *Journal of Controlled Release* **2018**, *282*, 120-130.
81. Marshall, K. E.; Vadukul, D. M.; Staras, K.; Serpell, L. C., Misfolded amyloid- $\beta$ -42 impairs the endosomal-lysosomal pathway. *Cellular and Molecular Life Sciences* **2020**.
82. Kaganovich, D.; Kopito, R.; Frydman, J., Misfolded proteins partition between two distinct quality control compartments. *Nature* **2008**, *454*, 1088.
83. Rudra, J. S.; Khan, A.; Clover, T. M.; Endsley, J. J.; Zloza, A.; Wang, J.; Jagannath, C., Supramolecular Peptide Nanofibers Engage Mechanisms of Autophagy in Antigen-Presenting Cells. *ACS Omega* **2017**, *2* (12), 9136-9143.
84. Wang, Z.; Shang, Y.; Tan, Z.; Li, X.; Li, G.; Ren, C.; Wang, F.; Yang, Z.; Liu, J., A supramolecular protein chaperone for vaccine delivery. *Theranostics* **2020**, *10* (2), 657-670.
85. Ghislat, G.; Lawrence, T., Autophagy in dendritic cells. *Cellular & Molecular Immunology* **2018**, *15* (11), 944-952.
86. Zhang, Y.; Zhang, L.; Gao, J.; Wen, L., Pro-Death or Pro-Survival: Contrasting Paradigms on Nanomaterial-Induced Autophagy and Exploitations for Cancer Therapy. *Accounts of Chemical Research* **2019**, *52* (11), 3164-3176.



## Programming supramolecular peptide materials by modulating the intermediate steps in the complex assembly pathway: implications for biomedical applications

---

87. Dou, X.; Wu, B.; Liu, J.; Zhao, C.; Qin, M.; Wang, Z.; Schönherr, H.; Feng, C., Effect of Chirality on Cell Spreading and Differentiation: From Chiral Molecules to Chiral Self-Assembly. *ACS Applied Materials & Interfaces* **2019**, *11* (42), 38568-38577.
88. Liu, J.; Yuan, F.; Ma, X.; Auphedeous, D.-i. Y.; Zhao, C.; Liu, C.; Shen, C.; Feng, C., The Cooperative Effect of Both Molecular and Supramolecular Chirality on Cell Adhesion. *Angewandte Chemie International Edition* **2018**, *57* (22), 6475-6479.
89. Dou, X.; Mehwish, N.; Zhao, C.; Liu, J.; Xing, C.; Feng, C., Supramolecular Hydrogels with Tunable Chirality for Promising Biomedical Applications. *Accounts of Chemical Research* **2020**, *53* (4), 852-862.
90. Wang, M.; Zhou, P.; Wang, J.; Zhao, Y.; Ma, H.; Lu, J. R.; Xu, H., Left or Right: How Does Amino Acid Chirality Affect the Handedness of Nanostructures Self-Assembled from Short Amphiphilic Peptides? *Journal of the American Chemical Society* **2017**, *139* (11), 4185-4194.
91. Moore, A. N.; Hartgerink, J. D., Self-Assembling Multidomain Peptide Nanofibers for Delivery of Bioactive Molecules and Tissue Regeneration. *Accounts of Chemical Research* **2017**, *50* (4), 714-722.
92. Restuccia, A.; Hudalla, G. A., Tuning carbohydrate density enhances protein binding and inhibition by glycosylated  $\beta$ -sheet peptide nanofibers. *Biomaterials Science* **2018**, *6* (9), 2327-2335.
93. Restuccia, A.; Seroski, D. T.; Kelley, K. L.; O'Bryan, C. S.; Kurian, J. J.; Knox, K. R.; Farhadi, S. A.; Angelini, T. E.; Hudalla, G. A., Hierarchical self-assembly and emergent function of densely glycosylated peptide nanofibers. *Communications Chemistry* **2019**, *2* (1), 53.
94. Vantomme, G.; Meijer, E. W., The construction of supramolecular systems. *Science* **2019**, *363* (6434), 1396.
95. Frederix, P. W. J. M.; Idé, J.; Altay, Y.; Schaeffer, G.; Surin, M.; Beljonne, D.; Bondarenko, A. S.; Jansen, T. L. C.; Otto, S.; Marrink, S. J., Structural and Spectroscopic Properties of Assemblies of Self-Replicating Peptide Macrocycles. *ACS Nano* **2017**, *11* (8), 7858-7868.
96. Li, I. C.; Hartgerink, J. D., Covalent Capture of Aligned Self-Assembling Nanofibers. *Journal of the American Chemical Society* **2017**, *139* (23), 8044-8050.

### Summary of key references

Key references published within the period of review are highlighted as: \* of special interest; \*\* of outstanding interest

<sup>27\*\*</sup> This work shows the generality of LLPS in the formation of cross- $\beta$  peptide nanofibers. Furthermore, it has outlined the thermodynamics underpinning the LLPS and cross- $\beta$  nucleation process.

<sup>29\*\*</sup> This work outlines an experiment-complying theoretical model that describes the dynamics between different populations of assemblies present in a supramolecular peptide system (monomer, oligomer, nanofiber). It also highlights the probabilistic nature for peptide assemblies to progress through each stage of the self-assembly pathway.

<sup>30\*</sup> This work outlines the heterogenic and dynamic nature of oligomers present in peptide supramolecular systems by fitting experimental data of several unrelated amyloidogenic systems to their newly derived mechanistic models.

<sup>36\*\*</sup> Through in-situ monitoring of the amphiphilic assembly of a 0D nanovesicle, this work shows that LLPS act as the precursory step for the eventual vesicle formation. Furthermore, it demonstrates that the properties of the phase-separated droplets are vital in defining the properties of vesicles being formed.

<sup>45\*\*</sup> This work shows for the first time that right-handed nanofibers can be formed with L-amino acid constituting amyloid peptides. The cryo-EM structures reconstructed have described the hierarchical organization of the right-handed nanofibers.

<sup>50\*</sup> This work demonstrates the capability of the multidomain peptide to drive 1D nanofibers assembly with neutrally charged flanking residues. It shows the versatility of multidomain peptides that can suit well for different biomedical applications.

<sup>62\*</sup> This work shows that complementary charge interaction between peptide side chains can generate a precise supramolecular pattern in the 1D nanofiber being formed. It demonstrates the potential of controlling the multicomponent properties in the 1D nanofibers by encoding charge complimentary side-chain interaction in the peptide sequences.

<sup>74\*</sup> This work shows that hydrogels composed of 1D peptide nanofibers exhibit a more extended-release profile of cyclic dinucleotides than conventional hydrogels. This peptide hydrogel can potentially serve as a therapeutic platform to enhance the efficacy of cyclic dinucleotides immunotherapies.

<sup>80\*</sup> This work shows that, next to CD4+ T cell responses, peptide nanofibers can also elicit CD8+ T cell responses upon intranasal administration. It demonstrates the versatility of peptide nanofibers in enhancing the vaccination immune response.

<sup>81\*</sup> This work shows that peptide assemblies can disrupt the endosomal-lysosomal pathway and release the peptide into the cytosol. This functionality can be potentially exploited for drug delivery applications.

<sup>84\*</sup> This work shows that engagement with autophagy mechanisms is critical in inducing an effective immune response upon peptide nanofiber vaccination.

<sup>87\*\*</sup> This work describes the critical role of chirality at the molecular and supramolecular level of the constituent parts of hydrogel towards cellular behavior. This highlights the

## **Programming supramolecular peptide materials by modulating the intermediate steps in the complex assembly pathway: implications for biomedical applications**

---

potential drawback of tuning peptide nanofibers' helicity by switching between L- and -D amino acids.

<sup>93\*</sup> This work describes how glycan-modified peptide nanofiber is responsive to the crowded environment that causes fibrous bundling. Such emergent function can help devise a fibrillar network with more specific biological recognizability.



# Chapter 3

## **Control over the fibrillization yield by varying the oligomeric nucleation propensities of self-assembling peptides**

Chun Yin Jerry Lau<sup>1</sup>, Federico Fontana<sup>2,3</sup>, Laurens D.B. Mandemaker<sup>4</sup>, Dennie Wezendonk<sup>4</sup>, Benjamin Vermeer<sup>5</sup>, Alexandre M.J.J. Bonvin<sup>5</sup>, Renko de Vries<sup>6</sup>, Heyang Zhang<sup>7</sup>, Katrien Remaut<sup>7</sup>, Joep van den Dikkenberg<sup>1</sup>, João Medeiros-Silva<sup>5</sup>, Alia Hassan<sup>8</sup>, Barbara Perrone<sup>8</sup>, Rainer Kuemmerle<sup>8</sup>, Fabrizio Gelain<sup>2,3</sup>, Wim E. Hennink<sup>1</sup>, Markus Weingarth<sup>\*5</sup> and Enrico Mastrobattista<sup>\*1</sup>

<sup>1</sup>*Utrecht Institute for Pharmaceutical Sciences, Department of Pharmaceutics, Faculty of Science, Utrecht University, Universiteitsweg 99, 3584 CG Utrecht, The Netherlands*

<sup>2</sup>*IRCCS Casa Sollievo della Sofferenza, Opera di San Pio da Pietralcina, Viale Capuccini 1, 71013 San Giovanni Rotondo, Italy*

<sup>3</sup>*ASST Grande Ospedale Metropolitano Niguarda, Center for Nanomedicine and Tissue Engineering, Piazza dell'Ospedale Maggiore 3, 20162 Milan, Italy.*

<sup>4</sup>*Inorganic Chemistry and Catalysis group, Debye Institute for Nanomaterials Science, Department of Chemistry, Faculty of Science, Utrecht University. Universiteitsweg 99, 3584 CG Utrecht, The Netherlands*

<sup>5</sup>*NMR Spectroscopy, Bijvoet Centre for Biomolecular Research, Department of Chemistry, Faculty of Science, Utrecht University. Padualaan 8, 3584 CH Utrecht, The Netherlands.*

<sup>6</sup>*Laboratory of Physical Chemistry and Colloid Science, Wageningen University, Dreijenplein 6, 6703 HB Wageningen, The Netherlands*

<sup>7</sup>*Ghent Research Group on Nanomedicines, Laboratory of General Biochemistry and Physical Pharmacy Ghent University, Ottergemsesteenweg 460, 9000 Ghent, Belgium.*

<sup>8</sup>*Bruker BioSpin AG, Industriestrasse 26, CH-8117 Fällanden, Switzerland.*

### Abstract

Self-assembling peptides are an exemplary class of supramolecular biomaterials of broad biomedical utility. Mechanistic studies on the peptide self-assembly demonstrated the importance of the oligomeric intermediates towards the properties of the supramolecular biomaterials being formed. In this study, we demonstrate how the overall yield of the supramolecular assemblies is moderated through subtle molecular changes in the peptide monomers. This strategy is exemplified with a set of surfactant-like peptides (SLPs) with different  $\beta$ -sheet propensities and charged residues flanking the aggregation domains. By integrating different techniques, we show that these molecular changes can alter both the nucleation propensity of the oligomeric intermediates and the thermodynamic stability of the fibril structures. We demonstrate that the amount of assembled nanofibers are critically defined by the oligomeric nucleation propensities. Our findings offer guidance on designing self-assembling peptides for different biomedical applications, as well as insights into the role of protein gatekeeper sequences in preventing amyloidosis

# Control over the fibrillization yield by varying the oligomeric nucleation propensities of self-assembling peptides

---

## 1. Introduction

Self-assembling peptides, a prominent class of supramolecular polymers, can form well-ordered nanostructures via non-covalent interactions (i.e., van der Waal's forces, electrostatic forces, hydrogen bonding), the main modulators for material tailoring<sup>1</sup>. Due to the dynamic and reversible nature of their interactions, self-assembling peptides offer novel functional properties for practical exploitation, e.g., multicomponent modularity<sup>2-4</sup>, semiconductivity,<sup>5, 6</sup> and evolution-like adaptivity<sup>7</sup>.

In search for the link between the peptide monomers and the final assembly states, a number of previous reports on self-assembling peptides have studied the effect of changing the molecular properties of peptide monomers (e.g., sequences' residues or stereochemistry<sup>8, 9</sup>) towards the final assembled products. Many studies have treated the peptide self-assembly as a spontaneous thermodynamic process<sup>10</sup>. Therefore, the linear correlation between the properties of peptide monomers and the final assembled structures is often described in these studies. However, increasing evidence shows that to overcome the huge desolvation barrier, rather than a spontaneous thermodynamic process, supramolecular assembly of amphiphilic peptides proceed via a multistep<sup>11</sup> pathway, along which metastable oligomeric states are first formed before conversion to supramolecular nanofibers (Figure 1a)<sup>12-18</sup>. This implies that the state of the intermediates in the assembly pathway also exerts critical influence over the outcome of the peptide self-assembly<sup>19, 20</sup>. For example, the polymorphic form of the assembled peptide fibrils is influenced by the properties of the oligomeric intermediates<sup>21</sup>. However, despite progress in the mechanistic understanding, the inter-relationship between the molecular properties of the peptide monomers, the oligomeric intermediates, and the overall yield of the supramolecular assembly process remains largely elusive<sup>22</sup>.

Here, we used surfactant-like peptides (SLPs) to show that the yield of peptide fibrillization is controlled by the properties of the oligomeric intermediates, which can be moderated by subtle molecular variations in the peptide sequences. SLPs consist of two modular subunits (Figure 1b): hydrophobic tails that interact via van der Waals' forces (side chain) and hydrogen bonds (backbone), as well as hydrophilic headgroups that confer mutually repulsive electrostatic interactions and determine the overall charges of the peptides<sup>23</sup>. The modularity of SLPs allows us to single out one molecular property and study its effect in the downstream self-assembly pathway. We composed a set of cognate SLPs with small molecular variations (Figure 1b). Using combined experimental techniques and molecular dynamics (MD) simulations, we demonstrate that these molecular parameters (i.e.,  $\beta$ -sheet propensities and charged residues flanking the aggregation domains) can modulate the nucleation propensity oligomeric intermediates and the thermodynamic stability of the fibril structures. We demonstrate that the amount of peptide nanofibers being formed are critically defined by the oligomeric nucleation propensities. Altogether, our results offer a general molecular approach to moderate the properties of peptide assemblies for a variety of biomedical applications.

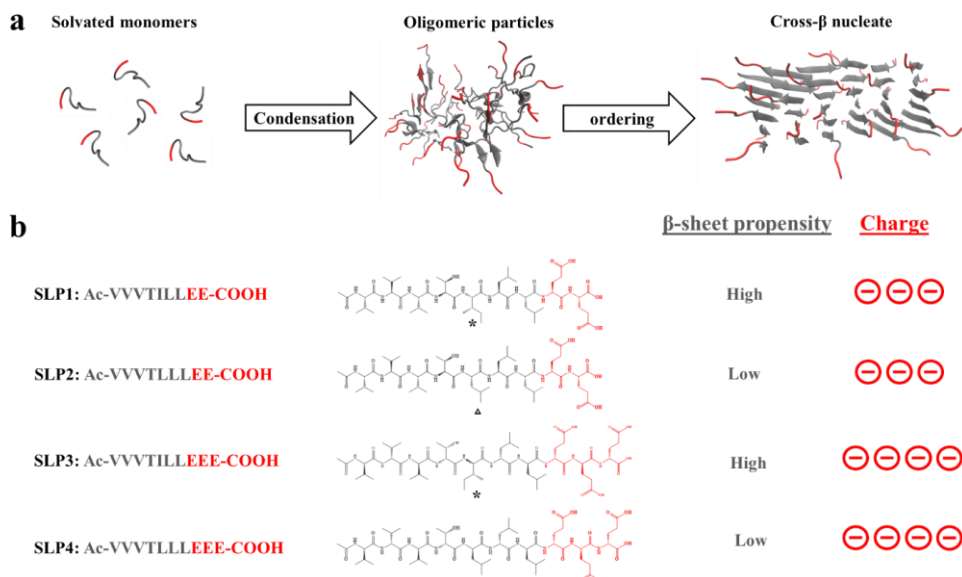


**Figure 1. Modularly engineered surfactant-like peptides (SLPs).** **a**) Schematic representation of the two-step nucleation mechanism of peptide self-assembly, in which peptides first assemble into oligomeric particles through condensation; nucleates are then formed within the oligomeric particles. **b**) Primary sequence and chemical structures of the studied SLPs. Hydrophobic tails and anionic headgroups are colored in grey and red, respectively. The mutated amino acids are highlighted by an asterisk for Ile and a triangle for Leu.

## 2. Results and Discussion

**Molecular design of surfactant-like peptides.** First, we designed a set of four cognate SLPs with different conformational propensities and headgroup charges in order to probe the effect of these molecular differences on the assembly pathway. We chose branched-chain amino acids (valine, leucine, isoleucine) as the major building blocks for the hydrophobic tail subunit, which are residues that often confer structural stability in proteins<sup>24</sup>. To limit the amount of molecular variability, we used Leu/Ile residue isomerism as the strategy for specific  $\beta$ -sheet propensity variation<sup>25</sup>. Ile has a higher  $\beta$ -sheet propensity compared to Leu, but substitution does not change the overall side-chain molecular volume and hydrophobicity. Since the sequence order can also influence the overall  $\beta$ -sheet propensity<sup>26</sup>, we employed the position scoring matrix WALTZ<sup>27</sup> to guide sequence design. The length of the tail group was chosen as N-terminal acetylated 7-mer peptide. An extra amino acid and an N-terminal acetyl cap were added to the 6-mer peptide sequence to minimize the influence of flanking effects by the charged residues<sup>28</sup>. The WALTZ database suggests that position 5 is a highly selective position for isoleucine, but not leucine, to drive cross- $\beta$  structures formation. We also placed threonine between two aliphatic amino acid trimers to create two  $\beta$ -sheet faces of different hydrophobicity. This allowed the assignment of the anisotropic side-chain interface that fits the statistical mechanical fibril assembly model (Figure S5)<sup>29,30</sup>. The statistical thermodynamics algorithm TANGO was used to determine the residual aggregation propensities along the whole sequence (Table S1)<sup>31</sup>.



## Control over the fibrillization yield by varying the oligomeric nucleation propensities of self-assembling peptides

Moreover, the number of charges in SLP was adjusted by altering the number of glutamic acid residues in the headgroup (Figure 1b).

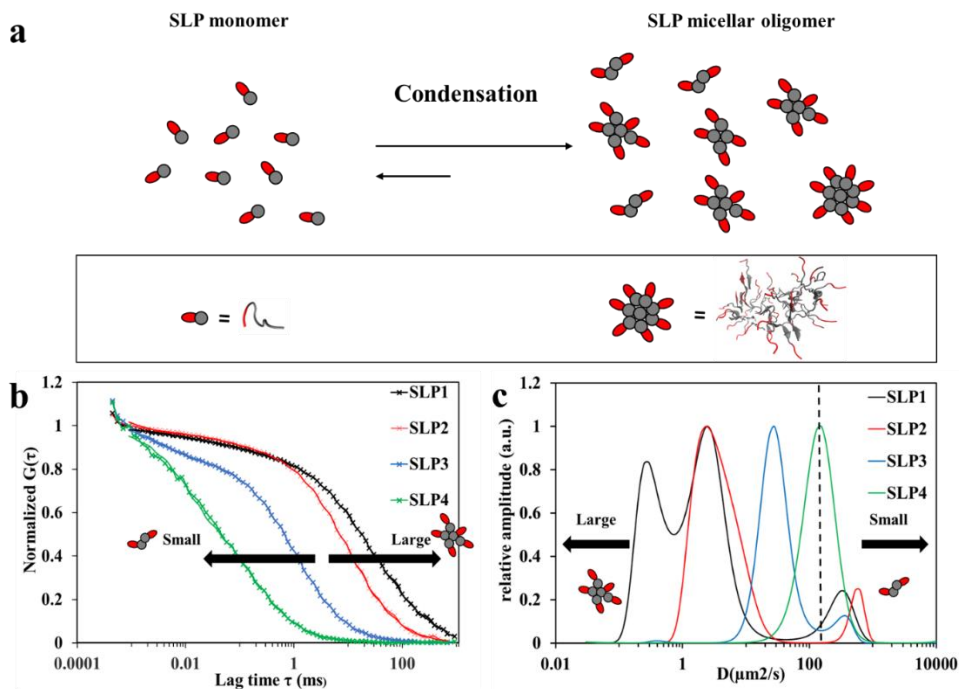


**Figure 2. Effect of headgroup charge on SLP oligomerization.** a) Illustration of the LLPS mechanism for SLPs. Micellar arrangement of the oligomers is caused by the amphiphilic nature of SLP<sup>59</sup>. Representative structures for monomer and micellar oligomers derived from MD simulations are shown below. b) Normalized autocorrelation curves of SLP1-4 determined by Fluorescence Correlation Spectroscopy (FCS) as performed for Cy5-labelled SLPs (black, red, blue, and green crosses). FCS data shows that the assemblies of SLP1-2 are globally larger than of SLP3-4. The measurement concentration was 4mM of SLPs in PBS (pH7.4), of which 1 out of 4000 peptides was labeled with Cy5. The FCS autocorrelation curves were fitted with the Maximum Entropy Method (MEM) for higher resolution analysis on size distribution, indicated by the solid lines. c) The size distribution of SLPs obtained from MEM analysis of the FCS measurements. The dashed line at  $D=150\mu\text{m}^2/\text{s}$  indicates the cut-off size between monomeric ( $D>150$ ) and oligomer ( $D<150$ ) populations. SLP1-2 with two glutamic acid residues in the headgroup formed oligomers with  $\sim 10$  times slower diffusivity than SLP3-4 with three glutamates in the headgroup.

**Headgroup charges regulate the size distribution of the oligomeric particles.** To study the effect of headgroup charges towards the size of the metastable oligomeric particles, we employed multiscale MD simulations to confirm the structural arrangement of the oligomeric particles (see Materials and Method). The final trajectory atomistic simulations suggested that the SLP oligomeric particles adopt a micellar arrangement with surface-exposed headgroups and buried tail groups (Figures 2a and S1-2). Next, given that higher surface electrostatic repulsive forces can impose higher repulsive forces between the oligomeric particles, thereby lowering their coalescence tendency<sup>32</sup>, we speculated that the size of the micellar oligomer with three glutamic acid residues in the headgroup (SLP3-4)

should be smaller than that with two glutamic acids (SLP1-2). To validate this hypothesis, we performed fluorescence correlation spectroscopy (FCS) measurements to study the diffusion properties of SLPs in the early phase of self-assembly. FCS was chosen to inspect the early assembly phase, as it gives high-resolution measurement for the small-sized oligomeric particles in solution state<sup>33</sup>. By comparing the autocorrelation graphs of SLP1-4 (Figure 2b), we could confirm that the size of oligomers decreases with the number of negative charges in the peptide headgroup, i.e., SLPs with two negative charges (SLP1-2) form larger oligomers than SLPs those with three negative charges (SLP3-4). To explore these size differences in more detail, we fitted the FCS data with a higher-order fitting model. The maximum entropy method (MEM) was chosen to account for the polydispersity of the oligomers. Each condensed fraction was treated as one quasi-continuous distribution, so as to provide widest data-complying size distribution (least chance of overinterpretation)<sup>34</sup>. We succeeded in resolving the monomeric peptides and oligomers for SLP1-3 (Figure 2c), whereas, due to their close size range, monomers and oligomers were represented as one continuous distribution for SLP4 (Figure 2c). In the MEM analysis, the diffusion coefficients of the SLP1-2 oligomers were ~10 fold smaller than for SLP3-4, clearly showing a correlation between headgroup charge and the size of oligomers, i.e., oligomers with two glutamates in the headgroup are considerably larger than those with three glutamates. Knowing that nucleation events only happen in a minority of the oligomer populations<sup>14, 35</sup>. Therefore, although this analysis does not allow us to distinguish between larger oligomers and the early nucleated structures (particularly the  $0.1-1\mu\text{m}^2/\text{s}$  SLP1 population in Figure 2c), as they fall in the same size range, we were able to validate our hypothesis that headgroup charges determine the size distribution of the oligomeric particles.

## Control over the fibrillization yield by varying the oligomeric nucleation propensities of self-assembling peptides

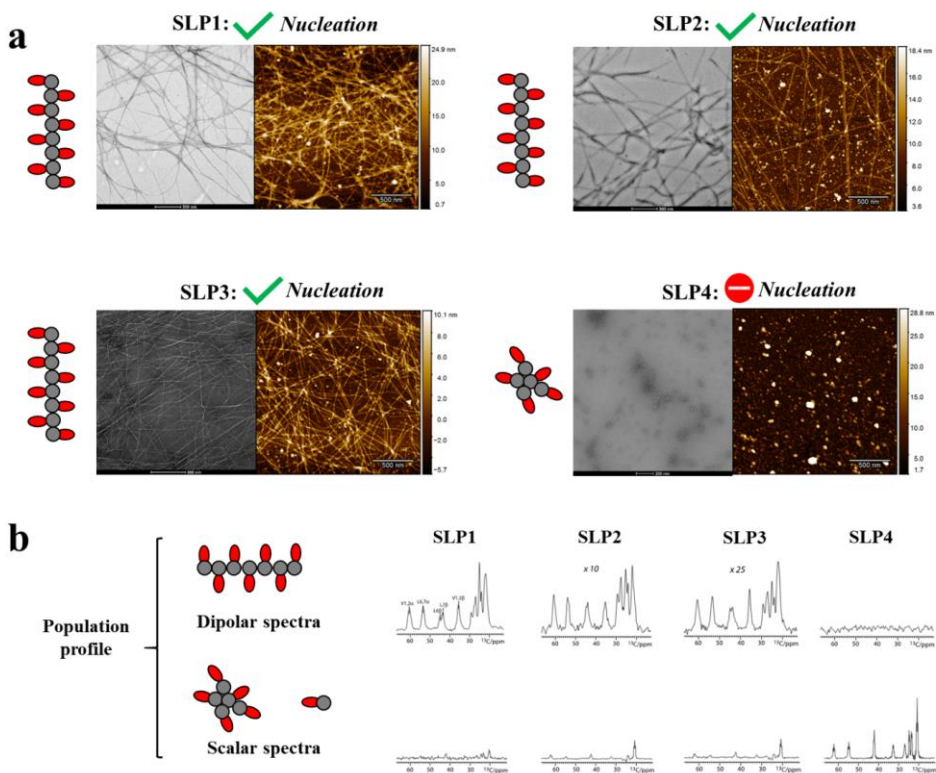


**Figure 3. Microscopy images of SLP assemblies and solid-state NMR-derived population profiles. a)** Negative staining TEM (left panel) and AFM images (right panel) showing the assembled structures of SLP1-4. 1D nanofibers are formed with SLP1-3, indicating nucleation events have taken place. Only 0D nanostructures are observed in SLP4, indicating no nucleation event has taken place. **b)** Population profiling of SLP assemblies by solid-state NMR spectroscopy. The dipolar cross-polarization (CP) spectra report on rigid 1D nanofibers, and the scalar INEPT spectra report on mobile species (micellar oligomers and monomeric SLP). The dipolar spectra were normalized (scaling factors of 10 and 25 for SLP2 and SLP3, respectively), while the intensity in scalar spectra directly reflects on the mobile population in the system. The spectra were measured at 500 MHz ( $^1\text{H}$ -frequency), 10 kHz magic angle spinning (MAS), and 280 K sample temperature.

**Mesoscale structure of SLP assemblies characterized by microscopy.** Next, we investigated the downstream effect of the differences in the size of oligomeric particles and  $\beta$ -sheet propensities on the supramolecular self-assembly. One of the pivotal events in defining supramolecular self-assembly is whether nucleation has taken place or not. This can be identified by the mesoscale structures of the assemblies after a certain time of incubation, e.g., the formation of 1D nanostructures is indicative for nucleation has taken place. We used negative-staining Transmission Electron Microscopy (TEM) and Atomic Force Microscopy (AFM) to compare SLPs that were assembled under the same preparation protocol (4mM, pH 7.4 in PBS for 3 days). We could indeed detect markedly different mesoscale structures in these SLP systems (Figure 3a; Figure S1). While SLP1-3 formed 1D nanofibers (~10nm in diameter, >1000nm long), we observed polydisperse 0D

nanostructures for SLP4 (diameter of 10-60nm). Based on these mesoscale evidences, we can deduce that nucleation occurred in SLP1-3, however not in SLP4.

**Determination of population size of fibril and non-fibril assemblies by solid-state NMR spectroscopy.** As a next step, we hypothesized that higher-resolution methods might disclose further differences in the properties of the SLP assemblies. To examine our hypothesis, we profiled the SLP1-4 assemblies using solid-state NMR (ssNMR) spectroscopy. Using the same conditions (4mM, pH 7.4 in PBS for 3 days), we acquired so-called dipolar cross-polarization (CP) ssNMR spectra and so-called scalar INEPT ssNMR spectra on isotopically ( $^{13}\text{C}$ ,  $^{15}\text{N}$ ) labeled SLP assemblies (see Materials and Methods), which enables to quantify rigid and mobile populations of peptide assemblies in the systems<sup>36</sup> (Figure 3b). While dipolar signals report on immobilized peptides in 1D assemblies, scalar spectra report on peptides with fast pico-to-nanosecond dynamics, which can either be monomeric peptides or micellar oligomers<sup>17, 32</sup>. We specifically labeled residues in the hydrophobic tail (Val1-2 and Leu6-7) responsible for the self-assembly. In line with the mesoscale differences observed by microscopy (Figure 3a), ssNMR showed stark differences in the population profiles of SLP1-3 and SLP4 (Figure 3b). SLP1-3 showed sizeable dipolar signals, indicating that a considerable number of peptides formed immobile assemblies, whereas dipolar signals were absent for SLP4, in line with the absence of 1D nanofibers for SLP4. A closer inspection into the population profiles of SLP1-3 revealed a noticeable difference in the dipolar and scalar signals between SLP1-3. The intensity of the dipolar spectra correlates with the amount of rigid cross- $\beta$  structure present in the system. We observe that the intensities of the dipolar signal of SLP1 are larger than SLP2 (normalization scaling factor of 10, Figure 3b) and SLP3 (normalization scaling factor of 25, Figure 3b), which indicate that the relative fibrillization yield of SLP1>SLP2>SLP3. Besides, the scalar signals were higher for SLP2-3 than SLP1, which means that SLP2-3 has more mobile peptides than SLP1.

Furthermore, ssNMR signals are sensitive reporters of the peptide conformation in the assemblies<sup>28, 36</sup>. We assigned  $^{15}\text{N}$  and  $^{13}\text{C}$  signals and amino protons in the assembled SLP1 system using 2D  $^{13}\text{C}$ - $^{13}\text{C}$  PARIS<sup>37</sup>, 2D C $\alpha$ N, and  $^1\text{H}$ -detected 2D C $\alpha$ (N)H experiments in combination with peptides in which only residues Val2 and Leu6 were isotope-labeled. These assignments unambiguously show that assembled peptides adopt  $\beta$ -strand configuration while the mobile population in the system is unstructured (Figure 4c).

## Control over the fibrillization yield by varying the oligomeric nucleation propensities of self-assembling peptides

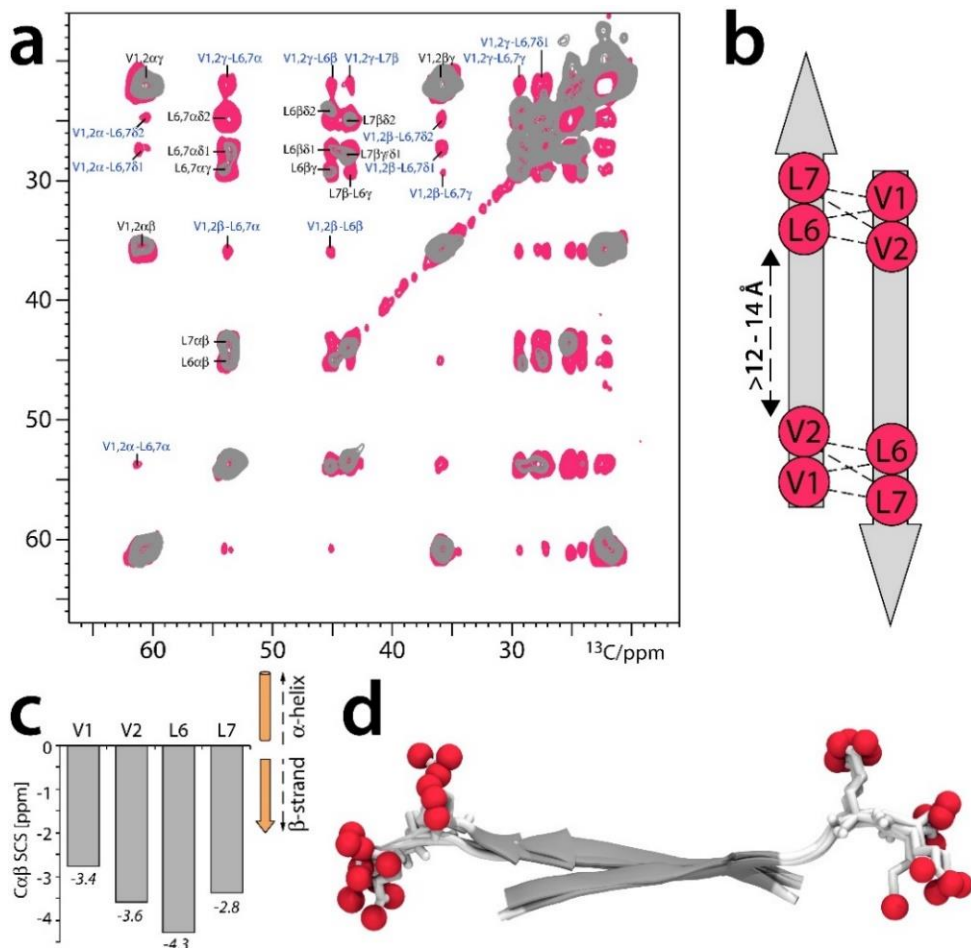


**Figure 4. Structure determination of the basic building blocks of the SLP fibers.** **a**) Superposition of 2D ssNMR PARIS  $^{13}\text{C}$ - $^{13}\text{C}$  spectra of  $^{13}\text{C}$ , $^{15}\text{N}$ -(Val1, Val2, Leu6, Leu7)-labelled SLP1 acquired with 50 (gray) and 700 ms (magenta) magnetization transfer. Intra- and intermolecular correlations are labeled in black and blue, respectively. The spectrum with 700 ms magnetization transfer time was acquired with a CPMAS CryoProbe (Bruker Biospin). **b**) Interresidual magnetization transfer from Val1/Val2 to Leu6/Leu7 observed in the 2D  $^{13}\text{C}$ - $^{13}\text{C}$  ssNMR spectrum relates to intermolecular contacts between antiparallel  $\beta$ -strands. Distances are  $\text{C}\alpha$ - $\text{C}\alpha$  spacings. **c**) SSNMR  $\text{C}\alpha\text{C}\beta$  secondary chemical shifts show that the hydrophobic tails adopt a  $\beta$ -strand conformation in the SLP1 nanofiber, similar for SLP2 and SLP3 fibers<sup>60</sup>. **d**) SSNMR structure of the SLP1 dimer in the 1D nanofiber. A superposition of the three best structures is shown (backbone RMSD of 1.11 Å). Oxygen-atoms of the anionic C-termini are highlighted as red spheres.

**Reconstruction of fibril models.** Next, we sought to elucidate how these molecular variations can affect the thermodynamic properties of the fibril assemblies. Inspired by a previous computational approach<sup>38</sup>, we built models of the SLP fibrils and validated them with the help of X-Ray Diffraction (XRD) and ssNMR spectroscopy. SLP1-3 fibers exhibit typical cross- $\beta$  X-ray diffraction (XRD) pattern, showing reflections at  $\sim 4.7$  and  $9\text{--}11$  Å

(Figure 5c). Since XRD (sharp reflection at 4.7 Å in XRD) and ssNMR show that SLP1-3 share the same interstrand features (Figure 3b), we used SLP1 to represent elucidating the inter- $\beta$ -strand configuration. We acquired a 2D  $^{13}\text{C}$ - $^{13}\text{C}$  PARIS ssNMR spectrum with a long magnetization transfer time of 700 ms that probes distances between  $^{13}\text{C}$  nuclei with a threshold of  $\sim 8$  Å. Given that the  $\text{C}\alpha_i$ - $\text{C}\alpha_{i+5}$  distance within the same  $\beta$ -strand is 15-18 Å and hence markedly beyond the ssNMR distance threshold, our labeling scheme can conclusively distinguish parallel or antiparallel alignment of  $\beta$ -strands (Figure 4b).

However, measuring intermolecular contacts between the peptides in our dilute experimental concentration (4 mM) is a serious sensitivity challenge, and increasing the sample concentration was not possible because it could alter the kinetic pathway of fibril assembly. To this end, we used a CPMAS CryoProbe prototype (BioSolids CryoProbe<sup>TM</sup>, Bruker Biospin)<sup>39</sup> that markedly enhanced spectral NMR sensitivity. With this advanced experimental setup, we were able to observe a large number ( $>50$ ) of intermolecular peptide-peptide contacts and could unambiguously establish an antiparallel alignment of  $\beta$ -strand in the fibers (Figure 4a,b). Interestingly, while Leu6 showed intermolecular NMR correlations with all aliphatic carbons of Val1 and Val2, some intermolecular correlations were absent for Leu7. This suggests that the  $\beta$ -strand tails form interdigitated antiparallel arrangements from which the charged headgroups stick out in order to minimize electrostatic repulsion.<sup>28</sup> The antiparallel, interdigitated dimer configuration was confirmed by NMR structure determination (Figure 4d), for which we used NMR distance restraints and dihedral restraints<sup>40</sup>. The antiparallel alignment was also in line with  $^{15}\text{N}$   $\text{R1}_{\text{rho}}$  measurements that probe the slow microsecond dynamics of the assembly (Figure S4). While the  $\beta$ -strand residues Val1-Leu7 are generally highly rigid, residue Leu7 showed modestly enhanced dynamics, in line with the charge-flanking residue effect observed in antiparallel  $\beta$ -sheet arrangement previously<sup>28</sup>.

Next, we built structural models of the SLP fibrils. Therefore, based on the established interstrand configuration, we arranged side chain faces of different hydrophobicity following the blueprint outlined from previous statistical mechanical model<sup>29, 30</sup> (Figure S5) and built MD fibril models composed of 36 peptides for each of SLP1-3 (Figure 5a, S6). Each fibril model was simulated for 100ns. Fibrils remained stably associated over the entire trajectory. In agreement with previous reports, a left-handed twist was observed for all three fibril models due to the chirality of the constituting L-amino acids (Figure 5b, S6)<sup>29, 30</sup>. The RDF of the inter-backbone distances were calculated from the fibril model and cross-validated with XRD results. The RDF and XRD results are in mutual agreement, showing a signal peak at  $\sim 4.7$  and 9-11 Å (Figure 5c, 5d). The good match between several experimental results and our MD model strongly corroborates the validity of our fibril models.

## Control over the fibrillization yield by varying the oligomeric nucleation propensities of self-assembling peptides

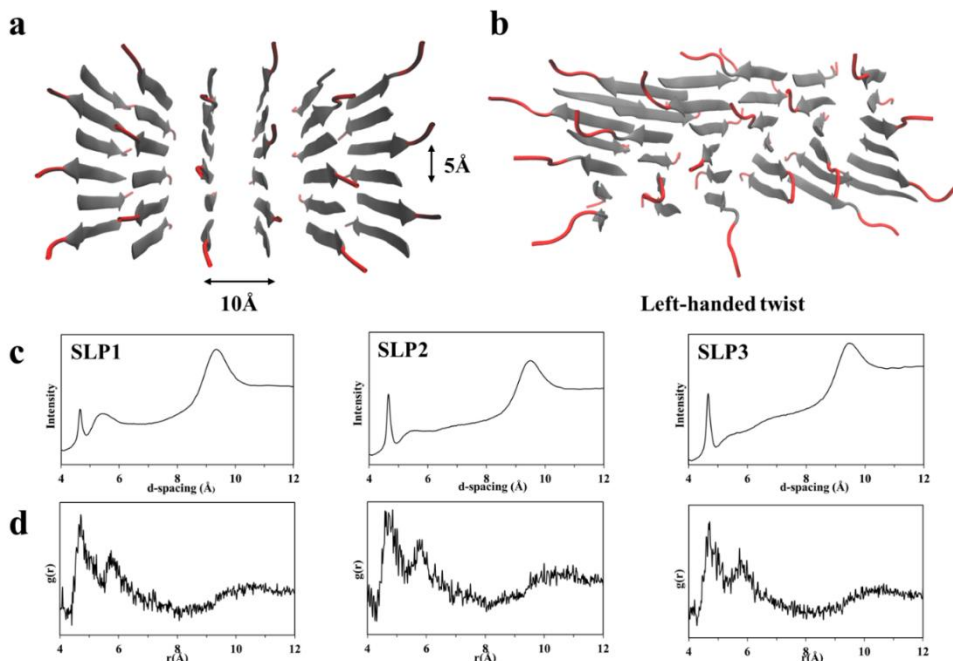


**Figure 5. Fibril models derived from MD simulations.** **a)** Representative atomistic manually built model of the starting fibril configuration with antiparallel SLPs. SLPs within a  $\beta$ -sheet is  $5\text{\AA}$  apart, and  $10\text{\AA}$  is the orthogonal distance between SLPs. **b)** Representative final configuration of the equilibrated molecular models after 100 ns of MD simulation. The chirality of the L-amino acids leads to a left-handed twist, as is observed in the SLP models. **c)** XRD pattern of the SLP1-3 fibrils. The reflection at  $\sim 4.7$  and  $9-11\text{\AA}$  represent the signatory of the cross- $\beta$  diffraction pattern. **d)** Radial Distribution Function (RDF) of the backbone-backbone distance calculated from the final MD configuration of SLP fibrils. In agreement with XRD, RDF also shows peaks at  $\sim 4.7\text{\AA}$  and  $9-11\text{\AA}$ , demonstrating a good match between MD fibril models and experimental data.

**Thermodynamic stability assessment by steered MD simulations.** As a next step, we evaluated the thermodynamic stability of the fibril models using Steered MD (SMD) simulations. Analogously, we also determined the thermodynamic stability of the oligomer structures. In these pulling simulations, an external mechanical force is applied to one SLP, which is then dragged from an aggregate core. With this approach, we derived a potential of mean force (PMF) profile, which is a good representation of the dissociation energy (fibril:  $\Delta G_d$ , oligomer:  $\Delta G_d'$ )<sup>49</sup>. Since the choice of the pull-out SLP within the molecular model determines the resultant PMF profiles, we chose one random-coil forming SLP and one  $\beta$ -sheet SLP (Figure 6a, S7). Each pull-out SLP was dragged along the x-direction (the reaction coordinate  $r$ ) for  $90\text{\AA}$ , while the application of a harmonic force constrained the other 35 SLPs. These results show that it takes  $\sim 3$  fold more energy to pull one SLP out from the fibril structure than from the oligomer structure (Figure 6a, S8). This means that fibril structures are much more stable configurations than the oligomer. For the fibril models, the increased headgroup charge in SLP3 caused a reduction in  $\Delta G_d$  and less fibril stability compared to SLP1,2. For the oligomer models, however, the charge differences in the peptide headgroups did not cause large differences in the  $\Delta G_d'$ . Since the magnitude of

the dissociation energy is an indicator for the thermodynamic stability of the supramolecular assemblies, these results suggested that an increasing number of charges in the headgroup caused more perturbations to the more ordered fibril structures than to the less ordered oligomer. We suspected that these differences were due to structural elasticity. The structural strain caused by increased electrostatic repulsion forces would be more detrimental to brittle rigid structures (fibrils) than flexible ones (oligomers). Such differences in structural elasticity are well supported by the strongly deviating sizes of the rigid and mobile equilibrium populations that we observed for SLP1-3 and SLP4 with the ssNMR experiments described above.

**The yield of nanofibers is moderated by the nucleation propensity in the oligomeric intermediates.** After characterizing the properties of SLP at the oligomer and fibril states, we sought to search for the underpinning reason behind the differences in yield of peptide nanofibers between SLP1-4. It was suggested that the final yield of the peptide nanofibers is determined by their structural stability<sup>10</sup>. However, with the high thermodynamic stability of the peptide nanofibers, the amount of monomeric peptide dissociation from fibrils is typically negligible<sup>41</sup>. Indeed, we have observed that SLP1 and SLP2, although their fibril exhibits similar thermodynamic stability, they show markedly different amounts of fibril and non-fibril assemblies. We, therefore, rationalize the difference in yields of nanofibers between SLP1-4 is instead influenced by the properties of the oligomer intermediates. Due to the heterogenic nature of the oligomeric species, it was reported that nucleation only happens in a minority of the oligomers<sup>14</sup>. Furthermore, the nucleation probability is correlated with the size of the oligomers, in which the chance of nucleation increases with the oligomer size<sup>17, 35</sup>. Indeed, we observed that SLP1-2, which forms larger-sized oligomers than SLP3-4, also gives higher nanofibers yields (Figure 3b). Besides, the nucleation probability is also influenced by the conformation propensity of the SLPs, which more  $\beta$ -sheet prone SLPs have a higher chance of forming cross- $\beta$  nucleates. Therefore, for the SLPs that bear the same headgroup charges, we consistently observed a higher yield of nanofibers for those with more  $\beta$ -sheet prone tail groups, *i.e.*, SLP1>2 and SLP3>4 (Figure 3b).

Our findings advance our fundamental understanding of the molecular design principles of SLPs (and self-assembling peptides in general) to tailor their properties for various applications (Figure S9). For applications requiring that SLPs stay in dynamic form, *e.g.*, the solubilization of membrane proteins, one should upper the charges and lower the  $\beta$ -sheet propensities of SLPs to prevent fibrillization we demonstrate it for SLP4. In contrast, for applications requiring the fibril infrastructure, *e.g.*, therapeutic scaffolds<sup>2-4</sup>, one should engineer the SLP with higher  $\beta$ -sheet propensities and lower charges to maximize the yield of fibril structures (like SLP1). In addition, for applications that use 1D nanofibers as a reservoir for hydrophobic drug release<sup>42</sup>, the micellar oligomer co-present in the system can affect the overall drug release profile. At last, with respect to protein aggregation, previous genome-wide sequence analysis revealed that in close proximity to the aggregation-prone  $\beta$ -strand regions in proteins, charged "gatekeeper" residues often prevent the  $\beta$ -strand sequences from aggregating<sup>43</sup>. Our current study implies that, besides preventing



## Control over the fibrillization yield by varying the oligomeric nucleation propensities of self-assembling peptides

aggregation, the charged protein gatekeeper sequences can also lower the chance of amyloid nucleation by lowering the oligomers' size.

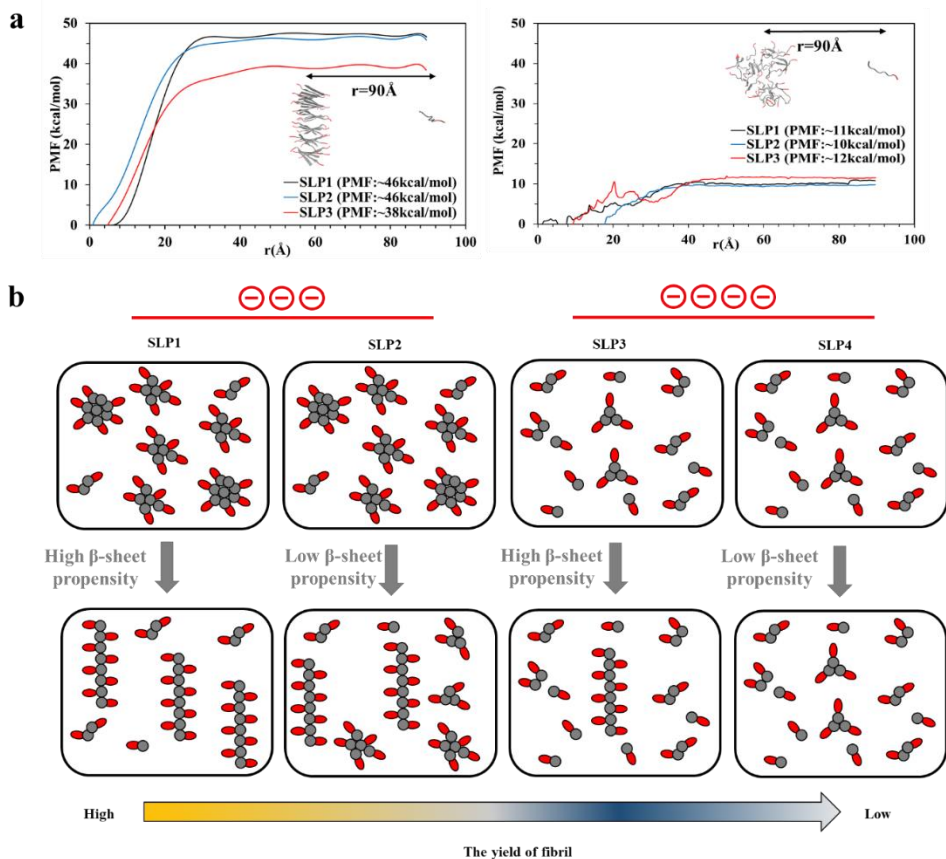


**Figure 6. Control over the fibrillization yield by varying the oligomeric nucleation propensities of surfactant-like peptides.** a) Potential of mean force (PMF) profiles of fibril (left) and oligomer (right) models along the reaction coordinate  $r$  derived from Steered MD (SMD) simulations provide information on the thermodynamic stability of fibril and oligomer structures. Increasing the number of charges of the headgroups reduced the fibrils' structural stability; however, not in the oligomers. A representative SMD trajectory is shown under each graph, during which a SLP monomer is dragged from the core of the oligomer and fibril model for  $90\text{Å}$  along with  $r$ . b) Graphical representation of the proposed mechanism leading to the different yields of nanofibrils between SLP 1-4. The size distribution of the oligomeric intermediates is controlled by the number of headgroup charges, in which the less charged SLPs form a bigger sized oligomer (2 on the left) and the more charged SLPs form smaller sized oligomers (2 on the right). Between the SLPs with the same charges, the fibrillization propensity is modulated by the  $\beta$ -sheet propensities of the tail group, with the SLP of higher  $\beta$ -sheet propensities giving higher yields of fibrils, *i.e.*, SLP1>2 and SLP3>4.

### 3. Conclusion

The data presented here demonstrated, for the first time, the molecular strategy to modulate the yield of the supramolecular polymerization process. The effect of the molecular changes

on the size distribution of the oligomeric particles and the thermodynamic stability of the fibrils are also evaluated, which helps define the mechanism leading to the differential polymerization yield. Thereby, our study enhances our understanding of the important role of oligomeric intermediates in defining the outcome of self-assembly systems and advances the rational design principles of self-assembling peptides that give different supramolecular properties for a wide latitude of applications<sup>2-4, 42, 44</sup>. Moreover, our findings suggest that charged protein gatekeeper sequences<sup>43</sup> can prevent amyloidosis by lowering the size of the oligomeric particles. This knowledge will be instrumental in the design of strategies to prevent amyloidosis.

### 4. Methods

**Materials.** Preloaded Fmoc-Glu(OtBu)-Wang resin was purchased from Novabiochem GmbH (Hohenbrunn, Germany), 2-(1H-Benzotriazol-1-yl)-1,1,3,3-tetramethyluronium hexafluorophosphate (HBTU) and 9-fluorenylmethoxycarbonyl (Fmoc)-protected amino acids, and trifluoroacetic acid (TFA) were purchased from Iris Biotech (Marktredwitz, Germany). Peptide grade N-methyl-2-pyrrolidone (NMP), dichloromethane (DCM), piperidine, N,N-diisopropylethylamine (DIPEA), and HPLC grade acetonitrile were purchased from Biosolve BV (Valkenswaard, Netherlands). 1-hydroxy-benzotriazole hydrate (HOBt), triisopropylsilane (TIPS), BioUltra grade ammonium bicarbonate, and sodium bicarbonate were purchased from Sigma-aldrich Chemie BV (Zwijndrecht, Netherlands). <sup>13</sup>C, <sup>15</sup>N-labelled Fmoc-amino acids were purchased from Cortec-net (Les Ulis, France).

**Bioinformatic analysis.** To predict the aggregation and fibrillization propensity of the designer SLPs, statistical thermodynamics algorithm, TANGO<sup>31</sup>, and position scoring matrices WALTZ<sup>27</sup> were used to calculate the respective scores (available at <http://tango.crg.es/tango.jsp> and <http://waltz.switchlab.org/>).

**Solid-phase peptide synthesis and characterization.** The SLP was synthesized using a standard Fmoc solid phase peptide synthesis using a Symphony peptide synthesizer (Protein Technologies, US). NMP was used as the coupling and washing solvent for the whole synthesis process. For each coupling step, Fmoc-amino acids were activated by 4eq HBTU/HOBt and 8eq DIPEA to react with the free N-terminal amino acids in the resin for one hour. After each coupling step, the Fmoc group was removed by four-fold treatment of 20% piperidine for ten minutes. TFA/water/TIPS (95/2.5/2.5) was used to simultaneously cleave the peptide off the resin and remove the side chain protecting groups. Peptides were purified by Prep-HPLC using Reprosil-Pur C18 column (10 μm, 250 × 22 mm) eluted with water-acetonitrile gradient 5% to 80% acetonitrile (10mM ammonium bicarbonate) in 40 minutes at flow-rate of 15.0 ml/min with UV detection at 220 nm. Purity was confirmed to be >90% by analytical RP-HPLC using Waters XBridge C18 column (5μm, 4.6 x 150mm) eluted with water-acetonitrile gradient 10% to 80% ACN (10mM ammonium bicarbonate) in 20 minutes at a flow rate of 1.0 ml/min and UV detection at 220 nm. Mass spectrometry (MS) analysis was performed using ESI-LC/MS instrument (Note S1-8).

## Control over the fibrillization yield by varying the oligomeric nucleation propensities of self-assembling peptides

---

Peptides for Cy5 modification were synthesized as described above with the addition of one lysine to the C-terminus. Peptides were then dissolved in 0.1M sodium bicarbonate solution (pH 8.3), and Cy5 NHS ester (10 eq in 1/10 volume of DMF) was added and incubated overnight. Cy5 conjugated peptides were purified by Prep-HPLC. Mass spectrometry (MS) analysis was performed using the ESI-MS instrument (Note S9-12).

**Sample preparation.** Peptide assemblies were prepared by dissolving peptide powders in nine volumes of 10mM sodium hydroxide in a 1.5ml Eppendorf tube. One volume of phosphate-buffered saline (10X) was added to make a sample of pH7.4±0.2 and a final concentration of 4mM. The solution was vortexed for 5 seconds and incubated statically for three days at room temperature before proceeding for measurements.

**X-ray diffraction (XRD).** XRD measurements were carried out on a Bruker-AXS D8 Advance powder X-ray diffractometer in Bragg–Brentano mode equipped with an automatic divergence slit (0.6 mm 0.3 °) and a PSD Vântec-1 detector. The radiation used was Co-K $\alpha$ 1,2,  $\lambda = 1.79026 \text{ \AA}$ , operated at 30 kV, 45 mA.

**Negative-staining TEM.** Samples prepared at 4 mM were diluted ten-fold with 1× PBS. Formvar/carbon-coated 400 mesh copper grid (Polysciences Inc.) was placed on top a droplet of 20  $\mu\text{L}$  of diluted samples. After 2 min incubation, the grid was washed three times with 0.2  $\mu\text{m}$  filtered mili-Q water and blotted dry with filter paper. Negative staining was performed for 1 min with 2% w/v uranyl acetate in water. The staining solution was blotted off with filter paper. Samples were imaged on a Tecnai 20 transmission electron microscope (FEI, Eindhoven, the Netherlands) equipped with a 4 K square pixel Eagle CCD camera (FEI, Eindhoven, the Netherlands) operated at 200 kV accelerating voltage.

**Atomic force microscopy (AFM) imaging.** AFM micrographs were recorded using a Bruker MultiMode 8 (ScanAsyst Air silicon nitride probes, spring constant 0.4 N/m, nominal tip radius 2 nm) and post-processed by a plane subtraction and line alignment. Three different spots (one in the main text, two in Figure S3) were measured on the sample to confirm uniformity and get a comprehensive view of the sample's features.

**Fluorescence Correlation Spectroscopy.** Fluorescence time traces were obtained by focusing a 640 nm laser line through a water immersion objective lens (60x Plan Apo VC, N.A. 1.2, Nikon, Japan) at ~50  $\mu\text{m}$  above the bottom of the glass-bottom 96-well plate (Grainer Bio-one, Frickenhausen, Germany). The measurement concentration was 1 $\mu\text{M}$  Cy5-SLP in 4mM of unlabeled SLPs, PBS (pH7.4). After 5 minutes of preparatory work, 50  $\mu\text{l}$  of the sample was measured with a confocal microscope (Nikon C1). A photon-counting instrument (PicoHarp 300, PicoQuant) was used to record time traces by binning the photon counts in intervals of 600 s. Autocorrelation curves were fitted by using Quickfit 3.0<sup>45</sup> using three-dimensional diffusion with a triplet as described below:

$$G(\tau) = \sum_{i=1}^N \alpha_i \left(1 + \frac{\tau}{\tau_{D_i}}\right)^{-1} \left(1 + \frac{\tau}{\gamma^2 \tau_{D_i}}\right)^{-\frac{1}{2}}$$

where  $\tau$  represents lag time,  $\tau_{D_i}$  is the diffusion time of the sample component, and  $\gamma$  is the aspect ratio of the focal volume ( $\sim 6$  for the common confocal microscope),  $N$  is the number of discretization steps to sample the maximum entropy distribution (MEM),  $\alpha_i$  is the relative amplitude of the component. The MEM methodology works towards the maximization of Shannon-Jaynes entropy ( $S$ ), which is defined as

$$S = - \sum_{j=1}^N \rho_j \ln \rho_j$$

where  $\rho_j$  represents the probability of detecting a component in the confocal volume.

$$\rho_j = \frac{\alpha_j \tau_{D_j}}{\sum_{i=1}^N \alpha_i \tau_{D_i}}$$

The diffusion coefficient  $D$  is derived from:

$$D = \frac{w_{xy}^2}{4\tau_D}$$

where  $w_{xy}$  is the lateral radius of the focal volume.  $w_{xy}$  was calibrated with a solution of Alexa-647 ( $D=330 \mu\text{m}^2/\text{s}$  at  $25^\circ\text{C}$ ), giving  $w_{xy} \sim 300 \text{ nm}$ .

**Solid-state NMR Spectroscopy.** 1D cross-polarization<sup>46</sup> and scalar<sup>47</sup> ssNMR experiments to probe rigid and mobile populations, respectively, were acquired at 11.7 T magnetic field (500 MHz ( $^1\text{H}$ -frequency)) with 10 kHz magic angle spinning (MAS) and 280 K sample temperature. 2D  $^{13}\text{C}$ - $^{13}\text{C}$  and 2D C $\alpha$ N for peptide assignments were also performed at similar conditions<sup>37</sup>. 2D Ca(N)H experiments for  $^{15}\text{N}$ T<sub>1rho</sub> relaxation studies were performed at 950 MHz magnetic field strength with 60 kHz.  $^{13}\text{C}$  was detected in the indirect dimension because of spectral overlap in the  $^{15}\text{N}$  dimension. The 2D  $^{13}\text{C}$ - $^{13}\text{C}$  PARIS<sup>37</sup> experiment with the CPMAS CryoProbe<sup>39</sup> to measure intermolecular peptide contacts was performed at 600 MHz and 12 kHz MAS using 700 ms magnetization transfer and a  $^1\text{H}$  recoupling amplitude of 6 kHz.

**NMR structure determination.** An NMR structure of the SLP1 dimer was obtained using HADDOCK version 2.4<sup>48</sup> using default parameters. In total, we used six NMR chemical shift-derived<sup>40</sup> dihedral angle restraints and sixty intermolecular NMR distance restraints. The resulting dimer structure was very well-defined and scored all within the same cluster.

### MD simulations

Coarse-grained (CG) MD simulations were performed with the Martini force field version 2.2<sup>49</sup> and GROMACS 5.0.4<sup>50</sup>. 36 SLPs were randomly immersed into a box with water beads to which 140 mM of NaCl was added (including neutralizing counterions). The systems were energy minimized and simulated for 3  $\mu\text{s}$  (150,000,000 steps of 25fs) using

## Control over the fibrillization yield by varying the oligomeric nucleation propensities of self-assembling peptides

---

standard settings for nonbonded interactions in an NPT ensemble with periodic boundary conditions. Simulated systems were weakly coupled to a pressure bath at 1 bar ( $\tau_p = 3$  ps) and coupled to a heat bath of 300 K temperature ( $\tau_T = 1.0$  ps) using Berendsen algorithm<sup>51</sup>. Since Ile and Leu share the same CG beads in the Martini force field, SLP1-2 and SLP3-4 share the same CG models. The secondary structure of the SLPs was assigned as a random coil with the martinize.py script. Random coil secondary structures were used in CGMD simulations to represent the initial steps of self-assembly. Polar P4 backbone beads were used to represent the N-terminal acetylate group. The final trajectories were transformed<sup>52</sup> to the atomistic coordinates and subject to the atomistic simulation.

Atomistic MD simulations were performed with the g53a6 force field<sup>53</sup> in GROMACS 5.0.4<sup>50</sup>. The fibril and oligomer models were first immersed into a box of a simple point charge (SPC) water<sup>54</sup> to which 140 mM of NaCl (including neutralizing counterions). The systems were energy minimized, then equilibrated for 100 ps in NVT ensemble at 300 K using V-rescale thermostat<sup>55</sup>. After that, 100 ps of NPT equilibration were performed at 1.0 bar using Parrinello–Rahman barostat<sup>56</sup>. Finally, the systems were simulated for 100 ns without restraints. The trajectories are available as Supplementary Data 1.

**Steered MD simulation.** Steered MD simulations were performed with the g53a6 force field<sup>53</sup> in GROMACS 4.5.5<sup>50</sup>. The equilibrated (100ns) structures from the atomistic MD simulation were transferred to larger rectangular boxes of SPC water, to which 140 mM of NaCl was added (including neutralizing counterions). The systems were energy minimized, then briefly equilibrated for 100ps in NVT ensemble at 300 K, followed by 100 ps in an NPT ensemble at 1.0 bar. After that, 200 ps of NVE ensemble was performed with position restrained peptides to optimize the charged side-chain orientations. Following the NVE equilibration, 1 SLP was pulled-out from the core of each structures along x-coordinate using a force constant of 1000 kJ mol<sup>-1</sup>nm<sup>2</sup> and pull-rate of 0.01 nm ps<sup>-1</sup>. The other 35 SLPs were constrained by applying a harmonic force along the x-direction. The measurements of force and displacement of individual trajectories were saved every 10 fs. From these recorded trajectories, we derived the potential of mean force (PMF) profiles using Jarzisky's equality<sup>57, 58</sup>. The trajectories are available in Supplementary Data 1.

### 5. Data availability

The MD trajectories used in this study are available as Supplementary Data 1. Other related data that support the findings of this study are available from the corresponding authors upon reasonable request.

### 6. Code availability

WALTZ and TANGO are freely accessible for academic and non-profit users at <http://tango.crg.es/tango.jsp> and <http://waltz.switchlab.org/>. QuickFit 3.0 is freely accessible for academic and non-profit users at <https://github.com/jkriege2/QuickFit3>.

### 7. Competing interests

There are no conflicts to declare

### 8. Acknowledgments

C.Y.J.L. acknowledges the support from the European Union (Horizon 2020 NANOMED Grant 676137). We thank Lione Willems (Wageningen University, The Netherlands) for her support in AFM and the Netherlands Center for Multiscale Catalytic Energy Conversion (MCEC), an NWO Gravitation program funded by the Ministry of Education, Culture and Science of the government of The Netherlands, for the financial support with the AFM measurements; Javier Sastre Toraño (Utrecht University, The Netherlands) for his support in ESI-MS. Kevin Braeckmans (Ghent University, Belgium) for his advice on MEM analysis. M.W. acknowledges financial support (project numbers 723.014.003 and 711.018.001) from the Dutch Research Council (NWO). F.F. and F.G. acknowledge the support from the Italian Ministry of Health (Ricerca Corrente 2018-2020). The secondment of F.F. at Utrecht University was granted by the Erasmus Traineeship Program of University of Milano-Bicocca. We thank prof. dr. Alexander Kros (Leiden University, The Netherlands) for critically reviewing this manuscript before submitting it for publication.

### 9. Author contributions

C.Y.J.L., A.J.J.B. and M.W. contributed to the coarse-grained and atomistic molecular dynamics (MD) simulation. C.Y.L, F.F. and F.G. contributed to the Steered MD simulation. C.Y.J.L, H.Z. and K.R. contributed to the FCS measurement and analysis. L.D.M. and R.d. V. contributed to the AFM measurement. D.W. contributed to the XRD measurement. J.v.D. contributed to the negative-staining TEM measurement. J.M.S., B.V., M.W., A.H., B.P., R.K. contributed to the ssNMR measurements. C.Y.J.L., W.H., M.W. and E.M. provided advice on the design of the whole experiments, C.Y.J.L., M.W. and E.M. designed the research concept, managed the project and were the main contributors to the manuscript writing

## Control over the fibrillization yield by varying the oligomeric nucleation propensities of self-assembling peptides

---

### References

1. Zhang, S., Fabrication of novel biomaterials through molecular self-assembly. *Nature Biotechnology* **2003**, *21*, 1171.
2. Hudalla, G. A.; Sun, T.; Gasiorowski, J. Z.; Han, H.; Tian, Y. F.; Chong, A. S.; Collier, J. H., Gradated assembly of multiple proteins into supramolecular nanomaterials. *Nature Materials* **2014**, *13*, 829.
3. Bakker, M. H.; Lee, C. C.; Meijer, E. W.; Dankers, P. Y. W.; Albertazzi, L., Multicomponent Supramolecular Polymers as a Modular Platform for Intracellular Delivery. *ACS Nano* **2016**, *10* (2), 1845-1852.
4. Shah, R. N.; Shah, N. A.; Del Rosario Lim, M. M.; Hsieh, C.; Nuber, G.; Stupp, S. I., Supramolecular design of self-assembling nanofibers for cartilage regeneration. *Proceedings of the National Academy of Sciences* **2010**, *107* (8), 3293.
5. Tao, K.; Makam, P.; Aizen, R.; Gazit, E., Self-assembling peptide semiconductors. *Science* **2017**, *358* (6365).
6. Kumar, M.; Ing, N. L.; Narang, V.; Wijerathne, N. K.; Hochbaum, A. I.; Ulijn, R. V., Amino-acid-encoded biocatalytic self-assembly enables the formation of transient conducting nanostructures. *Nature Chemistry* **2018**, *10* (7), 696-703.
7. Sadownik, J. W.; Mattia, E.; Nowak, P.; Otto, S., Diversification of self-replicating molecules. *Nature Chemistry* **2016**, *8* (3), 264-269.
8. Ozawa, Y.; Sato, H.; Kayano, Y.; Yamaki, N.; Izato, Y.-i.; Miyake, A.; Naito, A.; Kawamura, I., Self-assembly of tripeptides into  $\gamma$ -turn nanostructures. *Physical Chemistry Chemical Physics* **2019**, *21* (21), 10879-10883.
9. Mendes, A. C.; Baran, E. T.; Reis, R. L.; Azevedo, H. S., Self-assembly in nature: using the principles of nature to create complex nanobiomaterials. *WIREs Nanomedicine and Nanobiotechnology* **2013**, *5* (6), 582-612.
10. O'Nuallain, B.; Shivaprasad, S.; Kheterpal, I.; Wetzel, R., Thermodynamics of A $\beta$ (1-40) Amyloid Fibril Elongation. *Biochemistry* **2005**, *44* (38), 12709-12718.
11. Gazit, E., Diversity for self-assembly. *Nature Chemistry* **2010**, *2* (12), 1010-1011.
12. Hsieh, M.-C.; Lynn, D. G.; Grover, M. A., Kinetic Model for Two-Step Nucleation of Peptide Assembly. *The Journal of Physical Chemistry B* **2017**, *121* (31), 7401-7411.
13. Yuan, C.; Levin, A.; Chen, W.; Xing, R.; Zou, Q.; Herling, T. W.; Challa, P. K.; Knowles, T. P. J.; Yan, X., Nucleation and Growth of Amino Acid and Peptide Supramolecular Polymers through Liquid-Liquid Phase Separation. *Angewandte Chemie International Edition* **2019**, *58* (50), 18116-18123.
14. Michaels, T. C. T.; Šarić, A.; Curk, S.; Bernfur, K.; Arosio, P.; Meisl, G.; Dear, A. J.; Cohen, S. I. A.; Dobson, C. M.; Vendruscolo, M.; Linse, S.; Knowles, T. P. J., Dynamics of oligomer populations formed during the aggregation of Alzheimer's A $\beta$ 42 peptide. *Nature Chemistry* **2020**, *12* (5), 445-451.
15. Childers, W. S.; Anthony, N. R.; Mehta, A. K.; Berland, K. M.; Lynn, D. G., Phase Networks of Cross- $\beta$  Peptide Assemblies. *Langmuir* **2012**, *28* (15), 6386-6395.
16. Liang, C.; Hsieh, M.-C.; Li, N. X.; Lynn, D. G., Conformational evolution of polymorphic amyloid assemblies. *Current Opinion in Structural Biology* **2018**, *51*, 135-140.
17. Sementilli, A.; Rengifo, R.; Kim, Y.; Liang, C.; Li, N.; Mehta, A.; Lynn, D., Liquid-like phases pre-order peptides for supramolecular assembly. *ChemSystemsChem* **2020**, *n/a* (n/a).

18. Anthony, N. R.; Mehta, A. K.; Lynn, D. G.; Berland, K. M., Mapping amyloid- $\beta$ (16-22) nucleation pathways using fluorescence lifetime imaging microscopy. *Soft Matter* **2014**, *10* (23), 4162-4172.
19. Korevaar, P. A.; George, S. J.; Markvoort, A. J.; Smulders, M. M. J.; Hilbers, P. A. J.; Schenning, A. P. H. J.; De Greef, T. F. A.; Meijer, E. W., Pathway complexity in supramolecular polymerization. *Nature* **2012**, *481* (7382), 492-496.
20. Mattia, E.; Otto, S., Supramolecular systems chemistry. *Nature Nanotechnology* **2015**, *10* (2), 111-119.
21. Pellarin, R.; Schuetz, P.; Guarnera, E.; Caflisch, A., Amyloid Fibril Polymorphism Is under Kinetic Control. *Journal of the American Chemical Society* **2010**, *132* (42), 14960-14970.
22. Vantomme, G.; Meijer, E. W., The construction of supramolecular systems. *Science* **2019**, *363* (6434), 1396.
23. Zhao, X.; Pan, F.; Xu, H.; Yaseen, M.; Shan, H.; Hauser, C. A. E.; Zhang, S.; Lu, J. R., Molecular self-assembly and applications of designer peptide amphiphiles. *Chemical Society Reviews* **2010**, *39* (9), 3480-3498.
24. Kathuria Sagar, V.; Chan Yvonne, H.; Nobrega, R. P.; Özen, A.; Matthews, C. R., Clusters of isoleucine, leucine, and valine side chains define cores of stability in high-energy states of globular proteins: Sequence determinants of structure and stability. *Protein Science* **2015**, *25* (3), 662-675.
25. Street, A. G.; Mayo, S. L., Intrinsic  $\beta$ -sheet propensities result from van der Waals interactions between side chains and the local backbone. *Proceedings of the National Academy of Sciences* **1999**, *96* (16), 9074.
26. Bhattacharjee, N.; Biswas, P., Position-specific propensities of amino acids in the  $\beta$ -strand. *BMC Structural Biology* **2010**, *10* (1), 29.
27. Maurer-Stroh, S.; Debulpaep, M.; Kuemmerer, N.; Lopez de la Paz, M.; Martins, I. C.; Reumers, J.; Morris, K. L.; Copland, A.; Serpell, L.; Serrano, L.; Schymkowitz, J. W.; Rousseau, F., Exploring the sequence determinants of amyloid structure using position-specific scoring matrices. *Nature methods* **2010**, *7* (3), 237-242.
28. Rad-Malekshahi, M.; Visscher, K. M.; Rodrigues, J. P.; de Vries, R.; Hennink, W. E.; Baldus, M.; Bonvin, A. M.; Mastrobattista, E.; Weingarth, M., The Supramolecular Organization of a Peptide-Based Nanocarrier at High Molecular Detail. *Journal of the American Chemical Society* **2015**, *137* (24), 7775-7784.
29. Nyrkova, I. A.; Semenov, A. N.; Aggeli, A.; Boden, N., Fibril stability in solutions of twisted  $\beta$ -sheet peptides: a new kind of micellization in chiral systems. *The European Physical Journal B - Condensed Matter and Complex Systems* **2000**, *17* (3), 481-497.
30. Aggeli, A.; Nyrkova, I. A.; Bell, M.; Harding, R.; Carrick, L.; McLeish, T. C. B.; Semenov, A. N.; Boden, N., Hierarchical self-assembly of chiral rod-like molecules as a model for peptide  $\beta$ -sheet tapes, ribbons, fibrils, and fibers. *Proceedings of the National Academy of Sciences* **2001**, *98* (21), 11857.
31. Fernandez-Escamilla, A. M.; Rousseau, F.; Schymkowitz, J.; Serrano, L., Prediction of sequence-dependent and mutational effects on the aggregation of peptides and proteins. *Nature biotechnology* **2004**, *22* (10), 1302-1306.
32. Yu, X.; Wang, Q.; Zheng, J., Structural determination of Abeta25-35 micelles by molecular dynamics simulations. *Biophysical journal* **2010**, *99* (2), 666-674.



## Control over the fibrillization yield by varying the oligomeric nucleation propensities of self-assembling peptides

---

33. Eigen, M.; Rigler, R., Sorting single molecules: application to diagnostics and evolutionary biotechnology. *Proceedings of the National Academy of Sciences* **1994**, *91* (13), 5740.
34. Sengupta, P.; Garai, K.; Balaji, J.; Periasamy, N.; Maiti, S., Measuring Size Distribution in Highly Heterogeneous Systems with Fluorescence Correlation Spectroscopy. *Biophysical Journal* **2003**, *84* (3), 1977-1984.
35. Levin, A.; Mason, T. O.; Adler-Abramovich, L.; Buell, A. K.; Meisl, G.; Galvagnion, C.; Bram, Y.; Stratford, S. A.; Dobson, C. M.; Knowles, T. P. J.; Gazit, E., Ostwald's rule of stages governs structural transitions and morphology of dipeptide supramolecular polymers. *Nature Communications* **2014**, *5*, 5219.
36. Jekhmane, S.; Prachar, M.; Pugliese, R.; Fontana, F.; Medeiros-Silva, J.; Gelain, F.; Weingarth, M., Design Parameters of Tissue-Engineering Scaffolds at the Atomic Scale. *Angewandte Chemie International Edition* **2019**, *58* (47), 16943-16951.
37. Weingarth, M.; Demco, D. E.; Bodenhausen, G.; Tekely, P., Improved magnetization transfer in solid-state NMR with fast magic angle spinning. *Chemical Physics Letters* **2009**, *469* (4), 342-348.
38. Garzoni, M.; Baker, M. B.; Leenders, C. M. A.; Voets, I. K.; Albertazzi, L.; Palmans, A. R. A.; Meijer, E. W.; Pavan, G. M., Effect of H-Bonding on Order Amplification in the Growth of a Supramolecular Polymer in Water. *Journal of the American Chemical Society* **2016**, *138* (42), 13985-13995.
39. Hassan, A.; Quinn, C. M.; Struppe, J.; Sergeyev, I. V.; Zhang, C.; Guo, C.; Runge, B.; Theint, T.; Dao, H. H.; Jaroniec, C. P.; Berbon, M.; Lends, A.; Habenstein, B.; Loquet, A.; Kuemmerle, R.; Perrone, B.; Gronenborn, A. M.; Polenova, T., Sensitivity boosts by the CPMAS CryoProbe for challenging biological assemblies. *Journal of Magnetic Resonance* **2020**, *311*, 106680.
40. Shen, Y.; Delaglio, F.; Cornilescu, G.; Bax, A., TALOS+: a hybrid method for predicting protein backbone torsion angles from NMR chemical shifts. *Journal of Biomolecular NMR* **2009**, *44* (4), 213-223.
41. Wei, G.; Su, Z.; Reynolds, N. P.; Arosio, P.; Hamley, I. W.; Gazit, E.; Mezzenga, R., Self-assembling peptide and protein amyloids: from structure to tailored function in nanotechnology. *Chemical Society reviews* **2017**, *46* (15), 4661-4708.
42. Cao, M.; Lu, S.; Zhao, W.; Deng, L.; Wang, M.; Wang, J.; Zhou, P.; Wang, D.; Xu, H.; Lu, J. R., Peptide Self-Assembled Nanostructures with Distinct Morphologies and Properties Fabricated by Molecular Design. *ACS Applied Materials & Interfaces* **2017**, *9* (45), 39174-39184.
43. De Baets, G.; Van Durme, J.; Rousseau, F.; Schymkowitz, J., A genome-wide sequence-structure analysis suggests aggregation gatekeepers constitute an evolutionary constrained functional class. *Journal of Molecular Biology* **2014**, *426* (12), 2405-2412.
44. Veith, K.; Martinez Molledo, M.; Almeida Hernandez, Y.; Josts, I.; Nitsche, J.; Löw, C.; Tidow, H., Lipid-like Peptides can Stabilize Integral Membrane Proteins for Biophysical and Structural Studies. *ChemBioChem* **2017**, *18* (17), 1735-1742.
45. Krieger, J. W.; Langowski, J., QuickFit 3.0 (compiled: 2015-10-29, SVN: 4465): A data evaluation application for biophysics , [web page] <http://www.dkfz.de/Macromol/quickfit/> [Accessed on 2019/04/17] **2010-2019**.
46. Jekhmane, S.; Medeiros-Silva, J.; Li, J.; Kümmerer, F.; Müller-Hermes, C.; Baldus, M.; Roux, B.; Weingarth, M., Shifts in the selectivity filter dynamics cause modal gating in K<sup>+</sup> channels. *Nature Communications* **2019**, *10* (1), 123.

47. Lewandowski, J. R.; Sass, H. J.; Grzesiek, S.; Blackledge, M.; Emsley, L., Site-Specific Measurement of Slow Motions in Proteins. *Journal of the American Chemical Society* **2011**, *133* (42), 16762-16765.
48. van Zundert, G. C. P.; Rodrigues, J. P. G. L. M.; Trellet, M.; Schmitz, C.; Kastiritis, P. L.; Karaca, E.; Melquiond, A. S. J.; van Dijk, M.; de Vries, S. J.; Bonvin, A. M. J. J., The HADDOCK2.2 Web Server: User-Friendly Integrative Modeling of Biomolecular Complexes. *Journal of Molecular Biology* **2016**, *428* (4), 720-725.
49. de Jong, D. H.; Singh, G.; Bennett, W. F. D.; Arnarez, C.; Wassenaar, T. A.; Schäfer, L. V.; Periole, X.; Tieleman, D. P.; Marrink, S. J., Improved Parameters for the Martini Coarse-Grained Protein Force Field. *Journal of Chemical Theory and Computation* **2013**, *9* (1), 687-697.
50. Abraham, M. J.; Murtola, T.; Schulz, R.; Páll, S.; Smith, J. C.; Hess, B.; Lindahl, E., GROMACS: High performance molecular simulations through multi-level parallelism from laptops to supercomputers. *SoftwareX* **2015**, *1-2*, 19-25.
51. Berendsen, H. J. C.; Postma, J. P. M.; van Gunsteren, W. F.; DiNola, A.; Haak, J. R., Molecular dynamics with coupling to an external bath. *The Journal of Chemical Physics* **1984**, *81* (8), 3684-3690.
52. Wassenaar, T. A.; Pluhackova, K.; Böckmann, R. A.; Marrink, S. J.; Tieleman, D. P., Going Backward: A Flexible Geometric Approach to Reverse Transformation from Coarse Grained to Atomistic Models. *Journal of Chemical Theory and Computation* **2014**, *10* (2), 676-690.
53. Oostenbrink, C.; Villa, A.; Mark, A. E.; Van Gunsteren, W. F., A biomolecular force field based on the free enthalpy of hydration and solvation: The GROMOS force-field parameter sets 53A5 and 53A6. *Journal of Computational Chemistry* **2004**, *25* (13), 1656-1676.
54. Berendsen, H. J. C.; Postma, J. P. M.; van Gunsteren, W. F.; Hermans, J., Interaction Models for Water in Relation to Protein Hydration. In *Intermolecular Forces: Proceedings of the Fourteenth Jerusalem Symposium on Quantum Chemistry and Biochemistry Held in Jerusalem, Israel, April 13-16, 1981*, Pullman, B., Ed. Springer Netherlands: Dordrecht, 1981; pp 331-342.
55. Bussi, G.; Donadio, D.; Parrinello, M., Canonical sampling through velocity rescaling. *The Journal of Chemical Physics* **2007**, *126* (1), 014101.
56. Parrinello, M.; Rahman, A., Polymorphic transitions in single crystals: A new molecular dynamics method. *Journal of Applied Physics* **1981**, *52* (12), 7182-7190.
57. Jarzynski, C., Nonequilibrium Equality for Free Energy Differences. *Physical Review Letters* **1997**, *78* (14), 2690-2693.
58. Jarzynski, C., Equilibrium free-energy differences from nonequilibrium measurements: A master-equation approach. *Physical Review E* **1997**, *56* (5), 5018-5035.
59. Ianiro, A. et al. Liquid-liquid phase separation during amphiphilic self-assembly. *Nature Chemistry* **11**, 320-328, doi:10.1038/s41557-019-0210-4 (2019).
60. Wang, Y. & Jardetzky, O. Probability-based protein secondary structure identification using combined NMR chemical-shift data. *Protein Science* **11**, 852-861, doi:10.1110/ps.3180102 (2002).

**Control over the fibrillization yield by varying the oligomeric nucleation propensities of self-assembling peptides**

---

## Supporting Information

### Control over the fibrillization yield by varying the oligomeric nucleation propensities of self-assembling peptides

Chun Yin Jerry Lau, Federico Fontana, Laurens D.B. Mandemaker, Dennie Wezendonk, Benjamin Vermeer, Alexandre M.J.J. Bonvin, Renko de Vries, Heyang Zhang, Katrien Remaut, Joep van den Dikkenberg, João Medeiros-Silva, Alia Hassan, Barbara Perrone, Rainer Kuemmerle, Fabrizio Gelain, Wim E. Hennink, Markus Weingarth\* and Enrico Mastrobattista\*

## Control over the fibrillization yield by varying the oligomeric nucleation propensities of self-assembling peptides

**Table S1: TANGO and WALTZ scoring**

To predict the aggregation and fibrillization propensity of the designer SLPs, the statistical thermodynamics algorithm TANGO and the position scoring matrices WALTZ were used to calculate the respective scores (available at <http://tango.crg.es/tango.jsp> and <http://waltz.switchlab.org/>).

### A) SLP1: Ac-VVVTTILLEE-COOH

Sequence	Ac	V	V	V	T	I	L	L	E	E
TANGO	0.00	96.23	98.61	98.89	98.69	98.69	74.31	27.73	0.00	0.00
WALTZ	/	97.66	97.66	97.66	97.66	97.66	97.66	97.66	/	/

### B) SLP3: Ac-VVVTLLEEE-COOH

Sequence	Ac	V	V	V	T	L	L	L	E	E
TANGO	0.00	94.98	97.33	97.41	97.41	97.41	73.34	27.36	0.00	0.00
WALTZ	/	86.29	86.29	86.29	86.29	86.29	86.29	86.29	/	/

### C) SLP2: Ac-VVVTTILLEEE-COOH

Sequence	Ac	V	V	V	T	I	L	L	E	E	E
TANGO	0.00	96.34	99.03	99.17	99.17	99.17	83.80	54.44	0.00	0.00	0.00
WALTZ	/	97.66	97.66	97.66	97.66	97.66	97.66	97.66	/	/	/

### D) SLP4: Ac-VVVTLLEEE-COOH

Sequence	Ac	V	V	V	T	L	L	L	E	E	E
TANGO	0.00	95.55	98.21	98.36	98.36	98.36	83.11	53.99	0.00	0.00	0.00
WALTZ	/	86.29	86.29	86.29	86.29	86.29	86.29	86.29	/	/	/

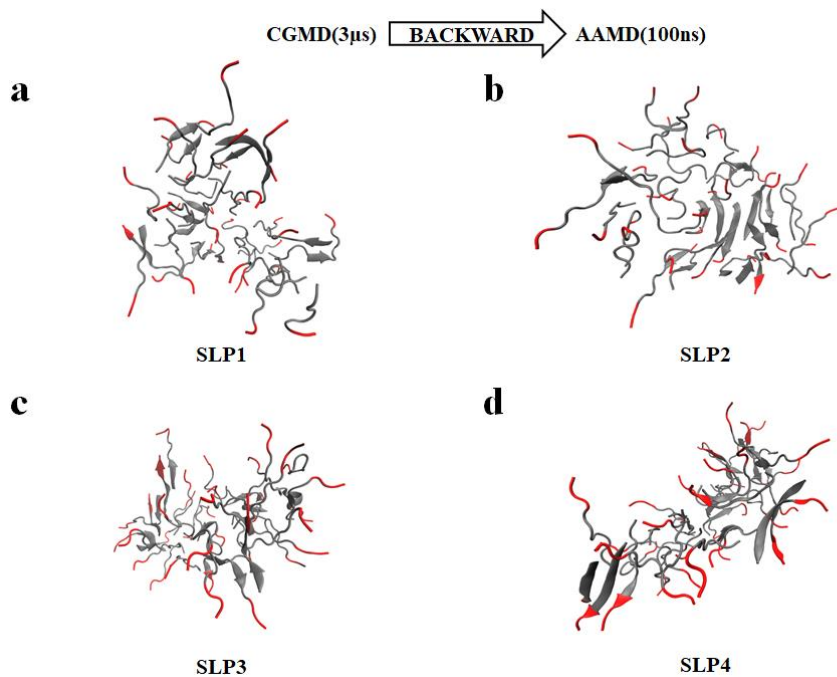


**Figure S1. Fine-grained micellar oligomers MD models.** Final trajectory of 100ns AAMD simulation after back transformation<sup>1</sup> from CGMD simulation.

## Control over the fibrillization yield by varying the oligomeric nucleation propensities of self-assembling peptides

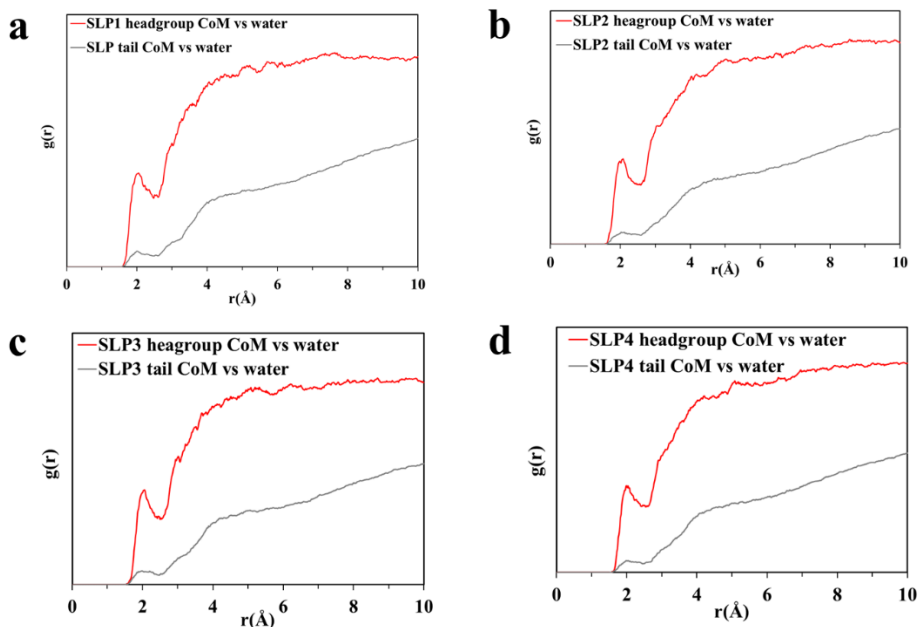
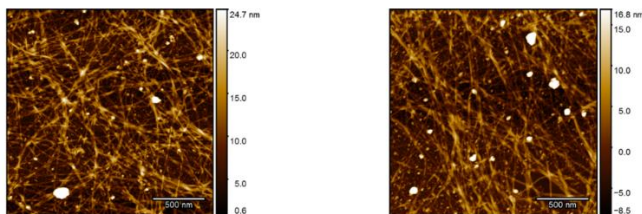
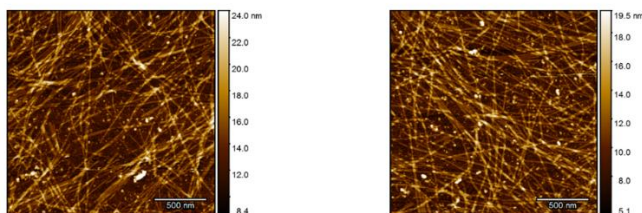


**Figure S2. Radial Distribution function (RDF) between Center of Mass (CoM) of tail/headgroup of SLP oligomers and water.** RDF functions of CoM of tail/headgroup and water is plotted for the final trajectory of fine-grained MD structures reported in Figure S1. It confirms the micellar arrangement in oligomers---tail clusters were desolvated, headgroups remained solvated.

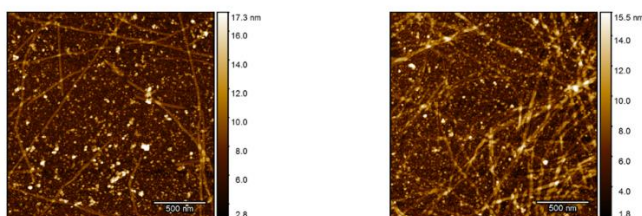
## a SLP1



## b SLP2



## c SLP3



## d SLP4

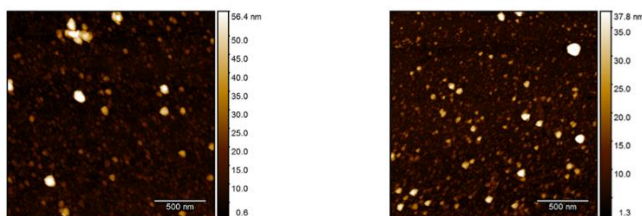
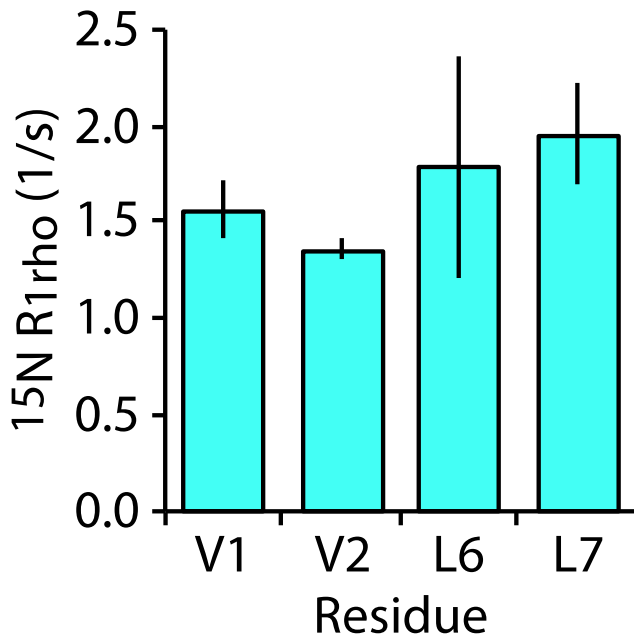


**Figure S3. Atomic force microscopy (AFM) imaging.** Freshly cleaved mica wafer was incubated for 5 min with 5 times diluted poly-L-lysine solution (150-300 kDa, 0.1%, Sigma-Aldrich, St. Louis, MO) and subsequently washed three times with MQ water. 4mM of peptide solution were diluted tenfold with PBS and a drop (50  $\mu$ L) of the solution was deposited on the coated mica and incubated for 5 minutes. The mica was washed three times with 500  $\mu$ L of dH<sub>2</sub>O to remove salts and dried under a stream of nitrogen. AFM micrographs were recorded using a Bruker MultiMode 8 (ScanAsyst Air silicon nitride probes, spring constant 0.4 N/m, nominal tip radius 2 nm) and post-processed by a plane subtraction and line alignment. Three different spots were measured on the sample to confirm uniformity and get a comprehensive view of the sample's features.

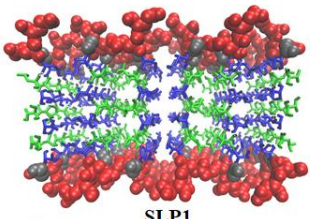
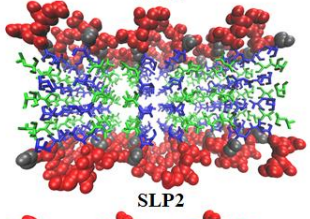
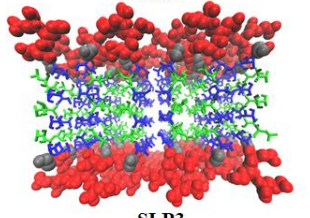


## Control over the fibrillization yield by varying the oligomeric nucleation propensities of self-assembling peptides

---



**Figure S4. Site-resolved  $^{15}\text{N } R_{1\rho}$  ssNMR dynamics of the SLP1 fibril.** Site-resolved  $^{15}\text{N } R_{1\rho}$  ssNMR dynamics of assembled SLP1 acquired at 60 kHz MAS and 950 MHz magnetic field (22.3 T  $^1\text{H}$  frequency). While the very slow relaxation shows that the  $\beta$ -structured residues are tightly assembled, the enhanced dynamics of Leu7 is in line with an interdigitated alignment in which the anionic C-terminus protrudes from the assembly. Spectra were measured with 2D  $^{13}\text{C}(^{15}\text{N})^1\text{H}$  experiments. The detour via the  $^{13}\text{C}$ -dimension was necessary due to spectral overlap of NH correlations.

	<u>Interface amino acids</u>	<u><math>\Delta G_{woct}</math> per cross-section (kcal/mol)</u>
 <p>SLP1</p>	Leu6 Thr4 Val2	-2.922
	Val2 Thr4 Leu6	
	Val1 Val3 Ile5 Leu7	
	Leu7 Ile5 Val3 Val1	-6.584
 <p>SLP2</p>	Leu6 Thr4 Val2	-2.922
	Val2 Thr4 Leu6	
	Val1 Val3 Leu5 Leu7	-6.84
	Leu7 Leu5 Val3 Val1	
 <p>SLP3</p>	Leu6 Thr4 Val2	-2.922
	Val2 Thr4 Leu6	
	Val1 Val3 Ile5 Leu7	
	Leu7 Ile5 Val3 Val1	-6.584

**Figure S5 Side chain interface assignment.** Molecular representation of two chemically anisotropic inter-side chain interfaces assigned for SLP1-3. Averaged hydrophobicity per amino acid and hydrophobicity per single cross-sectional face were calculated as the averaged value of free energies ( $\Delta G$ , kcal/mol) for transferring specific amino acid from water to n-octanol (woct)<sup>2</sup>.

## Control over the fibrillization yield by varying the oligomeric nucleation propensities of self-assembling peptides

---

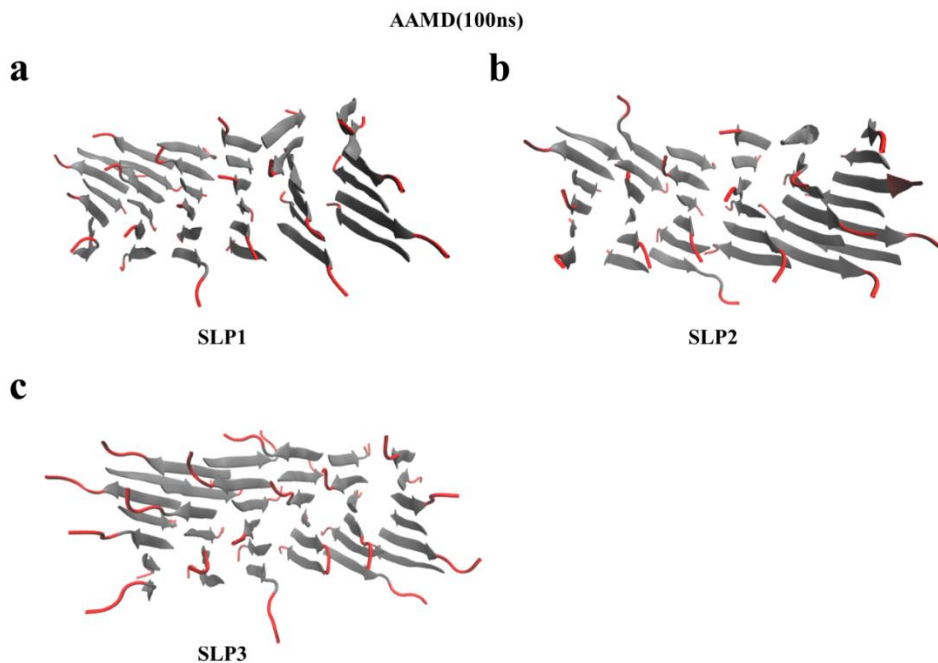


**Figure S6 Final (100ns) configuration of the equilibrated fibril molecular models.** The chirality of the L-amino acids leads to left-handed twist observed in the SLP models.

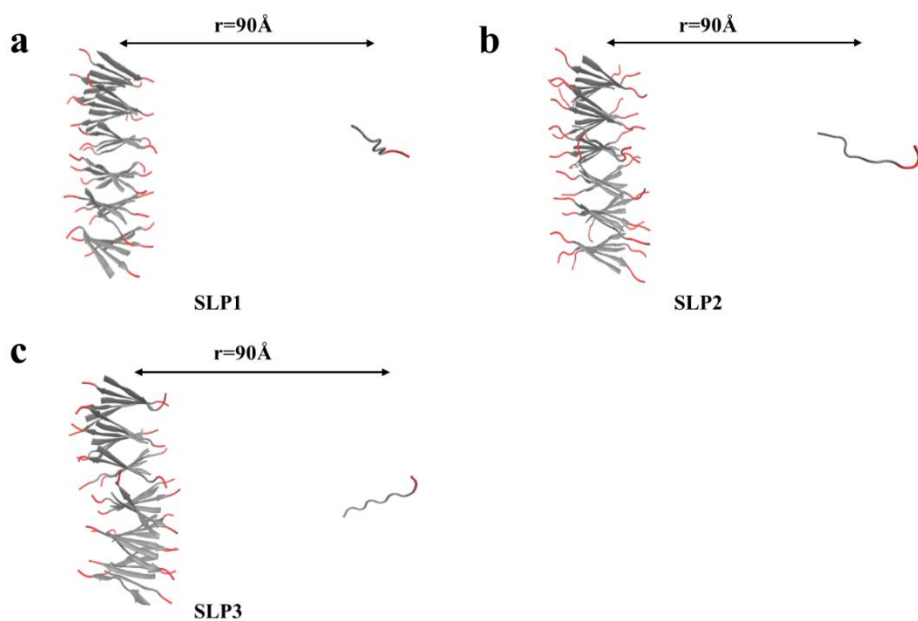


**Figure S7** Final trajectory snapshot of Steered MD simulation for SLP fibril structures. One  $\beta$ -sheet SLP was dragged from the core of the fibril models along the reaction coordinate  $r$  for  $90\text{\AA}$ .

## Control over the fibrillization yield by varying the oligomeric nucleation propensities of self-assembling peptides

---

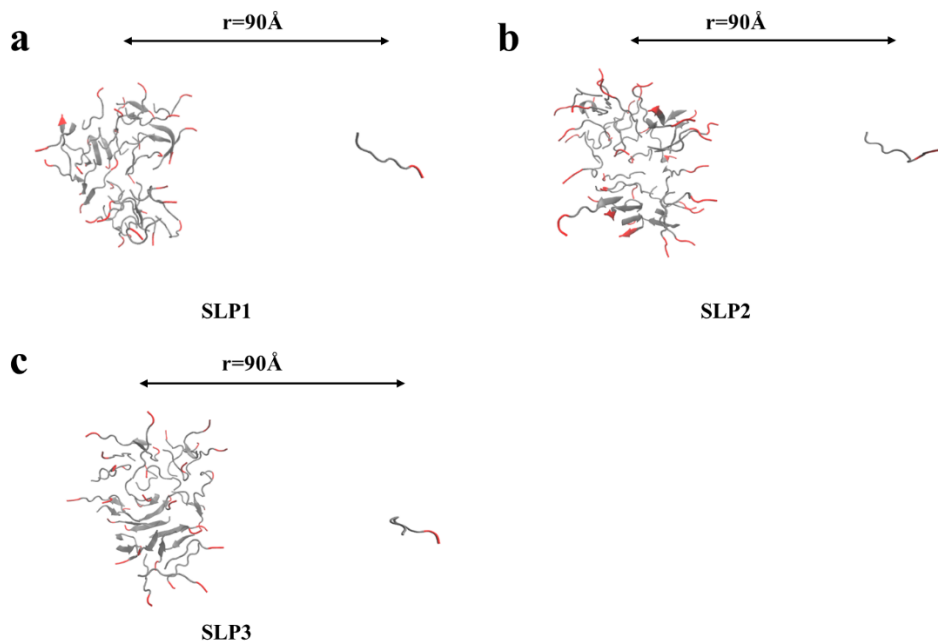


**Figure S8** Final trajectory snapshot of Steered MD simulation for SLP oligomeric structures. One random-coiled SLP was dragged from the core of the oligomer models along the reaction coordinate  $r$  for  $90\text{\AA}$ .

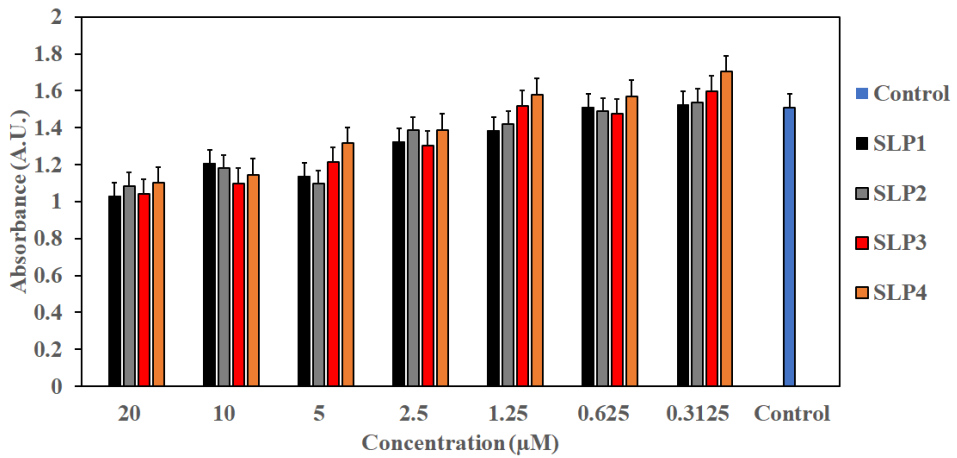


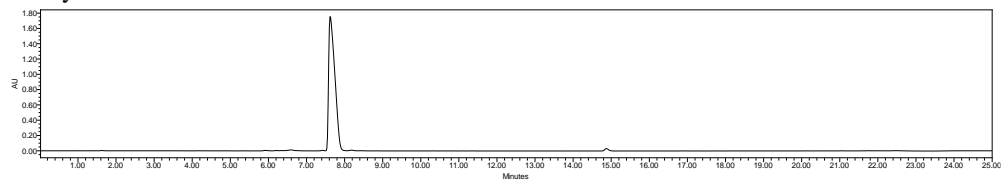
**Figure S9 Cell viability of exposing SLP assemblies at biological relevant concentration.** A431 cells (5000 cells/well) were exposed to SLP assemblies at a range of concentration (0.3125-20 μM) or phosphate buffered saline (1X, control) for 24 hours. The cell viability was then assessed with an MTS assay (absorbance at 490nm after 2 hours incubation). Results indicates that the working concentration for SLP 1-4 assemblies are recommended to be  $\leq 0.625\mu\text{M}$ . Values representative as average of a triplicate (mean  $\pm$  SEM).

# Control over the fibrillization yield by varying the oligomeric nucleation propensities of self-assembling peptides

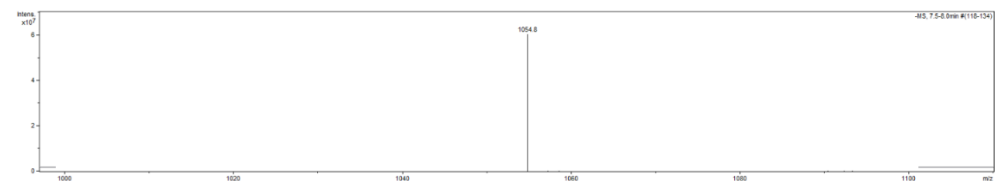
## Supplementary Note 1-12: HPLC-MS traces of synthesized SLPs

### Note S1. SLP1: Ac-VVVVTILLEE-COOH

#### Analytical RP-HPLC

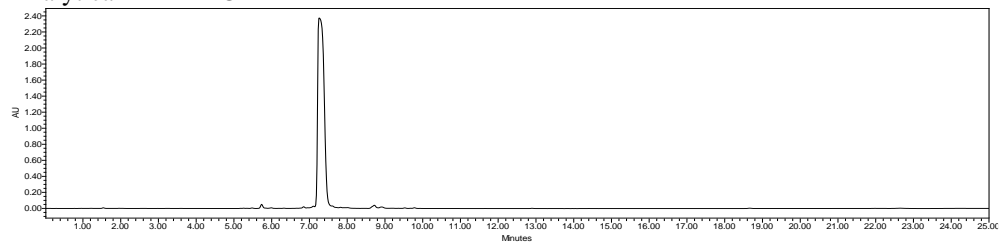


#### MS

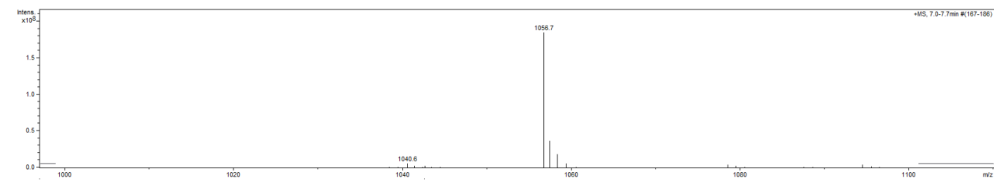


### Note S2. SLP2: Ac-VVVTLLEE-COOH

#### Analytical RP-HPLC



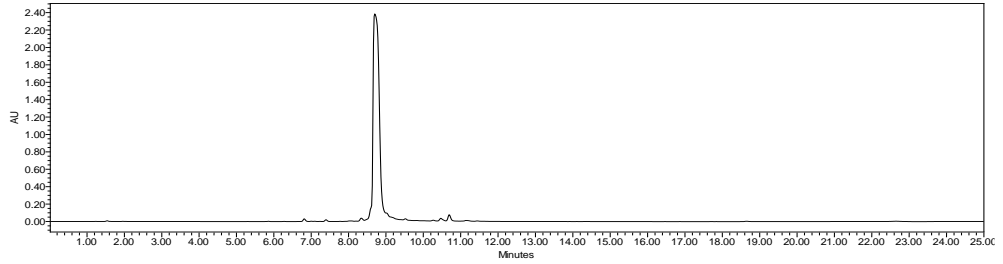
#### MS



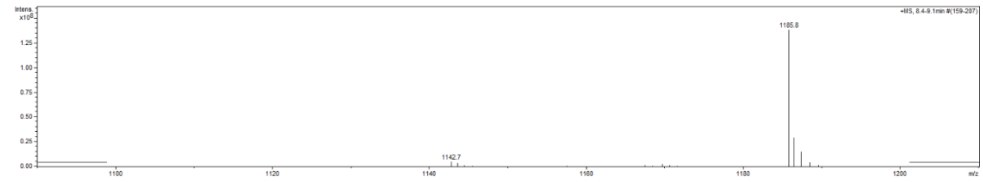
## Chapter 3

### Note S3. SLP3: Ac-VVVVTILLEEE-COOH

#### Analytical RP-HPLC

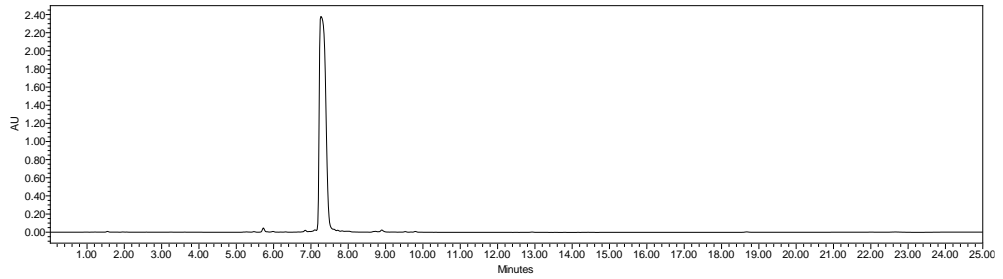


#### MS

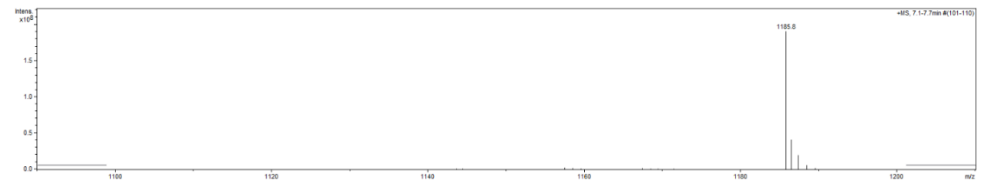


### Note S4. SLP4: Ac-VVVTLLEEE-COOH

#### Analytical RP-HPLC



#### MS

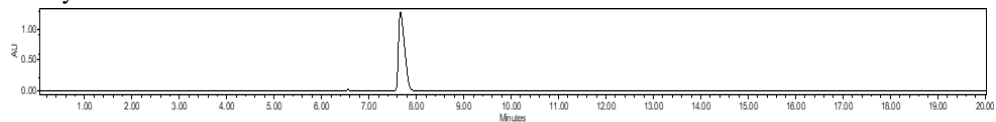




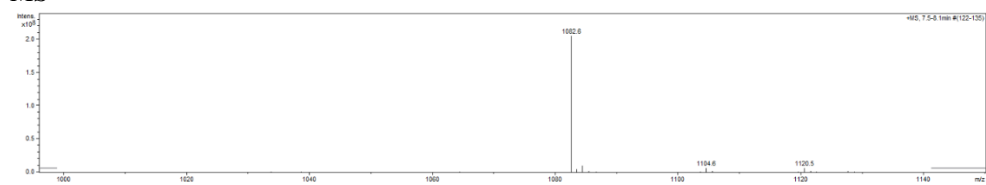
## Control over the fibrillization yield by varying the oligomeric nucleation propensities of self-assembling peptides

**Note S5.** SLP1: Ac-VVVTILLEE-COOH (isotopic  $^{13}\text{C}$ ,  $^{15}\text{N}$  labeling)

Analytical RP-HPLC

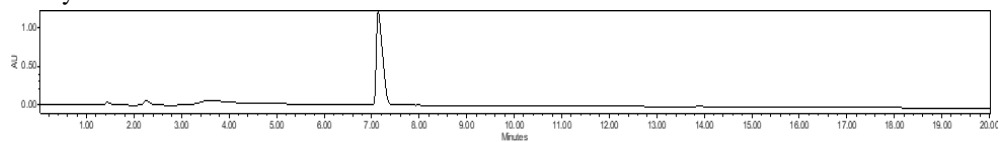


MS

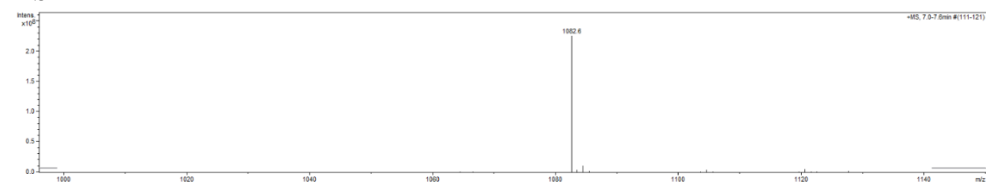


**Note S6.** SLP2: Ac-VVVTLLLEE-COOH (isotopic  $^{13}\text{C}$ ,  $^{15}\text{N}$  labeling)

Analytical RP-HPLC



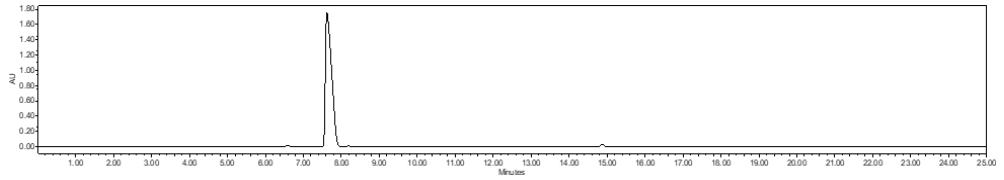
MS



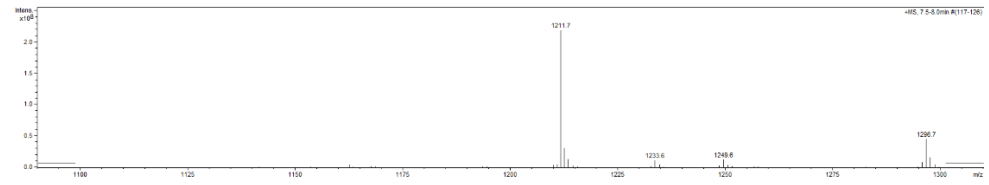
## Chapter 3

**Note S7.** SLP3: Ac-VVVTILLEEEE-COOH (isotopic  $^{13}\text{C}$ ,  $^{15}\text{N}$  labeling)

Analytical RP-HPLC

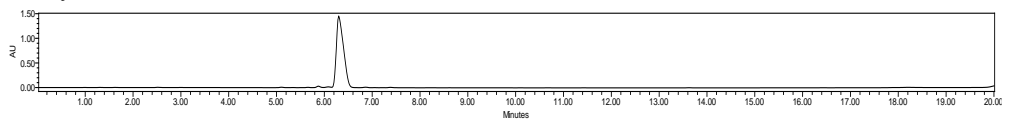


MS

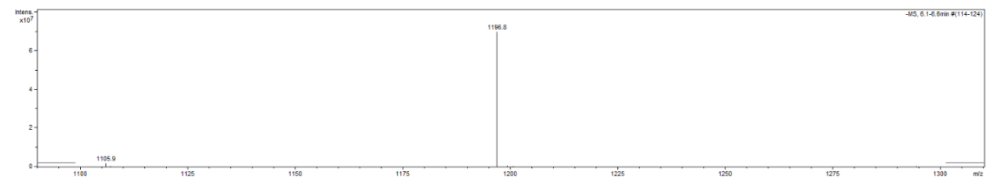


**Note S8.** SLP4: Ac-VVVTLLEEEE-COOH (isotopic  $^{13}\text{C}$ ,  $^{15}\text{N}$  labeling)

Analytical RP-HPLC



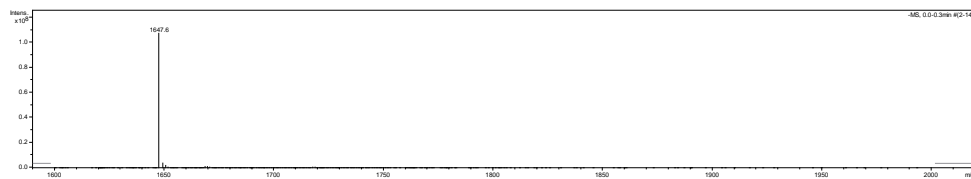
MS



# Control over the fibrillization yield by varying the oligomeric nucleation propensities of self-assembling peptides

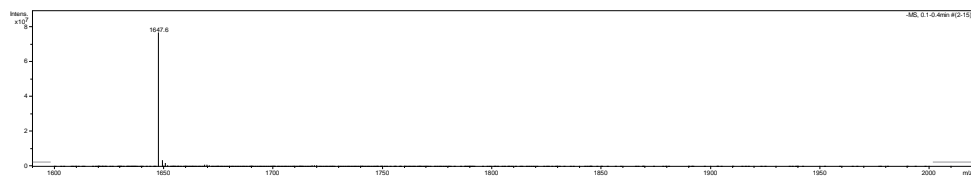
**Note S9.** SLP1: Ac-VVVVTTILLEEK(Cy5)-COOH

MS



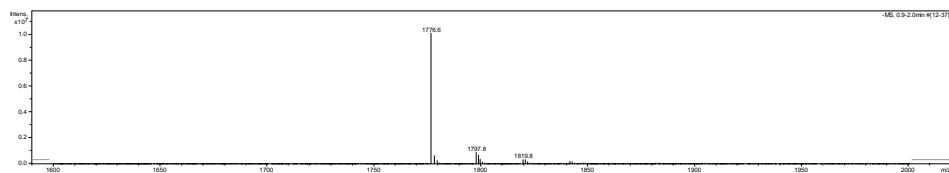
**Note S10.** SLP2: Ac-VVVVTLLEEK(Cy5)-COOH

MS



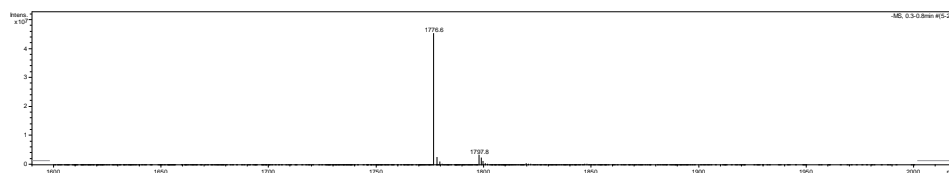
**Note S11.** SLP3: Ac-VVVVTTILLEEEK(Cy5)-COOH

MS



**Note S12.** SLP4: Ac-VVVVTLLEEEK(Cy5)-COOH

MS



### Supplementary References

- 1 Wassenaar, T. A., Pluhackova, K., Böckmann, R. A., Marrink, S. J. & Tieleman, D. P. Going Backward: A Flexible Geometric Approach to Reverse Transformation from Coarse Grained to Atomistic Models. *Journal of Chemical Theory and Computation* **10**, 676-690, doi:10.1021/ct400617g (2014).
- 2 Wimley, W. C., Creamer, T. P. & White, S. H. Solvation Energies of Amino Acid Side Chains and Backbone in a Family of Host–Guest Pentapeptides. *Biochemistry* **35**, 5109-5124, doi:10.1021/bi9600153 (1996).

# **Chapter 4**

## **The hierarchical structure of peptide nanofibers formed by self-assembly**

Chun Yin Jerry Lau<sup>1</sup>, Stuart C. Howes<sup>2</sup>, Wim E. Hennink<sup>1</sup>, Enrico Mastrobattista<sup>1</sup>

<sup>1</sup>*Department of Pharmaceutics, Utrecht Institute for Pharmaceutical Sciences, Utrecht University, 3584 CG Utrecht, The Netherlands*

<sup>2</sup>*Structural Biology, Bijvoet Centre, Utrecht University, Utrecht, The Netherlands, 3584 CH Utrecht, The Netherlands*

### Abstract

It has been shown in a variety of studies that peptide nanofibers are formed via hierarchical supramolecular assembly. The hierarchical organization of peptide nanofibers determines fiber morphology, which is critical for their biomedical applicability. In this study, we characterize the supramolecular organization of the nanofibers formed by self-assembly of a designer surfactant-like peptide (SLP 1) using cryo-EM analysis. We observed that SLP1 nanofibers displayed low twisting in physiological buffer (1XPBS, pH7.4, room temperature), which hinders the 3D reconstruction of the nanofibers using standard cryo-EM analysis. Taking a guide of the 2D class averages, we succeeded in unveiling the protofibril and fibrous organization for the SLP1 nanofibers. Furthermore, we highlight the possible cause of the low twisting of SLP1 nanofibers in light of the unveiled structural organization. Our findings offer guidance on the application of SLP1 nanofibers for tissue engineering and drug delivery purposes.

### 1. Introduction

Peptide nanofibers are formed via hierarchical supramolecular assembly<sup>1</sup>. The structural organization of peptides in the nanofibers is driven mainly by side-chain (van der Waals' forces) and backbone (hydrogen bonding) interactions<sup>1-3</sup>. The formation of peptide secondary structures ( $\alpha$ -helix,  $\beta$ -sheet) is the first step in directing the structural organization process. For peptide nanofibers, cross- $\beta$  structures are the most prevalent structures, which is specified by the orthogonal X-ray diffraction pattern at  $\sim 4.7\text{\AA}$  (inter- $\beta$ -strand) and  $10\text{\AA}$  (inter- $\beta$ -sheet). To arrive at the final energetically stable (kinetically trapped) fiber structure<sup>4</sup>, peptides assemble via a few metastable kinetic intermediate states rather than following a spontaneous thermodynamic process<sup>5</sup>. Once dissolved in water, peptides are entropically driven to form dynamic oligomeric particles, of which the majority of them are dissociated back into a monomeric state<sup>5</sup>. For the fibrilizing peptides, the dehydrated internal environment of the oligomeric particle cultivates the formation of cross- $\beta$  nucleates<sup>6</sup>. After such cross- $\beta$  nucleates are formed, the fibrous peptide structures are organized in the following hierarchical pathway: protofilaments are first assembled through nucleation-elongation of the cross- $\beta$  nucleates; subsequently, protofibrils are formed through the lateral association of the protofilaments; the final fibrous structures are formed via the longitudinal association of the protofibrils<sup>1</sup>.

Peptide nanofibers are used for biomedical applications such as drug delivery and tissue engineering. For example, high aspect ratio nanostructures containing bioactive moieties for cell adherence are employed as scaffolds for tissue engineering or delivery systems for antigen epitopes<sup>7</sup>. The viscoelastic nature of the fibrous network can be chemically attenuated, resulting in a mesh that resembles the extracellular matrix (e.g., stiffness of 200–5000Pa resembling the ECM of brain and skin<sup>8,9</sup>). Previous studies reveal that bioactive moieties can be incorporated into the peptide nanofibers in a modular fashion, bringing better bio-resemblance. Moreover, recent studies suggest that the spatial presentation of the bioactive moieties can influence the mechanotransduction of the cell embedded in the scaffold based on peptide nanofibers<sup>10</sup>. This suggests that the alteration in fiber morphology (e.g., helicity), which dictates this spatial orientation, can significantly alter the functionality of peptide nanofibers.

With recent developments of cryo-EM analysis, we can now study the polymorphic structures of peptide nanofiber with close to atomic resolution under near-native conditions. The hierarchical structures of several amyloid fibers are successfully characterized using this technique<sup>11,12</sup>, which offers us great insight into the complexity of the hierarchical process. For instance, the twist handedness of peptide nanofibers can be counteracted by the hierarchical process to generate nanofiber with a right-handed twist<sup>12</sup>. Recently, several molecular approaches have been reported for modulation of the fiber morphology<sup>13-15</sup>. However, the inter-relationship between molecular variations and the resultant supramolecular organization of the nanofibers at the protofibril and fibrous level remains largely elusive.<sup>16</sup> In the present work, we study the hierarchical fibrous structures assemble from a surfactant-like peptide (SLP1: Ac-VVVTILLLEE-COOH) using cryo-EM analysis. Since the protofilaments arrangement of SLP1 has been studied previously<sup>17</sup>, our focus is on the organization of protofilaments and fibrous organization in the SLP1 nanofibers.

**2. Results and Discussion**

**Low-twisted nanofiber assembled at physiological buffer.** Physiological buffers, such as phosphate-buffered saline (PBS), were frequently employed as solutes for biomedical applications of peptide nanofibers. In agreement with our previous report<sup>17</sup>, cryo-EM images showed that SLP1 assemble into fibrous structures when dispersed in PBS (Figure 1). Interestingly, the SLP1 nanofibers displayed a much lower twist and had a considerably larger helical pitch ( $3200 \pm 200 \text{ \AA}$ ,  $N=50$ ) than the amyloid fibril structures reported in the literature, which generally have a much smaller helical pitch ( $<500 \text{ \AA}$ )<sup>11</sup>.

---

<b>Ac-VVVTILLEE-COOH</b>	
<b>Data Collection</b>	
Magnification	x130,000
Defocus range ( $\mu\text{m}$ )	-1.0 to -3.0
Voltage (kV)	300
Microscope	Krios
Camera	K2 Summit
Frame exposure time (s)	0.15
# movie frames	38
Total electron dose ( $e^-/\text{\AA}^2$ )	50
Pixel size ( $\text{\AA}$ )	1.09
<b>Reconstruction</b>	
Box size (pixel)	260
Inter-box distance ( $\text{\AA}$ )	26
# segments extracted	234,613
# segments after Class2D	230,025
Resolution ( $\text{\AA}$ )	3.97

---



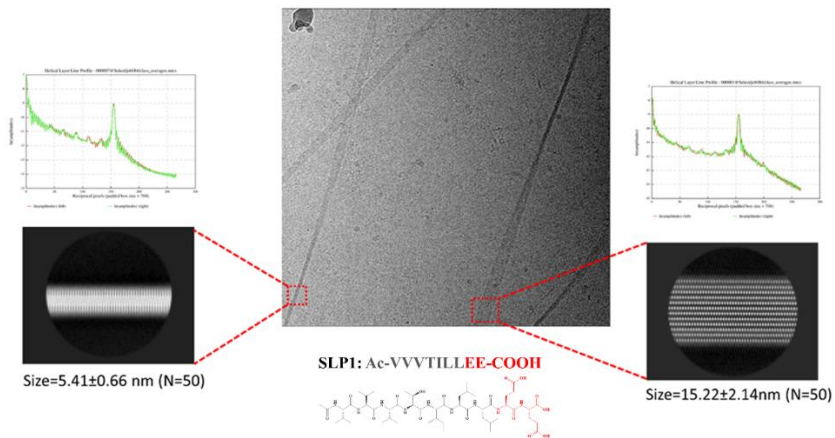


**Figure 1** Representative cryo-EM images of SLP1 nanofibers. The nanofibers displayed low helicity in the measurement condition (1XPBS). Two major 2D class averages were obtained from Relion. Each of the 2D classes displayed the same helical layer line profile, which demonstrates that they represent different views of the same nanofiber.

**Cryo-EM image analysis.** In a previous report, the supramolecular organization of a synthetic peptide nanofiber RADA-16 was scrutinized using solid-state NMR<sup>16</sup>. Though this study provided the molecular details of the organization of the RADA-16 protofilaments, the applied characterization strategy did not offer much structural insight into the protofibrils and fibrous organization. To investigate the protofibril/fibrous organization of SLP1 nanofibers, we proceeded to analyze the cryo-EM images using the statistical framework provided by REgularized LIkelihood OptimizatiON (RELION) 3.1. Using the helical reconstruction function, we dissected the fibrous structures with an overlapping box size of 260 Å. The 2D classification average showed a clear separation between the β-strand along the direction of the fibril axis. Additionally, we observed two major morphological classes within the 2D class averages, one class with a width of ~150 Å, another class with a width of 80 Å. This disparity in width suggested that they corresponded to different views of the fibrous structures: the flat and side view of the fiber. To confirm this, we performed the helical line profile analysis of these 2D classes. The helical line profile shows that the structures represented in these two 2D class averages shared the same interstrand distance of 5.0 Å.

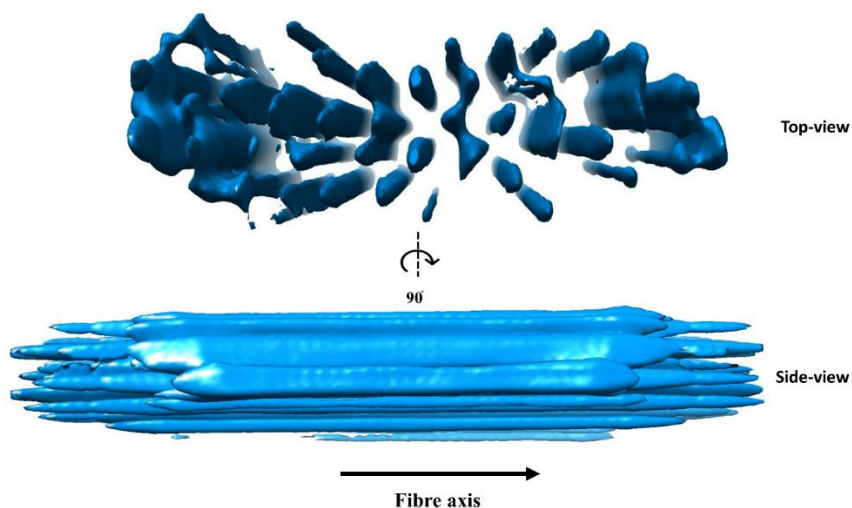


**Figure 2** 3D reconstruction of the SLP1 nanofiber using Relion. No  $\beta$ -strand separation was found in the reconstructed fibril models.

**Reconstruction of the hierarchical structure of peptide nanofibers.** Next, we proceeded to perform 3D classification. Using the `init3D` function, we generated a plausible starting fibril model for further analysis. However, after 2 rounds of 3D classification, we failed to observe  $\beta$ -strand separation in the fibril models, which is the benchmark for successful reconstruction (Figure 2). Further analysis suggested that such failure was due to the lack of view along with the cross-over pitch in the fibril. This was in good agreement with the 2D class averages, which shows only two major 2D classes.

To overcome this challenge of low helicity of the nanofibers, one common approach is to induce more twists through buffer exchange<sup>18</sup>. However, most fibrous structures existed in a kinetically trapped state rather than being in thermodynamic equilibrium<sup>4</sup>. An abrupt alteration of the buffer can trigger changes in the overall architecture of the peptide nanofibers, such as different constituents of protofilaments<sup>18</sup>. The possibility of structural alteration made the buffer exchange approach less suitable for this work. The aim here is to characterize the SLP1 fibrous structure in the application state, i.e., in PBS. Therefore, to derive the hierarchical organization of the SLP1 nanofibers, we modeled our molecular placement with the help of two major 2D class averages observed. For hierarchical nanostructures, the stronger non-covalent interactions dictate the assembly of lower-level structures, while the weaker interactions are responsible for the higher level of structural organization<sup>1</sup>. Concerning SLP1 nanofibers, we dissected the hierarchical molecular interactions in the following way: protofilament assembly is driven by the cooperative backbone hydrogen bonding, and van der Waals interactions induced by hydrophobic side chain faces (Val1, Val3, Ile5, Leu7)<sup>1</sup>; the protofibrils organization involved the interaction between side-chain faces (Val2, Thr4, Leu6)<sup>1</sup>; finally, the fibrous organization involved the edge-to-edge  $\beta$ -strand interactions. Using this organizational framework, we took a guide on the 2D class averages

## The hierarchical structure of peptide nanofibers formed by self-assembly

to reconstruct the molecular model of SLP1 nanofiber. In the flat-view of the 2D class average, we observed lateral alignment of 12  $\beta$ -sheets (Figure 1). Knowing that each protofilament consisted of 2  $\beta$ -sheets, we, therefore, assigned the protofibrils as composed of 6 protofilaments (Figure 3). Regarding the longitudinal association between the protofibrils, we observed two periodic structures in the side view of the 2D class averages (Figure 1). This suggests that the nanofiber structures consist of lateral association between two protofibrils (Figure 3). It is interesting to note that, though the flanking charged residues (glutamate dimers) were mutually repulsive, the longitudinal association could still be observed between the SLP1 protofibrils. One plausible explanation is the charge shielding effect caused by counterions presented in the buffer, which allows the association of protofibrils to take place.

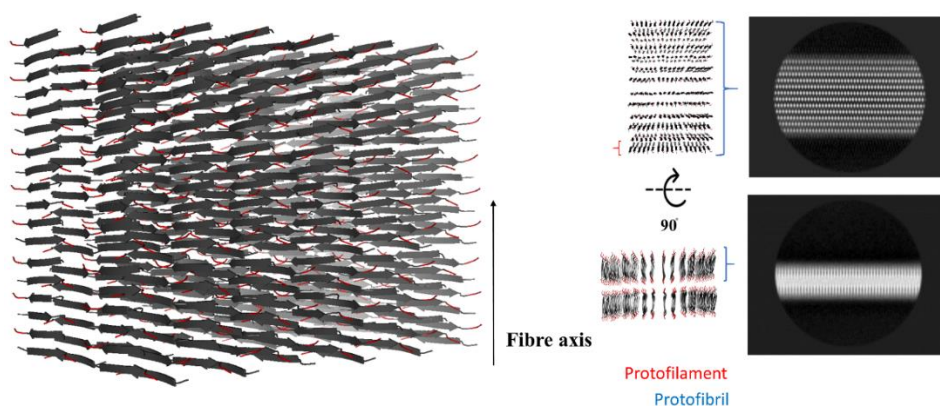


**Figure 3 Molecular model of an SLP1 nanofiber reconstructed based on the 2D class averages.** In the flat view 2D class (top), we observed lateral alignment of 12  $\beta$ -sheets, which is consistent with the association of 6 protofilaments. In the side view (bottom), we observed alignment of two periodic structures, which accounted for an association of 2 protofibrils

**Potential biomedical applications of SLP1 nanofibers.** Having unveiled the structural details of the SLP1, we can conjecture the potential fitting biomedical applications for the SLP1 nanofibers. First of all, we show that the SLP1 nanofibers have a low helical twist. Knowing that the helical twist of nanofibers was responsible for limiting the infinite growth of nanofibers both in the lateral and longitudinal direction, the comparatively low twist of the SLP1 nanofibers indicated that SLP1 has a low propensity for driving unidirectional growth of supramolecular assemblies. This low incentive for unidirectional growth can be attributed to the lack of directional non-covalent interactions, such as  $\pi$ - $\pi$ -stacking<sup>19</sup> and electrostatic attractions<sup>20-22</sup> in the side chain interface (van der Waals forces only). Besides, the counterion charge shielding of the mutually repulsive headgroup interactions also caused a lower incentive for the infrastructural twisting<sup>15, 23</sup>. Since nanofibers with low twisting can mechanically incur higher stem cell osteogenic potential through the activation of nuclear YAP<sup>10</sup>, SLP1 nanofibers are, therefore, a good candidate for tissue engineering. Secondly, for functionalizing SLP1 nanofibers with bioactive moieties that potentially interact with cells, our structural analysis showed that half of the displayed bioactive moieties

will likely be buried in the core of the hierarchical fibrous structures. Since effective cell activation typically requires a regulated display of multiple bioactive moieties, our structural analysis can serve as a guide on deciding the optimal ratio of functionalized vs non-functionalized SLP1 peptides for achieving optimal spacing. Thirdly, our structural analysis unveils that a hydrophilic pocket is present between two protofibrils. This hydrophilic channel can be potentially employed for the deposition of positively charged hydrophilic drugs (Figure 4). Lastly, knowing that structural flexibility is one major added value of using soft matter over rigid nanomaterials, it would be interesting to study the rigidity of peptide nanofibers with different degree of sophistication of structural ordering and correlate this to their bioactivity.

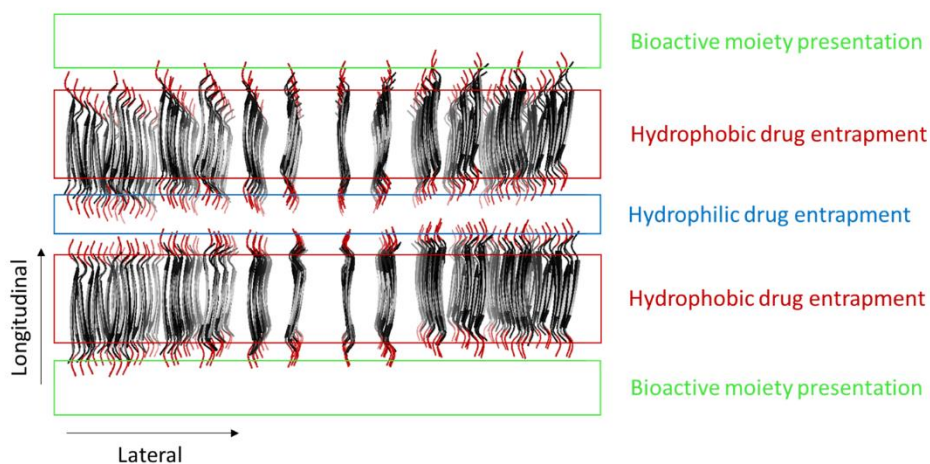


**Figure 4 Compartments of SLP1 nanofibers for various biomedical applications.** The green compartments may be used to display bioactive moieties, *e.g.*, for cell adhesion. The red compartments may provide hydrophobic drug entrapment in the inter- $\beta$  sheets. The blue compartment is suitable for potential hydrophilic drug entrapment.

### 3. Conclusion

In summary, we report the characterization of the supramolecular organization of a nanofiber assembled with a synthetic SLP1 peptide using cryo-EM analysis. Based on the 2D class averages derived with Relion analysis, we unveil the protofibril and fibrous organization in SLP1 nanofibers. We outline the plausible reasons for the low twisting of SLP1 nanofibers in PBS. Based on the characterized structural properties, we outline the functional implications of SLP1 nanofiber towards tissue engineering and drug delivery. Demonstrating the feasibility of reconstructing low-twisting peptide nanofibers paves the way for further structural investigations of other hierarchical nanofiber structures based on synthetic peptides.

### 4. Materials and Methods

**Materials.** Preloaded Fmoc-Glu(Otbu)-Wang resin was purchased from Novabiochem GmbH (Hohenbrunn, Germany), 2-(1H-Benzotriazol-1-yl)-1,1,3,3-tetramethyluronium hexafluorophosphate (HBTU) and 9-fluorenylmethoxycarbonyl (Fmoc)-protected amino acids were purchased from Iris Biotech (Marktredwitz, Germany). Peptide grade N-methyl-2-pyrrolidone (NMP), dichloromethane (DCM), piperidine, N,N-diisopropylethylamine (DIPEA), and HPLC grade acetonitrile were purchased from Biosolve BV (Valkenswaard, Netherlands). 1-hydroxy-benzotriazole hydrate (HOBt), triisopropylsilane (TIPS), trifluoroacetic acid (TFA), BioUltra grade ammonium bicarbonate, and sodium bicarbonate were purchased from Sigma-Aldrich Chemie BV (Zwijndrecht, Netherlands)

**Peptide synthesis.** Peptides were synthesized with standard Fmoc-solid-based chemistry and purified by Prep-RP-HPLC. Analytical RP-HPLC-MS was used to determine peptides' purity (>90% purity, Note S1).

**Sample preparation.** Purified synthetic surfactant-like peptide (>90% purity) was first dissolved in 450 $\mu$ l of 10mM sodium hydroxide solution. Subsequently, 50 $\mu$ l of 10X Dulbecco's PBS (27mM KCl, 15mM KH<sub>2</sub>PO<sub>4</sub>, 1380mM NaCl, 80mM Na<sub>2</sub>HPO<sub>4</sub>) was added to the solution to make the final concentration of peptide be 4mM (pH 7.2-7.6). The peptide solution was incubated for 3 days at 37°C before proceeding to subsequent measurements.

**Cryo-EM grid preparation.** A 5  $\mu$ l drop of the sample was placed on the surface of a glow-discharged 300 mesh Quantifoil R2/2 holey carbon grid (Quantifoil Micro Tools GmbH, Jena, Germany) for 30s held by the Vitrobot mark IV tweezer (FEI, Eindhoven, the Netherlands). Before introducing the sample into the Vitrobot, the environmental chamber of the Vitrobot was equilibrated at room temperature (22°C), and humidity was set at 100%. Samples were blotted for 4s at blot force 6. Grids were then released, plunged into liquid ethane at its freezing point, and stored under liquid nitrogen before imaging.

**Cryo-EM data collection.** Data collection was performed on a Titan Krios (FEI, Eindhoven, the Netherlands) transmission electron microscope equipped with a K2-Summit detector (Gatan) and operated at 300 kV accelerating voltage. Movies were collected using EPU (FEI) in superresolution counting mode, at a nominal magnification of 130,000 $\times$ , corresponding to a pixel size of 1.09Å at the specimen level. Further details were reported in Table 1

**Molecular model reconstruction.** The acquired super-resolution movie frames were imported to Relion 3.0.3<sup>24</sup>. Drift and beam-induced motion were corrected with MotionCor2<sup>25</sup>. Gctf<sup>26</sup> was used to estimate the contrast transfer function. Fiber segments were manually picked. Segment extraction was performed with an inter-box distance of 26 Å and box size of 260 Å. Reference-free 2D classification was performed with 200 Å mask, regularization value of T=2. 2D class averages showing helical repeat along the fiber axis were selected and used for 3D reconstruction. The initial models were refined with the first round of 3D classification with K=1 and T=20. The initial models were low-pass filtered to 20 Å and

used as a starting reference. Initial values of twist ( $-0.193^\circ$ ) and rise (4.98 Å) were calculated from the crossover distance and the layer line profiles of the 2D classes. The initial helical imposition gave clear  $\beta$ -strand separation. The resulting primary model was classified in another round of 3D classification with  $K=3$  and  $T=20$ . The 3D classes (2 out of 3) gave clear  $\beta$ -strand separation were manually selected and used for another round of 3D classification with local optimization of helical twist and rise ( $K=3$ ,  $T=20$ ).

2D class averages showing two different views of the nanofiber were used as a reference for molecular model building. A helical line profile was performed to confirm that both views share the same helicity. 50 EM images were chosen to measure the width and thickness of nanofiber (Table S1). The molecular model was reconstructed by aligning peptide monomers with the two different views of the fibrous structure.

### 5. Acknowledgement

C.Y.J.L acknowledges the support from the European Union (Horizon 2020 NANOMED Grant 676137). We thank Willie Geerts for his support in cryo-EM measurement.

### 6. Author contributions

C.Y.J.L. and S.H. contributed to the cryo-EM measurement and analysis. C.Y.J.L., W.H., and E.M. provided advice on the design of the whole experiments, C.Y.J.L. and E.M. designed the research concept, managed the project and were the main contributors to the manuscript writing.

### References

1. Aggeli, A.; Nyrkova, I. A.; Bell, M.; Harding, R.; Carrick, L.; McLeish, T. C. B.; Semenov, A. N.; Boden, N., Hierarchical self-assembly of chiral rod-like molecules as a model for peptide  $\beta$ -sheet tapes, ribbons, fibrils, and fibers. *Proceedings of the National Academy of Sciences* **2001**, *98* (21), 11857.
2. Tsemekhman, K.; Goldschmidt, L.; Eisenberg, D.; Baker, D., Cooperative hydrogen bonding in amyloid formation. *Protein Science* **2009**, *16* (4), 761-764.
3. Sawaya, M. R.; Sambashivan, S.; Nelson, R.; Ivanova, M. I.; Sievers, S. A.; Apostol, M. I.; Thompson, M. J.; Balbirnie, M.; Wiltzius, J. J. W.; McFarlane, H. T.; Madsen, A. Ø.; Riekel, C.; Eisenberg, D., Atomic structures of amyloid cross- $\beta$  spines reveal varied steric zippers. *Nature* **2007**, *447*, 453.
4. Pellarin, R.; Schuetz, P.; Guarnera, E.; Caflich, A., Amyloid Fibril Polymorphism Is under Kinetic Control. *Journal of the American Chemical Society* **2010**, *132* (42), 14960-14970.
5. Michaels, T. C. T.; Šarić, A.; Curk, S.; Bernfur, K.; Arosio, P.; Meisl, G.; Dear, A. J.; Cohen, S. I. A.; Dobson, C. M.; Vendruscolo, M.; Linse, S.; Knowles, T. P. J., Dynamics of oligomer populations formed during the aggregation of Alzheimer's A $\beta$ 42 peptide. *Nature Chemistry* **2020**, *12* (5), 445-451.
6. Yuan, C.; Levin, A.; Chen, W.; Xing, R.; Zou, Q.; Herling, T. W.; Challa, P. K.; Knowles, T. P. J.; Yan, X., Nucleation and Growth of Amino Acid and Peptide Supramolecular Polymers through Liquid-Liquid Phase Separation. *Angewandte Chemie International Edition* **2019**, *58* (50), 18116-18123.
7. Rudra, J. S.; Tian, Y. F.; Jung, J. P.; Collier, J. H., A self-assembling peptide acting as an immune adjuvant. *Proceedings of the National Academy of Sciences of the United States of America* **2010**, *107* (2), 622-627.
8. Gelain, F.; Cigognini, D.; Caprini, A.; Silva, D.; Colleoni, B.; Donegá, M.; Antonini, S.; Cohen, B. E.; Vescovi, A., New bioactive motifs and their use in functionalized self-assembling peptides for NSC differentiation and neural tissue engineering. *Nanoscale* **2012**, *4* (9), 2946-2957.
9. Silva, D.; Natalello, A.; Sani, B.; Vasita, R.; Saracino, G.; Zuckermann, R. N.; Doglia, S. M.; Gelain, F., Synthesis and characterization of designed BMHP1-derived self-assembling peptides for tissue engineering applications. *Nanoscale* **2013**, *5* (2), 704-718.
10. Arslan, E.; Hatip Koc, M.; Uysal, O.; Dikecoglu, B.; Topal, A. E.; Garifullin, R.; Ozkan, A. D.; Dana, A.; Hermida-Merino, D.; Castelletto, V.; Edwards-Gayle, C.; Baday, S.; Hamley, I.; Tekinay, A. B.; Guler, M. O., Supramolecular Peptide Nanofiber Morphology Affects Mechanotransduction of Stem Cells. *Biomacromolecules* **2017**, *18* (10), 3114-3130.
11. Fitzpatrick, A. W. P.; Debelouchina, G. T.; Bayro, M. J.; Clare, D. K.; Caporini, M. A.; Bajaj, V. S.; Jaroniec, C. P.; Wang, L.; Ladizhansky, V.; Müller, S. A.; MacPhee, C. E.; Waudby, C. A.; Mott, H. R.; De Simone, A.; Knowles, T. P. J.; Saibil, H. R.; Vendruscolo, M.; Orlova, E. V.; Griffin, R. G.; Dobson, C. M., Atomic structure and hierarchical assembly of a cross- $\beta$  amyloid fibril. *Proceedings of the National Academy of Sciences* **2013**, *110* (14), 5468.

12. Liberta, F.; Loerch, S.; Rennegarbe, M.; Schierhorn, A.; Westermark, P.; Westermark, G. T.; Hazenberg, B. P. C.; Grigorieff, N.; Fändrich, M.; Schmidt, M., Cryo-EM fibril structures from systemic AA amyloidosis reveal the species complementarity of pathological amyloids. *Nature Communications* **2019**, *10* (1), 1104.
13. Hu, Y.; Lin, R.; Zhang, P.; Fern, J.; Cheetham, A. G.; Patel, K.; Schulman, R.; Kan, C.; Cui, H., Electrostatic-Driven Lamination and Untwisting of  $\beta$ -Sheet Assemblies. *ACS Nano* **2016**, *10* (1), 880-888.
14. Clover, T. M.; O'Neill, C. L.; Appavu, R.; Lokhande, G.; Gaharwar, A. K.; Posey, A. E.; White, M. A.; Rudra, J. S., Self-Assembly of Block Heterochiral Peptides into Helical Tapes. *Journal of the American Chemical Society* **2020**, *142* (47), 19809-19813.
15. Sangji, M. H.; Sai, H.; Chin, S. M.; Lee, S. R.; R Sasselli, I.; Palmer, L. C.; Stupp, S. I., Supramolecular Interactions and Morphology of Self-Assembling Peptide Amphiphile Nanostructures. *Nano Letters* **2021**.
16. Cormier, A. R.; Pang, X.; Zimmerman, M. I.; Zhou, H.-X.; Paravastu, A. K., Molecular Structure of RADA16-I Designer Self-Assembling Peptide Nanofibers. *ACS Nano* **2013**, *7* (9), 7562-7572.
17. Lau, C. Y. J.; Fontana, F.; Mandemaker, L. D. B.; Wezendonk, D.; Vermeer, B.; Bonvin, A. M. J. J.; de Vries, R.; Zhang, H.; Remaut, K.; van den Dikkenberg, J.; Medeiros-Silva, J.; Hassan, A.; Perrone, B.; Kuemmerle, R.; Gelain, F.; Hennink, W. E.; Weingarth, M.; Mastrobattista, E., Control over the fibrillization yield by varying the oligomeric nucleation propensities of self-assembling peptides. *Communications Chemistry* **2020**, *3* (1), 164.
18. Seuring, C.; Verasdonck, J.; Ringler, P.; Cadalbert, R.; Stahlberg, H.; Böckmann, A.; Meier, B. H.; Riek, R., Amyloid Fibril Polymorphism: Almost Identical on the Atomic Level, Mesoscopically Very Different. *The Journal of Physical Chemistry B* **2017**, *121* (8), 1783-1792.
19. Gazit, E., A possible role for  $\pi$ -stacking in the self-assembly of amyloid fibrils. *The FASEB Journal* **2002**, *16* (1), 77-83.
20. Mehta, A. K.; Lu, K.; Childers, W. S.; Liang, Y.; Dublin, S. N.; Dong, J.; Snyder, J. P.; Pingali, S. V.; Thiyagarajan, P.; Lynn, D. G., Facial Symmetry in Protein Self-Assembly. *Journal of the American Chemical Society* **2008**, *130* (30), 9829-9835.
21. Hsieh, M.-C.; Liang, C.; Mehta, A. K.; Lynn, D. G.; Grover, M. A., Multistep Conformation Selection in Amyloid Assembly. *Journal of the American Chemical Society* **2017**, *139* (47), 17007-17010.
22. Zhang, S.; Holmes, T.; Lockshin, C.; Rich, A., Spontaneous assembly of a self-complementary oligopeptide to form a stable macroscopic membrane. *Proceedings of the National Academy of Sciences of the United States of America* **1993**, *90* (8), 3334-3338.
23. Hall, D. M.; Bruss, I. R.; Barone, J. R.; Grason, G. M., Morphology selection via geometric frustration in chiral filament bundles. *Nature Materials* **2016**, *15* (7), 727-732.
24. He, S.; Scheres, S. H. W., Helical reconstruction in RELION. *Journal of Structural Biology* **2017**, *198* (3), 163-176.



25. Zheng, S. Q.; Palovcak, E.; Armache, J.-P.; Verba, K. A.; Cheng, Y.; Agard, D. A., MotionCor2: anisotropic correction of beam-induced motion for improved cryo-electron microscopy. *Nature Methods* **2017**, *14* (4), 331-332.
26. Zhang, K., Gctf: Real-time CTF determination and correction. *Journal of Structural Biology* **2016**, *193* (1), 1-12.

## Supplementary Information

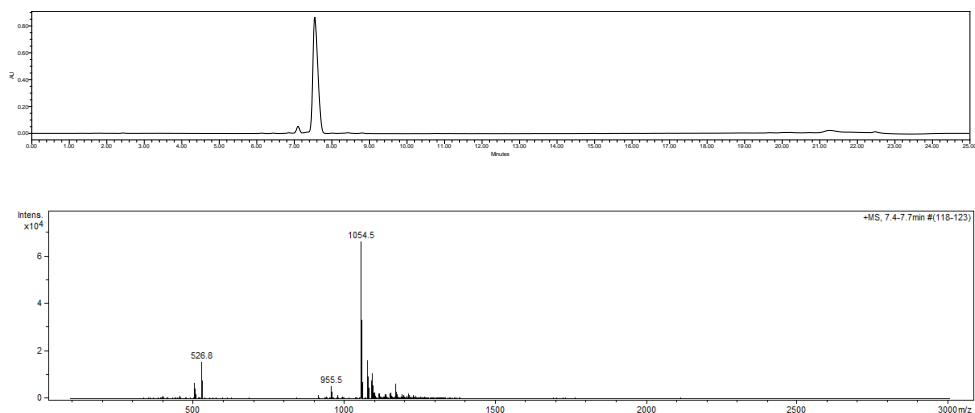
### The hierarchical structure of peptide nanofibers formed by self-assembly

Chun Yin Jerry Lau, Stuart C. Howes, Wim E. Hennink, Enrico Mastrobattista

### Note S1 HPLC-MS trace of SLP1

SLP1: Ac-VVVTILLEE-COOH (Theoretical mass=1056.3; mass found  $[M-H]^-$ =1054.5,  $[M-2H]^{2-}$ =526.8)

Purity was confirmed to be >90% by analytical HPLC (Xbridge C18 column, 4.6x150mm, 5 $\mu$ m) using eluted with water-acetonitrile gradient 5% to 80% ACN (10mM ammonium bicarbonate) in 20 minutes at flow rate 1.0 ml/min and UV detection at 220 nm. Mass spectrometry (MS) analysis was performed using micrOTOF-Q instrument running at negative mode.



## Chapter 4

---

**Table S1 Data table of nanofiber width and thickness measurement**

To validate the two major 2D classes averages observed are the representation of the SLP1 nanofiber in two different views, 50 images were chosen for nanofiber width and thickness measurement.

Image name	Width(nm)	Thickness(nm)
Follihole_20191018_1116-98289	13.7668	4.40
Follihole_20191018_1116-98290	14.1213	5.5150
	13.0072	4.11322
Follihole_20191018_1117-98291	12.4851	4.69586
Follihole_20191018_1121-98294	17.0542	5.72
	15.3593	5.2681
Follihole_20191018_1122-98296	15.00352	4.81578
	14.004	5.93024
Follihole_20191018_1125-98300	15.9125	4.87463
Follihole_20191018_1127-98301	14.9135	4.11322
	11.6991	3.51514
Follihole_20191018_1134-98312	12.1612	5.26821
Follihole_20191018_1136-98313	16.226	4.97117
Follihole_20191018_1145-98325	16.0315	3.72519
Follihole_20191018_1205-98351	15.0341	5.54937
Follihole_20191018_1211-98357	14.3417	5.51501
	15.4149	5.68474
Follihole_20191018_1214-98362	15.1663	5.93024
Follihole_20191018_1218-98366	14.6174	6.78257
Follihole_20191018_1218-98367	11.1415	5.93024
	19.2285	5.58352
Follihole_20191018_1224-98375	17.004	5.93024
Follihole_20191018_1225-98376	14.2018	5.46306
Follihole_20191018_1227-98379	16.4124	5.32206
Follihole_20191018_1245-98400	14.1951	6.28808
Follihole_20191018_1247-98402	13.1452	4.87463
Follihole_20191018_1259-98417	18.1713	6.05711
	17.2041	5.68474
Follihole_20191018_1259-98418	17.6405	5.86578
	18.385	6.43746
Follihole_20191018_1302-98421	19.4839	5.84955
	14.0876	6.05711
Follihole_20191018_1303-98422	17.6351	5.39302

## The hierarchical structure of peptide nanofibers formed by self-assembly

---

	17.44	4.97117
Follihole_20191018_1304-98424	15.3593	5.58352
	16.6937	6.28808
Follihole_20191018_1312-98433	15.8706	5.46306
Follihole_20191018_1320-98441	12.3473	5.25014
	10.7684	4.97117
	10.786	5.81697
	16.6024	5.46306
Follihole_20191018_1328-98449	17.9238	5.93024
Follihole_20191018_1335-98457	16.3427	4.93278
	17.0542	6.05711
Follihole_20191018_1336-98458	17.0263	5.86578
	13.08	5.32206
Follihole_20191018_1336-98459	15.7262	5.08459
Follihole_20191018_1345-98469	12.4699	5.25014
	16.0315	5.58352
Follihole_20191018_1346-98472	15.1098	5.68474



# Chapter 5

## Tuning surface charges of supramolecular nanofibers for induction of antigen-specific immune tolerance: an introductory study

Chun Yin Jerry Lau<sup>1</sup>, Naomi Benne<sup>2</sup>, Bo Lou<sup>1,3</sup>, Daniëlle ter Braake<sup>2</sup>, Esmeralda Bosman<sup>1</sup>, Nicky van Kronenburg<sup>1</sup>, Marcel Fens<sup>1</sup>, Wim E. Hennink<sup>1</sup>, Femke Broere<sup>2</sup>, Enrico Mastrobattista<sup>1</sup>

<sup>1</sup>*Utrecht Institute for Pharmaceutical Sciences, Department of Pharmaceutics, Faculty of Science, Utrecht University, Universiteitsweg 99, 3584 CG Utrecht, the Netherlands.*

<sup>2</sup>*Department of Infectious Diseases and Immunology, Faculty of Veterinary Medicine, Utrecht University, Yalelaan 1, 3584 CL Utrecht, the Netherlands*

<sup>3</sup>*Cardiovascular Research Institute, Department of Medicine, Yong Loo Lin School of Medicine, National University of Singapore, #08-01, MD6 Centre for Translational Medicine, 14 Medical Drive, 117599, Singapore*

### Abstract

Induction of antigen-specific immune tolerance has emerged as the next frontier in treating autoimmune disorders, including allergy and graft-vs-host reactions during transplantation. Nanostructures are widely under investigation as a platform for the coordinated delivery of critical components, i.e., the antigen epitope and tolerogenic agents, to the target immune cells and subsequently induce tolerance. In the present study, the utility of supramolecular peptide nanofibers to induce antigen-specific immune tolerance was explored. To study the influence of surface charges of the nanofibers towards the extent of the induced immune response, the flanking charge residues at both ends of the amphipathic fibrillization peptide sequences were varied. Dexamethasone, an immunosuppressive glucocorticoid drug, and model ovalbumin epitope were covalently linked at either end of the peptide sequences. It was shown that the functional extensions did not alter the structural integrity of the supramolecular nanofibers. Furthermore, the surface charges of the nanofibers were modulated by the inclusion of charged residues. Dendritic cell culture assays suggested that nanofiber of less negative  $\zeta$ -potential augmented the tolerogenic immune response. Conversely, nanofiber of more negative  $\zeta$ -potential resulted in a more robust tolerogenic response in in vivo studies. The discrepancy between the in vitro and in vivo results highlights the potential role of scavenger receptor Macrophage Receptor with COLlagenous structure (MARCO) in mediating the tolerogenic antigen presentation in macrophages, which can serve as a potential target for future development of tolerogenic immunotherapy.



# Tuning surface charges of supramolecular nanofibers for induction of antigen-specific immune tolerance: an introductory study

---

## 1. Introduction

Autoimmune disorders (e.g., allergy and graft-vs-host reactions during transplantation) are rising in developed and rapidly developing countries<sup>1</sup>. There is currently no cure for autoimmune disorders. Standard treatments of autoimmune disorders involve symptom alleviation through pharmacological intervention. However, most immunosuppressive interventions do not have a specific mode of action, which can undesirably lead to systemic immunodeficiency and life-changing side effects. Therefore, to incur higher disease specificity towards immunosuppression, antigen-specific immunotolerance has emerged as the next frontier in autoimmune disorder treatments<sup>2-4</sup>.

The establishment of antigen-specific immune tolerance requires 1) surface presentation of disease-specific antigen epitopes on antigen-presenting cells (APCs); and 2) steering APCs toward the tolerogenic phenotype, which leads to activation of antigen-specific regulatory T (Treg) cells. Nanomaterials are extensively explored as a platform for induction of antigen-specific immune tolerance, either through delivering antigen to APCs present in natural tolerogenic environments (e.g., liver)<sup>5,6</sup>, or co-delivery of tolerogenic pharmacological agents (e.g., dexamethasone) and antigens to the APCs. In particular, the latter approach can steer the recipient APCs toward a tolerogenic phenotype, thereby avoiding the "off-target" induction of pro-inflammatory response in the former approach<sup>7-9</sup> as well as limiting the systemic immunodeficient side effects, e.g., cancer promotion<sup>10</sup>. However, usage of conventional nanoparticles still encounters challenges in large-scale production<sup>11</sup> and stability and transport<sup>12,13</sup>.

Supramolecular peptide materials are extensively explored as immunomodulatory agents<sup>14,15</sup>. They represent promising vaccination agents thanks to their multivalent functionality<sup>16,17</sup>, simple preparation procedure, and high thermal stability<sup>18,19</sup>. Upon subcutaneous injection, these  $\beta$ -sheet rich nanofibers (<10nm in diameter, >200nm in length) can reach the site of action (lymphatic system) and elicit potent antigen-specific immune response<sup>15,20</sup>. Moreover, unlike conventional vaccine adjuvants (e.g., alum), nanofibers can induce antigen-specific immune responses without inducing local inflammation<sup>21</sup>. To decipher the relationship between physicochemical characteristics and the biological response, Collier et al. showed that the surface charge of the nanofibers is a pivotal parameter for adjusting their immunogenicity<sup>15</sup>. They showed that reducing the negative charges on the nanofiber surfaces can augment the dendritic cells (DCs) uptake, leading to more robust immune responses. However, they also showed that altering the surface charge of the nanofibers alone was insufficient to establish antigen-specific immune tolerance<sup>15</sup>. Besides, control over nanofibers' aspect ratio (diameter and length) is another approach often employed for modulating the immune response<sup>14,22</sup>. Due to the inherent structural helicity, the width of peptide nanofibers is energetically restrained<sup>23,24</sup>, with a diameter generally between 3-10nm<sup>22,25,26</sup>. Regarding the lengthwise control, Collier et al. showed that, in range of 200-1800nm, shorter nanofibers can induce a more robust CD8<sup>+</sup> T cell response<sup>22</sup>. However, they also showed that length alteration of the nanofibers does not cause significant effect towards CD4<sup>+</sup> T cell response.

In this study, we have investigated the effect of surface charge on the supramolecular nanofibers towards eliciting antigen-specific immunotolerance. We deployed multidomain peptides (MDPs), a well-studied  $\beta$ -sheet forming sequence (-SLSLSLSLSLSL-) developed by

the Hartgerink group, as the fibrillization domain<sup>27</sup>. Dexamethasone and the model ovalbumin (OVA) major histocompatibility complex (MHC) class II peptide epitope (OVA323: ISQAVHAAHAEINEAGR) were flanked at two ends of the fibrillization domain, spaced with either positively charged lysine (K) dimers or negatively charged glutamate (E) dimers (Figure 1a). The physicochemical properties of the supramolecular nanofibers' (morphology,  $\zeta$ -potential, secondary structure) were subsequently characterized. Finally, the pharmacological effect caused by the difference in physicochemical properties of nanofibers was studied using the bone marrow-derived dendritic cell (BMDC) and OTII adoptive transfer mouse model.

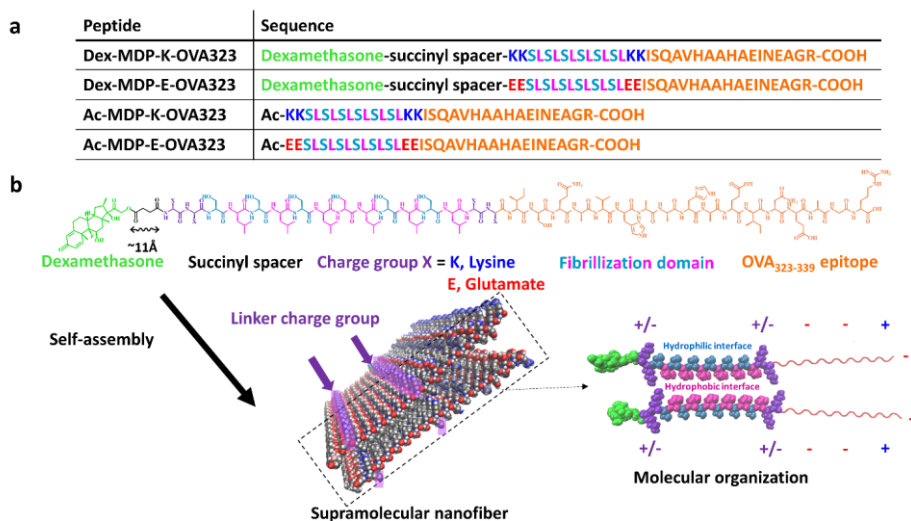


**Figure 1 Summary of peptides in this study and representation of the molecular arrangement in nanofibers.** a) list of peptides studied in this work. b) Graphical representation of the molecular organization of the supramolecular nanofibers. The chemical structure of the multidomain (MDP) fibrillization domain consists of alternative arrangements of serine (hydrophilic, in blue) and leucine residues (hydrophobic residue, in magenta). This structural chemical anisotropy aids the molecular arrangement of nanofibers into hydrophilic and hydrophobic interfaces. Due to the arrangement of the nanofiber in the form of an anisotropic tape, the flanking charge groups are exposed at the nanofiber surface. All the surface exposed charged residues are marked with + or -.

## 2. Results & Discussion

**Molecular design.** To systematically investigate the effect of linker charge groups on the formation of supramolecular nanofibers and antigen-specific tolerance induction, we designed a library of MDPs with either K or E flanking residues appended to both ends of the fibrillization domain (Figure 1a). Dexamethasone was conjugated to the N-terminus of the peptides via a biodegradable succinyl-spacer, which is susceptible to (intracellular) carboxylesterase degradation but is otherwise stable under physiological conditions<sup>28, 30, 31</sup>. Since carboxylesterases are ubiquitously expressed in the intracellular compartment<sup>32</sup> and whole blood<sup>33, 34</sup>, a short succinyl spacer (~11 Å extended length, Figure 1b) was used to

## Tuning surface charges of supramolecular nanofibers for induction of antigen-specific immune tolerance: an introductory study

ensure the ester bond was inaccessible to the catalytic binding site of carboxylesterase in the nanofiber state, thereby preventing premature release of dexamethasone from the nanofiber before taking up by the APCs<sup>35</sup>. Once the APCs take up the nanofibers, the fibrous structure will be processed through autophagy engagement<sup>36,37</sup>, followed by aminopeptidase (antigen epitope processing) and carboxylesterase (dexamethasone release) catalyzed degradation to exert its antigen-specific tolerogenic effect<sup>4,10</sup>(Figure 3a). To evaluate the effect of dexamethasone conjugation, two peptides composed of N-acetylated MDPs, Ac-MDP-K/E-OVA323 were included, for functional comparison with Dex-MDP-K/E-OVA323.

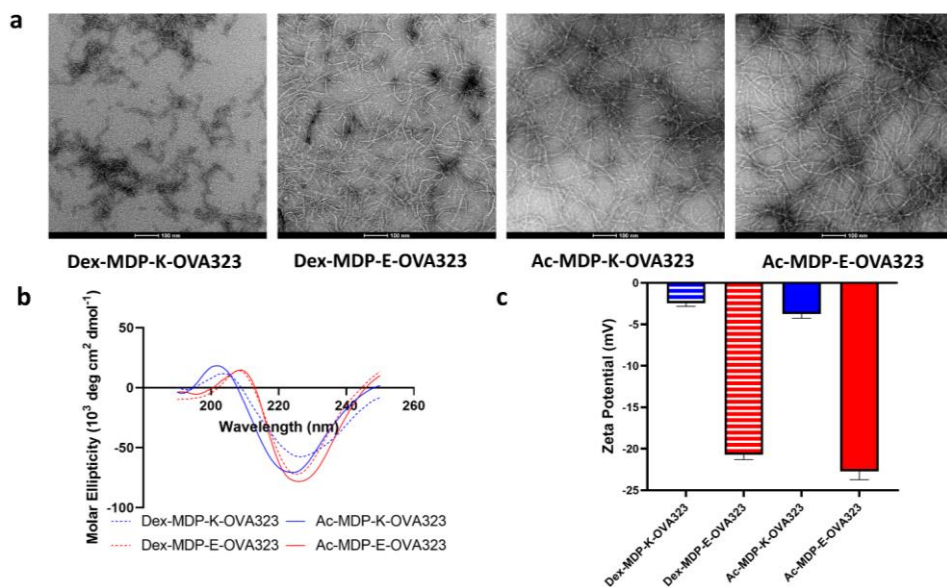


**Figure 2 Physicochemical properties of the formed peptide nanofibers.** a) Negative-stain TEM images show that MDP nanofiber formation is not disturbed by conjugation of dexamethasone and/or OVA323 epitopes. b) CD spectra of the peptides studied. All peptides display signature  $\beta$ -sheet patterns (negative minima: 220-230nm; positive band: 200-205nm). This shows that the  $\beta$ -sheet is the driving force for the fibrillization process. c)  $\zeta$ -potential of the peptide fibers studied. The K-containing nanofibers display a lower  $\zeta$ -potential (-2 to -4mV); while the E-containing nanofibers display a more negative  $\zeta$ -potential (-20 to -23mV). This shows that variation in charge of the flanking aa residues can alter the  $\zeta$ -potential of the nanofibers. The  $\zeta$ -potential Data expressed as the mean  $\pm$  standard deviations

**Supramolecular assembly & physicochemical characterization.** The morphology of the supramolecular assemblies was characterized by TEM. TEM images confirm that supramolecular nanofibers were formed from all four MDP-containing peptides (~4nm diameter, >500nm long) (Figure 2a). Next, we investigated the mode of fibrillization of these peptides. Previous studies showed that the MDP sequence initiated fibrillization through the  $\beta$ -sheet formation. Using CD spectrometry, a single negative minimum at 220-230 nm and a

positive band at 200-205 nm were observed in the different samples (Figure 2b), which signifies that the  $\beta$ -sheet conformation is the predominant secondary structure in the investigated nanofiber systems<sup>15</sup>. Regarding the use of 1×PBS as a buffer for  $\zeta$ -potential measurement, when compared to the lower ionic strength buffers (e.g., 10-25 mM HEPES, pH 7.4), its relatively high ionic strength and presence of multivalent ions (e.g.,  $\text{HPO}_4^{2-}$ ) can compress the electric double layer on the nanofiber surface, leading to a low  $\zeta$ -potential value<sup>38</sup>. However,  $\zeta$ -potential measurements in buffers of lower ionic strength can alter the nanofiber polymorph, thereby changing the resultant surface chemistry<sup>39</sup>. Therefore, 1×PBS was used to determine the  $\zeta$ -potential of the nanofibers. The  $\zeta$ -potential of the peptide nanofibers was influenced by the linker charge groups (Figure 2c). The K-containing nanofibers (Dex-/Ac-MDP-K-OVA323) exhibited less negative zeta potential (-2 to -4mV) when compared to the E-containing nanofibers (Dex-/Ac-MDP-E-OVA323, -20 to -23mV). This significant difference in  $\zeta$ -potential can be explained by the inherent chemical anisotropy in the fibrillization domain, causing the MDP nanofibers to molecularly arrange in the form of an anisotropic tape<sup>24</sup> (Figure 1b). Due to the molecular organization of the MDP nanofibers, the linker charge groups are exposed at the surface of the nanofibers (highlighted in purple in Figure 1b).

# Tuning surface charges of supramolecular nanofibers for induction of antigen-specific immune tolerance: an introductory study

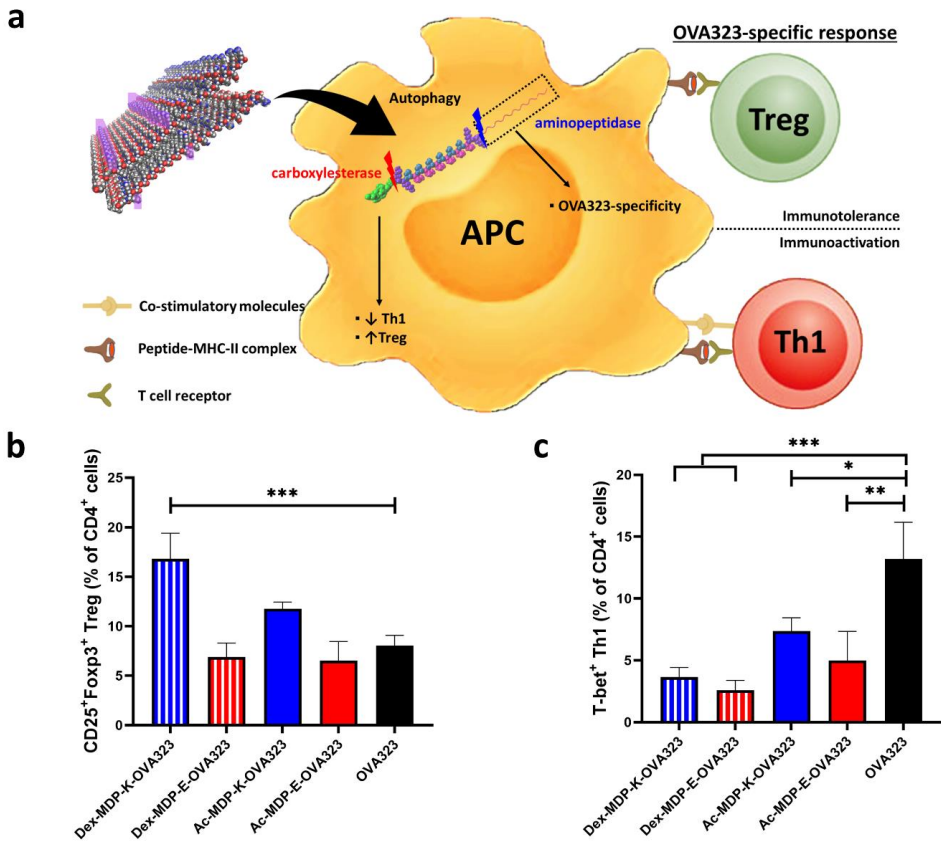


**Figure 3** *In vitro* tolerogenic effect of the nanofiber treatment. **a**) Graphical representation of the intracellular processing of the dexamethasone-containing nanofibers. The fibrous structure is first processed through autophagy engagement. Dexamethasone is then released by carboxylesterase catalyzed hydrolysis, which can upregulate regulatory T (Treg) level and lower the T helper 1 (Th1) level; while OVA323 epitope is processed by aminopeptidase to elicit antigen-specific response **b,c**) BMDCs were incubated with 10  $\mu$ M of peptide nanofiber dispersions for 2 days. Subsequently, CD4<sup>+</sup> OTII T cells were added and incubated for 3 days. **b**) The level of Treg was analyzed by flow cytometry. Significant Treg expansion was only observed for Dex-MDP-K-OVA323. **c**) The level of Th1 was analyzed by flow cytometry. All the nanofiber treatment groups significantly lowered the Th1 level when compared to treatment of the OVA323 epitope. Data were analyzed by one-way ANOVA with Dunnett's multiple comparison test (compared to the OVA323 group) and expressed as the mean  $\pm$  standard deviations (n=3); \* p<0.05, \*\* p<0.01, \*\*\*p<0.001.

**Dex-MDP-K-OVA323 upregulated *in vitro* OVA323-specific Treg.** To investigate whether Dex-MDP-OVA323 nanofibers can induce antigen-specific Tregs *in vitro*, BMDCs were incubated with the nanofibers for 2 days, followed by 3 days of co-culturing with CD4<sup>+</sup> T cells freshly isolated from the spleens of OTII mice. The level of OVA323-specific immune tolerance was probed by the level of the Treg cells. Since parallel activation of immunostimulatory effector T cells is undesirable for the potential treatment of autoimmune disorders<sup>40</sup>, the level of antigen-specific Th1 was monitored to validate the balance of the immune response. Since many disease-associated antigens are present in the physiological

environment<sup>3,41</sup>, the OVA323 epitope treatment group was used as the control for both the *in vitro* and *in vivo* studies. It was observed that only the Dex-MDP-K-OVA323 nanofiber formulation significantly expanded the Treg level amongst all the treatment groups (Figure 3b). The differential Treg induction effect between Dex-MDP-K-OVA323 and Ac-MDP-K-OVA323 showed that dexamethasone functionalization is essential for establishing antigen-specific immune tolerance. The failure for Ac-MDP-K/E-OVA323 to expand Treg concurred with the previous findings that variation in the nanofiber surface charge alone was insufficient to establish immune tolerance<sup>15</sup>. Finally, the differential Treg induction effect between Dex-MDP-K-OVA323 and Dex-MDP-E-OVA323 showed that reducing the surface negative charges can potentiate the tolerogenic response, which can be explained by the higher uptake of the nanofibers by the DCs due to the lower electrostatic repulsion between the negatively charged cell surface and nanofibers<sup>15</sup>. Next, it was observed that all treatment groups reduced the Th1 level compared to the OVA323 epitope treatment (Figure 3c). This observation concurred with the previous observation about the ability of nanofibers to serve as a non-inflammatory vaccine adjuvant<sup>21</sup>. Taken together, the results show that dexamethasone-incorporated nanofibers are capable of inducing antigen-specific immune tolerance without parallel pro-inflammatory immune activation. The extent of immune tolerance is increased by lowering the negative  $\zeta$ -potential of the peptide nanofibers, which likely results in a better uptake by DCs.

# Tuning surface charges of supramolecular nanofibers for induction of antigen-specific immune tolerance: an introductory study

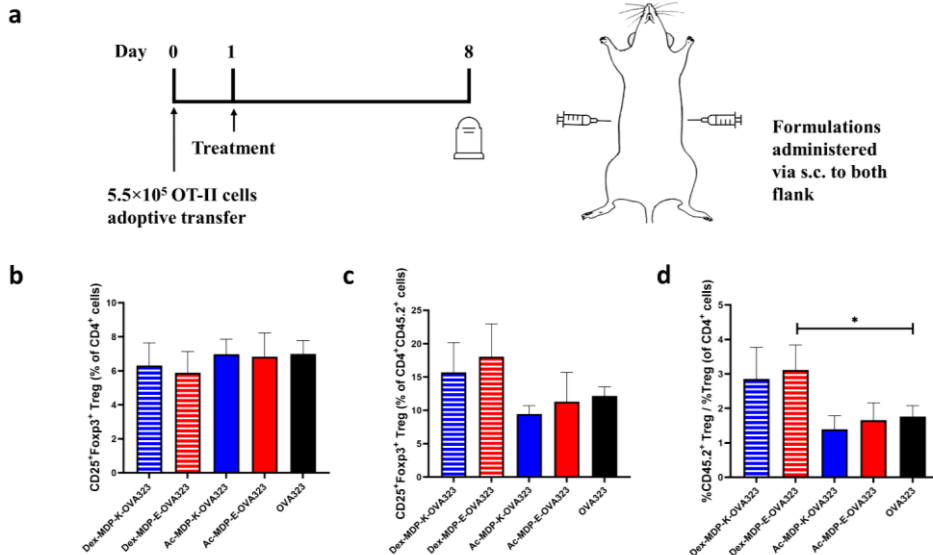


**Figure 4** *In vivo* tolerogenic effect of peptide nanofibers carrying dexamethasone and OVA323 epitopes. **a**) Outline of the OTII adoptive transfer model. On day 0,  $5.5 \times 10^5$  CD4<sup>+</sup>CD45.2<sup>+</sup> OTII T cells were adoptively transferred into C57BL/6-Ly5.1 mice via i.v. injection. On day 1, dispersions of nanofibers (200 nmol in total 100μl) were administered via s.c. injection at both flanks. Mice were sacrificed on day 8. The spleens of the mice were harvested for flow cytometry analysis. **b**) Percentage of Treg in all CD4<sup>+</sup> T cells. No statistical difference is detected between groups. **c**) Percentage of Treg in OTII CD4<sup>+</sup> T cells. No statistical significance between the nanofiber treatment groups and the control group was observed. **d**) Normalized Treg expression (CD4<sup>+</sup>CD45.2<sup>+</sup>/CD4<sup>+</sup>). Significant expansion of Treg was observed only for the Dex-MDP-E-OVA323 treatment group. Data were analyzed by one-way ANOVA with Dunnett's multiple comparison test (compared to the OVA323 group) and expressed as the mean ± standard deviation (n=5); \* p<0.05.

**Dex-MDP-E-OVA323 nanofiber upregulated *in vivo* OVA323-specific Treg.** To explore immune tolerance induction of the nanofibers *in vivo*, the OTII adoptive transfer mouse model was used to probe the OVA323-specific response (Figure 4a). We focused on the spleen as an indicator for induction of systemic immunotolerance as it is the largest secondary lymphoid organ in the body and an often-employed candidate for assaying the systemic immunotolerance<sup>42, 43</sup>. It was found that both Dex-MDP-K/E-OVA323 and Ac-MDP-K/E-OVA323 did not significantly affect the Treg level in the overall T cell population (Figure 4b). Since free dexamethasone can upregulate Treg in a non-antigen specific way<sup>44, 45</sup>, the lack of effect in the overall Treg level shows that the amount of dexamethasone prematurely released from the nanofibers was insignificant. Furthermore, though certain fluctuations in the Treg level in the OVA323-specific T cell subpopulation were observed, they failed to yield statistical differences compared to the control group (Figure 4c). However, through normalizing the OVA-specific Treg level with the intrinsic Treg expression in Ly5.1 mice (CD4<sup>+</sup>CD45.2<sup>+</sup>/CD4<sup>+</sup>), it was observed that Tregs were significantly upregulated only in the Dex-MDP-E-OVA323 treated group but not in other treatment groups

(Figure 4d). In agreement with the *in vitro* study, the tolerogenic response was only observed with nanofibers with conjugated dexamethasone. Furthermore, the *in vivo* results suggest that nanofiber with more negative  $\zeta$ -potential elicits a more robust tolerogenic response, which contradicts the *in vitro* findings. We conjectured that the discrepancy between the *in vitro* and *in vivo* results is due to the macrophage uptake mediated by the class A scavenger receptor (specifically the Macrophage Receptor with Collagenous structure (MARCO)). This MARCO scavenger receptor plays an important role in host defense against pathogens through taking up polyanionic nanostructures by macrophages<sup>46-48</sup>. Besides, the MARCO-mediated uptake of antigen-containing nanoparticles also regulates the tolerogenic response in macrophages<sup>49,50</sup>. As a result, though DCs uptake of Dex-MDP-E-OVA323 is hindered by higher mutual electrostatic repulsion<sup>15</sup> (as observed in the BMDC assay), the overall level of nanofiber uptake by APCs was compensated by the enhanced MARCO-mediated uptake by macrophages. Taken together, Dex-MDP-E-OVA323 can exert a higher OVA323-specific tolerogenic response than Dex-MDP-K-OVA323 in *in vivo* studies (Figure 4d).

### 3. Conclusion

In summary, the application of dexamethasone-incorporated peptide nanofibers for the induction of antigen-specific immune tolerance was explored. It was shown that the supramolecular organization of the nanofibers remained unaltered amid functional extension. Further, the incorporation of anionic or cationic amino acid residues at each end of the fibrillization domain was shown to be an effective approach in changing the  $\zeta$ -potential of the nanofibers. The extent of the tolerogenic response was found to be influenced by the  $\zeta$ -potential of the nanofibers. Nanofibers with less negative  $\zeta$ -potential gave a more robust tolerogenic response in the BMDC model, while a more potent tolerogenic response was observed for nanofibers with more negative  $\zeta$ -potential in the OTII adoptive transfer model. We conjectured that the discrepancy between these two models could be due to the scavenger receptor MARCO, which can mediate tolerogenic antigen presentation in macrophages. This can serve as a potential target for the future development of tolerogenic immunotherapy.

### 4. Methods

**Synthesis and preparation of the supramolecular peptide nanofibers.** Peptides (Figure 1a) were synthesized in-house with standard Fmoc solid-phase chemistry using a Liberty blue peptide synthesizer (CEM Corporation, US). Pre-loaded Fmoc-Arg(Pbf)-Wang resin (Novabiochem, Germany) was used as the starting material. For each coupling cycle, 5eq Fmoc-protected amino acids (Novabiochem, Germany) were activated with 5eq of Oxyma pure and N,N'-Diisopropylcarbodiimide (Biosolve BV, Netherlands) to react with the free N-terminal amino acids in the resin for 1 minute at 90°C. After each coupling step, the Fmoc group was removed by treatment with 20% piperidine for 1 minute at 90°C. Dexamethasone succinate was synthesized as described before (Figure 5a)<sup>28</sup> and conjugated to the free N-terminal of the protected peptide on the resin using the same coupling condition as



## Tuning surface charges of supramolecular nanofibers for induction of antigen-specific immune tolerance: an introductory study

with other Fmoc-amino acids (Figure 5b). A cleavage cocktail, trifluoroacetic acid/water/triisopropylsilane (95/2.5/2.5), was used to simultaneously cleave the peptide off the resin and remove the side chain protecting groups. Crude products were purified by preparative reverse-phase HPLC using Reprosil-Pur C18 column (10  $\mu$ m, 250  $\times$  22 mm) eluted with water-acetonitrile (MeCN) gradient 5% to 80% MeCN (0.1% formic acid for K-containing peptides, 10mM ammonium bicarbonate for E-containing peptides) in 35 minutes at a flowrate of 15.0ml/min with UV detection at 220 nm. Purity was confirmed to be >90% by analytical HPLC-MS using Waters XBridge C18 column (5 $\mu$ m, 4.6 $\times$ 150 mm) eluted with water-MeCN gradient 5 to 80% MeCN (0.1% formic acid for K-containing peptides, 10mM ammonium bicarbonate for E-containing peptides) in 20 minutes at a flow rate 1.0 ml/min and UV detection at 220 and 280 nm. MS analysis was performed using a Bruker microTOF-Q instrument (Note S1-5).

The nanofibers were prepared by dissolving peptides in sterile ultrapure water at a concentration of 8 mM. After overnight incubation at 4 $^{\circ}$ C, the peptide solution was diluted to 2 mM in 1 $\times$  Dulbecco's phosphate-buffered saline (1 $\times$ PBS, 2.7mM KCl, 1.5mM KH<sub>2</sub>PO<sub>4</sub>, 138mM NaCl, 8mM Na<sub>2</sub>HPO<sub>4</sub>) buffer to reach pH value 7.3-7.5 followed by incubation at room temperature for 3 hours<sup>29</sup>.

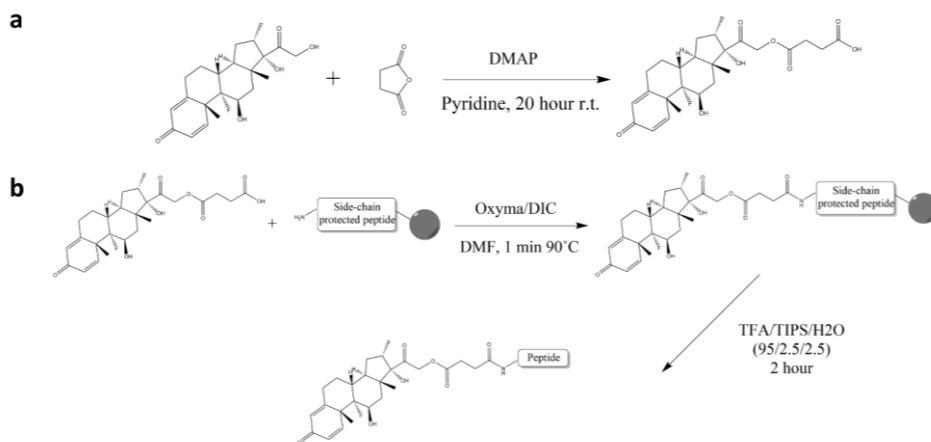


**Figure 5** Chemical synthetic pathway for a) dexamethasone succinate; b) dexamethasone-peptide conjugates.

**Circular dichroism (CD) &  $\zeta$ -potential measurement.** The dispersions of nanofibers (2 mM in 1 $\times$  PBS) were diluted to 0.2 mM with 1 $\times$ PBS buffer for both CD and  $\zeta$ -potential measurement. Far-UV CD spectra were recorded on a double beam DSM 1000 CD spectrometer (Online Instrument Systems, USA) from 260 to 180 nm in a quartz cuvette with 0.1 cm path length. Three accumulations were averaged for each sample, and the spectra were expressed in molar ellipticity (10<sup>3</sup> deg cm<sup>2</sup> dmol<sup>-1</sup>).  $\zeta$ -Potential was measured with a DTS1070 folded capillary cell on a Malvern Zetasizer Nano-Z (Malvern Instruments, UK).

Samples were equilibrated for 3 min at room temperature and measured 3 times, and results were shown as averaged.

**Negative-staining transmission electron microscopy (TEM).** The dispersions of nanofiber (2 mM) were diluted five-fold with 1X PBS buffer. Formvar/carbon-coated 400 mesh copper grid (Polysciences Inc., US) was placed on top of a droplet of 20  $\mu$ L of diluted samples. After 2 min incubation, the grid was washed three times with 0.2  $\mu$ m filtered milli-Q water and blotted dry with filter paper. Negative staining was performed for 1 min with 2% w/v uranyl acetate in water. The staining solution was removed by blotting with filter paper. Samples were imaged on a Tecnai 20 microscope equipped with a 4 K square pixel Eagle CCD camera (FEI, the Netherlands).

**Mice.** Female C57BL/6-Ly5.1 and C57BL/6-Tg(TcraTcrb)425Cbn/Crl (OTII) mice were purchased from Charles River, France, and kept under standard conditions at the central animal facility. Mice were provided with water and food ad libitum. All experiments were approved by the Animal Experiment Committee of Utrecht University.

**BMDCs.** Bone marrow cells were isolated from the tibias and femurs of C57BL/6 mice, and a single-cell suspension was obtained using a 70  $\mu$ m cell strainer (Greiner Bio-One B.V., Netherlands). The bone marrow cells were seeded at  $9 \times 10^5$  cells per well in a 6 well-plate and incubated for 7 days in IMDM medium supplemented with 2 mM glutamine, 10% FCS, 20 ng/mL GM-CSF, 100 U/mL penicillin/streptomycin, and 50  $\mu$ M  $\beta$ -mercaptoethanol. The cells were cultured at 37  $^{\circ}$ C. The medium was refreshed every other day.

**In vitro OVA-specific tolerogenic assay.** BMDCs were incubated with 10  $\mu$ M of Dex-MDP-K/E-OVA, Ac-MDP-K/E-OVA nanofiber, or OVA323 epitope for 2 days. Afterward, CD4<sup>+</sup> T cells were isolated from the spleens of OTII mice using a CD4<sup>+</sup>T cell isolation kit (Miltenyi Biotec B.V., Netherlands). The purified CD4<sup>+</sup> T cells were added at a density of  $1 \times 10^5$  cells per well and incubated for 3 days in a complete RPMI 1640 medium (Lonza, Switzerland) supplemented with 2 mM glutamine, 10% FCS, 100 U/mL penicillin/streptomycin, and 50  $\mu$ M  $\beta$ -mercaptoethanol. The cells were stained for viability using ViaKrome 808 Fixable Viability Dye (Beckman, USA, Cat# C36628). Cells were further stained with monoclonal antibodies specific for mouse CD4 (eBioscience, USA, Cat# 11-0042-82), CD25 (BD, USA, Cat# 553866), Foxp3 (eBioscience, USA, Cat# 45-5773-82) and T-bet (eBioscience, USA, Catalog # 17-5825-82). The proportion of Treg (CD25<sup>+</sup>Foxp3<sup>+</sup>) and T-helper 1 (T-bet<sup>+</sup>) cells in the live CD4<sup>+</sup> T cell population was analyzed by flow cytometry using a Gallios flow cytometer (Beckman Coulter, USA) and FlowJo 7.6.5.

**In vivo induction of OVA-specific immunotolerance.** On day 0, a total of  $5.5 \times 10^5$  CD45.2<sup>+</sup>CD4<sup>+</sup> OTII T cells were adoptively transferred into each CD45.1<sup>+</sup> Ly5.1 mouse via tail-vein injection. On day 1, the peptide fibers (2 mM) dispersions were subcutaneously injected into both right and left flanks (50  $\mu$ l each). Mice were sacrificed on day 8, and the spleens were harvested for flow cytometry analysis. The proportion of CD25<sup>+</sup>Foxp3<sup>+</sup> Treg

## **Tuning surface charges of supramolecular nanofibers for induction of antigen-specific immune tolerance: an introductory study**

---

in the CD4<sup>+</sup> and CD45.2<sup>+</sup>CD4<sup>+</sup> T cell population was analyzed by flow cytometry using a Gallios flow cytometer (Beckman Coulter, USA) and FlowJo 7.6.5.

**Statistical analysis.** Statistical analysis was performed in GraphPad Prism v.9.1.1 using one-way ANOVA with Dunnett's multiple comparison test. Data are presented as average± standard deviations unless otherwise indicated. Significant statistical difference is annotated as \* p<0.05, \*\* p<0.01, \*\*\*p<0.001.

### **5. Acknowledgment**

C.Y.J.L acknowledges the support from the European Union (Horizon 2020 NANOMED Grant 676137).

### **6. Author contributions**

C.Y.J.L., contributed to the organic synthesis and physicochemical characterization. C.Y.L, N.B., and B.L. contributed to the BMDC assay. C.Y.L, N.B., B.L., D.t.B., N.v.K. and M.F. contributed to the animal experiment. C.Y.J.L. and E.B. contributed to the negative-staining TEM measurement. N.B., D.t.B. and F.B. contributed to the flow cytometry analysis. C.Y.J.L., W.H. and E.M. provided advice on the design of the whole experiments, C.Y.J.L., W.H. and E.M. designed the research concept, managed the project and were the main contributors to the manuscript writing.

### References

1. Laayouni, H.; Oosting, M.; Luisi, P.; Ioana, M.; Alonso, S.; Ricaño-Ponce, I.; Trynka, G.; Zhernakova, A.; Plantinga, T. S.; Cheng, S.-C.; van der Meer, J. W. M.; Popp, R.; Sood, A.; Thelma, B. K.; Wijmenga, C.; Joosten, L. A. B.; Bertranpetit, J.; Netea, M. G., Convergent evolution in European and Roma populations reveals pressure exerted by plague on Toll-like receptors. *Proceedings of the National Academy of Sciences* **2014**, *111* (7), 2668.
2. Sakaguchi, S.; Miyara, M.; Costantino, C. M.; Hafler, D. A., FOXP3+ regulatory T cells in the human immune system. *Nature Reviews Immunology* **2010**, *10* (7), 490-500.
3. Pishesha, N.; Harmand, T.; Smeding, L. Y.; Ma, W.; Ludwig, L. S.; Janssen, R.; Islam, A.; Xie, Y. J.; Fang, T.; McCaul, N.; Pinney, W.; Sugito, H. R.; Rossotti, M. A.; Gonzalez-Sapienza, G.; Ploegh, H. L., Induction of antigen-specific tolerance by nanobody–antigen adducts that target class-II major histocompatibility complexes. *Nature Biomedical Engineering* **2021**.
4. Pickens, C. J.; Christopher, M. A.; Leon, M. A.; Pressnall, M. M.; Johnson, S. N.; Thati, S.; Sullivan, B. P.; Berkland, C., Antigen-Drug Conjugates as a Novel Therapeutic Class for the Treatment of Antigen-Specific Autoimmune Disorders. *Molecular Pharmaceutics* **2019**, *16* (6), 2452-2461.
5. Pearson, R. M.; Casey, L. M.; Hughes, K. R.; Miller, S. D.; Shea, L. D., In vivo reprogramming of immune cells: Technologies for induction of antigen-specific tolerance. *Advanced Drug Delivery Reviews* **2017**, *114*, 240-255.
6. Liu, Q.; Wang, X.; Liu, X.; Kumar, S.; Gochman, G.; Ji, Y.; Liao, Y.-P.; Chang, C. H.; Situ, W.; Lu, J.; Jiang, J.; Mei, K.-C.; Meng, H.; Xia, T.; Nel, A. E., Use of Polymeric Nanoparticle Platform Targeting the Liver To Induce Treg-Mediated Antigen-Specific Immune Tolerance in a Pulmonary Allergen Sensitization Model. *ACS Nano* **2019**, *13* (4), 4778-4794.
7. Kishimoto, T. K.; Maldonado, R. A., Nanoparticles for the Induction of Antigen-Specific Immunological Tolerance. *Frontiers in Immunology* **2018**, *9*, 230.
8. Kim, S.-H.; Moon, J.-H.; Jeong, S.-U.; Lee, C.-K., Induction of Antigen-Specific Immune Suppression Using Biodegradable Nanoparticles Containing Antigen and Dexamethasone. *The Journal of Immunology* **2019**, *202* (1 Supplement), 177.3.
9. Liu, Q.; Wang, X.; Liu, X.; Liao, Y.-P.; Chang, C. H.; Mei, K.-C.; Jiang, J.; Tseng, S.; Gochman, G.; Huang, M.; Thatcher, Z.; Li, J.; Allen, S. D.; Lucido, L.; Xia, T.; Nel, A. E., Antigen- and Epitope-Delivering Nanoparticles Targeting Liver Induce Comparable Immunotolerance in Allergic Airway Disease and Anaphylaxis as Nanoparticle-Delivering Pharmaceuticals. *ACS Nano* **2021**, *15* (1), 1608-1626.
10. Sands, R. W.; Tabansky, I.; Verbeke, C. S.; Keskin, D.; Michel, S.; Stern, J.; Mooney, D. J., Steroid–Peptide Immunoconjugates for Attenuating T Cell Responses in an Experimental Autoimmune Encephalomyelitis Murine Model of Multiple Sclerosis. *Bioconjugate Chemistry* **2020**, *31* (12), 2779-2788.

## Tuning surface charges of supramolecular nanofibers for induction of antigen-specific immune tolerance: an introductory study

---

11. Bresseleers, J.; Bagheri, M.; Storm, G.; Metselaar, J. M.; Hennink, W. E.; Meeuwissen, S. A.; van Hest, J. C. M., Scale-Up of the Manufacturing Process To Produce Docetaxel-Loaded mPEG-b-p(HPMA-Bz) Block Copolymer Micelles for Pharmaceutical Applications. *Organic Process Research & Development* **2019**, *23* (12), 2707-2715.
12. Ojha, T.; Hu, Q.; Colombo, C.; Wit, J.; van Geijn, M.; van Steenberg, M. J.; Bagheri, M.; Königs-Werner, H.; Buhl, E. M.; Bansal, R.; Shi, Y.; Hennink, W. E.; Storm, G.; Rijcken, C. J. F.; Lammers, T., Lyophilization stabilizes clinical-stage core-crosslinked polymeric micelles to overcome cold chain supply challenges. *Biotechnology Journal* **2021**, *16* (6), 2000212.
13. Crommelin, D. J. A.; Anchordoquy, T. J.; Volkin, D. B.; Jiskoot, W.; Mastrobattista, E., Addressing the Cold Reality of mRNA Vaccine Stability. *Journal of Pharmaceutical Sciences* **2021**, *110* (3), 997-1001.
14. Hainline, K. M.; Fries, C. N.; Collier, J. H., Progress Toward the Clinical Translation of Bioinspired Peptide and Protein Assemblies. *Advanced Healthcare Materials* **2018**, *7* (5), 1700930.
15. Wen, Y.; Waltman, A.; Han, H.; Collier, J. H., Switching the Immunogenicity of Peptide Assemblies Using Surface Properties. *ACS Nano* **2016**, *10* (10), 9274-9286.
16. Pompano, R. R.; Chen, J.; Verbus, E. A.; Han, H.; Fridman, A.; McNeely, T.; Collier, J. H.; Chong, A. S., Titrating T-Cell Epitopes within Self-Assembled Vaccines Optimizes CD4+ Helper T Cell and Antibody Outputs. *Advanced Healthcare Materials* **2014**, *3* (11), 1898-1908.
17. Shores, L. S.; Kelly, S. H.; Hainline, K. M.; Suwanpradid, J.; MacLeod, A. S.; Collier, J. H., Multifactorial Design of a Supramolecular Peptide Anti-IL-17 Vaccine Toward the Treatment of Psoriasis. *Frontiers in Immunology* **2020**, *11*, 1855.
18. Sun, T.; Han, H.; Hudalla, G. A.; Wen, Y.; Pompano, R. R.; Collier, J. H., Thermal stability of self-assembled peptide vaccine materials. *Acta Biomaterialia* **2016**, *30*, 62-71.
19. Kelly, S. H.; Opolot, E. E.; Wu, Y.; Cossette, B.; Varadhan, A. K.; Collier, J. H., Tabletized Supramolecular Assemblies for Sublingual Peptide Immunization. *Advanced Healthcare Materials* **2021**, *n/a* (n/a), 2001614.
20. Rudra, J. S.; Tian, Y. F.; Jung, J. P.; Collier, J. H., A self-assembling peptide acting as an immune adjuvant. *Proceedings of the National Academy of Sciences of the United States of America* **2010**, *107* (2), 622-627.
21. Chen, J.; Pompano, R. R.; Santiago, F. W.; Maillat, L.; Sciammas, R.; Sun, T.; Han, H.; Topham, D. J.; Chong, A. S.; Collier, J. H., The use of self-adjuncting nanofiber vaccines to elicit high-affinity B cell responses to peptide antigens without inflammation. *Biomaterials* **2013**, *34* (34), 8776-8785.
22. Fries, C. N.; Wu, Y.; Kelly, S. H.; Wolf, M.; Votaw, N. L.; Zauscher, S.; Collier, J. H., Controlled Lengthwise Assembly of Helical Peptide Nanofibers to Modulate CD8+ T-Cell Responses. *Advanced Materials* **2020**, *32* (39), 2003310.
23. Aggeli, A.; Nyrkova, I. A.; Bell, M.; Harding, R.; Carrick, L.; McLeish, T. C. B.; Semenov, A. N.; Boden, N., Hierarchical self-assembly of chiral rod-like molecules as

a model for peptide  $\beta$ -sheet tapes, ribbons, fibrils, and fibers. *Proceedings of the National Academy of Sciences* **2001**, 98 (21), 11857.

24. Hall, D. M.; Bruss, I. R.; Barone, J. R.; Grason, G. M., Morphology selection via geometric frustration in chiral filament bundles. *Nature Materials* **2016**, 15 (7), 727-732.
25. Fitzpatrick, A. W. P.; Debelouchina, G. T.; Bayro, M. J.; Clare, D. K.; Caporini, M. A.; Bajaj, V. S.; Jaroniec, C. P.; Wang, L.; Ladizhansky, V.; Müller, S. A.; MacPhee, C. E.; Waudby, C. A.; Mott, H. R.; De Simone, A.; Knowles, T. P. J.; Saibil, H. R.; Vendruscolo, M.; Orlova, E. V.; Griffin, R. G.; Dobson, C. M., Atomic structure and hierarchical assembly of a cross- $\beta$  amyloid fibril. *Proceedings of the National Academy of Sciences* **2013**, 110 (14), 5468.
26. Lau, C. Y. J.; Fontana, F.; Mandemaker, L. D. B.; Wezendonk, D.; Vermeer, B.; Bonvin, A. M. J. J.; de Vries, R.; Zhang, H.; Remaut, K.; van den Dikkenberg, J.; Medeiros-Silva, J.; Hassan, A.; Perrone, B.; Kummerle, R.; Gelain, F.; Hennink, W. E.; Weingarth, M.; Mastrobattista, E., Control over the fibrillization yield by varying the oligomeric nucleation propensities of self-assembling peptides. *Communications Chemistry* **2020**, 3 (1), 164.
27. Lopez-Silva, T. L.; Leach, D. G.; Azares, A.; Li, I. C.; Woodside, D. G.; Hartgerink, J. D., Chemical functionality of multidomain peptide hydrogels governs early host immune response. *Biomaterials* **2020**, 231, 119667.
28. Acedo, M.; Tarrason, G.; Piulats, J.; Mann, M.; Wilm, M.; Eritja, R., Preparation of oligonucleotide-dexamethasone conjugates. *Bioorganic & Medicinal Chemistry Letters* **1995**, 5 (15), 1577-1580.
29. Leach, D. G.; Dharmaraj, N.; Piotrowski, S. L.; Lopez-Silva, T. L.; Lei, Y. L.; Sikora, A. G.; Young, S.; Hartgerink, J. D., STINGel: Controlled release of a cyclic dinucleotide for enhanced cancer immunotherapy. *Biomaterials* **2018**, 163, 67-75.
30. Li, J.; Kuang, Y.; Shi, J.; Zhou, J.; Medina, J. E.; Zhou, R.; Yuan, D.; Yang, C.; Wang, H.; Yang, Z.; Liu, J.; Dinulescu, D. M.; Xu, B., Enzyme-Instructed Intracellular Molecular Self-Assembly to Boost Activity of Cisplatin against Drug-Resistant Ovarian Cancer Cells. *Angewandte Chemie International Edition* **2015**, 54 (45), 13307-13311.
31. Tang, W.; Zhao, Z.; Chong, Y.; Wu, C.; Liu, Q.; Yang, J.; Zhou, R.; Lian, Z.-X.; Liang, G., Tandem Enzymatic Self-Assembly and Slow Release of Dexamethasone Enhances Its Antihepatic Fibrosis Effect. *ACS Nano* **2018**, 12 (10), 9966-9973.
32. Hatfield, J. M.; Wierdl, M.; Wadkins, R. M.; Potter, P. M., Modifications of human carboxylesterase for improved prodrug activation. *Expert Opinion on Drug Metabolism & Toxicology* **2008**, 4 (9), 1153-1165.
33. Kalicharan, R. W.; Bout, M. R.; Oussoren, C.; Vromans, H., Where does hydrolysis of nandrolone decanoate occur in the human body after release from an oil depot? *International Journal of Pharmaceutics* **2016**, 515 (1), 721-728.
34. Kalicharan, R. W.; Oussoren, C.; Schot, P.; de Rijk, E.; Vromans, H., The contribution of the in-vivo fate of an oil depot to drug absorption. *International Journal of Pharmaceutics* **2017**, 528 (1), 595-601.

## Tuning surface charges of supramolecular nanofibers for induction of antigen-specific immune tolerance: an introductory study

---

35. Conda-Sheridan, M.; Lee, S. S.; Preslar, A. T.; Stupp, S. I., Esterase-activated release of naproxen from supramolecular nanofibres. *Chemical Communications* **2014**, 50 (89), 13757-13760.
36. Rudra, J. S.; Khan, A.; Clover, T. M.; Endsley, J. J.; Zloza, A.; Wang, J.; Jagannath, C., Supramolecular Peptide Nanofibers Engage Mechanisms of Autophagy in Antigen-Presenting Cells. *ACS Omega* **2017**, 2 (12), 9136-9143.
37. Kaganovich, D.; Kopito, R.; Frydman, J., Misfolded proteins partition between two distinct quality control compartments. *Nature* **2008**, 454, 1088.
38. Bhattacharjee, S., DLS and zeta potential – What they are and what they are not? *Journal of Controlled Release* **2016**, 235, 337-351.
39. Seuring, C.; Verasdonck, J.; Ringler, P.; Cadalbert, R.; Stahlberg, H.; Böckmann, A.; Meier, B. H.; Riek, R., Amyloid Fibril Polymorphism: Almost Identical on the Atomic Level, Mesoscopically Very Different. *The Journal of Physical Chemistry B* **2017**, 121 (8), 1783-1792.
40. Hansson, G. K.; Nilsson, J., Developing a vaccine against atherosclerosis. *Nature Reviews Cardiology* **2020**, 17 (8), 451-452.
41. Leonard, J. D.; Gilmore, D. C.; Dileepan, T.; Nawrocka, W. I.; Chao, J. L.; Schoenbach, M. H.; Jenkins, M. K.; Adams, E. J.; Savage, P. A., Identification of Natural Regulatory T Cell Epitopes Reveals Convergence on a Dominant Autoantigen. *Immunity* **2017**, 47 (1), 107-117.e8.
42. Krienke, C.; Kolb, L.; Diken, E.; Streuber, M.; Kirchhoff, S.; Bukur, T.; Akilli-Öztürk, Ö.; Kranz, L. M.; Berger, H.; Petschenka, J.; Diken, M.; Kreiter, S.; Yogev, N.; Waisman, A.; Karikó, K.; Türeci, Ö.; Sahin, U., A noninflammatory mRNA vaccine for treatment of experimental autoimmune encephalomyelitis. *Science* **2021**, 371 (6525), 145.
43. Lewis, S. M.; Williams, A.; Eisenbarth, S. C., Structure and function of the immune system in the spleen. *Science Immunology* **2019**, 4 (33), eaau6085.
44. Chen, X.; Oppenheim, J. J.; Winkler-Pickett, R. T.; Ortaldo, J. R.; Howard, O. M. Z., Glucocorticoid amplifies IL-2-dependent expansion of functional FoxP3+CD4+CD25+ T regulatory cells in vivo and enhances their capacity to suppress EAE. *European Journal of Immunology* **2006**, 36 (8), 2139-2149.
45. Chen, X.; Murakami, T.; Oppenheim, J. J.; Howard, O. M. Z., Differential response of murine CD4+CD25+ and CD4+CD25- T cells to dexamethasone-induced cell death. *European Journal of Immunology* **2004**, 34 (3), 859-869.
46. Novakowski, K. E.; Yap, N. V. L.; Yin, C.; Sakamoto, K.; Heit, B.; Golding, G. B.; Bowditch, D. M. E., Human-Specific Mutations and Positively Selected Sites in MARCO Confer Functional Changes. *Molecular Biology and Evolution* **2018**, 35 (2), 440-450.
47. Thelen, T.; Hao, Y.; Medeiros, A. I.; Curtis, J. L.; Serezani, C. H.; Kobzik, L.; Harris, L. H.; Aronoff, D. M., The Class A Scavenger Receptor, Macrophage Receptor with Collagenous Structure, Is the Major Phagocytic Receptor for Clostridium sordellii Expressed by Human Decidual Macrophages. *The Journal of Immunology* **2010**, 185 (7), 4328.

48. Arredouani, M. S.; Palecanda, A.; Koziel, H.; Huang, Y.-C.; Imrich, A.; Sulahian, T. H.; Ning, Y. Y.; Yang, Z.; Pikkarainen, T.; Sankala, M.; Vargas, S. O.; Takeya, M.; Tryggvason, K.; Kobzik, L., MARCO Is the Major Binding Receptor for Unopsonized Particles and Bacteria on Human Alveolar Macrophages. *The Journal of Immunology* **2005**, *175* (9), 6058.
49. Wermeling, F.; Chen, Y.; Pikkarainen, T.; Scheynius, A.; Winqvist, O.; Izui, S.; Ravetch, J. V.; Tryggvason, K.; Karlsson, M. C. I., Class A scavenger receptors regulate tolerance against apoptotic cells, and autoantibodies against these receptors are predictive of systemic lupus. *Journal of Experimental Medicine* **2007**, *204* (10), 2259-2265.
50. Wang, X.-Y.; Facciponte, J.; Chen, X.; Subjeck, J. R.; Repasky, E. A., Scavenger Receptor-A Negatively Regulates Antitumor Immunity. *Cancer Research* **2007**, *67* (10), 4996.



## Supplementary Information

### Tuning surface charges of supramolecular nanofibers for induction of antigen-specific immune tolerance: an introductory study

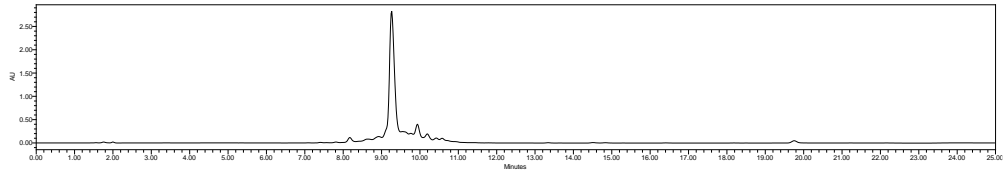
Chun Yin Jerry Lau, Naomi Benne, Bo Lou, Daniëlle ter Braake, Esmeralda Bosman, Nicky van Kronenburg, Marcel Fens, Wim E. Hennink, Femke Broere, Enrico Mastrobattista

**Supplementary Note 1-5: HPLC-MS traces of the synthesized peptide constructs**

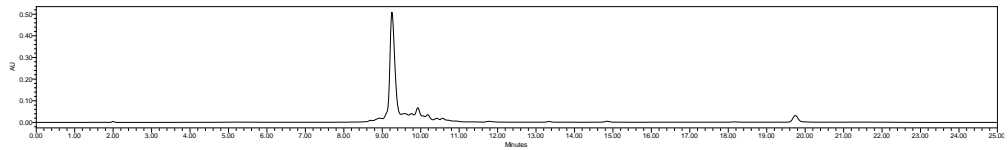
**S1:** DEX-MDP-K-OVA (Theoretical mass=3962.6 Da;  $[M+2H]^{2+}=1982.3$ ,  
 $[M+3H]^{3+}=1321.9$ ,  $[M+4H]^{4+}=991.6$ ,  $[M+5H]^{5+}=793.5$ )

Analytical HPLC

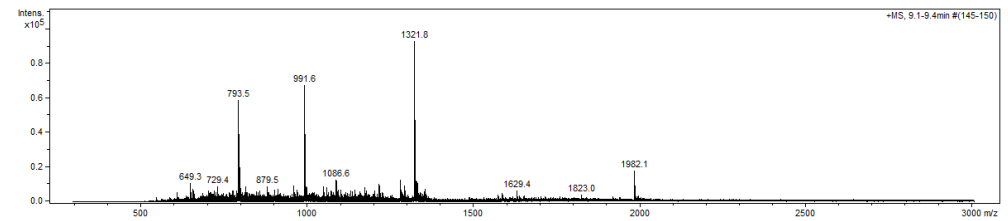
220nm



280nm



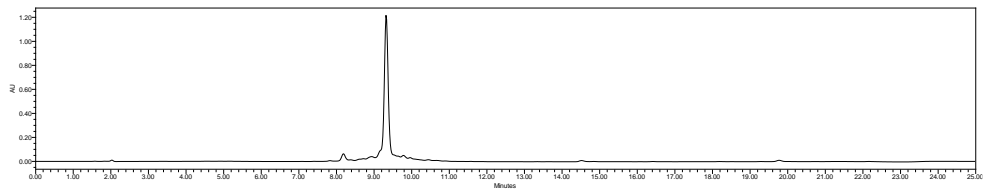
MS



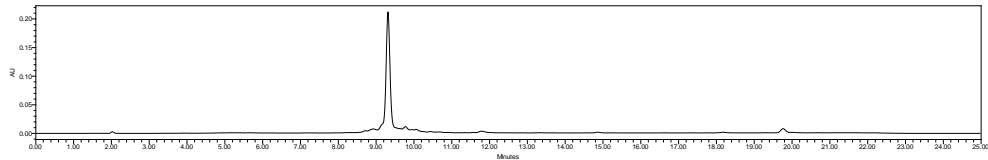
**S2:** DEX-MDP-E-OVA (Theoretical mass=3966.4 Da;  $[M+H]^{2+}=1984.2$ ,  
 $[M+3H]^{3+}=1323.1$ )

Analytical HPLC

220nm

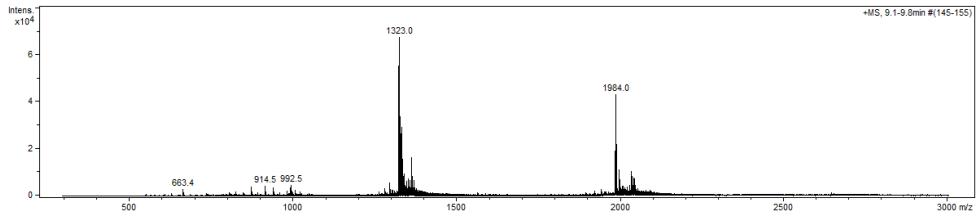


280nm



# Tuning surface charges of supramolecular nanofibers for induction of antigen-specific immune tolerance: an introductory study

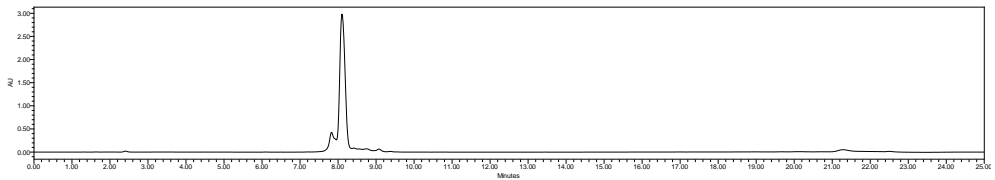
MS



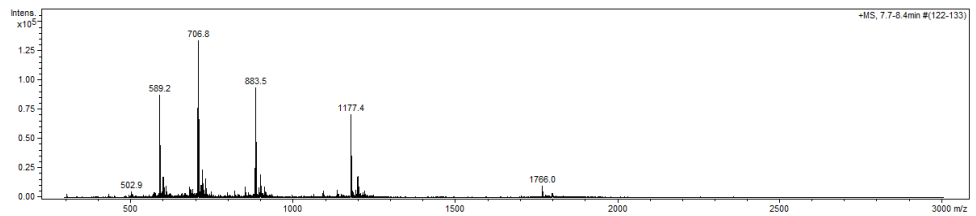
**S3:** Ac-MDP-K-OVA (Theoretical mass=3530.1 Da;  $[M+3H]^{3+}=1177.7$ ,  $[M+4H]^{4+}=883.5$ ,  $[M+5H]^{5+}=707.0$ ,  $[M+6H]^{6+}=589.4$ )

Analytical HPLC

220nm

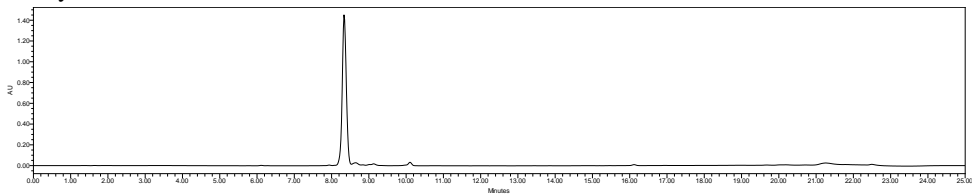


MS

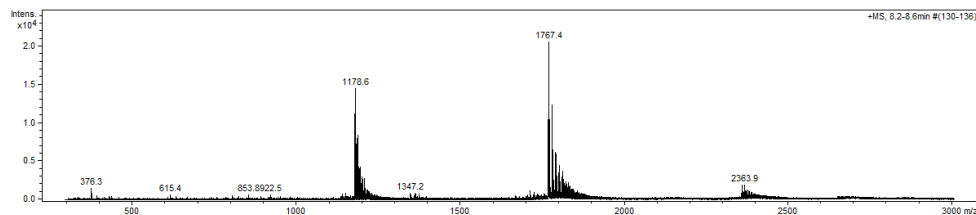


**S4:** Ac-MDP-E-OVA (Theoretical mass=3533.9 Da;  $[M+2H]^{2+}=1768.0$ ,  $[M+3H]^{3+}=1179.0$ )

Analytical HPLC



MS



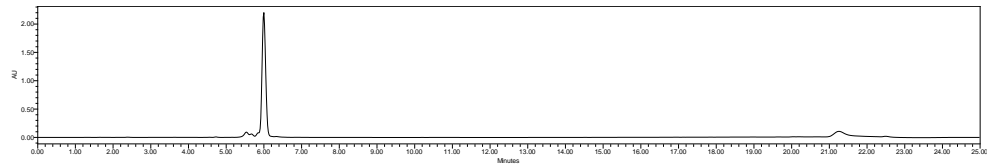
## Chapter 5

---

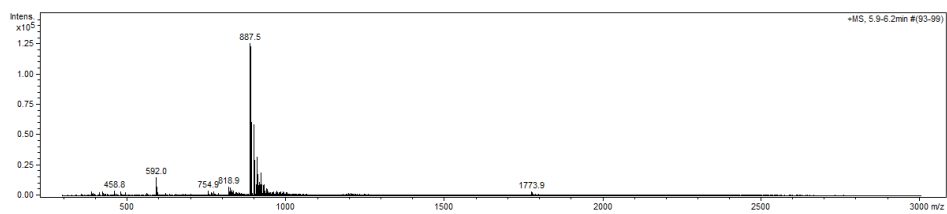
**S5:** OVA323 ((Theoretical mass=1773.9 Da;  $[M+2H]^{2+}=888.0$ )

Analytical HPLC

220nm



MS



# Chapter 6

## Complementary hydrophobic-electrostatic interactions enhance albumin association with dexamethasone-antigen conjugates leading to a more robust tolerogenic response

Chun Yin Jerry Lau<sup>1</sup>, Naomi Benne<sup>2</sup>, Bo Lou<sup>1,3</sup>, Daniëlle ter Braake<sup>2</sup>, Nicky van Kronenburg<sup>1</sup>, Marcel Fens<sup>1</sup>, Wim E. Hennink<sup>1</sup>, Femke Broere<sup>2</sup>, Enrico Mastrobattista<sup>1</sup>

<sup>1</sup>*Utrecht Institute for Pharmaceutical Sciences, Department of Pharmaceutics, Faculty of Science, Utrecht University, Universiteitsweg 99, 3584 CG Utrecht, the Netherlands. E-mail: e.mastrobattista@uu.nl*

<sup>2</sup>*Department of Infectious Diseases and Immunology, Faculty of Veterinary Medicine, Utrecht University, Yalelaan 1, 3584 CL Utrecht, the Netherlands*

<sup>3</sup>*Cardiovascular Research Institute, Department of Medicine, Yong Loo Lin School of Medicine, National University of Singapore, #08-01, MD6 Centre for Translational Medicine, 14 Medical Drive, 117599, Singapore*

### Abstract

The therapeutic potential of antigen-specific regulatory T (Treg) cells has been extensively explored and has led to the development of several tolerogenic vaccines. Dexamethasone-antigen conjugates represent a prominent class of tolerogenic vaccines that enable coordinated delivery of antigen and immunosuppressive drug dexamethasone to target immune cells. However, with their relatively small size (<5 nm), these immunoconjugates can, upon subcutaneous administration, bypass lymphatic transport through direct blood capillaries drainage and rapidly excreted by the kidney. Albumin association is a proven strategy to overcome this setback and increase the circulation times of small molecule-peptide conjugates. Herein, inspired by the peptide-protein complexation mechanism, the use of complementary hydrophobic-electrostatic interactions to enhance the association propensities between albumin and the dexamethasone-antigen conjugates was explored. By varying the charged residues in the spacer of the dexamethasone-antigen conjugates, the association propensities between albumin and the immunoconjugates were successfully modulated. Furthermore, through evaluating the electrostatic surface potential of albumin and the immunoconjugates, the albumin binding moiety of Dex-K4-OVA323 was shown to exhibit higher electrostatic complementarity to albumin than that of Dex-E4-OVA323 (K: lysine, E: glutamate). The OTII (C57BL/6-Tg(Tcr $\alpha$ Tcr $\beta$ )425Cbn/Crl) adoptive transfer model showed that Dex-K4-OVA323 can selectively upregulate OVA323-specific Treg, while no significant effect was observed for Dex-E4-OVA323. Our findings offer a molecular guide to augment the immune response of the immunoconjugates for potential application in tolerogenic immunotherapy.

# **Complementary hydrophobic-electrostatic interactions enhance albumin association with dexamethasone-antigen conjugates leading to a more robust tolerogenic response**

## **1. Introduction**

The therapeutic potential of antigen-specific regulatory T cells (Treg, Foxp3<sup>+</sup>CD4<sup>+</sup>CD25<sup>+</sup>) in mitigating autoimmune disorders has been extensively explored<sup>1-3</sup>. The antigen-specific Treg plays a crucial role in alleviating and remodeling pathological autoimmunity by responding to disease-associated antigens, e.g., atherosclerosis<sup>4,5</sup> and Type I Diabetes<sup>2,6</sup>. Tolerogenic vaccines are under development for *de novo* induction of antigen-specific Treg, which generally requires coordinated delivery of disease-associated antigen and tolerogenic adjuvants (e.g., dexamethasone, an immunosuppressive drug) to the antigen-presenting cells<sup>7-10</sup>. In particular, antigen-adjuvant conjugates are a convenient and effective approach to enable coordinated cargo delivery to the target immune cells, thereby avoiding the side effects experienced by their stochastic distribution in the body, e.g., off-target immune activation, nonspecific immunosuppression<sup>8</sup>. However, the relatively small size of the immunoconjugate monomers (< 5 nm) makes them, upon subcutaneous administration, susceptible to bypassing lymphatic transport through direct blood capillaries drainage<sup>11,12</sup> and subsequent rapid renal clearance<sup>13,14</sup>. Since the lymphatic systems are the primary site for cultivating the antigen-specific Treg, consideration needs to be taken to optimize the lymphatic retention of the immunoconjugates.

Albumin is the most abundant plasma protein present in different body compartments (e.g., lymphatic, interstitial fluid, blood). It plays a key role in regulating the colloid osmotic pressure in the body through its movement between blood circulation and the lymphatic system--albumin leaves the blood through capillaries end to reach the interstitial fluid, from which it rejoins the blood circulation via the lymphatic system<sup>15</sup>. Besides, albumin also plays a significant role in transporting endogenous and exogenous molecules via transient association<sup>16,17</sup>. In fact, albumin is one of the essential carrier proteins for small-molecule drugs to prolong their physiological half-life<sup>18</sup>. Through exploiting this transport mechanism, in several studies, molecular constructs were designed to enhance their lymphatic retention<sup>19-22</sup> (Figure 1a). For example, Chen *et al.* designed a molecular vaccine that formed an *in-situ* supramolecular complex with albumin upon subcutaneous injection, which led to enhanced lymphatic accumulation and elicitation of robust antigen-specific immune responses<sup>23</sup>. Therefore, the albumin-association approach has good scrutinization potential for augmenting the immunoactivity of the immunoconjugates.

Dexamethasone, a tolerogenic glucocorticoid, is transported primarily via albumin upon systemic administration<sup>24,25</sup>. It has been shown that the hydrophobic cavities residing in the subdomain IIA and IIIA of this protein are the binding sites for dexamethasone<sup>26,27</sup>, with a more specific binding area recently identified between subdomain IIA and IIB<sup>28</sup>. Hydrophobic interactions are dominant for the dexamethasone-albumin association, in which the only residing tryptophan (Trp214) in subdomain IIB acts as the moderator for the molecular binding of dexamethasone<sup>28</sup>. Furthermore, albumin displays a negative surface electrostatic potential at physiological conditions<sup>16</sup>. Consequently, it interacts with several cationic compounds through electrostatic interaction at physiological conditions<sup>29,30</sup>. To bridge these two modes of albumin interactions, Brandsdal *et al.* demonstrated that complementary hydrophobic-electrostatic interactions can enhance the association between small molecule-peptide conjugates and albumin<sup>30</sup>. Electrostatic interactions are influenced by 1) enthalpy of associative charging; and 2) entropy of counterions release<sup>31,32</sup>. In particular, electrostatic

interactions between peptide sequences with low charge density (<6 charged residues) are driven by the association enthalpy<sup>31</sup>. However, the association enthalpy is weaker when the oppositely charged residues are further apart<sup>33, 34</sup>. Drawing analogy to peptide-protein complexation mechanism<sup>33</sup>, through driving primary association, hydrophobic interactions can facilitate secondary electrostatic interactions by shortening the distance between small molecule-peptide conjugates and albumin. Therefore, this complementary mode of hydrophobic-electrostatic interactions can be explored as a general approach to aid the association between albumin and the dexamethasone-antigen conjugates.

In the present paper, the use of complementary hydrophobic-electrostatic interactions to enhance dexamethasone-antigen conjugate-albumin association was explored, and the effect it brings towards the induction of antigen-specific Treg was investigated. Dexamethasone and a model ovalbumin (OVA) major histocompatibility complex (MHC) class II peptide epitope (OVA323: ISQAVHAAHAEINEAGR) were conjugated via either cationic lysine (K) or anionic glutamate (E) tetramers to give immunoconjugates with oppositely charged albumin binding moieties (Figure 1b). The association propensities between immunoconjugates and albumin were evaluated through native polyacrylamide gel electrophoresis (PAGE) assay and electrostatic surface potential calculation. Finally, the biological effect caused by differential albumin association was evaluated with the tolerogenic response in OT-II adoptive mice model.

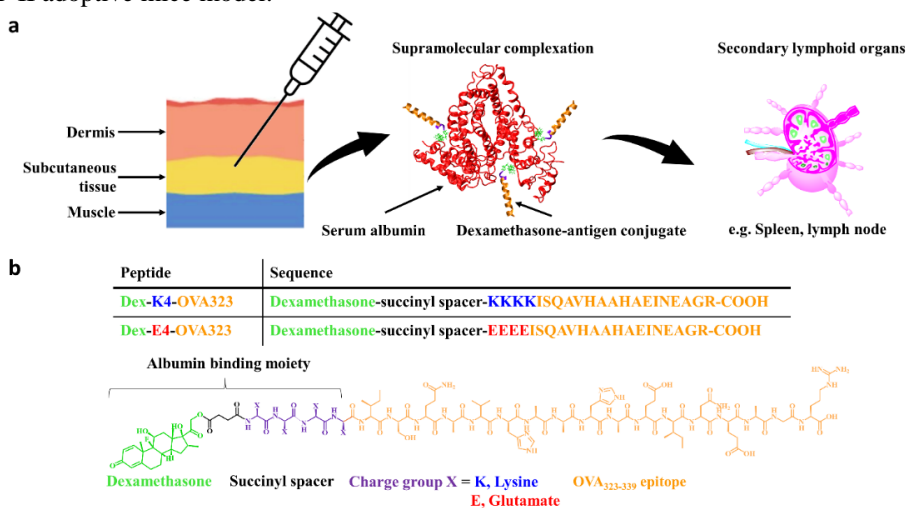


**Figure 1 Working mechanism and molecular details of the dexamethasone-antigen conjugates used in this study** **a)** Illustration of the proposed working mechanism of albumin binding. Upon administration to the subcutaneous tissue, the dexamethasone-antigen conjugates bind to albumin. Consequently, the supramolecular complexes are drained into the lymphatic system, thereby enhancing the accumulation of immunoconjugates to the secondary lymphoid organs. **b)** Chemical structures of the dexamethasone-antigen conjugates studied in this work. Dexamethasone was conjugated to the peptide sequences via a biodegradable succinyl linker. The N-terminus of the OVA323 epitope sequence was extended with four charged residues (K:+ve or E:-ve). The closely spaced dexamethasone and the charged residue tetramers constitute an albumin binding moiety.



# Complementary hydrophobic-electrostatic interactions enhance albumin association with dexamethasone-antigen conjugates leading to a more robust tolerogenic response

## 2. Results and Discussion

**Molecular design.** To study the effect of albumin-immunoconjugate electrostatic complementarity towards the induction of antigen-specific Treg, dexamethasone-antigen conjugates were designed and synthesized with differently charged residues in between the linker and the peptide epitope (K or E tetramers, Figure 1b). Since albumin possesses a negative surface electrostatic potential under physiological conditions<sup>16</sup>, the charge variation can cover the range of electrostatic interactions from attractive to repulsive. K and E were chosen as the cationic and anionic counterparts, as they have comparable molecular weights (K:146.2 Da, E:147.1 Da). The charged tetramer was appended to the N-terminus of the OVA323 epitope. Further, dexamethasone was conjugated to the N-terminus of the K/E4-OVA323 sequence via a biodegradable succinyl-spacer, which is prone to carboxylesterase cleavage but is otherwise physiologically stable<sup>8,35</sup>. Dexamethasone and the charged tetramers were placed in conjunction to foster the complementary hydrophobic-electrostatic interactions between immunoconjugates and albumin, thereby carving an albumin binding moiety (Figure 1b).

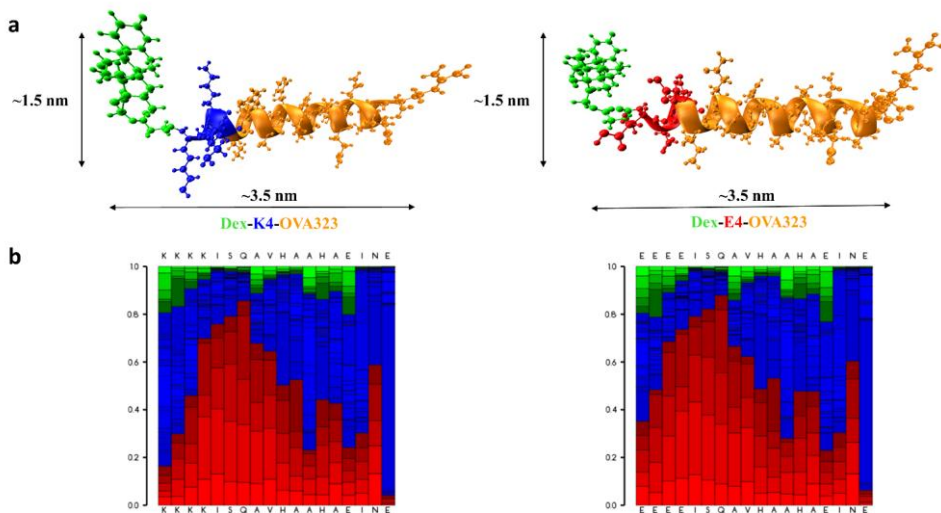


**Figure 2** Molecular conformation of the dexamethasone-antigen conjugates **a)** The best models of the immunoconjugate secondary structures predicted by PEP-FOLD3<sup>36,37</sup>. Both immunoconjugates adapt an  $\alpha$ -helical structure throughout the sequences. The monomeric size of these conjugates is susceptible for rapid renal clearance upon parenteral administration ( $<5\text{nm}$ )<sup>13</sup>. **b)** The structural alphabet prediction profile derived by PEP-FOLD3. The residual secondary structure probabilities are colored in red ( $\alpha$ -helix), blue (random coil), green ( $\beta$ -sheet). The output sequence in the profile is of the 3 residues subtracted from the input sequences.

**De novo prediction of the molecular conformation of the peptide conjugates.** To predict the molecular conformation of the immunoconjugates, a *de novo* structure prediction software program, PEP-FOLD3<sup>36,37</sup>, was used to derive the most probable molecular conformations of the peptide sequences. Since a small molecule N-terminal modifications generally have limited influence over the final secondary structure of a short peptide sequence<sup>38</sup>,

the K/E4-OVA323 sequences were used for the *de novo* prediction. The best models derived from free modeling parameters of K4-OVA323 and E4-OVA323 showed that they both adopt  $\alpha$ -helical structure throughout the sequence (Figure 2a). Furthermore, the structural alphabet prediction profile, based on 27 variations of peptide backbone conformation<sup>39</sup>, offered a colorimetric representation of the residual conformation probabilities (Figure 2b). By classifying the 27 conformational variabilities into 3 significant categories of secondary structures (red:  $\alpha$ -helix, blue: random coil, green:  $\beta$ -sheet, Figure 2b), observed that  $\alpha$ -helix prone residues (probability  $>0.5$ ) were distributed throughout the output sequences (3 residues deducted from the input sequences). This demonstrates that K/E4-OVA323 peptides adopt an  $\alpha$ -helical structure along the whole sequences. Next, we performed atomic coordinate parameterization with the dexamethasone succinate molecule using the LigParGen program<sup>40</sup>. The parameterized dexamethasone succinate was added to the N-terminal of the K/E4-OVA323 atomic model as an artificial amino acid (Figure 2a). Measurement of the monomeric size of the immunoconjugates (each  $\sim 1.5 \times 3.5$  nm) showed that both Dex-K/E4-OVA323 fell into the molecular size range that, upon subcutaneous administration, can bypass lymphatic transport through direct blood capillary drainage<sup>11, 12</sup> and subsequent rapid renal clearance<sup>13</sup>. Therefore, a strategy is needed to enhance the retention of immunoconjugates in the lymphatic system, which is the major site for antigen-specific Treg induction.

**Supramolecular complexation between immunoconjugates and albumin.** To decipher the plausible mechanism for enhancing the lymphatic retention of immunoconjugates, a native PAGE gel assay was performed to study the macromolecular complexes ( $>55$ kDa) form between immunoconjugates and biofluids. The supramolecular complexes were prepared by incubating  $20\mu\text{M}$  immunoconjugates with the biofluids at  $37^\circ\text{C}$  for one hour. 40% mouse plasma in phosphate-buffered saline (PBS) was used to emulate the biofluid of subcutaneous tissue<sup>41</sup>. Besides, knowing that albumin is a major carrier protein for small molecule drugs<sup>18</sup>, the HSA/immunoconjugate, and MSA/immunoconjugate complexes were prepared for molecular size comparison with the plasma/immunoconjugate complexes. To aid the recognition of immunoconjugates in the macromolecular complexes, the immunoconjugates were Cy5-labeled for fluorescence detection (Dex-K/E4-K<sub>(Cy5)</sub>OVA323). The fluorescent band of plasma/Dex-K4-K<sub>(Cy5)</sub>OVA323 complexes exhibited higher fluorescence intensity than the plasma/Dex-E4-K<sub>(Cy5)</sub>OVA323 complexes (Figure 3a). This shows that the cationic tetramer (K4) enhances the complexation propensities with plasma proteins when compared to the anionic tetramer (E4). Furthermore, it was observed that the fluorescent band of HSA/Dex-K4-K<sub>(Cy5)</sub>OVA323 and MSA/Dex-K4-K<sub>(Cy5)</sub>OVA323 complexes displayed similar size distribution with the plasma/Dex-K4-K<sub>(Cy5)</sub>OVA323 complexes (fluorescence bands at  $\sim 100$ kDa and  $>100$ kDa, Figure 3a). This suggests that albumin is a probable complexation partner with Dex-K4-OVA323 in the subcutaneous tissue. Interestingly, the size of supramolecular complexes formed between Dex-K4-K<sub>(Cy5)</sub>OVA323 and plasma/albumin were situated in the dimeric region (band at  $\sim 100$  kDa), which postulated its potential albumin dimerization properties caused by its cationic charges<sup>42</sup>.

## Complementary hydrophobic-electrostatic interactions enhance albumin association with dexamethasone-antigen conjugates leading to a more robust tolerogenic response

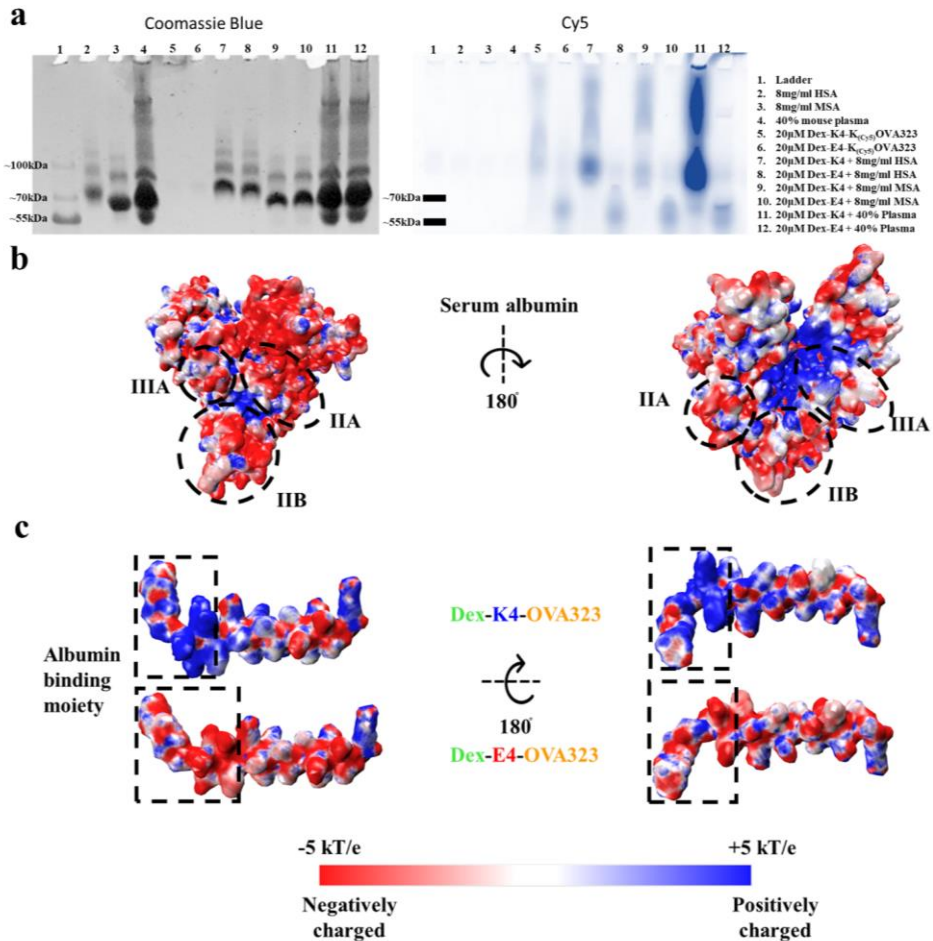


**Figure 3** Native PAGE gel assay of supramolecular complexes and the electrostatic surface potential of albumin (PDB ID: 1UOR) and dexamethasone-antigen conjugates. **a**) Association of fluorescently-labeled immunoconjugates with plasma proteins/albumin as assessed by native PAGE electrophoresis. The immunoconjugates were labeled with Cy5 to aid the recognition of immunoconjugates in the macromolecular-sized complexes. The protein in the system was visualized with Coomassie blue staining in the left, while the fluorescent signal was shown in the right. **b**) Albumin displays a predominantly negative surface potential. The electrostatic properties of the possible dexamethasone binding sites are circled in black (subdomain IIA, IIB, and IIIA). Both subdomain IIA and IIA display negatively charged surface properties, while subdomain IIIA has a balanced surface feature. **c**) Variation in the charged residues tetramer in the dexamethasone-antigen conjugates can successfully alter the electrostatic surface potential of the albumin binding moiety. The electrostatic surface potential is calculated using the APBS (Adaptive Poisson-Boltzmann Solver) software<sup>43</sup>. Potential isocontours are shown at -5 kT/e (red) and +5kT/e (blue). Structural representations were prepared with Visual molecular dynamics (VMD) software<sup>55</sup>.

**The electrostatic surface potential of the albumin binding sites and immunoconjugates.** Having demonstrated that the immunoconjugates bind to albumin, the connection between electrostatic complementarity and the albumin-conjugate association was then investigated. The electrostatic surface potential map of the albumin (PDB ID: 1UOR) and the

dexamethasone-antigen conjugates were calculated using the Adaptive Poisson-Boltzmann Solver (APBS) program<sup>43</sup>. The albumin model examined herein should be of good generality, as albumin shares high sequence homology across different species<sup>26, 28</sup>, especially domain II/III between humans and mice (Figure S2a-b)<sup>44</sup>. In agreement with the literature<sup>16</sup>, it is found that albumin displays a dominant-negative electrostatic surface potential (Figure 3b, S2c). Further, we observed that an area of positive electrostatic surface potential was centered around the core of the protein. The presence of oppositely charged area in the same protein can be partly explained by the evolutionary preservation of polar residues in the protein core, which plays a significant role in maintaining the overall protein folding (e.g., formation of salt-bridge)<sup>33, 45</sup>. Next, we assayed the electrostatic surface potential of the possible dexamethasone binding sites in the albumin. The mode of interaction of dexamethasone with albumin is via multisite association<sup>46</sup>, with one specific dexamethasone-binding site recently identified<sup>28</sup>. Therefore, we chose all plausible binding areas in the albumin for the electrostatic surface potential evaluation (subdomain IIA, IIB, IIIA)<sup>26-28</sup>. The electrostatic surface potential evaluation shows that both subdomain IIA and IIB display negative electrostatic surface potential (Figure 3b, S2c). Subdomain IIIA displays more balanced electrostatic surface potential (Figure 3b, S2c), which likely fosters higher binding capacity for hydrophobic drug molecules, e.g., digoxin, ibuprofen<sup>26</sup>. Finally, to assess the qualitative electrostatic complementarity between albumin and the immunoconjugates, we evaluated the electrostatic surface potential of Dex-K/E4-OVA323 (Figure 3c). It is shown that the charged linker residues alter the electrostatic surface potential of the albumin-binding moieties in the immunoconjugates. Therefore, the chosen peptide conjugates should represent good opposite models to study the effect of electrostatic complementarity between the dexamethasone-antigen conjugates and different binding sites in the albumin (Table 1).

**Table 1. Electrostatic complementarity between albumin and the dexamethasone-antigen conjugates**

Peptide	Albumin (whole)	Subdomain IIA	Subdomain IIB	Subdomain IIIA
Dex-K4-OVA323	High	High	High	Moderate
Dex-E4-OVA323	Low	Low	Low	Moderate

**Dex-K4-OVA323 specifically expands the OVA323-specific Treg population.** To explore the effect of albumin-immunoconjugate electrostatic complementarity towards the systemic tolerogenic response, the OVA323-specific response induced by the immunoconjugates in mice was evaluated. The OTII adoptive transfer model for the evaluation (Figure 4a) was used, in which each C57BL/6-Ly5.1 mouse received an injection of OTII CD4<sup>+</sup> T cells one day before the administration of the immunoconjugates. The mice were vaccinated subcutaneously with Dex-K/E4-OVA323, the OVA323 epitope, or 1×PBS (control) on day 0. Since carboxylesterase is not present in subcutaneous tissue<sup>47, 48</sup>, this tissue offers an inert environment for the immunoconjugates to preserve their molecular integrity before

## **Complementary hydrophobic-electrostatic interactions enhance albumin association with dexamethasone-antigen conjugates leading to a more robust tolerogenic response**

association with albumin. Subsequently, the mice were sacrificed on day 7, and the splenocytes were analyzed by flow cytometry. Spleen was chosen for analysis because it is the largest secondary lymphoid organ in the body and was used for assaying the induction of systemic antigen-specific immunotolerance<sup>3, 49</sup>. The splenic T cell analysis (CD4<sup>+</sup>) showed that administration of Dex-K/E4-OVA323 did not cause a significant effect on the overall population of the Treg cells (CD25<sup>+</sup>Foxp3<sup>+</sup>) in the Ly5.1 mouse (Figure 4b). Since free dexamethasone can expand the overall Treg population in a non-antigen specific manner<sup>50, 51</sup>, the lack of overall Treg effect by Dex-K/E4-OVA323 treatment shows that the amount of dexamethasone released from the immunoconjugates in the physiological environment was minuscule. However, within the subpopulation of OVA323-specific T cells (CD4<sup>+</sup>CD45.2<sup>+</sup>), a significant expansion of Treg cells in the mice treated with Dex-K4-OVA323 compared to the PBS control group was observed, but not for those treated with Dex-E4-OVA323 or OVA323 epitope alone (Figure 4c). These results concur with the previous findings that, despite disease-associated antigens are endogenously expressed in the body<sup>52</sup>, tolerogenic adjuvants are required to trigger tolerogenic antigen presentation<sup>7-10</sup>. Furthermore, the obtained results demonstrate that the systemic tolerogenic antigen presentation level is attenuated by the charged linker residues in the immunoconjugates. In particular, the differential response between Dex-K4-OVA323 and Dex-E4-OVA323 postulates the correlation between the albumin-immunoconjugate electrostatic complementarity and the level of antigen-specific Treg induction. Further studies are planned to substantiate the claim of this work, including molecular dynamics simulation (elucidate the molecular association mechanism), cell uptake (explore cellular transportability of albumin<sup>23, 53</sup>), and bio-distribution studies.

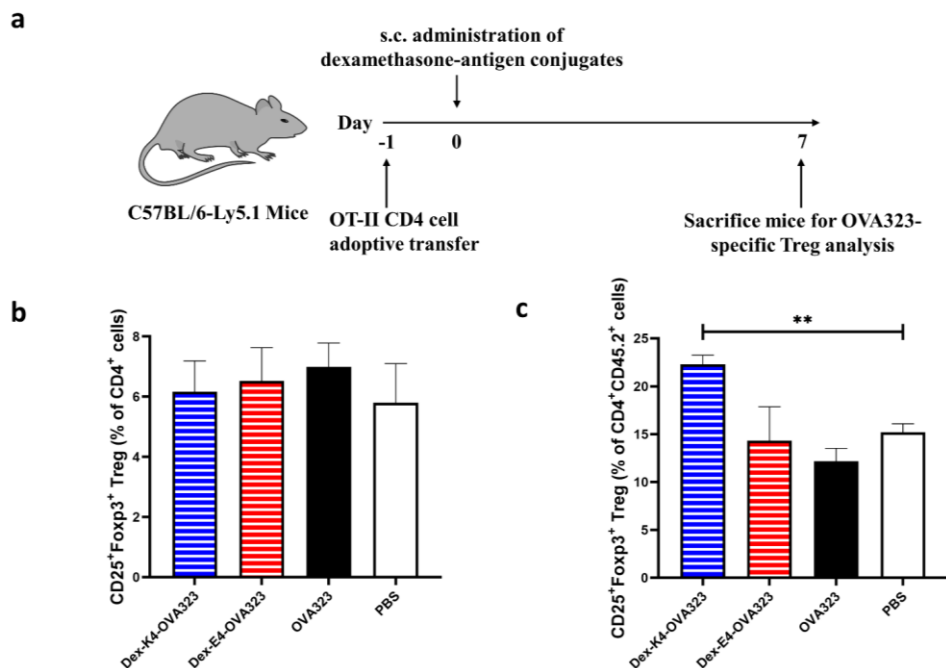


**Figure 4** The Dex-K4-OVA323 conjugates specifically upregulate the OVA323-specific Treg level. **a**) The CD45.1<sup>+</sup> C57BL/6-Ly5.1 mice receive an adoptive transfer of OTII CD45.2<sup>+</sup>CD4<sup>+</sup> T cells on day -1. The Ly5.1 mice are treated with phosphate-buffered saline (PBS, control), 200 $\mu$ g of dexamethasone-antigen conjugates, or OVA323 epitope via subcutaneous injection to both flanks (50 $\mu$ l each). The mice are sacrificed on day 7, and the spleen is harvested for flow cytometry analysis. **b**) Percentage of Treg (CD25<sup>+</sup>Foxp3<sup>+</sup>) in all CD4<sup>+</sup> T cells. No statistical difference is observed between the control and the immunoconjugate or epitope treatment groups. **c**) Percentage of Treg in OTII CD45.2<sup>+</sup> T cells. Significant expansion of Treg is observed in Dex-K4-OVA323 only. It shows that higher electrostatic complementarity between albumin and immunoconjugates can augment the tolerogenic response. Besides, it shows that antigen epitope alone is insufficient to establish a tolerogenic response. Data were analyzed by one-way ANOVA with Dunnett's multiple comparison test (compared to the control group) and expressed as the mean  $\pm$  standard deviations (n=5); \*\* p<0.01.

### 3. Conclusion

In summary, we have studied the connection between localized charge group variation within dexamethasone-antigen conjugates and the induction level of antigen-specific Treg. We show that the monomeric immunoconjugates because of their small size ( $\sim 1.5 \times 3.5$  nm), are susceptible to rapid renal clearance upon subcutaneous administration. Employing gel electrophoresis of supramolecular complexes, we show that immunoconjugates/plasma protein complexes are formed in the emulated biofluid of subcutaneous tissue, with albumin as a probable complexation partner. By evaluating the electrostatic surface potential of both albumin and the dexamethasone-antigen conjugates, we show that the charge variation in the spacer of the immunoconjugates yields binding moieties with binding moieties different electrostatic complementarity to the albumin. Furthermore, we demonstrate that immunoconjugates with higher electrostatic complementarity with albumin (Dex-K4-OVA323) induced significantly higher levels of OVA323-specific Treg, while no significant effect was

## **Complementary hydrophobic-electrostatic interactions enhance albumin association with dexamethasone-antigen conjugates leading to a more robust tolerogenic response**

observed for the immunoconjugates with lower electrostatic complementarity (Dex-E4-OVA323) or the antigen epitope alone (OVA323). These results postulate the correlation between albumin-immunoconjugate electrostatic complementarity and the level of antigen-specific Treg induction. Further experimental data are required to unveil the mechanistic link between albumin association and the enhanced tolerogenic response. Our finding offers a simple chemical approach to augment the immune response of the immunoconjugates for potential application in tolerogenic immunotherapy.

### **4. Materials and Methods**

**Synthesis of dexamethasone-antigen conjugates.** The peptides were synthesized with standard Fmoc solid-phase chemistry using a Liberty blue peptide synthesizer (CEM corporation). In brief, for each coupling cycle, 5eq Fmoc-protected amino acids were activated with 5eq of Oxyma pure and N,N'-Diisopropylcarbodiimide to react with the free N-terminal exposed on resin for 1 minute at 90°C. After each amino acid coupling, the Fmoc group was deprotected by treatment with 20% piperidine for 1 minute at 90°C. The dexamethasone succinate derivate was prepared as described previously<sup>35</sup>. This compound was subsequently coupled to the side chain protected sequence on resin using the same solid phase chemistry as other Fmoc-amino acids. The dexamethasone-antigen conjugate was cleaved with cocktail trifluoroacetic acid/water/triisopropylsilane (95/2.5/2.5) for 2 hours at room temperature and purified by preparative reverse-phase HPLC using a Reprosil-Pur 120 C18-AQ column (10µm, 250 × 25mm). The purity of the immunoconjugates was confirmed to be >90% by analytical HPLC using a Waters XBridge C18 column (5µm, 4.6 × 150mm), and Mass Spectrometry (MS) analysis was performed using a Bruker microTOF-Q instrument (Note S1-2).

**LigParGen parameterization.** The chemical structure of dexamethasone succinate was downloaded from PubChem (<https://pubchem.ncbi.nlm.nih.gov/>) and optimized with Avogadro software. The MOL file of the structurally optimized dexamethasone succinate was uploaded to the LigParGen web server for atomic coordinate parametrization<sup>40</sup>. The parameterized dexamethasone succinate was used as an artificial amino acid for further analysis.

**PEP-FOLD3 secondary structure prediction.** The *ab initio* secondary structure prediction of the charge group flanked OVA323 sequences was performed using the PEP-FOLD3.0 server<sup>36,37</sup>. Standard free modeling parameters were chosen for the sequence modeling. The best models (PDB files) were chosen for further analysis. The structural alphabet prediction profile was generated for representing the conformation propensities per residue in the output sequences (3 residues subtracted from the input sequences).

**Gel electrophoresis of supramolecular complexes.** *In vitro* supramolecular complexation was performed by incubating 20 µM immunoconjugates with biofluids, including 40% plasma, 8 mg/ml HSA or 8mg/ml MSA (Sigma Aldrich) in 1×PBS (2.7mM KCl, 1.5mM

KH<sub>2</sub>PO<sub>4</sub>, 138mM NaCl, 8mM Na<sub>2</sub>HPO<sub>4</sub>), at 37°C for one hour. Subsequently, the macromolecular complexation products were analyzed using NativePAGE™ 4-16% Bis-Tris gel (Thermo Fisher) running with 1× Tris-acetate-EDTA buffer (Figure S1). The dexamethasone-antigen conjugates were Cy5-labeled via the addition of Fmoc-Lys(Cy5)-OH (AAT Bioquest) to the N-terminal of OVA323 sequence during the solid phase synthesis (*i.e.*, Dex-K/E4-K<sub>(Cy5)</sub>OVA323, Note S3-4). Thereby, the distribution of the immunoconjugates in the macromolecular complexes (>55 kDa) can be identified by fluorescence signal (ex700/em750 nm) detected by ChemiDoc Imaging System (Bio-Rad Laboratories). Furthermore, the protein in the gel was visualized with Coomassie blue staining.

**Electrostatic surface potential analysis.** The electrostatic surface potential of the human serum albumin and dexamethasone-antigen conjugates were calculated using the APBS (Adaptive Poisson–Boltzmann Solver) software<sup>43</sup>. In brief, the PDB files of human serum albumin (PDB ID: 1UOR) and the dexamethasone-antigen conjugates were converted to PQR files using PDB2PQR<sup>54</sup>. Subsequently, the PQR files were analyzed by APBS with default charges and atomic radii to generate the surface potential map. Structural representations were prepared with Visual molecular dynamics (VMD, version 1.9.3)<sup>55</sup>.

**Mice.** All animal work was conducted under the approved protocol from the Animal Experiment Committee of Utrecht University. Female C57BL/6-Ly5.1 and C57BL/6-Tg(TcraTcrb)425Cbn/Crl (OTII) mice (8 weeks) were purchased from Charles River and kept under standard conditions at the animal facility.

**Antibodies for flow cytometry analysis.** The monoclonal antibodies for mouse CD4 (eBioscience, Cat# 11-0042-82), CD25 (BD, Cat# 553866), CD45.2 (eBioscience, Cat# 45-0454-82), Foxp3 (eBioscience, Cat# 45-5773-82) were used according to the manufacturer's instruction, including antibody dilution. Flow cytometry was performed on a Gallios flow cytometer (Beckman Coulter). Data were analyzed using FlowJo 7.6.5.

**OTII adoptive transfer model for tolerogenic assay.** On day -1, OTII mice were sacrificed. CD4<sup>+</sup> T cells were isolated from the spleen of OTII mice using a CD4<sup>+</sup> T-cell magnetic bead isolation kit (Miltenyi Biotec). A total of 5.5×10<sup>5</sup> CD45.2<sup>+</sup>CD4<sup>+</sup> OT-II T cells were adoptively transferred into each CD45.1<sup>+</sup> Ly5.1 mouse via tail-vein injection. On day 0, samples (200 µg) were subcutaneously injected to both right and left flank of the Ly5.1 mouse (50 µl each in 1× PBS). Mice were sacrificed on day 7. The spleens of the different mice were isolated, and the splenocytes were analyzed by flow cytometry.

**Statistical analysis.** Statistical analysis was performed in GraphPad Prism v.9.1.1 using one-way ANOVA with Dunnett's multiple comparison test. Data were presented as average± standard deviations unless otherwise indicated. Significant statistical difference was annotated as \*\* p<0.01.



## **Complementary hydrophobic-electrostatic interactions enhance albumin association with dexamethasone-antigen conjugates leading to a more robust tolerogenic response**

### **5. Acknowledgment**

C.Y.J.L acknowledges the support from the European Union (Horizon 2020 NANOMED Grant 676137). We thank Danny Wilbie for his help with Native PAGE analysis.

### **6. Author contributions**

C.Y.J.L. contributed to the organic synthesis, structural bioinformatics analysis and the native PAGE gel studies. C.Y.L., N.B., B.L., D.t.B., N.v.K. and M.F. contributed to the animal experiment. N.B., D.t.B. and F.B. contributed to the flow cytometry analysis. C.Y.J.L., W.H. and E.M. provided advice on the design of the whole experiments, C.Y.J.L., W.H. and E.M. designed the research concept, managed the project and were the main contributors to the manuscript writing.

### References

1. Sakaguchi, S.; Miyara, M.; Costantino, C. M.; Hafler, D. A., FOXP3+ regulatory T cells in the human immune system. *Nature Reviews Immunology* **2010**, *10* (7), 490-500.
2. Esensten, J. H.; Muller, Y. D.; Bluestone, J. A.; Tang, Q., Regulatory T-cell therapy for autoimmune and autoinflammatory diseases: The next frontier. *Journal of Allergy and Clinical Immunology* **2018**, *142* (6), 1710-1718.
3. Krienke, C.; Kolb, L.; Diken, E.; Streuber, M.; Kirchhoff, S.; Bukur, T.; Akilli-Öztürk, Ö.; Kranz, L. M.; Berger, H.; Petschenka, J.; Diken, M.; Kreiter, S.; Yogev, N.; Waisman, A.; Karikó, K.; Türeci, Ö.; Sahin, U., A noninflammatory mRNA vaccine for treatment of experimental autoimmune encephalomyelitis. *Science* **2021**, *371* (6525), 145.
4. Hansson, G. K.; Nilsson, J., Developing a vaccine against atherosclerosis. *Nature Reviews Cardiology* **2020**, *17* (8), 451-452.
5. Nilsson, J.; Hansson, G. K., Vaccination Strategies and Immune Modulation of Atherosclerosis. *Circulation Research* **2020**, *126* (9), 1281-1296.
6. Spence, A.; Purtha, W.; Tam, J.; Dong, S.; Kim, Y.; Ju, C.-H.; Sterling, T.; Nakayama, M.; Robinson, W. H.; Bluestone, J. A.; Anderson, M. S.; Tang, Q., Revealing the specificity of regulatory T cells in murine autoimmune diabetes. *Proceedings of the National Academy of Sciences* **2018**, *115* (20), 5265.
7. Maldonado, R. A.; LaMothe, R. A.; Ferrari, J. D.; Zhang, A.-H.; Rossi, R. J.; Kolte, P. N.; Griset, A. P.; O’Neil, C.; Altreuter, D. H.; Browning, E.; Johnston, L.; Farokhzad, O. C.; Langer, R.; Scott, D. W.; von Andrian, U. H.; Kishimoto, T. K., Polymeric synthetic nanoparticles for the induction of antigen-specific immunological tolerance. *Proceedings of the National Academy of Sciences* **2015**, *112* (2), E156.
8. Sands, R. W.; Tabansky, I.; Verbeke, C. S.; Keskin, D.; Michel, S.; Stern, J.; Mooney, D. J., Steroid–Peptide Immunoconjugates for Attenuating T Cell Responses in an Experimental Autoimmune Encephalomyelitis Murine Model of Multiple Sclerosis. *Bioconjugate Chemistry* **2020**, *31* (12), 2779-2788.
9. Pickens, C. J.; Christopher, M. A.; Leon, M. A.; Pressnall, M. M.; Johnson, S. N.; Thati, S.; Sullivan, B. P.; Berkland, C., Antigen-Drug Conjugates as a Novel Therapeutic Class for the Treatment of Antigen-Specific Autoimmune Disorders. *Molecular Pharmaceutics* **2019**, *16* (6), 2452-2461.
10. Cifuentes-Rius, A.; Desai, A.; Yuen, D.; Johnston, A. P. R.; Voelcker, N. H., Inducing immune tolerance with dendritic cell-targeting nanomedicines. *Nature Nanotechnology* **2021**, *16* (1), 37-46.
11. Trevaskis, N. L.; Kaminskas, L. M.; Porter, C. J. H., From sewer to saviour — targeting the lymphatic system to promote drug exposure and activity. *Nature Reviews Drug Discovery* **2015**, *14* (11), 781-803.
12. Ryan, G. M.; Kaminskas, L. M.; Porter, C. J. H., Nano-chemotherapeutics: Maximising lymphatic drug exposure to improve the treatment of lymph-metastatic cancers. *Journal of Controlled Release* **2014**, *193*, 241-256.
13. Longmire, M.; Choyke, P. L.; Kobayashi, H., Clearance properties of nano-sized particles and molecules as imaging agents: considerations and caveats. *Nanomedicine* **2008**, *3* (5), 703-717.
14. Bertrand, N.; Leroux, J.-C., The journey of a drug-carrier in the body: An anatomico-physiological perspective. *Journal of Controlled Release* **2012**, *161* (2), 152-163.

## **Complementary hydrophobic-electrostatic interactions enhance albumin association with dexamethasone-antigen conjugates leading to a more robust tolerogenic response**

15. Ellmerer, M.; Schaupp, L.; Brunner, G. A.; Sendlhofer, G.; Wutte, A.; Wach, P.; Pieber, T. R., Measurement of interstitial albumin in human skeletal muscle and adipose tissue by open-flow microperfusion. *American Journal of Physiology-Endocrinology and Metabolism* **2000**, *278* (2), E352-E356.
16. Fanali, G.; di Masi, A.; Trezza, V.; Marino, M.; Fasano, M.; Ascenzi, P., Human serum albumin: From bench to bedside. *Molecular Aspects of Medicine* **2012**, *33* (3), 209-290.
17. Czub, M. P.; Venkataramany, B. S.; Majorek, K. A.; Handing, K. B.; Porebski, P. J.; Beeram, S. R.; Suh, K.; Woolfork, A. G.; Hage, D. S.; Shabalin, I. G.; Minor, W., Testosterone meets albumin – the molecular mechanism of sex hormone transport by serum albumins. *Chemical Science* **2019**, *10* (6), 1607-1618.
18. Czub, M. P.; Handing, K. B.; Venkataramany, B. S.; Cooper, D. R.; Shabalin, I. G.; Minor, W., Albumin-Based Transport of Nonsteroidal Anti-Inflammatory Drugs in Mammalian Blood Plasma. *Journal of Medicinal Chemistry* **2020**, *63* (13), 6847-6862.
19. Abdallah, M.; Müllertz, O. O.; Styles, I. K.; Mörsdorf, A.; Quinn, J. F.; Whittaker, M. R.; Trevaskis, N. L., Lymphatic targeting by albumin-hitchhiking: Applications and optimisation. *Journal of Controlled Release* **2020**, *327*, 117-128.
20. Liu, H.; Moynihan, K. D.; Zheng, Y.; Szeto, G. L.; Li, A. V.; Huang, B.; Van Egeren, D. S.; Park, C.; Irvine, D. J., Structure-based programming of lymph-node targeting in molecular vaccines. *Nature* **2014**, *507* (7493), 519-522.
21. Yousefpour, P.; Varanko, A.; Subrahmanyam, R.; Chilkoti, A., Recombinant Fusion of Glucagon-Like Peptide-1 and an Albumin Binding Domain Provides Glycemic Control for a Week in Diabetic Mice. *Advanced Therapeutics* **2020**, *3* (10), 2000073.
22. Kwak, G.; Kim, H.; Park, J.; Kim, E. H.; Jang, H.; Han, G.; Wang, S. Y.; Yang, Y.; Chan Kwon, I.; Kim, S. H., A Trojan-Horse Strategy by In Situ Piggybacking onto Endogenous Albumin for Tumor-Specific Neutralization of Oncogenic MicroRNA. *ACS Nano* **2021**, *15* (7), 11369-11384.
23. Zhu, G.; Lynn, G. M.; Jacobson, O.; Chen, K.; Liu, Y.; Zhang, H.; Ma, Y.; Zhang, F.; Tian, R.; Ni, Q.; Cheng, S.; Wang, Z.; Lu, N.; Yung, B. C.; Wang, Z.; Lang, L.; Fu, X.; Jin, A.; Weiss, I. D.; Vishwasrao, H.; Niu, G.; Shroff, H.; Klinman, D. M.; Seder, R. A.; Chen, X., Albumin/vaccine nanocomplexes that assemble in vivo for combination cancer immunotherapy. *Nature Communications* **2017**, *8* (1), 1954.
24. Cummings, D. M.; Larijani, G. E.; Conner, D. P.; Ferguson, R. K.; Rocci, M. L., Characterization of Dexamethasone Binding in Normal and Uremic Human Serum. *DICP* **1990**, *24* (3), 229-231.
25. Peets, E. A.; Staub, M.; Symchowicz, S., Plasma binding of betamethasone3H, dexamethasone-3H, and cortisol-14C— A comparative study. *Biochemical Pharmacology* **1969**, *18* (7), 1655-1663.
26. He, X. M.; Carter, D. C., Atomic structure and chemistry of human serum albumin. *Nature* **1992**, *358* (6383), 209-215.
27. Naik, P. N.; Chimatadar, S. A.; Nandibewoor, S. T., Interaction between a potent corticosteroid drug – Dexamethasone with bovine serum albumin and human serum albumin: A fluorescence quenching and fourier transformation infrared spectroscopy study. *Journal of Photochemistry and Photobiology B: Biology* **2010**, *100* (3), 147-159.

28. Shabalina, I. G.; Czub, M. P.; Majorek, K. A.; Brzezinski, D.; Grabowski, M.; Cooper, D. R.; Panasiuk, M.; Chruszcz, M.; Minor, W., Molecular determinants of vascular transport of dexamethasone in COVID-19 therapy. *IUCrJ* **2020**, *7* (Pt 6), 1048-58.
29. Marszałek, M.; Konarska, A.; Szajdzinska-Pietek, E.; Wolszczak, M., Interaction of Cationic Protoberberine Alkaloids with Human Serum Albumin. No Spectroscopic Evidence on Binding to Sudlow's Site 1. *The Journal of Physical Chemistry B* **2013**, *117* (50), 15987-15993.
30. Sivertsen, A.; Isaksson, J.; Leiros, H.-K. S.; Svenson, J.; Svendsen, J.-S.; Brandsdal, B. O., Synthetic cationic antimicrobial peptides bind with their hydrophobic parts to drug site II of human serum albumin. *BMC Structural Biology* **2014**, *14* (1), 4.
31. Singh, A. N.; Yethiraj, A., Driving Force for the Complexation of Charged Polypeptides. *The Journal of Physical Chemistry B* **2020**, *124* (7), 1285-1292.
32. Rathee, V. S.; Sidky, H.; Sikora, B. J.; Whitmer, J. K., Role of Associative Charging in the Entropy–Energy Balance of Polyelectrolyte Complexes. *Journal of the American Chemical Society* **2018**, *140* (45), 15319-15328.
33. Zhou, H.-X.; Pang, X., Electrostatic Interactions in Protein Structure, Folding, Binding, and Condensation. *Chemical Reviews* **2018**, *118* (4), 1691-1741.
34. Lee, K. K.; Fitch, C. A.; García-Moreno E, B., Distance dependence and salt sensitivity of pairwise, coulombic interactions in a protein. *Protein Science* **2002**, *11* (5), 1004-1016.
35. Acedo, M.; Tarrason, G.; Piulats, J.; Mann, M.; Wilm, M.; Eritja, R., Preparation of oligonucleotide-dexamethasone conjugates. *Bioorganic & Medicinal Chemistry Letters* **1995**, *5* (15), 1577-1580.
36. Shen, Y.; Maupetit, J.; Derreumaux, P.; Tufféry, P., Improved PEP-FOLD Approach for Peptide and Mini-protein Structure Prediction. *Journal of Chemical Theory and Computation* **2014**, *10* (10), 4745-4758.
37. Lamiable, A.; Thévenet, P.; Rey, J.; Vavrusa, M.; Derreumaux, P.; Tufféry, P., PEP-FOLD3: faster de novo structure prediction for linear peptides in solution and in complex. *Nucleic Acids Res* **2016**, *44* (W1), W449-54.
38. Crusca Jr, E.; Rezende, A. A.; Marchetto, R.; Mendes-Giannini, M. J. S.; Fontes, W.; Castro, M. S.; Cilli, E. M., Influence of N-terminus modifications on the biological activity, membrane interaction, and secondary structure of the antimicrobial peptide hylin-a1. *Peptide Science* **2011**, *96* (1), 41-48.
39. Camproux, A. C.; Gautier, R.; Tufféry, P., A Hidden Markov Model Derived Structural Alphabet for Proteins. *Journal of Molecular Biology* **2004**, *339* (3), 591-605.
40. Dodda, L. S.; Cabeza de Vaca, I.; Tirado-Rives, J.; Jorgensen, W. L., LigParGen web server: an automatic OPLS-AA parameter generator for organic ligands. *Nucleic Acids Research* **2017**, *45* (W1), W331-W336.
41. Rutili, G.; Arfors, K.-E., Protein Concentration in Interstitial and Lymphatic Fluids from the Subcutaneous Tissue. *Acta Physiologica Scandinavica* **1977**, *99* (1), 1-8.
42. Li, X.; Jeong, K.; Lee, Y.; Guo, T.; Lee, D.; Park, J.; Kwon, N.; Na, J.-H.; Hong, S. K.; Cha, S.-S.; Huang, J.-D.; Choi, S.; Kim, S.; Yoon, J., Water-Soluble Phthalocyanines Selectively Bind to Albumin Dimers: A Green Approach Toward Enhancing Tumor-Targeted Photodynamic Therapy. *Theranostics* **2019**, *9* (22), 6412-6423.

## **Complementary hydrophobic-electrostatic interactions enhance albumin association with dexamethasone-antigen conjugates leading to a more robust tolerogenic response**

43. Baker, N. A.; Sept, D.; Joseph, S.; Holst, M. J.; McCammon, J. A., Electrostatics of nanosystems: Application to microtubules and the ribosome. *Proceedings of the National Academy of Sciences* **2001**, *98* (18), 10037.
44. Nilsen, J.; Bern, M.; Sand, K. M. K.; Grevys, A.; Dalhus, B.; Sandlie, I.; Andersen, J. T., Human and mouse albumin bind their respective neonatal Fc receptors differently. *Scientific Reports* **2018**, *8* (1), 14648.
45. Worth, C. L.; Blundell, T. L., On the evolutionary conservation of hydrogen bonds made by buried polar amino acids: the hidden joists, braces and trusses of protein architecture. *BMC evolutionary biology* **2010**, *10*, 161-2148-10-161.
46. Sandblad, P.; Arnell, R.; Samuelsson, J.; Fornstedt, T., Approach for Reliable Evaluation of Drug Proteins Interactions Using Surface Plasmon Resonance Technology. *Analytical Chemistry* **2009**, *81* (9), 3551-3559.
47. Kalicharan, R. W.; Bout, M. R.; Oussoren, C.; Vromans, H., Where does hydrolysis of nandrolone decanoate occur in the human body after release from an oil depot? *International Journal of Pharmaceutics* **2016**, *515* (1), 721-728.
48. Kalicharan, R. W.; Oussoren, C.; Schot, P.; de Rijk, E.; Vromans, H., The contribution of the in-vivo fate of an oil depot to drug absorption. *International Journal of Pharmaceutics* **2017**, *528* (1), 595-601.
49. Lewis, S. M.; Williams, A.; Eisenbarth, S. C., Structure and function of the immune system in the spleen. *Science Immunology* **2019**, *4* (33), eaau6085.
50. Chen, X.; Oppenheim, J. J.; Winkler-Pickett, R. T.; Ortaldo, J. R.; Howard, O. M. Z., Glucocorticoid amplifies IL-2-dependent expansion of functional FoxP3+CD4+CD25+ T regulatory cells in vivo and enhances their capacity to suppress EAE. *European Journal of Immunology* **2006**, *36* (8), 2139-2149.
51. Chen, X.; Murakami, T.; Oppenheim, J. J.; Howard, O. M. Z., Differential response of murine CD4+CD25+ and CD4+CD25- T cells to dexamethasone-induced cell death. *European Journal of Immunology* **2004**, *34* (3), 859-869.
52. Wolf, D.; Gerhardt, T.; Winkels, H.; Michel, N. A.; Pramod, A. B.; Ghosheh, Y.; Brunel, S.; Buscher, K.; Miller, J.; McArdle, S.; Baas, L.; Kobiyama, K.; Vassallo, M.; Ehinger, E.; Dileepan, T.; Ali, A.; Schell, M.; Mikulski, Z.; Sidler, D.; Kimura, T.; Sheng, X.; Horstmann, H.; Hansen, S.; Mitre, L. S.; Stachon, P.; Hilgendorf, I.; Gaddis, D. E.; Hedrick, C.; Benedict, C. A.; Peters, B.; Zirlik, A.; Sette, A.; Ley, K., Pathogenic Autoimmunity in Atherosclerosis Evolves From Initially Protective Apolipoprotein B100- Reactive CD4+ T-Regulatory Cells. *Circulation* **2020**, *142* (13), 1279-1293.
53. Roopenian, D. C.; Akilesh, S., FcRn: the neonatal Fc receptor comes of age. *Nature Reviews Immunology* **2007**, *7* (9), 715-725.
54. Dolinsky, T. J.; Czodrowski, P.; Li, H.; Nielsen, J. E.; Jensen, J. H.; Klebe, G.; Baker, N. A., PDB2PQR: expanding and upgrading automated preparation of biomolecular structures for molecular simulations. *Nucleic Acids Research* **2007**, *35* (suppl\_2), W522-W525.
55. Humphrey, W.; Dalke, A.; Schulten, K., VMD: Visual molecular dynamics. *Journal of Molecular Graphics* **1996**, *14* (1), 33-38.

## Supplementary Information

### Complementary hydrophobic-electrostatic interactions enhance albumin association with dexamethasone-antigen conjugates leading to a more robust tolerogenic response

Chun Yin Jerry Lau, Naomi Benne, Bo Lou, Daniëlle ter Braake, Nicky van Kronenburg, Marcel Fens, Wim E. Hennink, Femke Broere, Enrico Mastrobattista

## Complementary hydrophobic-electrostatic inter-actions enhance albumin association with dexamethasone-antigen conjugates leading to a more robust tolerogenic response

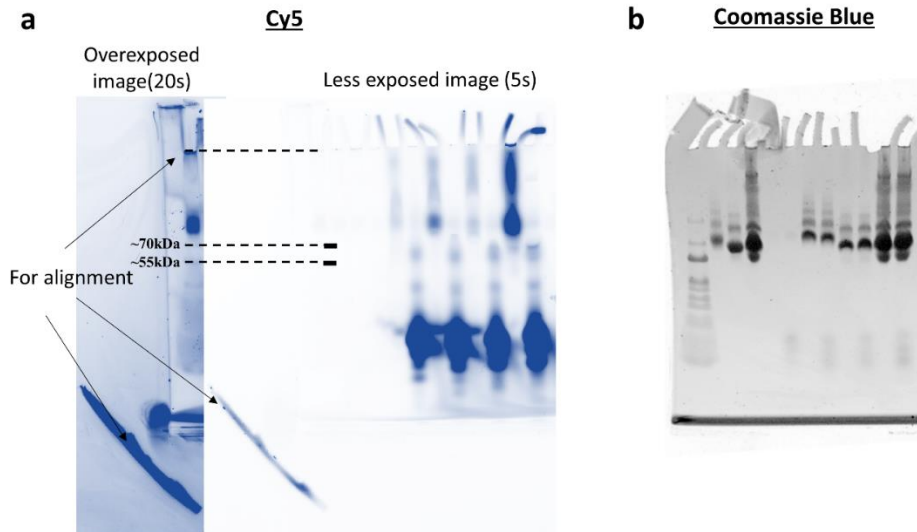


**Figure S1 Protein ladder alignment in fluorescence channel of native PAGE gel of immunoconjugates-biofluid complexes a)** The full native PAGE gel of the supramolecular complexes formed between immunoconjugates and biofluids. The protein ladder (55, 70kDa) in the fluorescence channel was assigned by exaggerating the exposure time (20s), followed by alignment to the less exposed image (5s). **b)** The whole native PAGE gel with Coomassie blue staining, which visualized the protein present in the system.

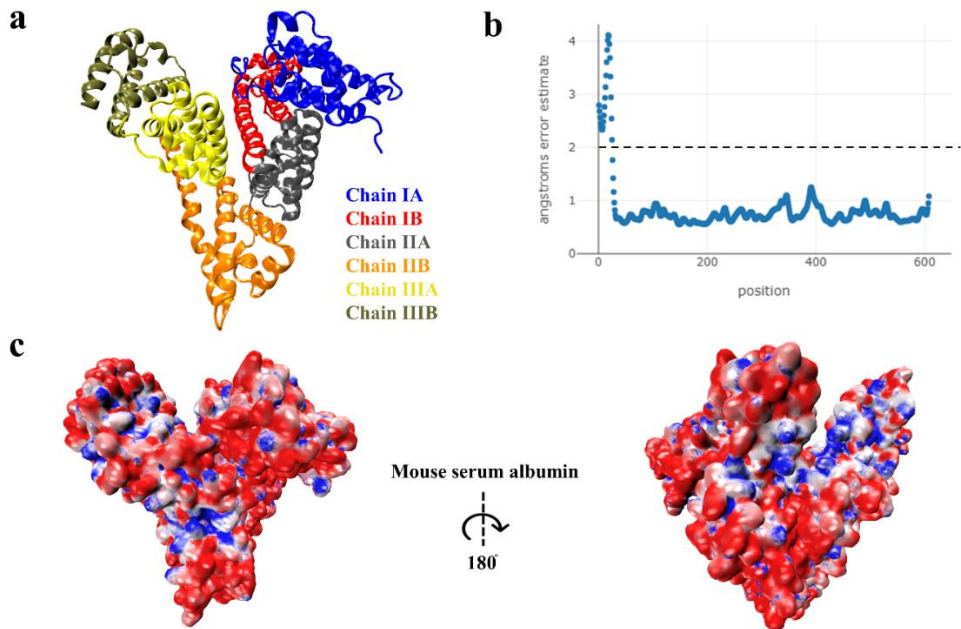


**Figure S2 RoseTTAFold<sup>1</sup> model and electrostatic surface potential analysis of mouse serum albumin (MSA).** **a)** The RoseTTAFold model ( $<2\text{\AA}$  error) of MSA (26-608) with a global distance test (GDT) score of 0.9. **b)** Plot of per-residue error estimates for the selected MSA model (1-608). It shows that residue 26-608 has  $<2\text{\AA}$  per-residue error. **c)** The electrostatic surface potential of the selected MSA model calculated using the APBS (Adaptive Poisson-Boltzmann Solver) software<sup>2</sup>. Potential isocontours are shown at  $-5\text{ kT/e}$  (red) and  $+5\text{ kT/e}$  (blue). Structural representations were prepared with Visual molecular dynamics (VMD) software<sup>3</sup>.



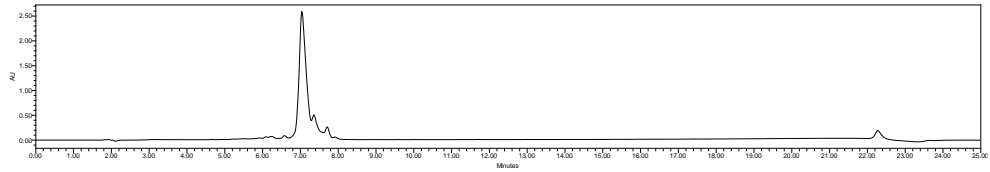
# Complementary hydrophobic-electrostatic inter-actions enhance albumin association with dexamethasone-antigen conjugates leading to a more robust tolerogenic response

## Supplementary Note 1-2: HPLC-MS traces of Dexamethasone-antigen conjugates

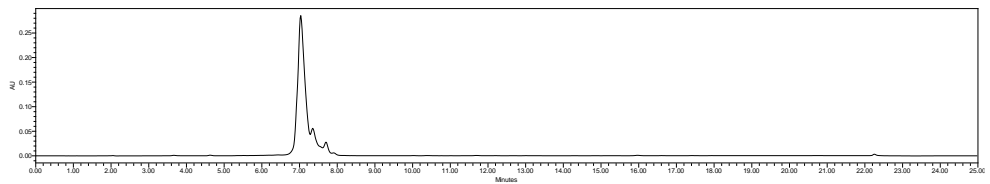
**Note S1:** DEX-K4-OVA (Theoretical mass=2761.1 Da;  $[M+2H]^{2+}=1381.6$ ,  $[M+3H]^{3+}=921.4$ ,  $[M+4H]^{4+}=691.3$ )

Analytical HPLC (5% to 100% acetonitrile in 20 min, 0.1% formic acid)

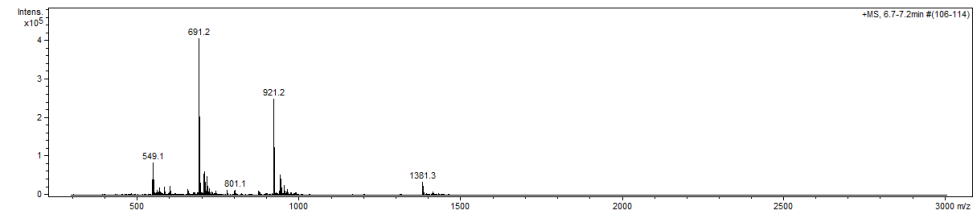
220nm



280nm



MS

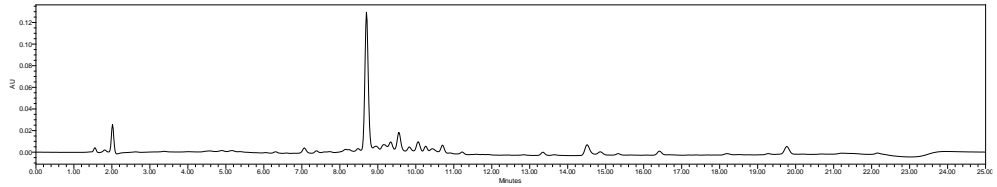


## Chapter 6

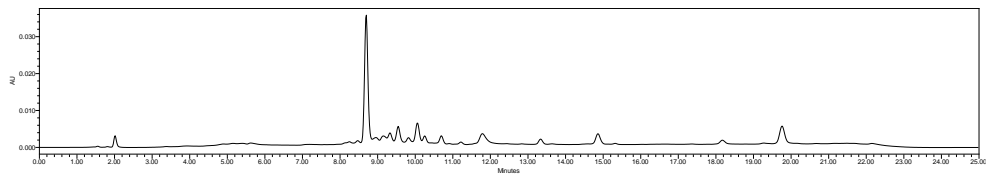
**Note S2:** Dex-E4-OVA (Theoretical mass=2764.9 Da;  $[M+2H]^{2+}=1383.5$ ,  
 $[M+3H]^{3+}=922.6$ )

Analytical HPLC (5% to 80% acetonitrile in 20 min, 10mM ammonium bicarbonate)

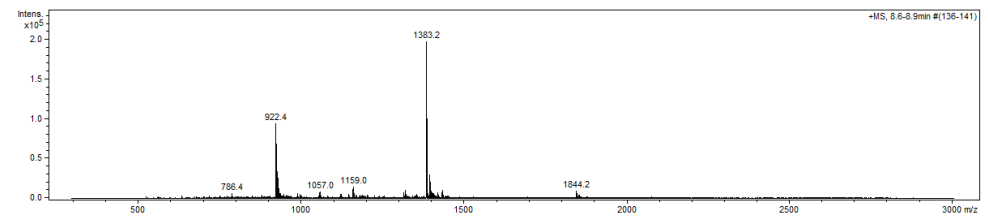
220nm



280nm



MS

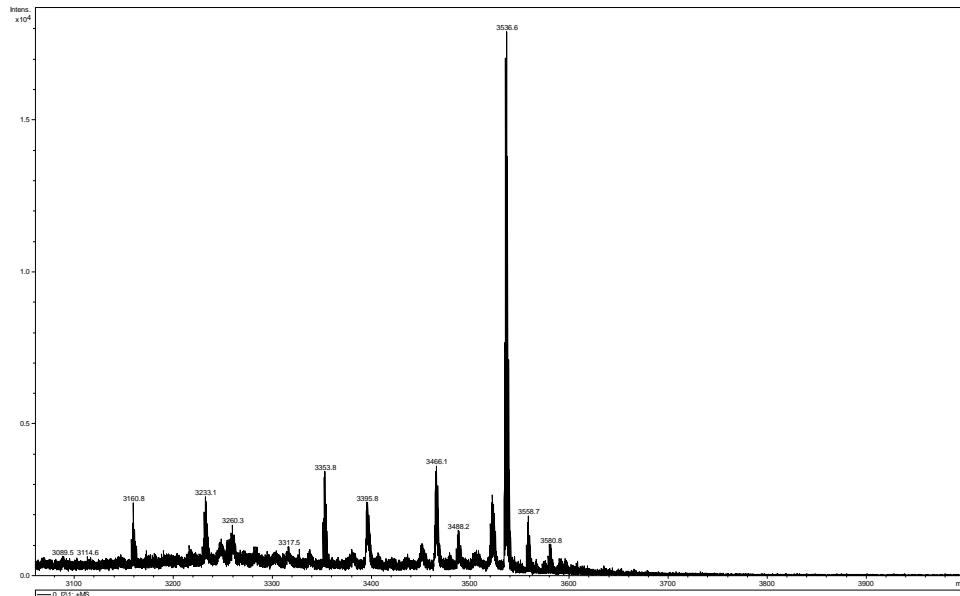


## Complementary hydrophobic-electrostatic inter-actions enhance albumin association with dexamethasone-antigen conjugates leading to a more robust tolerogenic response

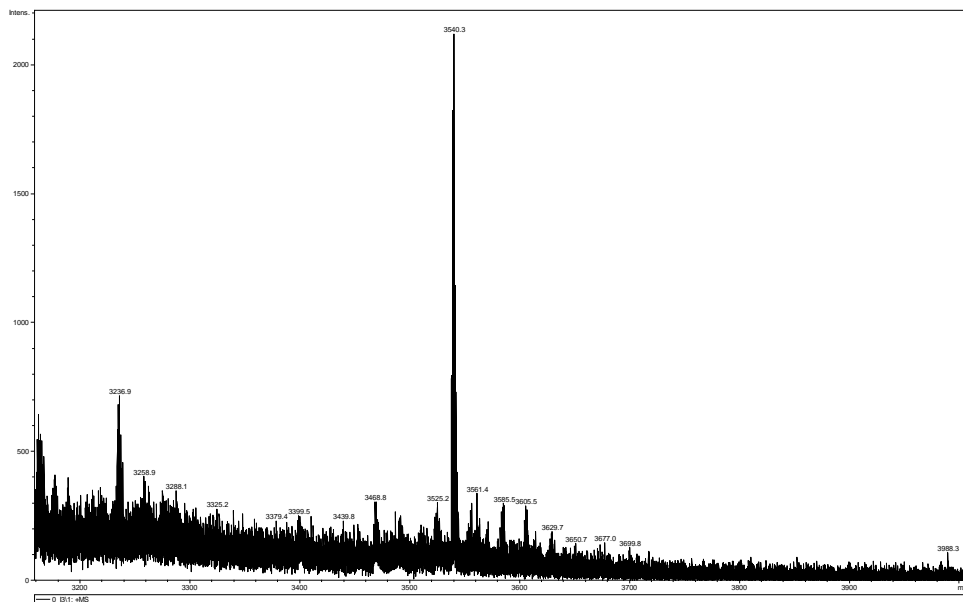
### Supplementary Note 3-4: MALDI-TOF/TOF MS traces of Cy5 labeled Dexamethasone-antigen conjugates

Note S3: Dex-K4-K(Cy5)ISQAVHAAHAEINEAGR (Theoretical  $[M+Na]^+$ :3536.1)

MALDI-TOF/TOF (Bruker ultrafleXtreme,  $\alpha$ -Cyano-4-hydroxycinnamic acid matrix)



**Note S4:** Dex-E4-K(Cy5)ISQAVHAAHAEINEAGR (Theoretical [M+Na]<sup>+</sup>:3539.9)  
MALDI-TOF/TOF (Bruker ultrafleXtreme,  $\alpha$ -Cyano-4-hydroxycinnamic acid matrix)



1. Baek, M.; DiMaio, F.; Anishchenko, I.; Dauparas, J.; Ovchinnikov, S.; Lee, G. R.; Wang, J.; Cong, Q.; Kinch, L. N.; Schaeffer, R. D.; Millán, C.; Park, H.; Adams, C.; Glassman, C. R.; DeGiovanni, A.; Pereira, J. H.; Rodrigues, A. V.; van Dijk, A. A.; Ebrecht, A. C.; Opperman, D. J.; Sagmeister, T.; Buhlheller, C.; Pavkov-Keller, T.; Rathinaswamy, M. K.; Dalwadi, U.; Yip, C. K.; Burke, J. E.; Garcia, K. C.; Grishin, N. V.; Adams, P. D.; Read, R. J.; Baker, D., Accurate prediction of protein structures and interactions using a three-track neural network. *Science* **2021**, eabj8754.
2. Baker, N. A.; Sept, D.; Joseph, S.; Holst, M. J.; McCammon, J. A., Electrostatics of nanosystems: Application to microtubules and the ribosome. *Proceedings of the National Academy of Sciences* **2001**, 98 (18), 10037.
3. Humphrey, W.; Dalke, A.; Schulten, K., VMD: Visual molecular dynamics. *Journal of Molecular Graphics* **1996**, 14 (1), 33-38.

# **Chapter 7**

Summary and Perspectives

### 1. Summary

This thesis explores the potential immunological applications of supramolecular peptide materials using the roadmap for functional supramolecular materials development described by Meijer et al. <sup>1</sup>. This roadmap can be summarized as 1) optimization of the non-covalent synthesis of the materials; 2) in-depth characterization of the material properties; and 3) effective integration of materials to the application sites to deliver its overarching functionality. **Chapter 1** provides a short introduction to the background and considerations for developing supramolecular peptide materials targeting immunological applications.

**Optimization of the non-covalent synthesis of the materials.** Since the non-covalent synthesis of supramolecular materials consists of multiple steps, the intermediate states play a significant role in deciding the outcome of the supramolecular products. The parameters for optimizing the non-covalent synthesis of the supramolecular peptide materials are discussed in **chapter 2**. Using the zero-/one-dimensional nanostructure selectivity over the  $\beta$ -sheet assembly pathway as an example, we highlighted the internal and external factors that can modulate the intermediates and discussed how those factors can influence the assembly outcome. In **chapter 3**, we investigated the molecular parameters governing the nucleation propensities of the oligomeric intermediates. Using a cognate set of self-assembling peptides, we showed that lowering the mutually repulsive electrostatic charges between the peptide building blocks and increasing the  $\beta$ -sheet propensities of the peptide sequence can increase the nucleation propensities of the oligomeric intermediates. We showed that the oligomeric nucleation propensities critically define the fibrillization yield.

**In-depth characterization of the material properties.** Precise understanding of the structural organization of supramolecular products can not only give us better insights into their material properties but also provide clues into the energy constraints these structures are encountering. In **chapter 4**, we used cryo-EM analysis to study the supramolecular organization of peptide nanofibers formed by supramolecular assembly of surfactant-like peptide 1 (SLP1). We observed that SLP1 nanofibers (diameter  $\sim$ 4nm, length  $>$ 500nm) display low twists under physiological conditions. This physicochemical property hinders the 3D reconstruction of the structure using a commonly used cryo-EM image processing method, REgularised LIkelihood Optimisation (RELION)<sup>2</sup>. Taking a guide from the 2D class averages of cryo-EM, we succeed in elucidating the protofibril and fibrous organization of the SLP1 nanofibers. Based on the reconstructed structures, we conjectured the possible causes of the low twist of SLP1 nanofibers in physiological buffer and outlined the functional implications of SLP1 nanofiber towards tissue engineering and drug delivery. These insights demonstrate how a high-level understanding of the supramolecular organization can aid future molecular design and functional exploitation of supramolecular materials.

**Effective functional integration of materials to the application sites.** To deliver the overarching biomedical functionality of the supramolecular materials, the materials must be effectively integrated into the application sites. Two main approaches of functional

integration of materials are being pursued---1) reconciling the fabricated supramolecular materials and the administration sites, or 2) incorporating the supramolecular materials as modalities in the application sites. In **chapter 5 and 6**, we explored the potential application of supramolecular peptide materials as tolerogenic vaccines using these two respective functional integration approaches. In **chapter 5**, we deployed nanofibers as scaffolds for the co-delivery of antigen epitopes and tolerogenic adjuvants (dexamethasone). In agreement with the previous findings<sup>3</sup>, we showed that the fiber scaffold with more negative  $\zeta$ -potential can enhance macrophage receptor with collagenous structure (MARCO)-mediated uptake, thereby leading to a more robust tolerogenic response. In **chapter 6**, inspired by the peptide-protein complexation mechanism, we explored the use of complementary hydrophobic-electrostatic interactions to enhance the association propensities between albumin and the dexamethasone-antigen conjugates. Through varying the electrostatic surface potential of the albumin binding moiety in the dexamethasone-antigen conjugate, we discovered that immunoconjugates of higher electrostatic complementarity with albumin are prone to a higher *in-situ* association. We found that immunoconjugates with higher albumin association propensity gave more robust tolerogenic responses upon *in vivo* administration.

### 2. Immediate steps forward

**Cryo-EM characterization of functionalized supramolecular nanofibers.** Having characterized the hierarchical structure of non-functionalized SLP1 nanofibers in **chapter 4**, the next step will be to understand how nanofiber functionalization (e.g., drug conjugation) can influence its supramolecular organization. In particular, small molecule drugs are generally hydrophobic. As hydrophobic interactions are the primary driver of structural ordering in proteinaceous materials<sup>4</sup>, adding the hydrophobic moieties to nanofibers can likely trigger structural organization cascades. For example, dexamethasone functionalization of the nanofibers in **chapter 5** can likely enhance the sophistication of their hierarchical assembly pathway<sup>5</sup>. Therefore, a high-level understanding of the supramolecular organization of the functionalized nanofibers (e.g., the surface exposure of drug molecules) is crucial to further their application exploitation.

**Explore translatability of dexamethasone-antigen conjugates for autoimmune disease treatments.** Having shown that dexamethasone-antigen conjugate with high albumin association propensities elicits the most robust antigen-specific tolerogenic response among all the candidates studied in **chapter 5 and 6**, the next step will be to explore its clinical translatability in autoimmune disease models. Several issues need to be considered for effective translation. First, the number of charged residues in the immunoconjugates needs to be adjusted according to the physicochemical properties of the disease-associated epitopes (e.g., number of anionic residues) to maintain a net positive electrostatic surface potential for albumin association. Second, to utilize the ability of the immunoconjugates in upregulating splenic regulatory T (Treg) cells, autoimmune diseases with a direct link to splenic immunity should be chosen for preliminary investigations. For example, heightened proinflammatory antigen-specific activity in the cardiosplenic axis is shown to cause pathological cardiac remodelling (e.g., heart failure)<sup>6,7</sup>. Therefore, induction of

cardioprotective splenic Treg by the immunoconjugates presents a promising strategy in alleviating these pathological symptoms<sup>8</sup>.

**Utilize supramolecular properties of dexamethasone-antigen conjugates to assist conventional nanomedicine preparation.** On top of exploring the translatability in autoimmune disease treatment, the supramolecular properties of the dexamethasone-antigen conjugates can also be harnessed for assisting conventional nanomedicines preparation. For example, electrostatic attractions can increase the encapsulation efficiency of charged residues modified antigens into nanogels<sup>9</sup>. Since many nanomedicines are amphiphilic in nature (e.g., lipid nanoparticles), this makes dexamethasone-antigen conjugates a suitable interaction partner with them through complimentary hydrophobic-electrostatic interactions.

### 3. Perspective

**Quantifying the system plurality of the supramolecular materials.** Due to the inherent system plurality, one major challenge in developing functional supramolecular materials is consistently manufacturing well-defined structures. Due to the pathway complexity of constructing supramolecular materials, different intermediate stages can lead to the formation of different supramolecular products<sup>10, 11</sup>. For example, in **chapter 3**, we observed that the fibrillization process can give rise to a mixture of rigid (nanofiber) and mobile (oligomer) structures. Two common strategies to tackle this challenge are 1) optimizing the non-covalent synthesis yield or 2) purifying the supramolecular products. For example, due to the high thermodynamic stability of peptide nanofibers, the amount of peptide dissociates from the nanofibers is, in most cases, minimal<sup>12, 13</sup>. Therefore, peptide nanofibers can be purified from their oligomer counterparts (e.g., prepare liquid crystalline filamentous colloids<sup>14, 15</sup>). However, making more homogenous materials (e.g., pure nanofibers with low oligomers content) does not always guarantee better application outcomes. The ability to formulate a complex molecular system is one of the unique strengths of supramolecular materials<sup>1</sup>. For example, the co-existence of peptide nanofibers and oligomers can act synergistically in tissue engineering applications (e.g., nanofibers serve as matrix scaffolds<sup>16, 17</sup>, oligomers for stabilizing the native folding of the locally concentrated growth factors in the matrix<sup>18, 19</sup>). Therefore, it will be useful to develop tools to quantify the system plurality of supramolecular materials.

**Bridging the static and dynamic analysis of the supramolecular materials.** Thanks to the advancement of cryo-EM technology, it is now possible to characterize the molecular organization of supramolecular materials in near-atomic resolution. However, cryo-EM measurement is performed with samples in near-native but static conditions. As a result, it could not capture the dynamic properties of the sample, which is also a critical feature of supramolecular materials. For example, structural defects in supramolecular peptide nanofibers can instigate heterogeneity in their secondary nucleation kinetics and resultant fiber morphology<sup>20</sup>. Therefore, there are ongoing endeavours to bridge the static and dynamic analysis of the supramolecular material properties. For example, Baker et al.



utilized the high-level structural details resolved with cryo-EM to engineer the assembly and disassembly kinetics of supramolecular peptide filaments<sup>21</sup>; while Patterson et al. elucidated the liquid-liquid phase separation events during the nanovesicles self-assembly through bridging the liquid-phase EM (dynamic) with the cryo-EM (static) analysis<sup>22</sup>. This comprehensive knowledge of supramolecular materials would be paramount to further their functional development.

**Holistic consideration of molecules surrounding the supramolecular materials.** The structural properties of supramolecular materials (e.g., size, morphology, hydrophobicity) are crucial parameters in moderating their biocompatibility and functionality<sup>23, 24</sup>. However, the organization of molecules surrounding the supramolecular materials (e.g., water, counterions) also play a significant role in determining their biocompatibility and functionality<sup>25-28</sup>. For example, Stupp et al. showed that water ordering on the surface of the nanofibers plays an integral part in their structural organization, and liberation of these ordered water molecules surrounding the surface of these epitope-functionalized nanofibers can provide entropic incentives for the ligand-receptor interactions<sup>25</sup>. Furthermore, they showed that replacing counterions  $\text{Na}^+$  to  $\text{Ca}^{2+}$  on the nanofiber surface can reduce its structural fluidity<sup>25</sup>, which could lower its cytotoxicity<sup>29</sup>. Therefore, the molecules surrounding the supramolecular materials should be holistically considered in their future functional development. (e.g., fabricating transient nanofibers with surface retarded chaotropic ions)

**Development of environment-responsive supramolecular systems for immunological applications.** The development of synthetic immune niches is considered the next frontier in immunotherapy<sup>30, 31</sup>. The implanted synthetic immune niches can offer a systemic environment to continuously modify immune cell functionality by providing a biocompatible and resilient scaffold with the spatiotemporal release of immunomodulatory factors. Current approaches in constructing synthetic immune niches involve modular integration of different functional biomaterials<sup>30, 32</sup>. However, these biomaterials are often independent of each other, making these artificial systems less sustainable if their fabricated configuration is perturbed. In contrast, the multiple supramolecular products formed via non-covalent synthesis can be interconnected in the form of mutualistic biopolymer networks, *i.e.*, each assembly state is in equilibrium with the other<sup>13, 33, 34</sup>. This makes artificial systems constructed with supramolecular materials more adaptive towards perturbation. For example, when mechanical stress is applied to the synthetic immune niches composed of supramolecular peptide materials (*e.g.*, peptide nanofibers as a matrix scaffold, oligomers as native folding stabilizing agents of immunological factors), the fractured peptide nanofibers in the system can trigger secondary nucleation events to increase the overall nanofibers contents<sup>35</sup>. As a result, the increased fibrous content can enhance the mechanical resilience of synthetic immune niches. The systemic stimuli-responsiveness of supramolecular materials can potentially enhance the sustainability of synthetic immune niches compared with the conventional use of independent biomaterial ensembles.

### 4. Conclusion

In summary, this thesis systematically explores the immunomodulatory potential of supramolecular peptide materials. The parameters to optimize the non-covalent synthesis process and to govern the hierarchical organization of peptide nanofibers were studied on the example of surfactant-like peptides. Using peptide nanofibers as a scaffold, we explored the application potential of these ordered materials in inducing antigen-specific tolerance. Furthermore, we examined the application potential of dynamic assemblies between albumin and dexamethasone-antigen conjugates to enhance the level of tolerogenic response induced. Finally, we discussed the perspective on the future development of supramolecular materials targeting immunological application.

### References

1. Vantomme, G.; Meijer, E. W., The construction of supramolecular systems. *Science* **2019**, *363* (6434), 1396.
2. Zivanov, J.; Nakane, T.; Forsberg, B. O.; Kimanius, D.; Hagen, W. J.; Lindahl, E.; Scheres, S. H., New tools for automated high-resolution cryo-EM structure determination in RELION-3. *Elife* **2018**, *7*.
3. Getts, D. R.; Martin, A. J.; McCarthy, D. P.; Terry, R. L.; Hunter, Z. N.; Yap, W. T.; Getts, M. T.; Pleiss, M.; Luo, X.; King, N. J. C.; Shea, L. D.; Miller, S. D., Microparticles bearing encephalitogenic peptides induce T-cell tolerance and ameliorate experimental autoimmune encephalomyelitis. *Nature Biotechnology* **2012**, *30* (12), 1217-1224.
4. Camilloni, C.; Bonetti, D.; Morrone, A.; Giri, R.; Dobson, C. M.; Brunori, M.; Gianni, S.; Vendruscolo, M., Towards a structural biology of the hydrophobic effect in protein folding. *Scientific Reports* **2016**, *6* (1), 28285.
5. Matern, J.; Dorca, Y.; Sánchez, L.; Fernández, G., Revising Complex Supramolecular Polymerization under Kinetic and Thermodynamic Control. *Angewandte Chemie International Edition* **2019**, *58* (47), 16730-16740.
6. Bansal, S. S.; Ismahil, M. A.; Goel, M.; Patel, B.; Hamid, T.; Rokosh, G.; Prabhu, S. D., Activated T Lymphocytes are Essential Drivers of Pathological Remodeling in Ischemic Heart Failure. *Circulation: Heart Failure* **2017**, *10* (3), e003688.
7. Ismahil, M. A.; Hamid, T.; Bansal, S. S.; Patel, B.; Kingery, J. R.; Prabhu, S. D., Remodeling of the Mononuclear Phagocyte Network Underlies Chronic Inflammation and Disease Progression in Heart Failure. *Circulation Research* **2014**, *114* (2), 266-282.
8. Rieckmann, M.; Delgobo, M.; Gaal, C.; Büchner, L.; Steinau, P.; Reshef, D.; Gil-Cruz, C.; Horst, E. N. t.; Kircher, M.; Reiter, T.; Heinze, K. G.; Niessen, H. W. M.; Krijnen, P. A. J.; van der Laan, A. M.; Piek, J. J.; Koch, C.; Wester, H.-J.; Lapa, C.; Bauer, W. R.; Ludewig, B.; Friedman, N.; Frantz, S.; Hofmann, U.; Ramos, G. C., Myocardial infarction triggers cardioprotective antigen-specific T helper cell responses. *The Journal of Clinical Investigation* **2019**, *129* (11), 4922-4936.
9. Kordalivand, N.; Tondini, E.; Lau, C. Y. J.; Vermonden, T.; Mastrobattista, E.; Hennink, W. E.; Ossendorp, F.; Nostrum, C. F. v., Cationic synthetic long peptides-loaded nanogels: An efficient therapeutic vaccine formulation for induction of T-cell responses. *Journal of Controlled Release* **2019**, *315*, 114-125.
10. Baskakov, I. V.; Legname, G.; Baldwin, M. A.; Prusiner, S. B.; Cohen, F. E., Pathway Complexity of Prion Protein Assembly into Amyloid. *Journal of Biological Chemistry* **2002**, *277* (24), 21140-21148.
11. Korevaar, P. A.; George, S. J.; Markvoort, A. J.; Smulders, M. M. J.; Hilbers, P. A. J.; Schenning, A. P. H. J.; De Greef, T. F. A.; Meijer, E. W., Pathway complexity in supramolecular polymerization. *Nature* **2012**, *481* (7382), 492-496.
12. Wei, G.; Su, Z.; Reynolds, N. P.; Arosio, P.; Hamley, I. W.; Gazit, E.; Mezzenga, R., Self-assembling peptide and protein amyloids: from structure to tailored function in nanotechnology. *Chemical Society reviews* **2017**, *46* (15), 4661-4708.

13. Cao, Y.; Adamcik, J.; Diener, M.; Kumita, J. R.; Mezzenga, R., Different Folding States from the Same Protein Sequence Determine Reversible vs Irreversible Amyloid Fate. *Journal of the American Chemical Society* **2021**, *143* (30), 11473-11481.
14. Nyström, G.; Arcari, M.; Mezzenga, R., Confinement-induced liquid crystalline transitions in amyloid fibril cholesteric tactoids. *Nature Nanotechnology* **2018**, *13* (4), 330-336.
15. Woltman, S. J.; Jay, G. D.; Crawford, G. P., Liquid-crystal materials find a new order in biomedical applications. *Nature Materials* **2007**, *6* (12), 929-938.
16. Chau, Y.; Luo, Y.; Cheung, A. C. Y.; Nagai, Y.; Zhang, S.; Kobler, J. B.; Zeitels, S. M.; Langer, R., Incorporation of a matrix metalloproteinase-sensitive substrate into self-assembling peptides – A model for biofunctional scaffolds. *Biomaterials* **2008**, *29* (11), 1713-1719.
17. Cormier, A. R.; Pang, X.; Zimmerman, M. I.; Zhou, H.-X.; Paravastu, A. K., Molecular Structure of RADA16-I Designer Self-Assembling Peptide Nanofibers. *ACS Nano* **2013**, *7* (9), 7562-7572.
18. Zhang, S., Discovery and design of self-assembling peptides. *Interface Focus* **2017**, *7* (6), 20170028.
19. Veith, K.; Martinez Molledo, M.; Almeida Hernandez, Y.; Josts, I.; Nitsche, J.; Löw, C.; Tidow, H., Lipid-like Peptides can Stabilize Integral Membrane Proteins for Biophysical and Structural Studies. *ChemBioChem* **2017**, *18* (17), 1735-1742.
20. Pinotsi, D.; Buell, A. K.; Galvagnion, C.; Dobson, C. M.; Kaminski Schierle, G. S.; Kaminski, C. F., Direct Observation of Heterogeneous Amyloid Fibril Growth Kinetics via Two-Color Super-Resolution Microscopy. *Nano Letters* **2014**, *14* (1), 339-345.
21. Shen, H.; Fallas, J. A.; Lynch, E.; Sheffler, W.; Parry, B.; Jannetty, N.; Decarreau, J.; Wagenbach, M.; Vicente, J. J.; Chen, J.; Wang, L.; Dowling, Q.; Oberdorfer, G.; Stewart, L.; Wordeman, L.; De Yoreo, J.; Jacobs-Wagner, C.; Kollman, J.; Baker, D., De novo design of self-assembling helical protein filaments. *Science* **2018**, *362* (6415), 705.
22. Ianiro, A.; Wu, H.; van Rijt, M. M. J.; Vena, M. P.; Keizer, A. D. A.; Esteves, A. C. C.; Tuinier, R.; Friedrich, H.; Sommerdijk, N. A. J. M.; Patterson, J. P., Liquid–liquid phase separation during amphiphilic self-assembly. *Nature Chemistry* **2019**, *11* (4), 320-328.
23. Sato, K.; Hendricks, M. P.; Palmer, L. C.; Stupp, S. I., Peptide supramolecular materials for therapeutics. *Chemical Society Reviews* **2018**, *47* (20), 7539-7551.
24. Fromchuk, E.; Carey, S. T.; Edwards, C.; Jewell, C. M., Self-Assembly as a Molecular Strategy to Improve Immunotherapy. *Accounts of Chemical Research* **2020**, *53* (11), 2534-2545.
25. Ortony, J. H.; Qiao, B.; Newcomb, C. J.; Keller, T. J.; Palmer, L. C.; Deiss-Yehiely, E.; Olvera de la Cruz, M.; Han, S.; Stupp, S. I., Water Dynamics from the Surface to the Interior of a Supramolecular Nanostructure. *Journal of the American Chemical Society* **2017**, *139* (26), 8915-8921.

26. Deshmukh, S. A.; Solomon, L. A.; Kamath, G.; Fry, H. C.; Sankaranarayanan, S. K. R. S., Water ordering controls the dynamic equilibrium of micelle–fibre formation in self-assembly of peptide amphiphiles. *Nature Communications* **2016**, *7* (1), 12367.
27. Cho, Y.; Christoff-Tempesta, T.; Kaser, S. J.; Ortony, J. H., Dynamics in supramolecular nanomaterials. *Soft Matter* **2021**, *17* (24), 5850-5863.
28. Snyder, P. W.; Lockett, M. R.; Moustakas, D. T.; Whitesides, G. M., Is it the shape of the cavity, or the shape of the water in the cavity? *The European Physical Journal Special Topics* **2014**, *223* (5), 853-891.
29. Newcomb, C. J.; Sur, S.; Ortony, J. H.; Lee, O.-S.; Matson, J. B.; Boekhoven, J.; Yu, J. M.; Schatz, G. C.; Stupp, S. I., Cell death versus cell survival instructed by supramolecular cohesion of nanostructures. *Nature Communications* **2014**, *5* (1), 3321.
30. Weiden, J.; Tel, J.; Figdor, C. G., Synthetic immune niches for cancer immunotherapy. *Nature Reviews Immunology* **2018**, *18* (3), 212-219.
31. Adu-Berchie, K.; Mooney, D. J., Biomaterials as Local Niches for Immunomodulation. *Accounts of Chemical Research* **2020**, *53* (9), 1749-1760.
32. Li, A. W.; Sobral, M. C.; Badrinath, S.; Choi, Y.; Graveline, A.; Stafford, A. G.; Weaver, J. C.; Dellacherie, M. O.; Shih, T.-Y.; Ali, O. A.; Kim, J.; Wucherpennig, K. W.; Mooney, D. J., A facile approach to enhance antigen response for personalized cancer vaccination. *Nature Materials* **2018**, *17* (6), 528-534.
33. Childers, W. S.; Anthony, N. R.; Mehta, A. K.; Berland, K. M.; Lynn, D. G., Phase Networks of Cross- $\beta$  Peptide Assemblies. *Langmuir* **2012**, *28* (15), 6386-6395.
34. Bai, Y.; Chotera, A.; Taran, O.; Liang, C.; Ashkenasy, G.; Lynn, D. G., Achieving biopolymer synergy in systems chemistry. *Chemical Society Reviews* **2018**, *47* (14), 5444-5456.
35. Michaels, T. C. T.; Šarić, A.; Curk, S.; Bernfur, K.; Arosio, P.; Meisl, G.; Dear, A. J.; Cohen, S. I. A.; Dobson, C. M.; Vendruscolo, M.; Linse, S.; Knowles, T. P. J., Dynamics of oligomer populations formed during the aggregation of Alzheimer's A $\beta$ 42 peptide. *Nature Chemistry* **2020**, *12* (5), 445-451.



# **Appendices**

Nederlandse Samenvatting  
Curriculum Vitae  
List of Publications  
Acknowledgement

### **Nederlandse Samenvatting**

Dit proefschrift heeft de mogelijke immunologische toepassingen van supramoleculaire peptide materialen onderzocht aan de hand van het stappenplan voor de ontwikkeling van functionele supramoleculaire materialen zoals beschreven door Meijer et al.<sup>1</sup>. Dit stappenplan kan worden samengevat als 1) optimalisatie van de niet-covalente synthese van de materialen; 2) diepgaande analyse van de materiaaleigenschappen; en 3) effectieve integratie van de materialen in verschillende toepassingsgebieden om een gewenste functionaliteit, in dit geval optimale immuun stimulatie, te leveren. **Hoofdstuk 1** geeft een korte inleiding in de ontwikkeling van supramoleculaire peptide materialen voor immunologische toepassingen.

#### ***1. Optimalisatie van de niet-covalente synthese van de materialen***

Aangezien de niet-covalente synthese van supramoleculaire materialen uit meerdere stappen bestaat, spelen de intermediaire toestanden een belangrijke rol bij het bepalen van het eindresultaat van het assemblage proces. De parameters voor het optimaliseren van de niet-covalente synthese van de supramoleculaire peptide materialen zijn besproken in **hoofdstuk 2**. Met de 0/1-dimensionale nanostructuur selectiviteit boven de  $\beta$ -sheet assemblage route als voorbeeld, belichtten we de interne en externe factoren die de tussenproducten kunnen beïnvloeden en daarmee dus ook het eindproduct. In **hoofdstuk 3** hebben we de moleculaire parameters onderzocht die bepalen of oligomere tussenproducten via nucleatie verder aggregeren of niet. Met behulp van een set zelf-assemblerende peptiden hebben we aangetoond dat het verlagen van de wederzijdse afstotende elektrostatische ladingen tussen de peptide bouwstenen en het verhogen van het vermogen om  $\beta$ -sheets te vormen de nucleatie van de oligomere tussenproducten kan verhogen. We toonden aan dat de mate van oligomere nucleatie bepalend is voor de uiteindelijke opbrengst van de gevormde fibrillen.

#### ***2. Diepgaande analyse van de materiaaleigenschappen***

Een nauwkeurig begrip van de structurele organisatie van supramoleculaire producten kan ons niet alleen een beter inzicht geven in hun materiaaleigenschappen, maar ook aanwijzingen geven over de energetische beperkingen die deze structuren ondervinden. In **hoofdstuk 4** hebben we cryo-EM analyse gebruikt om de supramoleculaire organisatie van peptide nanofilamenten te bestuderen die gevormd zijn door supramoleculaire assemblage van zeep-achtige peptide 1 (SLP1). We hebben waargenomen dat de SLP1 nanofilamenten (diameter  $\sim$ 4nm, lengte  $>$ 500nm) een lage draaiing vertonen onder fysiologische condities. Deze fysisch-chemische eigenschap belemmert de 3D-reconstructie van de structuur met behulp van conventionele cryo-EM beeldverwerkingsmethodes. Gebruik makend van de 2D-klasse gemiddelden van cryo-EM, slaagden we erin om de protofibril en organisatie van de SLP1 nanofilamenten op te helderen. Gebaseerd op de gereconstrueerde structuren, doen we een uitspraak over de mogelijke oorzaken van de lage twist van SLP1 nanofilamenten in fysiologische buffer en schetsen we de functionele implicaties van SLP1 nanofilamenten voor tissue engineering en drug delivery. Deze inzichten tonen aan hoe een goed begrip van



de supramoleculaire organisatie kan helpen bij het toekomstige moleculaire ontwerp en de functionele exploitatie van supramoleculaire materialen.

### *3. Doeltreffende functionele integratie van materialen voor specifieke toepassingen*

Voor biomedische toepassing van supramoleculaire materialen zullen deze effectief moeten worden geïntegreerd met andere materialen. Twee belangrijke benaderingen van functionele integratie van materialen worden nagestreefd---1) het verenigen van de gefabriceerde supramoleculaire materialen met het bestaande materiaal/weefsel, of 2) het incorporeren van de supramoleculaire materialen als modaliteiten op de plek van toediening. In **hoofdstuk 5 en 6** hebben we de potentiële toepassing van supramoleculaire peptide materialen als vaccins onderzocht. In **hoofdstuk 5** hebben we nanofilamenten gebruikt als dragersystemen voor antigeen epitopen en immunosuppressiva (dexamethason). In overeenstemming met de eerdere bevindingen<sup>2</sup>, toonden we aan dat de nanofilamenten met een meer negatieve  $\zeta$ -potentiaal beter werden opgenomen door immuuncellen door binding aan de MARCO-receptor (macrofaag receptor met collageen structuur), wat leidde tot een meer robuuste tolerogene respons. In **hoofdstuk 6** onderzochten we het gebruik van complementaire hydrofobe-elektrostatische interacties om de binding tussen albumine en de dexamethason-antigeen conjugaten te verbeteren. Door de elektrostatische oppervlaktepotentiaal van het albuminebindende deel in het dexamethason-antigeen conjugaat te variëren, ontdekten we dat immunoconjugaten met een betere elektrostatische complementariteit met albumine een sterkere binding aan dit eiwit lieten zien. Dit leidde vervolgens tot robuustere antigeen-specifieke tolerogene reacties in de muis. Dit werk laat zien dat via een rationele benadering peptide-drug conjugaten verbeterd kunnen worden om een gewenst immunologisch effect te krijgen en biedt mogelijkheden voor de ontwikkeling van nieuwe therapieën voor de behandeling van auto-immuunziekten.



### Curriculum vitae

Chun Yin Jerry Lau was born on 3<sup>rd</sup> July 1991 in British Hong Kong. In 2010, he graduated from high school in Hong Kong, during which he obtained a licentiate diploma (violin performance) from the Trinity College London, United Kingdom. From 2010 to 2014, he studied the Master of Pharmacy program at the University of Bath, United Kingdom. Afterward, he performed one year of pre-registration pharmacist training in Belfast, Northern Ireland, followed by a half-year work as a research assistant at the Chinese University of Hong Kong. In April 2016, he started his Ph.D. in the pharmaceuticals department, Utrecht University, which was part of the E.U.'s Marie Skłodowska-Curie Innovative training network (NANOMED-ITN). He was supervised by prof Enrico Mastrobattista and prof dr ir Wim Hennink. His research focused on developing supramolecular peptide materials aimed at immunological applications (tolerogenic immunotherapy).

### List of Publications

#### *This thesis:*

C.Y.J. Lau, F. Fontana, L.D.B. Mandemaker, D. Wezendonk, B. Vermeer, A.M.J.J. Bonvin, R. de Vries, H. Zhang, K. Remaut, J. van den Dikkenberg, J. Medeiros-Silva, A. Hassan, B. Perrone, R. Kuemmerle, F. Gelain, W.E. Hennink, M. Weingarth, E. Mastrobattista, Control over the fibrillization yield by varying the oligomeric nucleation propensities of self-assembling peptides, *Communications Chemistry*, 3, 164, 2020

C.Y.J. Lau, E. Mastrobattista, Programming supramolecular peptide materials by modulating the intermediate steps in the complex assembly pathway: implications for biomedical applications, *Current Opinion in Colloid & Interface Science*, 51, 101396, 2020

C.Y.J. Lau, N. Benne, B. Lou, O. Zharkova, D. ter Braake, N. van Kronenburg, M. Fens, F. Broere, W.E. Hennink, J.W. Wang, E. Mastrobattista, Collaborative hydrophobic-electrostatic interactions assisted dexamethasone-antigen conjugates/albumin association for tolerogenic immunotherapy, in preparation

C.Y.J. Lau, S. Howes, N. Benne, F. Broere, W.E. Hennink, E. Mastrobattista, Cryo-EM structure of dexamethasone-functionalized supramolecular nanofibers, in preparation

#### *Other publications:*

B. Lou, C.Y.J. Lau, W.E. Hennink, E. Mastrobattista, Preparation of mRNA polyplexes with post-conjugated endosome-disruptive peptides, *Methods in Molecular Biology*, 2355, 275-286, 2021

M.K.N Twilhaar, L. Czentner, J. Grabowska, A.J. Affandi, C.Y.J. Lau, Katarina Olesek, H. Kalay, C.F. van Nostrum, Y. van Kooyk, G. Storm, J.M.M. den Haan, Optimization of liposomes for antigen targeting to splenic CD169+ macrophages, *Pharmaceutics*, 12(12), 1138, 2020

## List of Publications

---

N. Kordalivand, E. Tondini, C.Y.J. Lau, T. Vermonden, E. Mastrobattista, W.E. Hennink, F. Ossendorp, C.F. van Nostrum, Cationic Synthetic Long Peptide-Loaded Nanogels: An Efficient Therapeutic Vaccine formulation for induction of T-cell Responses, *Journal of Controlled Release*, 315:114–125, 2019

B. Lou, S. De Koker, C.Y.J. Lau, W.E. Hennink, E. Mastrobattista, mRNA Polyplexes with Post-Conjugated GALA Peptides Efficiently Target, Transfect, and Activate Antigen Presenting Cells, *Bioconjugate Chemistry*, 30:461–475, 2019

E. Carter, C.Y. Lau, D. Tosh, S.G. Ward, R.J. Mrsny, Cell penetrating peptides fail to induce an innate immune response in epithelial cells in vitro: implications for continued therapeutic use, *European Journal of Pharmaceutics and Biopharmaceutics*, 85:12–19, 2013

D. ter Braake, N. Benne, C.Y.J. Lau, E. Mastrobattista, F. Broere, Retinoic acid-containing liposomes for the induction of antigen-specific regulatory T cells as a treatment for autoimmune diseases, *Pharmaceutics*, submitted

### Acknowledgment

Out of my unquenchable joy and excitement, I would like to express my heartfelt gratitude to all those who have supported me throughout the past five years. Your help is fundamental to the completion of my doctoral research.

I would like to express my most profound appreciation to **Enrico**. Words cannot adequately express my gratitude for your guidance and patience throughout my doctoral studies. Thanks for providing me with the resources and freedom to fulfill my ambition and have a profound belief in my work when the results did not look great. You have provided me with the most ideal and vibrant environment to embark on my career as an early-stage researcher.

I would also like to extend my deepest gratitude to **Wim**. Thanks very much for your scientific insights and advice for scientific writings. I am particularly grateful for your insights into instilling personality into the semantic network of science (*i.e.*, addressing works by the PI's name). It offers me immeasurable help in navigating through the enormous volume of scientific literature.

The completion of my thesis would not have been possible without the support and nurturing of **Markus**. Thanks for showing me how to bring scientific works to fruition through an unswerving commitment to excellence. You are my very role model as an emerging scientist, and I sincerely hope we can collaborate again in the foreseeable future.

I would like to acknowledge the assistance of **Alexandre, Renko, Federico, Heyang, Katrien, Laurens, Dennie, Joep, and Joao** for all your help in my first research project. Your contributions are pivotal for the successful completion of our work.

In addition, I would like to extend my sincere thanks to **Stuart**. Thanks for introducing me to the field of cryoEM and offering me countless support in the EM research (*e.g.*, grid preparation, Relion analysis). Thanks also to **Mihajlo** and **Miguel** for all your computational assistance.

I also wish to thank **Naomi** for your support for animal studies. Your expertise and help in organ processing and FACS analysis cannot be overestimated. Thanks also to **Marcel, Nicky, Danielle, and Femke** for your help in the animal studies.

I had the great pleasure of participating in part of the NANOMED ITN network. It is a life-changing experience for me to learn from and grow together with all of you (**Molood, Shirin, Jaleesa, Mona, Mahsa, Roxane, Esra, Vangelis, Shoupeng, Roberta, Jelle, Conor, Vijay, and Mike**). Thanks for the company and discussions during the consortium meetings. Special thanks to **Jan** for your unwavering efforts in coordinating the consortium.

## Acknowledgement

---

I would like to recognize the assistance and advice I received from **Bo**. Thanks for your lunch companion and, in particular, your help in setting up the animal work in NUS. Your advice and insights play an immeasurable role in my career development. Thanks also to **Jiongwei** and **Olga** for your help in the biodistribution studies.

I am also grateful to **Koichi**. Thanks for your insights and advice about Japanese academia. It helps me enormously in making my postdoctoral research plan. Special thanks to my paronyms **Danny** and **Erik**. Thanks for taking the responsibility on short notice. Thanks for your coffee time companion and our (serious) discussion on science and anime, **Danny**. Thanks for your generous reception for our ensemble night, **Erik**. I would also like to acknowledge the companion of the biopharmacy lunch group, **Ada, Ator, Barbara, Bas, Blessings, Cristina, Danny, Erik, Johanna, Lucas, Martina, Matthijs, Olivier** and **Stefania**. Your lunch break companion helps bring forth a grand daily renewal of academic philosophy spirits. Our (weekly?) borrel also help to enlighten the start of my weekend. I also profoundly enjoyed your companion throughout my doctoral studies, **Carl, Charis, Daiki, Everaldo, Genoveva, Jeffrey, Karina, Lies, Lucia, Marzieh, Massi, Mert, Neda, Roderick, Sjaak, and Thijs**. All our fond memories together formulate an unforgettable page of my life. Thanks also to **Ru-Pan** for your accompany and discussion about research and life. I would also like to thank the Chinese community in our group, **Bo, Boning, Dandan, Feilong, Haili, Mengshan, Xiangjie, Yan, Yanna** and **Yinan**. 與君離別意，同是宦遊人。海內存知己，天涯若比鄰。

I'd like to acknowledge the assistance from our technicians, **Esmeralda, Imro, Kim, Mies, Roel, and Louis**. Special thanks to **Esmeralda** for your help in the cryoEM measurement. Thanks also to **Mies** for your daily technical assistance. The daily assistance from **Imro, Kim, Roel, and Louis** was also very helpful to me. Thanks also to **Barbara** for all your administrative support throughout my doctoral studies. Thanks also to the students I supervised, **Wahwah, Matthijs, Annet, and Sanaz**. Your input and support helped me immensely in the completion of this work.

Last but not least, I would like to thank my parents and grandparents for their constant emotional support throughout my doctoral studies. Your support is the steadfast anchor for me to get through this turbulent and uncertain doctoral research journey. 尊前慈母在，浪子不覺寒。

Jerry